University of Bath

UNIVERSITY OF BATH

PHD

Design of Aerospace Laminates for Multi-Axis Loading and Damage Tolerance

Nielsen, Mark

Award date:
2018

Awarding institution:
University of Bath

[Link to publication](#)

Design of Aerospace Laminates for Multi-Axis Loading and Damage Tolerance

Mark William Degn Nielsen

A thesis submitted for

the degree of Doctor of Philosophy

University of Bath

Department of Mechanical Engineering

November 2017

COPYRIGHT

Attention is drawn to the fact that copyright of this thesis rests with the author. A copy of this thesis has been supplied on condition that anyone who consults it is understood to recognise that its copyright rests with the author and that they must not copy it or use material from it except as permitted by law or with the consent of the author.

Declaration

Declaration of any previous submission of the work

The material presented here for examination for the award of a higher degree by research has not been incorporated into a submission for another degree.

Candidates signature:

Declaration of authorship

I am the author of this thesis, and the work described therein was carried out by myself personally, with the exception of part of Chapter 4 where 50% of the work was carried out by other researchers. The manufacturing eigen-mode analysis and the non-standard angle stiffness matching presented is the full authorship of my colleagues Kevin Johnson, Andrew Rhead and Richard Butler at the University of Bath. It has been included in this thesis for completeness as it formed part of a joint journal article, referenced fully in my publications.

Candidates signature:

Contents

List of Figures

List of Tables

Acknowledgements

I would like to thank my supervisors Andrew Rhead and Richard Butler for their support and guidance throughout and for encouraging me to do a PhD in the first place. It has led to a period of my life that I have very much enjoyed, maintaining my interest in research that I hope will continue into the future. Thanks also to Rich Newley for providing useful industrial insight into the broader relevance of my work.

I would also like to thank my parents Harald and Janet for always encouraging my sister Charlotte and I to follow our own path in life and to do what makes us happy.

Thanks are also in order for my colleagues in the Supreme Composites Research Office for their help and camaraderie which has created a friendly and joyful atmosphere to be a part of. Special mentions go to Lucie for her amazing support and above board help at times, and to Hua for being a great friend throughout it all.

Abstract

Acknowledging the goal of reduced aircraft weight, there is a need to improve on conservative design techniques used in industry. Minimisation of laminate in-plane elastic energy is used as an appropriate in-plane performance marker to assess the weight saving potential of new design techniques. MATLAB optimisations using a genetic algorithm were used to find the optimal laminate variables for minimum in-plane elastic energy and/or damage tolerance for all possible loadings.

The use of non-standard angles was able to offer equivalent, if not better in-plane performance than standard angles, and are shown to be useful to improve the ease of manufacture. Any standard angle laminate stiffness was shown to be able to be matched by a range of two non-standard angle ply designs. This non-uniqueness of designs was explored.

Balancing of plus and minus plies about the principal loading axes instead of the manufacturing axes was shown to offer considerable potential for weight saving as the stiffness is better aligned to the load.

Designing directly for an uncertain design load showed little benefit over the 10% ply percentage rule in maintaining in-plane performance. This showed the current rule may do a sufficient job to allow robustness in laminate performance. This technique is seen useful for non-standard angle design that lacks an equivalent 10% rule.

Current use of conservative damage tolerance strain limits for design has revealed the need for more accurate prediction of damage propagation. Damage tolerance modelling was carried out using fracture mechanics for a multi-axial loading considering the full 2D strain energy and improving on current uni-axial models. The non-conservativeness of the model was evidenced to be from assumptions of zero post-buckled stiffness. Preliminary work on conservative multi-axial damage tolerance design, independent of thickness, is yet to be confirmed by experiments.

Publications

The following thesis is created in part by publications, either published in international journals or presented at conferences, that are listed here:

Journal Publications:

M.W.D. Nielsen, K.J. Johnson, A.T. Rhead, and R. Butler. "Laminate design for optimised in-plane performance and ease of manufacture," *Compos Struct*, vol. 177, no. 1, pp. 119-128, 2017.

Submitted for publication:
M.W.D. Nielsen, A.T. Rhead, and R. Butler. "Minimum mass laminate design for uncertain in-plane loading," *Composites Part A*, 2018.

Conference Papers:

M.W.D. Nielsen, A.T. Rhead, and R. Butler. "Structural efficiency via minimisation of elastic energy in damage tolerant laminates," in *Proceedings of the 16th European Conference on Composite Materials*, (Seville, Spain), $22\text{-}26^{th}$ June, 2014.

M.W.D. Nielsen, A.T. Rhead, and R. Butler. "Minimum mass laminate design for uncertain in-plane loading," in *Proceedings of the 20th International Conference on Composite Materials*, (Copenhagen, Denmark), $19\text{-}24^{th}$ July, 2015.

M.W.D. Nielsen, K.J. Johnson, A.T. Rhead, and R. Butler. "Laminate design with non-standard ply angles for optimised in-plane performance," *Proceedings of the 21st International Conference on Composite Materials*, (Xi'an, China), $20\text{-}25^{th}$ August, 2017.

Nomenclature

Acronyms

BVID   Barely Visible Impact Damage

CAI   Compression After Impact

CLT   Classical Laminate Theory

GA   Genetic Algorithm

NSA   Non-Standard Angle (0°-180°)

QI   Quasi-Isotropic

SA   Standard Angle (0°, ±45° & 90°)

SAI   Shear After Impact

SERR   Strain Energy Release Rate

TAI   Tension After Impact

Formulae Symbols

$$\begin{bmatrix} \kappa_x \\ \kappa_y \\ \kappa_{xy} \end{bmatrix}$$ κ Laminate curvatures and twist components at the mid-plane

$$\begin{bmatrix} \sigma_x \\ \sigma_y \\ \tau_{xy} \end{bmatrix}$$ In-plane axial, transverse and shear laminate stresses

$$\begin{bmatrix} \varepsilon_x \\ \varepsilon_y \\ \gamma_{xy} \end{bmatrix}$$ ε In-plane axial, transverse and shear laminate strains

$$\begin{bmatrix} M_x \\ M_y \\ M_{xy} \end{bmatrix}$$ Moment resultants

$$\begin{bmatrix} N_x \\ N_y \\ N_{xy} \end{bmatrix}$$ Force resultants

$$\begin{bmatrix} Q_{11} & Q_{12} & 0 \\ Q_{12} & Q_{22} & 0 \\ 0 & 0 & Q_{66} \end{bmatrix}$$ Ply stiffness matrix

δl Infinitesimal length of unbuckled element used for propagation

η Misalignment angle of the balancing axes from the principal loading axes

γ Non-standard angle proportions

λ_i Eigenvalues of the laminate stiffness matrix, $i = 1, 2, 3$

ν_{12} Major Poisson's Ratio

$\overline{U}$ Normalised in-plane elastic energy

ψ, ϕ, θ Non-standard angles

$\sigma_{I,II}$ Principal loading stresses

$\sigma_{th}\sqrt{T_{SL}}$ Normalised damage tolerance stress

σ_{th} Threshold propagation stress

ε_C Critical sublaminate buckling strain

$\varepsilon_{th}\sqrt{T_{SL}}$ Normalised damage tolerance strain

ε_{th} Threshold propagation strain

$\xi_{1,2}$ In-plane lamination parameters

E_{11} Axial modulus

E_{22} Transverse modulus

F Factor of strain on chosen base strain vector

F_C Buckling factor of strain on chosen base strain vector

F_{th} Threshold factor of strain on chosen base strain vector

G SERR

G_{12} Shear modulus

G_C Critical SERR

G_{IC} Mode I (peeling) critical SERR

G_{IIC}	Mode II (sliding shear) critical SERR
G_{IIIC}	Mode III (tearing) critical SERR
T	Full laminate thickness
t_k	Single ply thickness
T_{SL}	Sublaminate thickness
$U_{1,2,3,4,5}$	Stiffness invariants
$[\overline{Q}]$	Laminate in-plane stiffness matrix
$[\overline{Q}_{SL}]$	Sublaminate in-plane stiffness matrix
$[A_{SL}]$	Sublaminate in-plane stiffness matrix
$\mathbf{A}$, $[A]$	Laminate in-plane stiffness matrix
$\mathbf{B}$, $[B]$	Laminate in-plane/out-of-plane stiffness matrix
$\mathbf{D}$, $[D]$	Laminate out-of-plane stiffness matrix
U_b	Bending energy
U_m	Membrane energy
U_{ult}	In-plane ultimate elastic energy per unit volume

Chapter 1

Introduction

The aircraft industry is growing. Predictions made by the International Air Transport Association (IATA) in 2016 foresee that passenger demand over the next 20 years will nearly double. This forecast is driving airlines to place more aircraft orders, with most of the increase expected in the Asia-Pacific region [1]. However, in conjunction with increased aircraft use, restrictions and penalties associated with increased CO2 emissions create a challenge for the air tourism industry. For sustainability, the Carbon Offsetting and Reduction Scheme for International Aviation (CORSIA) was agreed upon by 65 governments on the 6th October 2016 at International Civil Aviation Organization (ICAO) Assembly in Montreal. These 65 governments collectively are responsible for more than 86.5% of the current international aviation activity, and more than 80% of the growth expected in CO2 emissions after 2020. CORSIA is a plan for carbon neutral growth from 2020 onwards. Any increase in emissions from the 2019 to 2020 average is required to be offset for every year above those levels [2, 3]. From the perspective of the airlines, any reduction in emissions, due to decreased fuel consumption, produces desirable operating cost savings. Improvements in aircraft engine design, aerodynamics and weight are sought in order to increase fuel economy. In this research, the focus is placed on the reduction of the aircraft structural weight.

In an effort to produce lighter aircraft, there has been a switch from using aluminium alloy to Carbon Fibre Reinforced Plastic (CFRP) materials in the semi-monocoque primary structures of aircraft. CFRPs have the advantage of offering a higher specific in-plane strength and modulus, tailoring of mechanical properties and better fatigue and corrosion properties. CFRP features heavily in the new Airbus A350 XWB and Boeing 787 Dreamliner aircraft with benefits not only in weight reduction but from a financial perspective with reduced inspection and maintenance checks due to the improved fatigue and corrosion resistance.

CFRP laminates, unlike homogeneous metals, feature orthotropic unidirectional

(UD) plies stacked upon each other allowing tailored anisotropic mechanical properties. The behaviour of these laminates is also more complex due to this heterogeneity through thickness. The orthotropy of the UD plies arises from directionality of the stiff parallel carbon fibres surrounded by the resin matrix. The four standard ply orientations used in industry are 0°, +45°, -45° and 90° and seen in an example laminate in Fig. 1.1.
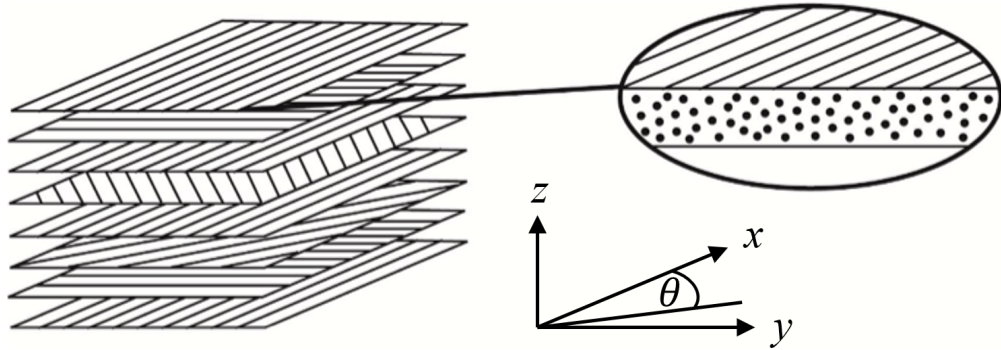
Figure 1.1: *Example laminate stacking sequence of UD plies, $[0/90/0/-45/0/45/90/0]$, with cross-section detail of a single ply.*

From the airworthiness regulations, discussed in depth in Chapter 2, laminates must perform to allow the structure to meet the ultimate load strength requirements. Numerous laminate failure behaviours including in-plane failure, panel buckling and damage tolerance failure must be prevented up to these ultimate load cases. In design, none of these behaviours can be ignored if an airworthy laminate is desired. The goal is one of minimising the laminate weight subject to these strength constraints when given a general laminate loading condition as seen in Fig. 1.2.

CFRP laminates are relatively new applications to the mainstream aerospace industry and thus a lot of conservatism surrounds their use, despite being researched for over 50 years [4]. This leaves a large scope to improve upon the current design methods that are not fully exploiting the potential of CFRP to reduce weight. Current design methodologies incorporate [5–8]:

  (i) Sole use of Standard Angles (SA): 0°, +45°, -45° and 90°.

 (ii) At least 10% thickness of each SA.

(iii) Symmetry about the laminate mid-plane.

(iv) Balancing of plus and minus plies about the manufacturing /geometric axis.

 (v) Ply unblocking to ensure a maximum of 4-6 plies or 1 mm of similar orientation plies in a row to reduce edge effects from an accumulation of interlaminar shear stress [5].

(vi) Reduced angular separation between plies, e.g. $\leq 45°$ angular separations between adjacent plies if possible for reduced interlaminar shear stress.

(vii) $\pm 45°$ near the surface for damage tolerance and buckling performance.
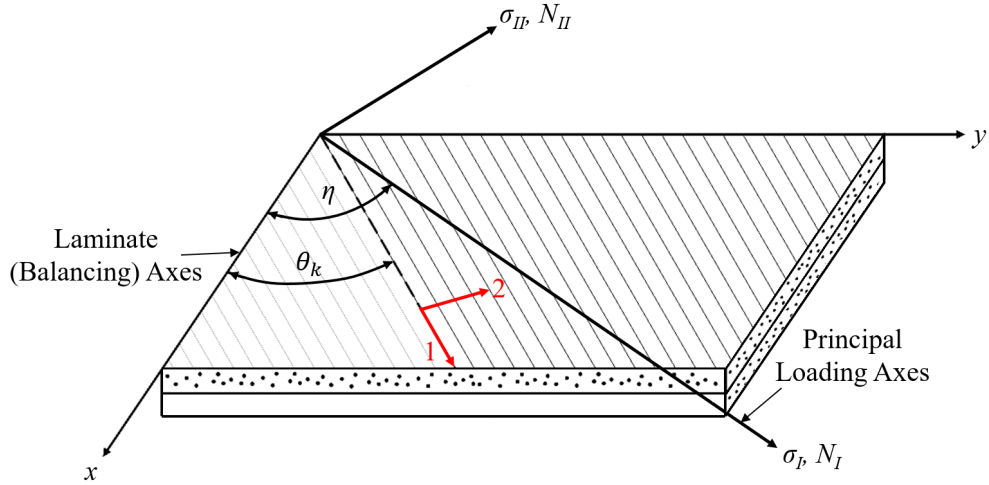
Figure 1.2: *Local ply axes (1-2) and laminate (balancing) axes (x-y). The principal loading axes (σ_I-σ_{II}) and misalignment angle η of the balancing axes are also shown, allowing simplification of any general in-plane loading condition N_x, N_y and N_{xy}.*

The 10% rule ensures the laminate is robust to deviations and uncertainty in the flight loads by maintaining some base stiffness properties in all directions. This rule is seemingly arbitrary as, although there is little known about the uncertainty of aircraft loads, the range of ultimate loads are known. From a design perspective, as long as the laminate will withstand these loads without failure, the laminate is airworthy. Non-Standard Angle (NSA) plies potentially offer greater performance and weight reduction over SAs through greater tailoring of ply orientations where angles can be anywhere from 0°-180° [9]. A novel idea of balancing plies about the principal loading axis instead of the geometrical/manufacturing axis is suggested for potential weight reduction as the stiffness is allowed to be aligned symmetrically and thus more efficiently with the load. This introduces extension-shear and bend-twist coupling in the manufacturing axis if it is not already present.

In this thesis, the laminate design rules of (i) SA use, (ii) the 10% rule, and (iii) balancing in the geometric/manufacturing axis are challenged. To assess the potential of the new design methods laminate design optimisations are undertaken in Chapters 4 and 5 using laminate in-plane elastic strain energy (compliance) as a measure of weight saving ability in accordance to in-plane fibre based failure mechanisms. Prager and Taylor showed that minimum elastic energy, or maximum stiffness under load, coincides with minimum weight in isotropic materials, where the material stiffness is used most efficiently [10]. This is a simple and computationally efficient

performance marker that can provide an avenue into the use of new techniques. The applicability of elastic energy to predict the strength relationship of laminates is discussed in Chapter 3.

A major problem with CFRP use is the low out-of-plane strength and the reduction of in-plane strength when impacted in the thickness direction [11]. Particularly severe are the undetectable but critical inter-ply delaminations, called Barely Visible Impact Damage (BVID), caused by impacts in manufacture or service from runway debris, hail, ground equipment or tools, discussed further in Chapter 2. Other damage such as matrix cracks and fibre fracture can occur during impact but the reduction in residual compressive strength is insignificant compared to delamination. Barely visible impact damage is the most critical damage. Low-velocity impacts create surface indentations that usually fall below the threshold for detectability in the scheduled visual inspection process and thus is barely visible. BVID is problematic because it reduces the Compression After Impact Strength (CAIS) of the structure without knowledge of any damage being present. In compression, buckling of the sublaminates above delaminations gives rise to potential propagation of the delamination that is complex to understand. Therefore the regulations require aircraft structures be damage tolerant of all BVID damage up to the ultimate load of the aircraft with no growth of damage occurring and for the lifetime of the aircraft, discussed further in the Regulations in Chapter 2.

Due to the complexity in the damage behaviour, prevalence and location, current design methods use conservative structural damage tolerance strain allowables empirically derived from vast experimental tests, below which the BVID does not grow [12]. Further weight saving is suggested through use of modelling techniques that reduce the conservatism associated with the failure mechanism, allowing the removal of strain allowables. Accurate modelling prediction is possible through FEA when knowing the damage characteristics [13–15], but due to the uncertainty in the damage and FEAs time consuming nature, it does not lend to the quick laminate initial design process. A general mechanistic understanding of the behaviour is desired so that analytically based modelling and computationally efficient design capabilities can be produced that allow the design conservativeness to be lowered and thus save weight. Current analytical models exist that predict CAIS well for uni-axial loading using fracture mechanics [13, 16–18]. A general model for multi-axial loading is desired and is explored through modelling and experimental comparison in Chapter 6.

Damage tolerance optimisation of sublaminate and laminate variables for any multi-axial load is carried out using a multi-axial propagation model derived in Chapter 6. Damage tolerance stress/strain maximisation as well as constraint application is investigated. The ability to design laminates independent of thickness and for

multi-axial loads is novel.

Potential improvements to the current industry methods apply mainly to the initial design process where there exists the greatest potential to affect the structural design and thus save weight. In later stages, there is greater inflexibility in design choices and starting off with ill designed parts can lead to problems and solutions that result in sacrificing the CFRP advantage over metals. In the final stages detailed FEA modelling and larger scale structural testing allow the structure's performance to be confirmed. The aims of this thesis are to investigate new initial design methods to allow greater weight saving, including (i) introducing new laminate efficiency diagrams and techniques, (ii) improving on laminate design rules, and (iii) removal of DT strain allowables through efficient design modelling.

Chapter 2

Literature Review

This review of the literature will cover the current state of the research with regards to the topics of (i) initial laminate design techniques and (ii) the modelling of damage tolerance to aid in the initial design. Both aspects potentially allow less conservative lower weight designs to be produced whilst still meeting the structural requirements set out by the CS-25 and FAR-25 (Certification Specification and Federal Aviation Regulation) regulations for large aircraft- [19, 20]. However, it is first important to gain an understanding of what these regulations are so they can be accounted for in optimisation routines.

2.1   Regulations

CS-25 and FAR-25 are the European airworthiness requirements set by the European Aviation Safety Agency (EASA) and the American airworthiness requirements set by the Federal Aviation Administration (FAA) respectively for large/transport aeroplanes [19, 20]. The majority of the documents requirements are identical, with clear communication between the two agencies. The aircraft must comply with these requirements in order to receive a Type-Certificate signifying airworthiness.

2.1.1   General Structure

The general structural requirements for airworthiness are included in CS-25.3 and FAR-25.3 or Sub-Part C of the documents. CS-25.307 (a) states

'Compliance with the strength and deformation requirements of this Subpart must be shown for each critical loading condition.'

with CS-25.333 (a) stating:

'*The strength requirements must be met at each combination of airspeed and load factor on and within the boundaries of the representative manoeuvring envelope.*'

CS-25.305 (a) talks of the strength and deformation requirements:

'*The structure must be able to support limit loads without detrimental permanent deformation*' and (b) '*The structure must be able to support ultimate loads without failure for at least 3 seconds.*'

These limit loads are decided by the aircraft's manoeuvre envelope and the ultimate loads are set at 1.5x the limit loads.

Compliance with these regulations is nevertheless aided by the authorities, with guidance given to the aircraft designers in ways in which they can comply with the requirements. These can be seen in the AMC 25.3 documentation for CS-25 for the general requirements. Specific documentation for guidance with composite materials are seen in the close to identical AMC 20-29 (Acceptable Means of Compliance) from EASA and AC 20-107B (Advisory Circular) from FAA, which outline acceptable means of compliance but not the only means [21, 22]. The aircraft manufacturer is ultimately responsible for providing sufficient evidence for compliance with the requirements, whether they use the guidance documents or not.

2.1.2   Damage Tolerance

The damage tolerance requirements are detailed in CS-25.571 and FAR-25.571. CS-25.571 states:

'*The residual strength evaluation must show that the remaining structure is able to withstand loads (considered as static ultimate loads) corresponding to the following conditions:*'

The conditions that follow this ((b)(1) to (b)(6)) are the various typical critical flight conditions, from which are calculated static forces, expected to place the structure under the maximum load possible in service multiplied by the safety factor of 1.5. CS-25.571 later states:

'*The residual strength requirements of this sub-paragraph (b) apply, where the critical damage is not readily detectable.*'

Therefore for all BVID the residual strength of the structure must be at least above or equal to the ultimate load expected for the structure. The document states:

'*On the other hand, in the case of damage which is readily detectable within a short period, smaller loads than those of sub-paragraphs (b)(1) to (b)(6) inclusive may be used by agreement with the Authority.*'

This refers to damage that can be seen from a visual inspection or noticed by a clear reduction in a function, such as reduction in cabin pressure, generally found within a period of around 50 flights. This does not refer to damage seen during the scheduled detailed inspection, which covers Visible Impact Damage (VID).

Overall the regulations require that the damage tolerant structure can be supported by sufficient evidence showing that there will be no catastrophic failure throughout the aircraft's lifetime. Compliance is achieved by producing in depth analysis and testing of the structures, providing the evidence required, along with outlining the appropriate inspection intervals to cope with damage that has a reasonable chance of occurring. In the main document (CS-25.571 and FAR-25.571), specifics regarding the use of different materials in damage tolerance are not covered. Composite materials and the typical damage classifications such as BVID and VID are not mentioned here.

The AMC 20-29 document details in more depth how the requirements can be satisfied for composite materials. Fig. 2.1 taken from this document shows the different severities of damage categorised and the loads that are required to be maintained whilst each damage type is present.
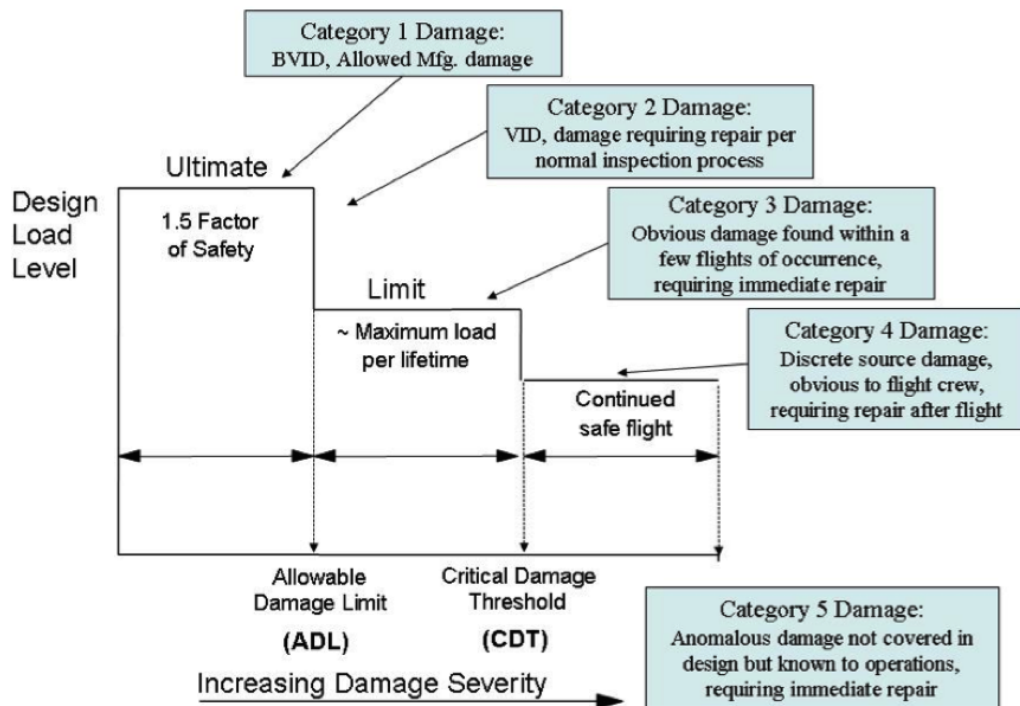
Figure 2.1: *The residual strength requirements of different damage severities [21].*

BVID falls under Category 1, allowable damage that could go undetected; a structure with this level of damage must be able to maintain ultimate load carrying capabilities due to a non-testable residual strength.

If the damage is more severe from the initial impact, and is visible during the scheduled detailed inspection, then the structure will be repaired back to ultimate load carrying capability. This VID is not obvious enough to be seen from a large distance. Design is required to ensure this damage does not reduce the residual strength lower than the limit load of the aircraft during the time period between inspections. Therefore the structure will have adequate residual strength in service with no immediate repair required. More severe obvious damage requires repair as soon as it is noticed or detected (after the flight) and is generally allowed a lower residual strength.

The no-growth condition means that the structure must have no damage growth under repeated loads or up to a certain static load. This is used for the majority of composite damage tolerant parts because it is difficult to predict how fast the growth will be and if it is stable. This condition assures no further deterioration of the structure under loading. For BVID and VID the residual strength will remain above the ultimate and limit load respectively. This approach is shown alongside the slow-growth approach used for metal parts (can be applied to composites) on the diagram in Fig. 2.2 taken from AMC 20-29.
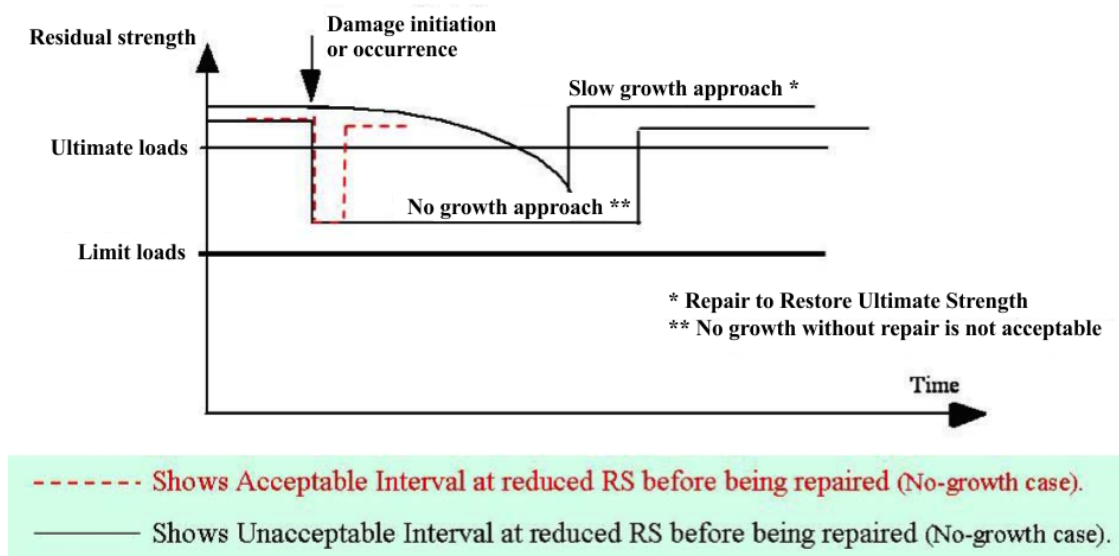
Figure 2.2: *The acceptable no-growth approach to damage [21].*

In industry, a conservative method of designing for damage tolerance is used. Instead of initially designing a part with its own calculated damage tolerant strength by predicting the load at which damage growth occurs, they enforce a maximum strain allowable for all parts of the same material, below which they assume no growth can occur. This accompanies the standard design rule of placing ±45° plies on the surface for better damage tolerance performance. The magnitude of the strain allowable is produced from extensive empirical testing and is conservative for any layup design, usually 4000-5000 μstrain. Consequently current designs may be too

conservative and are not enabling the greatest weight saving from composites to be established.

2.1.3 Regulations Summary

The static ultimate loads for which the composite structure must withstand without failure are generally known, unless there is significant change in the aircraft design. The recommended 'no growth' for any BVID damage up to the ultimate load condition for regulation compliance is known. Conservative empirically-derived design strain limits are enforced in industry, limiting the potential of composite laminates. Improved weight saving is possible with greater understanding of the damage failure characteristics allowing more accurate modelling predictions for the point of damage growth.

2.2 Laminate Design Optimisation

Industrial demand is driving the research for improvement on the current initial design techniques to allow fast and accurate identification of optimal designs [23]. Ideally any design process would initially produce well designed laminates, as initial designs constrain the flexibility at later design stages. Therefore the most optimal initial designs will allow the greatest weight saving to be achieved once the iterative design process is over and the final structure is designed. Optimisation of a laminate design generally requires manipulation of the composite to produce the best physical arrangement of material to meet a certain objective, e.g. maximum buckling load or minimum weight whilst meeting strength constraint requirements. The aerospace industry mainly uses straight fibre UD plies and there is still a large scope for improvement using current laminate manufacturing processes.

Optimised laminates should meet stiffness, strength, buckling and damage tolerance requirements for the range of loads that could be applied (see Section 2.1) whilst minimising the weight of the structure. Not all of these design requirements are generally considered in previous studies, and instead design requirements tend to be considered isolation. Techniques that may provide improvements of a part in isolation may no longer do so when applied to a full aircraft panel design scenario. The complex problem involving many laminate design variables and design constraints lends to the use of computers and numerical methods to solve such problems correctly and efficiently. This is in contrast with past techniques where experience was used to pick initial designs, and engineering judgement was used to make design iterations and often the most optimal design was not found [24].

Optimisation of laminated composite structures typically requires manipulation of discrete ply orientations, number of plies and stacking sequence. Plies have a pre-allocated thickness due to the current standardised manufacturing capabilities [25]. This discretises the design space often leading to compromises in performance when continuous design variables, such as lamination parameters, are used in the top-level optimisation before a real stacking sequence can be created using a following optimisation step [26]. Most optimisations use Classical Lamination Theory (CLT) to provide laminate stiffness and stress-strain relationships from which ply stress and strains can allow prediction of laminate behaviour when design loads are given as inputs [27]. Therefore this enables laminate performance characteristics to be quantified with models and tailored to meet requirements in the optimisation. Optimisation of the laminates has been undertaken to produce laminates for minimum weight, with constraints of buckling load, damage tolerance [28, 29], strength and stiffness for a given design loading [30, 31]. Optimisations have also been carried out to produce maximum performance in singular performance aspects such as buckling load [32], damage tolerance [33–35], strength [36, 37], and stiffness [38–41]. For further information on the optimisations carried out for many different types of fibre reinforced composite structures, a literature survey by Sonmez provides an extensive review [42].

The optimisation methods and objectives will be described and discussed next.

2.2.1 Discrete Variable Optimisation

The design space created using discrete variables is non-convex due to the trigonometric equations in CLT and so does not lend itself to gradient-based methods [43, 44]. A large number of local optima tend to be present and the global optimum is unlikely to be discovered. Genetic Algorithms (GAs) have been used popularly to successfully tackle the complex problem of finding the optimum stacking sequence for a composite panel by minimising an objective function, which may describe the weight or an aspect of laminate performance [33, 34, 45–48]. They are suited to this due to their ability to work on a complex design space, where the best designs are picked and either used (elite) and/or mutated (mutation) and/or combined with others (crossover) to form a population that is more likely to include a better design [49]. Le Riche and Haftka successfully found optimal stacking sequences for maximisation of the buckling load in fixed thickness laminates with the use of a GA. The reported positives of this method were the ability to find multiple designs that are optimal so that the designer could then pick a more favourable optimal design. There was also the fact of the ability to tune the genetic algorithm to search in a particular manner so that the optimum of a particular design problem can be

found more efficiently [48]. Park et al. [36] produced optimal stacking sequences using a genetic algorithm to maximize the strength of the laminate when different loading and boundary conditions were considered. The Tsai-Hill failure criterion was used as an accurate stress assessment in the optimisation (see Appendix B). The optima were efficiently found without any initial guess or auxiliary information at the input [44]. The benefit of a GA is the flexibility to handle complicated design spaces, thereby obtaining optimum designs. There are numerous other computational methods that work on laminate stacking sequence variables to find optimal solutions including simulated annealing algorithms [50, 51] branch and bound algorithms [25, 52], particle swarm optimisation [53] and many more [42]. More basic methods when the problem is less complex may use enumeration [54], parametric studies [55, 56] or analytical methods [57–59].

2.2.2   Lamination Parameters

Laminate in-plane and out-of-plane stiffness properties can be described by using lamination parameters, first introduced by Tsai and colleagues in 1968 [44]. They can describe a fully uncoupled laminate with just 4 variables, a symmetric and balanced laminate by 6 variables and a fully coupled laminate by 12, allowing for a less complex optimisation compared to discrete ply variables. Another feature is the convex continuous design space (proven in [43]) allowing the optimum to be found efficiently using gradient-based methods [6, 60–67]. The problem introduced with the use of lamination parameters is the need to convert the optimum lamination parameters back to discrete thicknesses, ply angles and stacking sequence [26]. The optimisation therefore inevitably becomes a two-stage optimisation. First a top-level optimisation is used to find optimum lamination parameters that meet constraints and then a second-stage optimisation is used to find the discrete solutions that can match the top-level solutions as closely as possible. This is called a bi-level optimisation. This technique has been used by Liu et al. [65] to minimise the material volume (weight) of a wing box made from standard angle (SA) laminates whilst meeting buckling, strain, and ply percentage constraints, as well as blending and manufacturing requirements. They found the lamination parameters for the minimum weight wing box whilst meeting the constraints. Optimisation runs were then used to shuffle the layers in order to meet the blending and manufacturing requirements whilst still satisfying the lamination parameters. Issues were discovered when a lower number of plies were used for the bottom skin, and the optimal lamination parameters were harder to obtain with fewer discrete variables to optimise with. Herencia et al. [66, 67] used a gradient-based top-level optimisation in two publications to find optimal lamination parameters for the minimum weight of a T-shaped stiffener subject to strength, buckling and stacking design rule constraints. The

difference in the approach utilised in each paper is in the second-stage optimisation. In the first [66] a GA was used to find the discrete layup solutions by minimising the distance in the design space to the optimum lamination parameters. It was found that the discrete solutions were always higher weight designs. In the work of Herencia et al. [67] a first-order Taylor series is used about the continuous optimum, assuming the optimal discrete solution is reasonably close to the continuous optimum, approximating the design constraints sufficiently. A GA is used to find the discrete solution that best satisfies this new constraint approximation and produces optimum designs 3.5% lighter than the previous technique. This highlights the potential problems of finding discrete optimum solutions from the optimal continuous lamination parameter solutions.

2.2.3   Stiffness/Strain Energy Optimisation

Stiffness can be either maximized [38, 40, 41, 68] or used as a constraint [30, 31] in an optimisation. Prager and Taylor [10] first outlined the optimality criteria justifying the technique of minimisation of elastic or compliance energy in order to maximise the global structural efficiency or stiffness to a given loading. This technique creates a structure that stores the least strain energy under a given load, and thus is thought to provide efficient use of material and align with a minimum weight design if material strength is critical [38, 39, 58, 59, 68–70]. Pedersen used this premise in composite materials to find analytical fibre angle solutions for minimum elastic energy in an orthotropic material (single layer) under combined in-plane strains [58]. However the complexities induced with a multi-ply laminate structure make an analytical approach unfeasible and thus optimisations using algorithmic methods must be used to find the optimal designs [38, 39, 59, 68–70]. The equation describing the elastic energy within the laminate would be used as the objective function in an optimisation of this type.

Recent techniques to simplify and generalise the laminate design process for in-plane strength and stiffness by Tsai and Melo [23] has shown that all unidirectional carbon-fibre composites have close to the same trace-normalised stiffness parameters for the in-plane stiffness matrix. The trace is a material constant defined by the sum of the leading diagonal of the terms in the laminate and ply in-plane stiffness matrices $\left[\overline{Q}\right]$ and $[Q]$, respectively. This then allows a master-ply of mechanical properties to be used to describe all carbon-epoxy materials. A given material's trace represents the stiffness performance of that material. Fewer material tests are shown to be required to establish reliable material properties. When creating a laminate, a single test can be used to establish all the mechanical properties. Any defects or effects from manufacture are automatically taken into account, and no

further tests are required to establish the whole laminate performance.

Stiffness Summary

Lamination parameters can be used to describe laminate stiffness properties with fewer variables as well as creating a convex design space which is easier to optimise. Drawbacks of this are the two-step optimisation required in order to discretise continuous optimums to a real stacking sequence. Minimisation of in-plane compliance or elastic energy can be used to create the most stiff laminate to a given in-plane load. It is a simple approach to provide efficient use of a composite material. It can be used to approximate maximum strength design but is not directly equivalent.

2.2.4 Strength Optimisation

Optimising for maximum in-plane strength is not as simple as minimisation of laminate elastic strain energy. This is due to the fact that the stresses in each individual ply must be calculated in order to assess when first-ply failure will occur, and then consequently the progressive failure until the final ply failure occurs. Failure criteria are generally used in the optimisation as a constraint [30, 31] or objective function [32, 36]. Composite material failure is usually assessed successfully using a quadratic stress criterion such as the Tsai-Wu failure criterion [71]. The Tsai-Hill failure criterion is used during maximum strength optimisation in Park [36] (see Appendix B for the difference in these criteria). The stresses here are calculated using the finite element method, and the points in the structure that fail earliest are evaluated and the laminate is optimised to iteratively increase the lowest strength point in the structure until the maximum laminate strength is reached. These models work on a ply level mesomechanic strength whereas other failure criteria that take into account the more detailed micromechanics of failure can produce more accurate failure predictions; such as the Puck criterion [72, 73] and Cuntze criterion [74, 75]. The World Wide Failure Exercise (WWFE) has shown the inconsistency of failure criteria in predicting the strength of composite pressure vessels [76–80]. Failure criteria still capture the laminate strength relationship as a whole and thus are still useful for the initial design optimisation purposes but more accurate modelling and/or experimental tests are needed to accurately quantify the real strength and behaviour of the designs. The end goal is to provide accurate design tools to be implemented by designers instead of the need for time and cost expensive FEA and experimental testing programmes. Tsai and Melo [23] introduce a general omni-strain envelope that predicts failure of the material irrespective of the stacking sequence and ply orientations within the design; an invariant-based failure criterion. This allows for the easy evaluation of a design with adequate in-plane strength for structural designers.

Strength Summary

Strength modelling has been shown to be notoriously hard due to the complex nature of composite materials. Models that account for the large range of micro, meso and macro-mechanical behaviour are found to perform best. Accurate and fast models are desirable to produce lower weight initial designs. Minimisation of in-plane elastic energy can be used to create the most globally stiff laminate for a given in-plane loading and is a simple way to consider efficient use of material, approximating a laminate with maximum in-plane strength.

2.2.5   Robust Design

Uncertainty exists in all parts of the real world engineering problem of aircraft design. These include the loads a structure may experience, uncertainty in material properties (due to manufacturing quality), and expected performance due to a lack of a truly complete understanding of the real structural behaviour. These uncertainties must be taken into account by using reliable statistical information where possible and producing conservative designs to ensure structural safety for the lifetime of the aircraft (see Regulations 2.1 [19,20]). Uncertainty quantification using real statistical data is allowing complex problems with conservative current solutions to be solved more accurately and quickly by making use of improved numerical methods [81–83].

However most optimisations in composites consider fixed design loadings and fixed material properties that are not representative of the real loads and properties. This may lead to unknown off-axis loading failure or unexpected failure modes as the material designs rely so much on their anisotropy to be optimal. To avoid these problems, current structures are conservatively designed for the range of possible ultimate loads that could be applied. It does not make sense to design solely for the most likely loads that the structure will experience but for all possible loads that could be experienced. Conservativeness in laminate performance is also built in through use of the 10% minimum ply percentage rule in the current industry laminate design practice discussed in Section 2.2.6. Accounting for the uncertainties directly would likely lead to designs of lower weight whilst still ensuring safety.

Taking into account uncertainty, Murotsu et al. [84] used the probability associated with the loads and the material properties (from manufacture). A series system model is used to optimize the laminates with respect to their failure probability to produce the most reliable laminates.

Lombardi and Haftka [85] produce a way to lower the computational cost of optimisation when considering anti-optimisation. Optimisation when uncertainty is present is shown to include the generally used technique of anti-optimisation, i.e.

finding the optimal design that has the best performance under the worst possible scenario that could be created from the uncertain inputs. Then it is checked whether this worst scenario is acceptable and thus if the design is robust or not.

Guo et al. [86] discuss optimisation considering uncertain inputs in anti-optimisations. It was recognised that most techniques do not sufficiently find the worst possible scenario of an optimal design from the range of scenarios created by the uncertainties. This is due to the use of search algorithms that tend to fall in local optima, putting the robustness of designs at risk. They outline that the anti-optimisation is often a non-convex problem and global optimality criteria must be used to make sure the optimal designs obtained are robust.

Verchery [87] has shown that Netting analysis, in which the fibres within a laminate are aligned in principal directions to carry principal stresses, can be treated as a limiting case of Classical Laminate Theory. His approach indicates that designs with fewer than three fibre directions produce mechanisms when subject to small disturbances in loading and thus the weak matrix becomes critical to prevent such an action to occur. This provides justification for the implementation of all the current standard fibre angles of 0°, +45°, -45° and 90° in a given design (see 10% rule in Section 2.2.6) in order to prevent this mechanism like behaviour when the loads are somewhat uncertain.

Robust Design Summary

Uncertainty is present in the material properties, laminate manufacture and applied loadings which all causes uncertainty in the laminate performance behaviour, assuming it modelled correctly in the first place. Design techniques that account for these uncertainties produce the most realistic designs and unnecessary conservatism can be removed. The 10% ply percentage rule that is applied to the currently used standard angle designs provides robustness to uncertainty in loading as well as providing a base stiffness in all directions. Its sweeping use in all designs suggests a potential area of weight saving potential if a laminate is instead directly designed for the loading uncertainty.

2.2.6   Industry Design Rules

Design rules are often placed as constraints on optimisations to ensure designs provide the performance and manufacturability characteristics desired. The common industry rules in place for the CFRP panels for aircraft structures are based on both experience, evidence and reasoning discussed elsewhere [5–8]. The design rules include:

(i) Sole use of Standard Angles (SA), 0°, +45°, -45° and 90°.

(ii) At least 10% thickness of each SA.

(iii) Symmetry about the laminate mid-plane, enforcing $\mathbf{B} = 0$.

(iv) Balancing of angle plies in the manufacturing /geometric axis, enforcing A_{16}, A_{26} = 0 (no. of +45°s = no. of -45°s).

(v) Ply unblocking to ensure a maximum of 4-6 plies or 1 mm of plies of the same/similar orientation in a row to reduce the inter-laminar shear stress and likelihood of edge failure [5]. Also allows reduction of thermal stresses built up during cure.

(vi) Reduced angular separation between plies, e.g. $\leq 45°$ angular separations between adjacent plies for reduced inter-laminar shear stress. A 90° switch from one ply to the next should be prevented if possible.

(vii) $\pm 45°$ near the surface for damage tolerance and buckling performance.

These rules are used in many optimisations [65, 88, 89]. Reasons for using all four standard angles can be seen from the robust truss like structure created with the standard-angle fibre directions [87]. However the use of the whole range of fibre angles (0°-180°) called non-standard angles or non-conventional angles, used in non-conventional laminates (NCL), has been shown to extend the stiffness landscape. All possible in-plane stiffnesses can be produced by just two plus minus non-standard angle pairs, the extent of the design space is seen with lamination parameters in Miki and Sugiyama. [90]. Weaver and Bloomfield. [9] have shown that use of non-standard angles has allowed increased buckling performance when plies can be orientated at any 5° angle. This is possible since the range of lamination parameters obtainable is greater for the same number of plies compared to standard angles. Use of non-standard angles has also provided increases in damage tolerance over standard angle designs via greater dispersion and fibre bridging effects [28]. The problem with non-standard angles are their lack of 10% ply percentage rule to ensure the design has robustness in its strength and stiffness performance in all directions when loading uncertainty exists. The 10% rule allows the laminate to rely on the fibres in all directions, creating a more stable strength and stiffness response than relying on solely the matrix in certain directions [87]. Experimental evidence for non-standard angle plies for $\pm 55°$ shows a markedly non-linear stiffness response that would not be desirable for a laminate required to have well understood loading characteristics [80]. Peeters and Abdalla [91] have shown the ability to optimise non-standard angle designs for maximum stiffness to a load whilst having a constraint ensuring a certain level of stiffness in all directions. This cleverly mimics the robust performance characteristics the 10% rule creates. Abdalla [92] has been able to apply a base

stiffness for NSAs in the in-plane lamination parameter space from which designs can be chosen that have a robust stiffness in all directions. This can be seen in Fig 2.3 showing the extent of the design space for SAs and NSAs with and without an effective 10% rule.
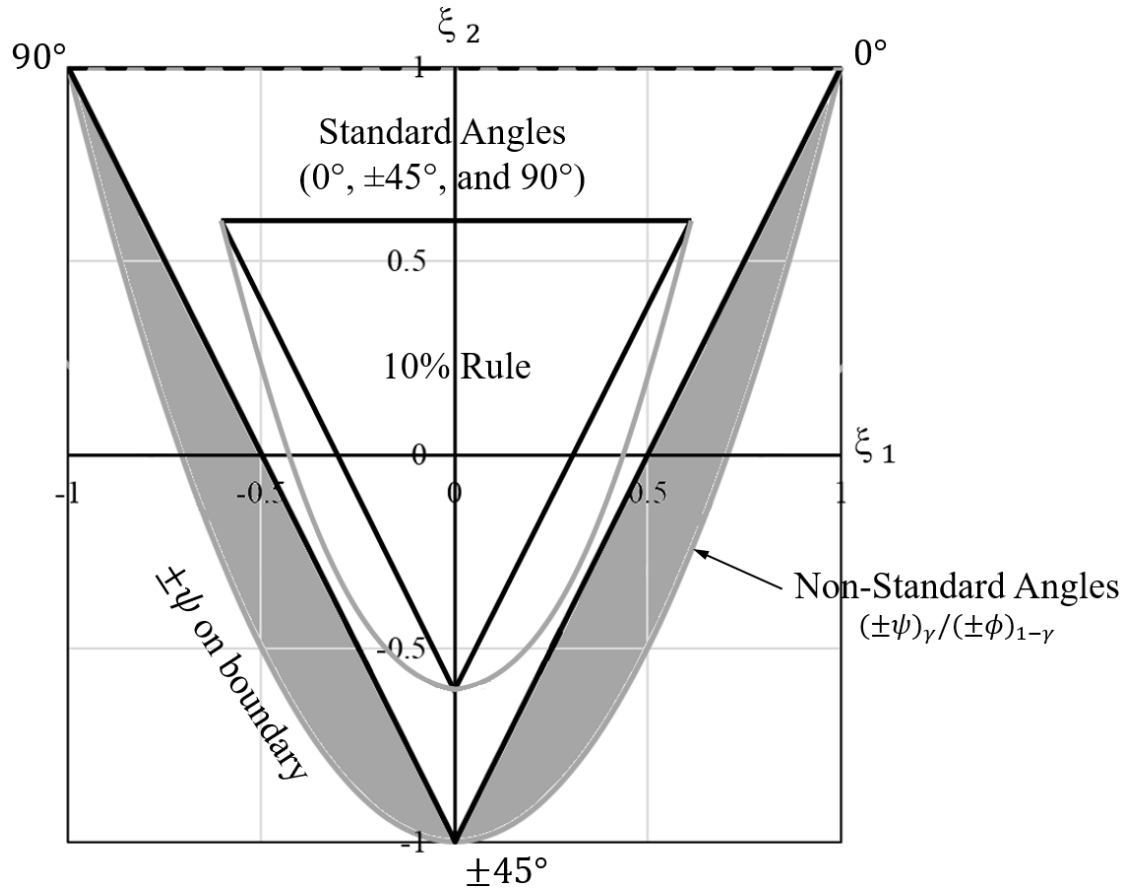
Figure 2.3: *In-plane lamination parameter space for SAs (triangle) ands the greater space for NSAs (parabola) and the effective 10% rule applied to both, reducing the design space to the smaller shapes.*

Symmetry is a common design rule used to prevent any in-plane to out-of-plane coupling behaviour and warping during manufacture that generally occur due to the presence of coupling terms in the stiffness matrix. Symmetry creates a structure that behaves more like a homogeneous material, allowing panels to be connected without much concern of their differing behaviours under load. Symmetry, however, is not required to produce a laminate with a $[B]$ matrix equal to zero, as seen by the specially orthotropic fully uncoupled 8 ply sequence from Caprino and Visconti [93]. York [94, 95] has shown that more special non-symmetric stacking sequences can provide the requirement of $[B] = 0$.

Balanced angle ply designs are generally required to stop twisting of the wing-box as the extension-shear coupling contributes to out-of-plane deformation. However twisting can be eliminated by having a lower skin which counteracts the extension-

shear coupling of the upper skin. Aero-elastic tailoring to purposefully induce wing twist for favourable lift characteristics as the wing bends has been demonstrated to be a potential exception to the rule [96–98]. Tsai [99] has also argued for the removal of the balancing rule and instead using the extension-shear coupling to help the performance of the laminate to further reduce weight. In the same paper it is suggested that symmetry can also be relaxed in order to seek greater weight saving. The $[B]$ matrix terms can be minimised by repeating the non-symmetric stacks many times and so the laminate behaviour becomes homogeneous [99, 100]. York [97] has shown that straying from the balanced and symmetric design rule can give rise to useful coupling behaviours and greater flexibility in design.

$\pm 45°$ surface plies increase damage tolerance due to their resistance to delamination formation during impact [101] as well as the increase in strain required for a sublaminate to buckle and propagate [102]. Thus they are generally placed at the surface.

Ply unblocking is required to prevent large in-plane shear stresses that can more easily promote failure at the adjacent interface and edge-failures when blocks of plies are too thick. Significant residual stress due to the thermal stresses locked in during the manufacturing cure cycle can also decrease the laminate strength. Reducing interface angle mismatch prevents the same problems as seen by ply blocks. A smaller mismatch in adjacent plies reduces these problems and reduces the heterogeneity of the laminate. Modelling is required to produce accurate predictions on the effect of ply unblocking angles and thickness of ply blocks to allow quantification of the residual stresses to determine when failure may occur. These models can then be applied to the optimisation instead of the ply unblocking rules, reducing the conservativeness associated with the design and potentially creating lower weight laminates.

Industry Design Rules Summary

Laminate design rules are used in optimisation to achieve appropriate laminate characteristics without directly optimising for a particular objective. Design rules, although simple and easy to use, remove the ability to directly optimise for the performance characteristic they are trying to provide and thus remove potential weight savings that could be had. The need for direct optimisation instead of applying somewhat arbitrary rules in a broad fashion is evident. The rules have generally dictated the use of solely SAs. Through the consideration of lamination parameters, the large majority of in-plane and out-of-plane stiffness has been shown to be captured by the use of solely standard angles. However, NSA laminates offer the full range of in-plane stiffness with the use of just two $\pm\theta$ angles. The disadvantage of

using standard angles is seen to be small for stiffness purposes but as ply numbers are lowered, greater variation in ply angle is likely required to capture a greater range of stiffness. There are a lack of equivalent design rules available for NSAs. Research optimisations incorporating a base in-plane stiffness in all directions for NSA designs has allowed an equivalent transfer of the industry 10% rule. Further consideration of design with NSA plies are required to create laminates with the required performance characteristics.

2.2.7 Laminate Optimisation Overview

Fast and accurate initial design tools are required to allow maximum weight saving in the final design. Current design using UD plies is still carried out in a conservative fashion, offering scope for greater weight savings to be achieved using current manufacturing processes.

Composite laminate optimisation is a complex problem involving many laminate design variables and design constraints that lends itself to the use of computational and numerical methods to solve such problems correctly and efficiently.

Laminate optimisation has been considered for all aspects of laminate design, including buckling resistance, damage tolerance, in-plane strength, stiffness and more. All of these need to be considered in a full laminate design problem. Laminate stress-strain behaviour is typically determined by CLT after which appropriate failure criteria and models can be applied to determine the laminate performance characteristics.

The choice of laminate design variables used in the literature varies. Discrete ply stacking sequences for specified loadings offer a complicated non-convex design space that suits GA use. The benefit of a GA is the flexibility to handle complicated design spaces, thereby obtaining optimum designs. Continuous lamination parameters allow for a convex design space and ease of initial optimisation analysis using fast gradient based methods. A general view of the design landscape for a performance parameter can be plotted on a lamination parameter diagram. A two-level optimisation method is required to convert these parameters back into a discrete ply design. This can be problematic as optimum discrete designs can be far from the continuous optimum and so the same discrete ply stack problem from above is formed as a second optimisation step.

A general view of design is important for understanding the nuances of cause and effect within the optimisation problem in order to assess if new techniques will offer an advantage over the current design techniques. This requires the ability to offer a view of optimum designs for a large range of loadings, including magnitude and

direction.

2.3 Damage Tolerance

2.3.1 Impact Damage

Composite aircraft parts can be impacted in a number of possible ways, and the types of impact can be categorised into overlapping ranges on the continuous velocity spectrum. Dropped tools during fabrication, assembly and service maintenance come under low-velocity impacts of around 1-10 m/s [103]. Hailstones at terminal velocity can be at the high end of the low-velocity impacts, 9 m/s, or more intermediate velocity, 40 m/s, depending on their diameter [104]. They are a concern due to their partially soft mechanical properties that readily create impact damage without surface indentation [105]. BVID (Barely Visible Impact Damage) caused by these low-velocity impacts is of critical concern and is extensively studied in the literature. The classification of BVID is determined by the indentation depth limit which is around 0.5 mm according to Gower et al. [106]. The maximum BVID delamination length is observed to be just over 9 times the laminate thickness [107].

It is important to know the BVID damage extent from low-velocity impact when using a model to assess the CAI strength. Therefore characterisation of this damage is desired.

Shivakumar et al. [108] outlined that low-velocity impact can be modelled as quasi-static. This is because there is sufficient time available for the entire structure to react. During shorter contact times at higher velocities, the stress wave does not have sufficient time to propagate across the plate and a local wave response is seen. Nettles and Douglas [103] confirmed low-velocity impact tests can be simulated using quasi-static static loading with the damage matching in both tests as long as the same maximum contact force, from impact, is used in the quasi-static loading. Jackson and Poe [109] agree by showing that for sufficiently large mass, low-velocity impacts (ie. quasi-static), the maximum impact force is the sole parameter influencing the size of the maximum delamination in simple plates. A comparison between static indentation in a circular window and dynamic impact in a circular window gave similar results. For a constant impact force and large enough impactor mass, velocity, impact mass (as a variable), plate size and boundary conditions have no effect on delamination diameter. Force matched testing by Highsmith [110] showed that in the impact tests conducted there was less damage than in the quasi-static tests, concluding that impact force is not a good measure of damage severity and therefore suggesting quasi-static tests can act as conservative test for damage. This

goes against Nettles and Douglas [103], whom outlined their results may only work for quasi-isotropic (QI) laminates. The results from Highsmith are however from QI laminates with non-standard plies ([0/+60/-60]), perhaps not representing the the QI SA deigns likely referred to by Nettles and Douglas. Therefore both stacking sequence and fibre orientation may play a role in the inability and ability to correctly represent impact tests with quasi-static loading tests. Thus it may be context specific that the deciding factor in delamination damage is the maximum contact force. Nevertheless at least if quasi-static tests are carried out the damage is evidenced to be conservative.
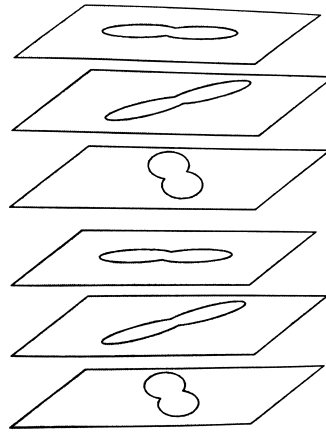
Figure 2.4: *Typical shape of delaminations at ply interfaces after impact.*

The shape of delaminations from impact are generally peanut shaped, see Fig. 2.4, and align with the fibre direction of the lower ply at the interface away from the impact face [111, 112]. A larger delamination is typically formed near the back face away from the impact face. Depending on the stacking sequence, conical delamination damage can often be seen through the thickness of the laminate where delaminations get progressively larger towards the back face [111]. Suesmasu and Majima [113] show this can be from the difference in SERRs (Strain Energy Release Rate) through the thickness; being higher at the back face.

Hong and Liu [114] show there is a linear relationship between impact energy and total delamination area, assuming all other variables are equal. Assuming the energy from impact is absorbed by the laminate then it is intuitive that any energy over the initiation energy for damage will be used to do work done in creating damage. It is also shown that the bending stiffness mismatch between adjacent plies is correlated to the delamination area at each interface. The authors note that thin composites plates under low-velocity impact behave similar to global bending.

Sjoblom et al. [115] show energy loss during impact is a better measure of total damage formed during impact than impact energy, since it is the energy that is

absorbed by the laminate which creates damage, not the impact energy. They also again confirm static tests correctly represent the lower range of low-velocity impacts in non-rate sensitive materials.

In the work of Hitchen and Kemp [101], it was found the maximum delamination area after impact dictates the compressive residual strength, with a larger area (more damage) producing less strength. The total delamination area is shown to be influenced by the stacking sequence and the energy absorbed during impact. The effect of using dissimilar ply angles at the surface, eg. $\pm 45°$ and similarly $0°/90°$, can increase the initiation energy reducing the energy for propagation during impact and therefore the overall damage can be lower, increasing the CAI strength for the same impact energy. Delamination shape was shown to be influenced by splitting and fibre fracture in the ply below the delamination. Pilchak et al. [116] show a smaller angle mismatch between plies gives a higher delamination resistance (greater initiation energy) with fibre bridging contributing to this effect, i.e. fibres overlapping (bridging) between adjacent plies preventing delamination at the shared interface.

Amaro et al. [117] showed impactor diameter and boundary conditions have an effect on the impact response. With greater diameters, the amount of deflection at a constant impact energy increases and thus creates more damage. Clamped boundary conditions which create a stiffer laminate, reduce the deflection of the laminate but increase the amount of energy absorbed by the laminate, therefore increasing the damage for the same energy and impactor diameter. Simply-supported boundary conditions give more displacement, however less energy is absorbed and so the damage is lower [118].

Bouvet et al. [119] modelled low-velocity impact damage using FE, taking into account matrix cracks locally and modelled fibre failure as a continuum variable. This was created as a qualitative model, the actual magnitude and extent of damage was not captured but the global response and damage morphology in each interface was in agreement with experimental C-scan results. They identify Mode I interlaminar peeling fracture as being fundamental to delamination propagation during impact but Mode II interlaminar shearing fracture potentially being more prominent depending on stacking sequence (see Fig. 2.5). They suggest the permanent indentation must be taken into account in the FE model since it can affect residual strength in compression.

Finally Bouvet et al. state:

'*A lot of work is still necessary to wholly simulate the DT of a composite panel and to take into account, at the same time, the damage during impact and the permanent indentation to evaluate the residual strength and to optimise the design of the composite structures in damage tolerance...*'

Mode I	Mode II	Mode III
Peeling, G_{IC}	Sliding Shear, G_{IIC}	Tearing, G_{IIIC}
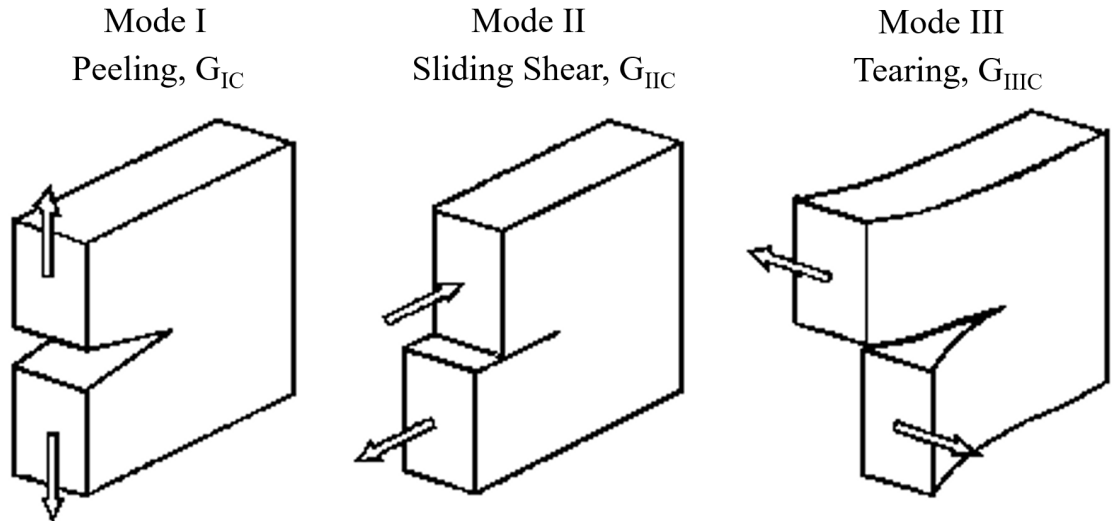
Figure 2.5: *The three modes of fracture*

Garnier et al. [120] noted that for all damage to be detected, several different techniques should be used, including optical and ultrasonic, in order to capture delamination sufficiently. However, C-scan does this to a reasonable degree of accuracy for understanding the extent of delamination damage for BVID. C-scans may be not reveal the full extent of delaminations as they become closed when not under load, as outlined by Chen et al. [121], where the extent of delamination can be seen to be larger when the sublaminate is under an out-of-plane load.

Lammerant and Verpoest [122] concluded that when using FE to predict initiation and growth of delaminations during impact, the possibility of matrix crack formation must be accounted for in the model, in addition to delamination, in order to get the impact damage and morphology correct.

Clark [123] used a 3D model to explain the behaviour of delaminations in impact damaged composites, showing the model accurately predicted delaminations/cracking for a range of different laminates and support conditions. It was found that the main variables controlling damage are the relative orientations of the 2 plies about an interface. The 2nd ply away from the interface has minor effects on the damage formation.

Davies and Olsson [118] produced a review from their experience and the literature, which covers impact damage, analysis capabilities and damage tolerance de-

sign tools. They concluded that the damage formed from impact and the residual strength are dependent on many variables such as the material properties, stacking sequence, geometry, laminate mass and stiffness. They also conclude that during impact, Mode II fracture involving interlaminar shear is the most dominant action in regards to damage formation and damage resistance relies on the Mode II toughness of the material. Additionally they highlight that analytical models have been developed that accurately predict the initiation of damage during impact on basic plates but the damage growth (during impact) and morphology is very complex and must be modelled using FE simulations that are computationally expensive. This means that at present it is not possible to know the nature of the damage that may occur until a part is fully designed, therefore assumptions must be made about the worst possible damage that could occur when designing for CAI strength.

Impact Damage Summary

Although the formation of impact damage and its prediction is not as important as accurately predicting the residual strength of damaged laminates, it aids this research by giving insight into the entire design problem. Therefore it could potentially offer overlap with ideas that can help create a CAI model or understand the behaviour. Several factors are found to be associated with the size, type and shape of damage formation after low-velocity impact.

Analytical models have been developed that accurately predict the initiation of damage during impact on basic plates but the damage growth (during impact) and morphology is very complex and is only possible to be modelled through use of FE simulations that are computationally expensive. Therefore during the initial design stage we cannot know with certainty the extent of BVID damage. This then directs us to using realistic estimates of the extent of BVID from NDT after impact experiments. NDT techniques such as C-scan are used to view the extent of damage. The complexity and uncertainty related to impact damage formation, as shown by the many factors that influence the damage formation, creates a reliance on experimental testing and conservative predictions to assess the damage of BVID for the use in a CAI model for the initial design stage.

2.3.2   Behaviour and Strength in CAI

The sublaminate buckle-driven delamination propagation mechanism is shown in Fig. 2.6, which represents the damage tolerance failure problem. Byers [11], carried out a series of tests for NASA, showing the highest reduction in compressive strength for BVID is 80%. This evidences the criticality of BVID damage to composite panel

design. It was found that the material with the highest interlaminar fracture toughness displayed the greatest compressive residual strength. Davies and Olsson [118] agree, with the Mode I interlaminar fracture (peeling) and Mode II interlaminar fracture (shearing) fracture toughness being key in the damage growth.

(a)   (b)   (c)
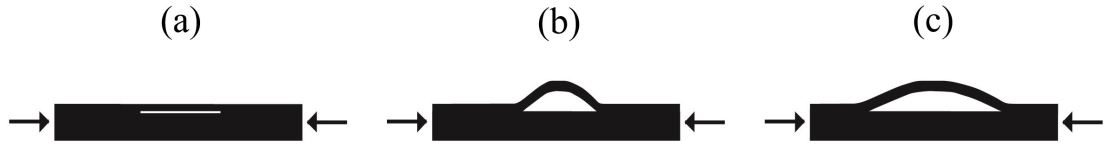
Figure 2.6: *The mechanism for sublaminate buckle-driven delamination propagation in 1D. (a) Near surface delamination damage present, (b) sublaminate buckles under compression and (c) delamination growth occurs under further compression.*

Hitchen and Kemp [101] showed CAI strength is dictated by the maximum delamination area, in the majority of cases being the very back interface; with a larger delamination area producing less strength. Amaro et al. [124] showed from experimental tests that CAI strength is correlated to delamination area as well as the number of delaminations. The stacking sequence was also shown to affect the point of buckling and subsequently the CAI strength. The effect of multiple delaminations was found to reduce the damage tolerance of laminates more than for a single delamination [125, 126]. From Aslan and Sahin [127], it can be seen that when considering the sizes of multiple delaminations the longest near-surface delamination in the direction of load dictates the interface and load at which sublaminate buckling and failure occurs. The size of delaminations below this near-surface delamination is not seen to have an effect on the damage tolerance performance. Suemasu et al. [128] show that for artificial delaminations that are spread through the thickness in a conical shape, the largest delamination would cause sublaminate buckling at the lowest load followed by the next largest delamination. The distribution, whether conical or constant size delaminations through thickness (based around the same average diameter over the total number of interfaces), was concluded to affect the behaviour significantly with larger CAI strengths seen with the constant size delaminations.

In Craven et al. [129], the size of delamination was modelled using FEA in ANSYS. It showed that with an increase in delamination size/area, a decrease in stiffness of the damage region occurred, which then lead to a lower damage tolerance with earlier buckling. This was also shown by Tafreshi and Oswald [130] when considering the delamination size as a proportion of overall panel area; increasing proportional delamination area decreases the damage tolerance.
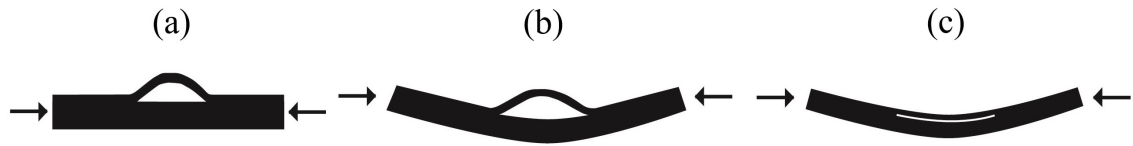
Figure 2.7: *Possible buckling failure from (a) local sublaminate buckling (b) local-global buckling interaction (delamination opening) and (c) global buckling (delamination closing).*

The buckling load of a sublaminate is dependent on delamination depth as shown theoretically in Hunt et al. [131]; with larger depths increasing the buckling load. An increase in size of the delamination has also been shown to decrease the buckling load in Kim and Kedward [132]. In Hunt et al. [131] depth of delamination was also theoretically shown to affect the mode of failure. Assuming a sublaminate blister can be modelled by a strut then for a strut that is twice as long as the delamination length, a delamination at a maximum depth of 25% laminate thickness would buckle. After buckling, the propagation mechanism is able to occur. However around 25% depth a delamination was theoretically shown to switch from an opening buckling mode to a closing mode and failure of the global laminate would occur through other means, see Fig. 2.7. Experimental data from Melin and Schön [133] showed the transition from opening to closing typically occurred in the 10-20% depth range. BVID would generally be seen around this range.

Sheinman et al. [134] produced a parametric study using a one-dimensional propagation model and showed that for a delaminated sublaminate there is no need for three-dimensional analysis since the classical plate theory holds true for the larger more important delaminations which have a sufficient length/thickness ratio. This ratio was shown to most affect the load at which delamination growth occurs. It is also noted that delaminations propagate in a mixed-mode fashion with a relatively high contribution from Mode II.

It has been shown in Greenhalgh and Singh [135] that for a buckle above a delamination, the growth mostly occurs in the direction of sublaminate fibres at the interface if they are in the direction more transverse to the applied load.

Behaviour and Strength in CAI Summary

The laminate strength reduction with BVID is a critical problem limiting the aircraft structural weight. The main fracture properties governing damage growth are Mode I interlaminar fracture (peeling) and Mode II interlaminar fracture (shearing), and need to be accounted for to model growth correctly. The largest near-surface delamination (its size and location) is a predictor of the CAI strength. The greater

the size of near-surface delamination the more severe the reduction in strength. The presence of multiple delaminations also produces a reduction in strength. Larger delaminations have lower buckling strains and tend to give lower CAI strengths. Whether the delamination will open is dictated by the delamination depth and its effective strut length. Growth of delaminations are in the direction of the sublaminate fibres at the interface if they are sufficiently perpendicular to the loading. 2D plate theory is sufficient to accurately describe the behaviour of sublaminates as long as the delamination is large. The general relationships between damage and CAI strength are well known, however quantifying their effects and interaction is more difficult.

2.3.3   CAI Models

Sublaminate Buckling

It has been shown that simple approximations of zero stiffness in the buckled sublaminate can produce predictions close to the experimental results for onset of propagation, even when using a rectangular buckled shape for the sublaminate [136]. Whereas in practice, the buckled shape may represent more of an ellipse as considered in multiple models [16, 108, 137, 138]. From a closed form solution using the Rayleigh Ritz method, it is possible to describe the state of an elliptical orthotropic buckle that most resembles actual damage. This should provide more accurate predictions as well as being time efficient, as shown in Shivakumar et al. [108]. However, the technique used could not predict all buckling strains due to not having the ability to analyse anisotropy, which directly affects the strain energy associated with out-of-plane displacement causing different mode shapes and buckling loads. Xiong et al. [137] went further with a Rayleigh Ritz method that can accurately predict buckling strains with asymmetry present.

To account for any possibility of sublaminate stiffness coupling, a fully general buckling analysis using efficient buckling analysis software can be used such as that of the infinite strip software VICONOPT [139]. This is used by Butler et al. [102] for a circular sublaminate which is represented by a finite number of same-width strips whilst assuming a shape for periodic buckling, see Fig. 2.8. The buckling shape equations for each strip can be solved exactly and the software can combine the strips to form a transcendental eigenvalue problem. Only 6 strips are needed to find a sufficiently accurate buckling strain and thus this technique is extremely efficient, and well suited for initial stage design use unlike FE modelling which, whilst accurate, is computationally expensive. It is noted by Xiong et al. [137] that the calculation of the buckling load is very important for the prediction of CAI strength. From the evidence, state of the art CAI model design is not limited by the calculation of the

correct buckling strain/load.
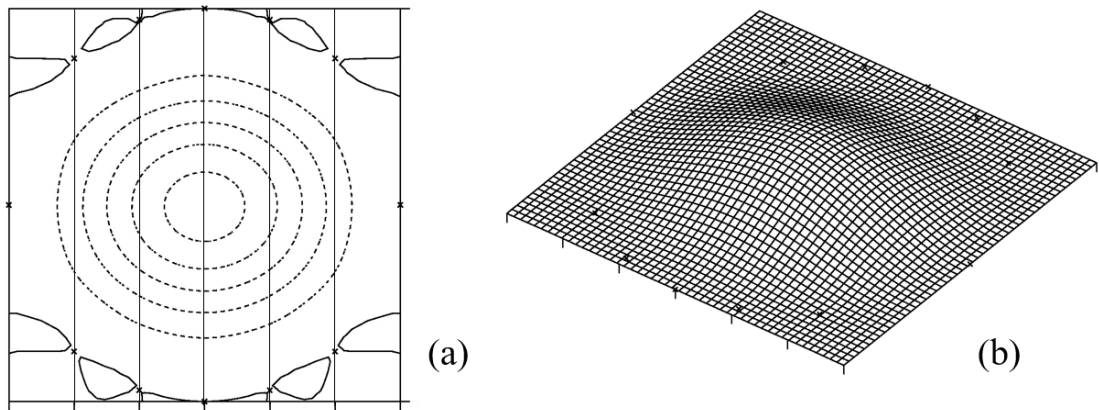
Figure 2.8: *Example VICONOPT output for a $[+30_4/ - 30_4]$ with extension-twist coupling and a large transverse compressive load component due to a large laminate Poisson's ratio compared to the laminate. (a) shows the the 6 strips and the 2D buckle contours and (b) shows the exaggerated 3D buckled shape [140].*

Delamination Propagation/Failure

In an early review by Baker et al. [141] it was highlighted that the feasible techniques for successfully predicting delamination growth are either strain energy density or strain energy release rate (SERR). They highlight the difficulty of using stress criteria due to the complex stress-field around the delamination that can only be accurately modelled using FE. This agrees with the approaches that have been most successful with predicting delamination growth. Zhang and Wang [125], whilst developing a fracture mechanics model concluded that a stress-based failure criterion was not appropriate for propagation prediction due to a stress singularity at the crack tip. Therefore most tend to the use of SERR criteria that only rely on knowing the shape of the buckle before and after propagation in order to accurately capture the point of growth [16–18, 102, 125]. The SERR is an adaptation of the J-integral [142]. The J-integral for isotropic materials calculates the energy available for release independent of the path around a crack it is evaluated over.

Models have successfully been applied to predict the growth of damage and have been adapted from Chai and Babcocks [143] original one-dimensional analytical model for propagation in a strut that uses the SERR method for prediction of growth. Rhead and Butler [107] adapted the strut model to two-dimensional propagation in a semi-analytical model that incorporates the use of the efficient buckling analysis in VICONOPT, discussed previously. The propagation strain, in quasi-isotropic uniaxial coupon tests with anisotropic sublaminates above artificial circular

delaminations, was predicted to within 16% using the model. The model assumes a conservative Mode I critical SERR to predict damage growth. To remain computationally efficient but with sufficient accuracy, the model effectively approximates the extent of delamination damage as a circle, also seen in Chai and Babcock [16] with an ellipse.

Butler et al. [102] further adapted the model to better account for transverse propagation and were able to predict conservatively and within 10% of experimental results for a range of quasi-isotropic laminates. The results agree strongly when the behaviour kept within the assumptions of remaining flat (thin-film assumption) and having weak elastic coupling in the post-buckled sublaminate. Strong coupling can cause global buckling interaction with the base laminate. A nonlinear FEA model using cohesive elements was also developed to predict buckling and propagation strain and agreed strongly with the experimental results whilst also making some non-conservative predictions. Due to the efficient nature of this semi-analytical model it was found suitable for optimum ply-stacking algorithms at the initial design stage. Sublaminate fibre angles of $\pm 45°$ were shown to be most damage tolerant and $0°$, the least.

Flanagan [17] produced a SERR model that incorporates buckling and the propagation of an ellipse, similar to the model by Chai and Babcock [16]. Close predictions were obtained for experiments that use artificial delaminations with a clamped boundary. Cairns et al. [18] produced a parametric study on a SERR model for an elliptical buckle and found agreement with experimental results whilst using a Mode I critical SERR. Delaminations were seen to grow perpendicular to the applied compressive load. Smaller delaminations were also shown to be have more unstable growth characteristics and higher propagation strains compared to larger delaminations. During the experiments any initial out-of-plane movement was seen to affect the result by lowering propagation strains compared to the model predictions.

Soutis and Curtis [144] used the same fracture toughness techniques introduced by earlier work [145] when considering compressive notch failure. To predict CAI strength they assume that the damage can be modelled as an open hole. C-scan images are used to obtain an equivalent hole diameter. A fracture toughness evaluation is used to assess whether microbuckling of fibres and subsequent growth has occurred, providing a value of CAI strength. The results agree within 10% of experimental values for a variety of SA quasi-isotropic laminates and materials. This confirms the similarities between open holes and impact damage in compression.

Attempts to apply the model from the work published by Butler et al. [102] when considering a greater range of sublaminate fibre angles ($\pm\theta$) has not been successful and the experimental results have disagreed with the model when $\pm 30°$ is present in the sublaminate. It is found that sub-laminate fibre angles between $\pm 0\text{-}40°$ have

the lowest damage tolerance due to their higher axial stiffnesses, and for angles between ±40-60° sublaminate buckling is delayed. This range of ply angles is also most damage tolerant due to their minimal combination of axial and transverse stiffnesses. Finally, sublaminate containing fibre angles from ±60-90° generally do not buckle before the full laminate. This is due to tensile transverse strains created across the sublaminate that tend to close the delamination. The transverse tensile strains are due to the negative Poissons Ratio mismatch between the sublaminate and full laminate. When ±30° fibre angles were present in the sublaminate, local buckling strains were higher than predicted by the semi-analytical strip model and FEA model. Delamination propagation was conversely found to occur at lower strains than predicted by the model and the FEA. It is suggested this may be due to large Poissons ratio mismatches present with ±30° having near a close-to-maximum Poissons Ratio. This can be expected as this mismatch is not taken into account post-buckling [146].

Xiong et al. [137] produced an analytical method that corresponded with experimental CAI strength results. The delaminations from impact testing in coupon experiments are scanned using a C-scan and represented as an elliptical soft inclusion in the model. The buckling stress of an elliptical sublaminate is then calculated using a Rayleigh Ritz method that accounts for asymmetric buckling. This is then used along with the known undamaged strength to calculate the reduced stiffness due to the buckle. Stress failure criteria are used just around the soft inclusion to pick up the elevated stresses to calculate the material failure. However, the model does not account for the growth of the delamination, which is likely to occur with delaminations close to the surface. A similar method used by Esrail and Kassapoglou [13] accounting for progressive failure of material around a delamination uses concentric ellipses (ellipses within ellipses) to create different reduced stiffness areas in an FE model. The progressive reduction in strength of the structure can be seen with the model. However, a problem arises in some cases when attempting to predict the CAI strength correctly because sublaminate buckling is not accounted for.

FE simulations have become more efficient, for example, the models by Kärger et al. [14, 15] for use at an early design stage. Simulations of the impact event are incorporated and use the same damage formed to simulate the failure and to find the residual strength of the laminate. This still does not have the ease of application of analytical tools that can easily change input parameters and account for different possible impacts. The models have been validated against experiments but it is acknowledged further work is still needed on the tools and their ability to manage any general problem, especially in impact damage prediction.

Davies and Olsson [118] highlight that one drawback of most models is that they are

verified under conditions that allow buckling-driven delamination failure to occur whilst suppressing other failure mechanisms. For example, the use of anti-buckling guides in CAI tests suppresses any global buckling interaction that can occur. They do not account for any interaction between different failure behaviours that have the possibility to reduce the CAI strength further. It is important to understand the mechanics of the entire problem so that a realistic model can be produced. It is acknowledged that the behaviour modelled in isolation does allow understanding of the parameters affecting the strength which facilitates further work and understanding.

CAI Models Summary

Fully anisotropic sublaminate buckling can be efficiently and accurately modelled by a circle or an ellipse. Buckling strain calculation is shown to be very important for CAI prediction and SERR evaluation. SERR fracture mechanics based methods are considered the most viable technique for modelling propagation, since stress-based criteria struggle due to a mathematical stress singularity at the crack tip. Models predicting delamination propagation correctly work with the assumption of a conservative Mode I critical SERR for the real mixed-mode behaviour that generally features a large Mode II component. Predictions are close to experimental results and conservative for QI SA laminates, but encounter problems when large Poissons ratio mismatch effects are introduced with non-standard sublaminate ply angles. Any significant coupling in the sublaminate also results in a poor prediction using these models. The loading accounted for is only uni-axial, with no analytical models describing the multi-axis loading state that would be more common in an actual structure. Modelling damage as an open hole and predicting propagation using notch failure works well for QI SA laminates under uni-axial loading but does not help us to understand the underlying mechanisms. These models may fail once the problems become more complex and the underlying mechanisms aren't captured appropriately. Models may need to account for matrix cracks and other damage behaviour to accurately predict the propagation failure mechanism. FEA models are not yet fast or flexible enough to create an initial stage design tool to predict growth accurately. Accurate and efficient models are required for general design of damage tolerant laminates for a multi-axis loading regime.

2.4　Aims and Objectives

2.4.1　Aims

The aims of this thesis are to investigate current initial design methods and to improve upon them to allow greater weight savings. This includes relaxation of laminate design rules and the replacement of the conservative damage tolerance strain allowables with efficient and accurate multi-axial design modelling.

2.4.2　Objectives

(i) Creation of new design techniques that take advantage of relaxation of the design rules.

(ii) Directly optimise design for the required laminate performance instead of indirectly with the use of design rules.

(iii) Implementing general design optimisations for a wide range of load directions and magnitudes to a show a general view of design in order to deduce whether new techniques are worthwhile compared to the current design practice.

(iv) Creation of a multi-axial damage tolerance model for design purposes.

(v) Optimise laminates for damage tolerance improving on the conservative industry strain allowables.

Chapter 3

Methods: Laminate Optimisation

This chapter outlines the general laminate design methods used in this thesis. The decision to use a genetic algorithm for laminate optimisation as well as the use of ply angles and ply percentages as design variables is justified. The general optimisation process is outlined for a multi-axial load state described by just two variables. Justification of minimum in-plane elastic energy as the laminate optimisation objective to represent in-plane strength is discussed. The non-optimality of design rule constraints used in the current industry design practice suggest that improvement could be made by optimising directly for the desired laminate behaviour. Use of non-standard angles, relaxation of stiffness coupling requirements, and an alternative to the 10% rule is also suggested to allow potentially greater weight savings.

3.1 Introduction

Rapid and accurate design tools are needed for the initial laminate design stage to produce the greatest weight savings from the use of composite materials. The use of conservative, and therefore constrained, design techniques limit the material's potential. Optimisation algorithms are useful to find optimal designs in a timely manner given design inputs and design requirements. Improved models for laminate failure prediction are needed, allowing for less conservative and lower weight designs to be produced. New models and techniques are ideally to be assessed for their minimum weight capability in a general sense and not just one design example i.e. for a variety of load cases in both magnitude and direction. Some of the techniques already investigated show improvement over the current design practice for buckling strength when using Non-Standard Angles (NSAs) compared to Standard Angles (SAs), e.g. allowing 5° increments [9, 147]. NSAs have also shown improvement for damage resistance and damage tolerance [28, 148]. They can also be employed to introduce extension-shear and bend-twist coupling to aid with wing bend-twist

characteristics for better flight performance [97, 98].

This body of work is attempting to produce new modelling and design techniques that allow lower weight design. A significant amount of literature is focused towards finding solutions more efficiently due to the real problem of a large number of degrees of freedom in modelling the complex micro to macro mechanical behaviour of a composite wing structure. This is where more mathematical and computer science based techniques provide an advantage, with multiscale modelling leading the way forward [149, 150].

It is prudent to first consider how any new techniques will be assessed to offer greater minimum weight capability and this includes the layout of the design optimisation process. The main considerations being the:

(i) Design Inputs

(ii) Design Variables

(iii) Optimisation Objective

(iv) Optimisation Routine

(v) Design Constraints

3.2   Design Inputs

3.2.1   Design Loadings

The range of critical design loadings that an aircraft must withstand without failing are defined by the flight envelope as per the regulations (see Section 2.1). The loads which a laminate must be designed for are extracted from this envelope.

The mechanical behaviour of a laminate is usually described by Classical Laminate Theory (CLT), where a state of plane stress is assumed (σ_z, τ_{xz}, $\tau_{yz} = 0$) and the in-plane load/moment-strain/curvature relationship is given as follows.

$$\begin{bmatrix} N \\ M \end{bmatrix} = \begin{bmatrix} A & B \\ B & D \end{bmatrix} \begin{bmatrix} \varepsilon \\ \kappa \end{bmatrix} \tag{3.1}$$

Assuming moment results are zero (M = 0) and that laminates are balanced and symmetric (ie. **B** = 0 and A_{16}, $A_{26} = 0$), CLT gives the in-plane load-strain relationship as

$$\begin{bmatrix} N_x \\ N_y \\ N_{xy} \end{bmatrix} = \begin{bmatrix} A_{11} & A_{12} & 0 \\ A_{12} & A_{22} & 0 \\ 0 & 0 & A_{66} \end{bmatrix} \begin{bmatrix} \varepsilon_x \\ \varepsilon_y \\ \gamma_{xy} \end{bmatrix} \tag{3.2}$$

where N_x, N_y, N_{xy} and ε_x, ε_y, ε_{xy} are the in-plane axial, transverse and shear loads per unit width and corresponding laminate strains, respectively. The A_{ij} terms represent the in-plane stiffnesses and subscript SL denotes sublaminate as opposed to laminate variables.

Since the objective is to allow designs and techniques to be assessed irrespective of load magnitude and laminate thickness, the in-plane design loads per unit width can be converted to in-plane laminate level stresses.

$$\{\sigma\} = \begin{Bmatrix} \sigma_x \\ \sigma_y \\ \tau_{xy} \end{Bmatrix} = \{N\}/T = \frac{1}{T} \begin{Bmatrix} N_x \\ N_y \\ N_{xy} \end{Bmatrix} = \begin{bmatrix} \overline{Q}_{11} & \overline{Q}_{12} & 0 \\ \overline{Q}_{12} & \overline{Q}_{22} & 0 \\ 0 & 0 & \overline{Q}_{66} \end{bmatrix} \begin{bmatrix} \varepsilon_x \\ \varepsilon_y \\ \gamma_{xy} \end{bmatrix} \tag{3.3}$$

Further, conversion to principal loadings σ_I and σ_{II}, and a misalignment angle η of the balancing axes from the principal loading axes is useful to simplify the design loading further. A converted general load state is shown in Figure 3.1. The equations for the derivation of the principal loading and η are as follows

$$\sigma_{I,II} = \frac{(\sigma_x + \sigma_y)}{2} \pm \sqrt{\left(\frac{(\sigma_x - \sigma_y)}{2}\right)^2 + \tau_{xy}^2} \tag{3.4}$$

$$\eta = \frac{1}{2} tan^{-1} \frac{2\tau_{xy}}{\sigma_x - \sigma_y)} \tag{3.5}$$
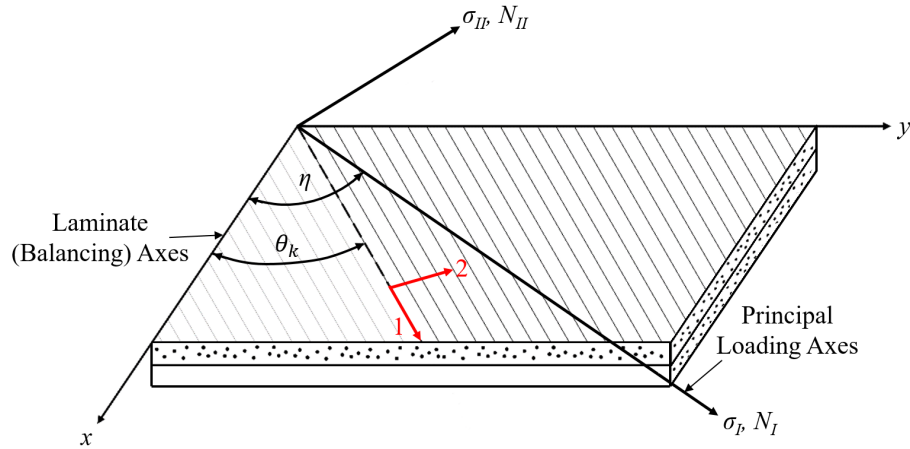
Figure 3.1: *Local ply axes (1-2) and laminate (balancing) axes (x-y). The principal loading axes (σ_I-σ_{II}) and misalignment angle η of the balancing axes are also shown, allowing simplification of any general in-plane loading condition N_x, N_y and N_{xy}.*

Removing the effect of load magnitude by converting to principal load ratios σ_I/σ_{II} allows input design loadings to be fully expressed by just two variables σ_I/σ_{II} and η. These are the input variables that can be varied for numerous optimisation runs to allow a global picture of design to be produced and assessed.

3.2.2   Design Variables

For a manufacturable, optimal laminate design solution, minimum weight discrete designs are required. The weight and thickness of the design depends on the force resultant that must be supported by the panel. Following the creation of general input loadings, and the idea of providing a general basis to assess new design techniques, creation of general laminate design variables that are independent of thickness and geometry are needed.

Design variables that are both continuous and non-dimensional in nature will allow ease of optimisation alongside providing visualisation of design results in a general manner. Optimisation using lamination parameters is often used due to their ability to provide a convex design space, allowing more efficient gradient-based optimisation methods to be incorporated [43]. Problems arise when converting from optimum lamination parameters to a discrete design, where another optimisation step often is required [26, 66]. This problem can be removed however, if continuous laminate variables are backed out from the lamination parameters instead of discrete values.

Considering the aim is not to improve optimisation processes but instead to improve design from a fundamental perspective by providing a general view of design to aid the designer, two types of laminate variables are chosen to be used: ply angles and continuous ply percentages, i.e. continuous proportions of each angle within the full stack. The continuous ply percentages allow optimisations to be straight forward as the design space is smooth, as well as the variables being easily understood by a designer.

Ply angles and continuous ply percentages can be used as laminate design variables without the need to define discrete ply thicknesses. These variables can provide enough information to assess the failure and minimum weight capability of a laminate and thus can be optimised. Optimum designs are applicable to many laminate thicknesses and if discretisation to realistic designs is required, then if the design variables are maintained then laminates will be theoretically minimum weight. As the aim is not to produce discrete designs from these general designs, optimality of discrete designs may be far from the general optimum design [66]. The lower the optimal ply number (weight) the smaller the design space and so the range of performance achievable is lowered. New techniques may show weight improvement in general but each real design scenario must be taken in context as they may not

provide any benefit in reality due to discretisation. Thus the maintenance of the optimum continuous design depends on its replication by a discrete equivalent.

Seen in later chapters, designs either use standard angles or non-standard angles and both sets can be described by their ply angles and ply percentages. The specific design variables used in this work are shown in Table 3.1.

The SA designs can be described fully by two variables (two ply percentages) and the non-standard designs by three or five (two angles and one percentage in Chapter 4, three angles and two percentages in Chapter 5). The non-standard angles have two pairs of balanced and symmetric $\pm$ angles (Chapter 4) or three angles in the form $[\pm\theta \mp \theta \mp \theta \pm \theta]$ creating fully uncoupled blocks about the mid-plane [93] (Chapter 5, also maintaining $[B] = 0$ and A_{16}, $A_{26} = 0$). Three angles ensure that any standard design is also a subset of the non-standard designs. However since all standard angle stiffnesses can be described by just two $\pm\theta$ non-standard angles (see Chapter 4 for full derivation and explanation) then for stiffness purposes only, three angles are not required [61]. For optimisations in this thesis, ply percentage variables are considered in a continuous fashion and the non-standard angles as integers from 0°-180° (discussed further in Section 3.5. Laminates are assumed to be balanced with no in-plane to out-of-plane coupling, i.e. $[B] = 0$, see Section 2.2.6.

	Chapter 4	Chapter 5	Chapter 9
Standard Angles	3 angles (0°, ±45° & 90°) 2 proportions (% 0's & % 45's)		Laminate: 3 angles (0°, ±45° & 90°) 2 proportions (γ_0, $\gamma_{\pm45}$, 1-($\gamma_0 + \gamma_{\pm45}$)) Sublaminate: 3 angles (0°, ±45° & 90°) 2 proportions (γ_0, $\gamma_{\pm45}$, 1-($\gamma_0 + \gamma_{\pm45}$))
Non-Standard Angles	2 angles, ψ & ϕ 1 proportion, γ ($\pm\psi_\gamma / \pm\phi_{1-\gamma}$)	3 angles, ψ, ϕ & θ 2 proportions, γ_ψ & γ_ϕ $\pm \mp \pm$ fully uncoupled stacks	N/A

Table 3.1: *Laminate angle variables and subsequent notation used for optimisation in Chapters 4, 5 and 9 respectively. Note that stacking sequences shown do not represent the order of plies in optimised designs.*

3.3 Optimisation Objective

3.3.1 Performance Marker Discussion

Optimised laminate designs are independent of thickness and therefore optimality cannot be determined by weight. Instead laminates can be assessed for their minimum weight capability entirely through a performance aspect that is assumed to be weight limiting. Optimisations are hereby carried out with the concept of minimising an objective function related to a performance aspect, and doing so by varying ply angles with continuous ply percentages. How well a technique fulfils the objective is decided by the value of the performance marker and thus its value is considered to relate to its minimum weight potential.

The performance aspect that is limiting to laminate weight depends on the loading, the laminate design itself and its thickness [5]. Thick laminates are inherently hard to buckle and not damage tolerance critical due to the large thickness of material maintaining residual strength. Compression after impact strength is normally the weight limiting performance aspect for thin composite laminates [5]. A full design scenario with performance aspects as constraints would automatically reveal the predicted critical performance aspect, which is generally always context specific.

A full design scenario with many design constraints will complicate the cause and effect of any results. Therefore what is considered to be the fundamental base of any design was initially considered to be designed for, barring application of suitable design rules. The in-plane stiffness and strength in the required directions forms the base of any laminate design and will become weight critical if fibres are not aligned sufficiently towards the loading. A laminate must first have enough fibre stiffness and strength to be able to carry the in-plane loads that may be applied. The stacking sequence/design may later be altered to provide sufficient buckling and damage tolerance performance. This includes placing the load bearing plies in the core and the soft $\pm 45°$s at the surface for damage tolerance and buckling [5, 102]. A Boeing stiffener patent in the blade section uses NSA ply angles ranging from 2°-12° in the core (α) and 50°-85° in the surface (β) [151].
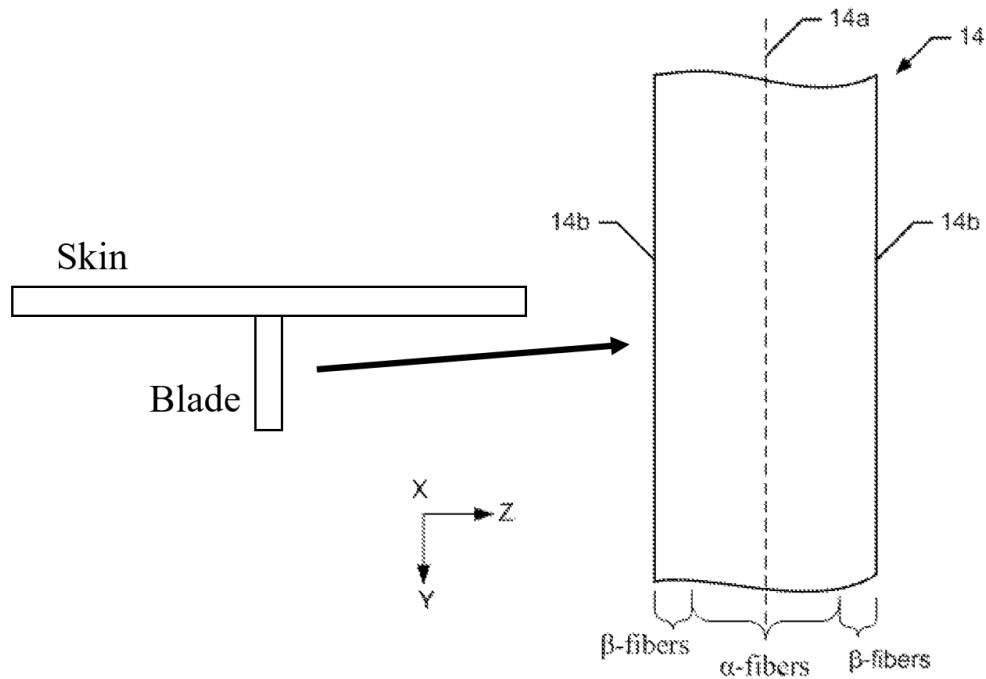
Figure 3.2: *Boeing Patent: Surface and core angles in the blade section of a stiffener.*

Typical angle percentage designs for a skin, stiffener and spar are 44/44/12, 60/30/10 and 10/80/10 respectively, corresponding to percentages of 0°/±45°/90°. The skin is composed of fibres that align with the axial (0°) and shear (±45°) loads caused by the bending of the wing. The stiffener is created from mostly 0° plies due to high axial loads and ±45°s plies to prevent buckling. The spar design is dominated by ±45° plies to carry a shear load. The designs reveal the need for a base in-plane stiffness and strength.

A performance marker that models the in-plane strength/stiffness is desired. Adequate strength places enough stiffness in the appropriate directions. Strength criteria such as the quadratic Tsai-Wu are often used in composite analysis and design. These models work on a ply level mesomechanic strength whereas other failure criteria that take into account the more detailed micromechanics of failure and can produce more accurate failure predictions; such as the Puck criterion [72, 73] or Cuntze criterion [74, 75]. The World Wide Failure Exercise (WWFE) has shown the inconsistency of failure criteria in predicting the strength of composite pressure vessels [76–80]. Even the best strength criteria have problems dealing with non-linear stiffness laminates and stiffnesses that can be seen in laminates with non standard $\pm\theta$ pairs and laminates with large Poisson's ratios [76]. Strength criteria that do predict failure for most cases somewhat accurately are complex to apply and timely to use in an optimisation run, hence more favourable analytical tools are desired. Tsai and Melo [23] introduce a general omni-strain envelope that predicts failure of the material irrespective of the stacking sequence and ply orientations within the

design; an invariant-based failure criterion. This allows for the easy evaluation of a design for adequate in-plane strength for structural designers.

3.3.2 In-Plane Elastic Energy Performance Marker

Due to the complexity involved in predicting laminate strength, especially for NSAs, and the desire to use a performance marker that can be applied easily to all laminate designs in a efficient manner, maximum global stiffness is sought as an objective; otherwise known as compliance minimisation. Stiffness is a simple approximation of laminate strength with stiff material generally placed in the directions of load. The global stiffness under load is represented by the value of the laminate in-plane elastic energy, as seen by the area in Fig. 3.3 where the objective is to minimise this area for a given stress, by changing the laminate design. Laminate in-plane elastic energy under multi-axial loads is proposed as a simple and easily calculated performance marker that can allow assessment of minimum weight capability for a variety of loads and thicknesses.

Minimisation of in-plane elastic energy in laminate design does not directly imply maximisation of in-plane strength of a composite material. Nevertheless, it is assumed to be sufficient to capture the in-plane strength relationship as fibres are aligned to best carry the applied multi-axial stresses, which is the case for maximum in-plane strength design in a Netting analysis regime [87,152]. Netting analysis, which ignores the support of the resin matrix and aligns fibres in principal directions to carry principal stresses, leads to laminate designs in which the stresses in fibres are limited to some value associated with failure i.e. fully-stressed fibre design. Verchery [87] has shown that Netting analysis, can be treated as a limiting case of Classical Laminate Theory.
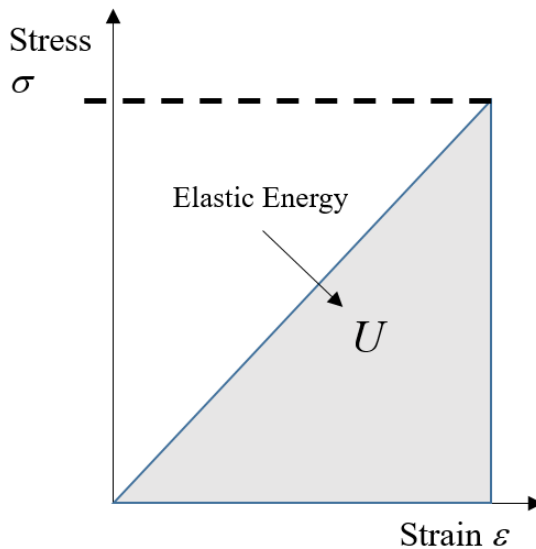
Figure 3.3: *In-plane elastic energy for a given stress loading.*

The caveat for this design technique is that for a given design problem, the optimum strength design may not be the same as the one found using minimum elastic energy. However if the in-plane strength is captured to a sensible degree then generalities with the use of certain technique should still hold true for the majority of design problems. Potential weight reduction that is suggested from the use of this technique may be non-existent if other laminate performance aspects are weight limiting. This is likely the case for the majority of laminates that are limited by damage tolerance or buckling performance [5].

3.4   In-Plane Elastic Energy Derivation

Given that the in-plane Hookean strain or elastic energy for a linear elastic solid is (see 3.3)

$$u = \frac{1}{2} \int \sigma^T \varepsilon \ dV \tag{3.6}$$

Eq. 3.6 then implies

$$u = \frac{1}{2} \int \sigma^T \overline{Q}^{-1} \sigma \ dV \tag{3.7}$$

Working per unit volume allows for laminate geometry to be ignored which further implies

$$U = \frac{1}{2} \sigma^T \overline{Q}^{-1} \sigma = \frac{1}{2} (q_{11}\sigma_x^2 + 2q_{12}\sigma_x\sigma_y + q_{22}\sigma_y^2 + q_{66}\tau_{xy}^2) \tag{3.8}$$

Division of Eq. 3.8 by the sum of the squares of the principal stresses normalises U, removing the effect of the magnitudes of the loads/stresses, and allows for an equal comparison between loading states of the same magnitude i.e.

$$\overline{U} = \frac{q_{11}\sigma_x^2 + 2q_{12}\sigma_x\sigma_y + q_{22}\sigma_y^2 + q_{66}\tau_{xy}^2}{2(\sigma_I^2 + \sigma_{II}^2)} \tag{3.9}$$

Where

$$\sigma_{I,II} = \frac{\sigma_x + \sigma_y}{2} \pm \sqrt{\left(\frac{\sigma_x - \sigma_y}{2}\right)^2 + \tau_{xy}^2} \tag{3.10}$$

Substitution of Eq. 3.10 into Eq. 3.9 gives the expression for normalised elastic energy per unit volume, representing the effective laminate compliance that is inde-

pendent of load magnitude and laminate thickness. A lower value corresponds to a higher global laminate stiffness and more efficient use of material [152].

$$\overline{U} = \frac{q_{11}\sigma_x^2 + 2q_{12}\sigma_x\sigma_y + q_{22}\sigma_y^2 + q_{66}\tau_{xy}^2}{2(\sigma_x^2 + \sigma_y^2 + 2\tau_{xy}^2)} \qquad (3.11)$$

If the laminate is not balanced, either for all axes, or in the axes in which the elastic energy is calculated then $q_{16}\sigma_x\tau_{xy}$ and $q_{26}\sigma_y\tau_{xy}$ terms appear in the numerator of Eq. 3.11.

Assuming a magnitude of U that causes failure U_{ult} and a required ultimate load vector, N_{ult}, that must be carried, then if the point of failure is at this critical loading, from Eq. 3.3, Eq. 3.8 becomes

$$U_{ult} = \frac{1}{2T^2} N_{ult}^T \overline{Q}^{-1} N_{ult} \qquad (3.12)$$

it follows that $T^2 \propto \overline{Q}^{-1}$ and $T \propto \sqrt{\overline{Q}^{-1}}$, thus the thickness (weight) of the laminate depends on the optimality of $\overline{Q}^{-1}$. Since $\overline{U} \propto \overline{Q}^{-1}$ then the weight $\propto \sqrt{\overline{U}}$.

There is no specific value of U_{ult} that corresponds to failure strength predictions and laminate weight determination. Despite this weight savings of one design technique over another can be calculated by comparing the values of $\sqrt{\overline{U}}$. $\overline{U}$ is used as a performance marker only, where the ability to rank designs is thought to be sufficient to find a suitable optimum design.

3.5 Optimisation Routine

3.5.1 Choice of Optimisation Method

The choice of ply angles and ply percentages for laminate design variables creates a stiffness design space that is non-convex, with local optima, due to the trigonometric equations in CLT and thus the global optimum may not be discovered using a gradient-based method [43, 44], unlike lamination parameters. Genetic Algorithms (GAs) have been used popularly to successfully tackle the complex problem of finding the optimum stacking sequence for a composite panel by minimising an objective function, which may describe the weight or an aspect of laminate performance [33, 34, 45–48]. They are suited to this due to their ability to work on a complex design space, where the best designs from each iteration are picked for use (elite) and/or mutated (mutation) and/or combined with others (crossover) to form a population that is more likely to include a better design [49]. Since the design variables are

continuous in nature (or almost continuous for NSAs, see Section 3.5.2), a genetic algorithm should have little problem finding the global optimum. As long as the optimal solution can be found efficiently to allow results to be produced then that is all that is required to show if techniques can improve the optimality of designs over the current practice.

3.5.2 Use of Genetic Algorithm

The performance of a laminate subject to a multi-axial state of stress is assumed to be represented by its Hookean strain energy or elastic energy; minimum energy indicates maximum performance. Laminates in this thesis are optimised using a Matlab Genetic Algorithm (GA) 'ga' [153–156]. Laminated aerospace structures are, in general, subject to a combination of in-plane axial, transverse and shear load. As described in Section 3.3.2, optimal laminate designs will efficiently distribute fibres to meet these loads producing a laminate with minimum elastic energy. For each design loading, the GA fulfils this objective by finding the laminate design that minimises the laminate elastic strain energy in Eq. 3.11 thus creating designs with $\overline{U}_{min}$. GA optimisation is halted if either the maximum number of iterations reaches 5000 or if the change in the elastic energy value between iterations is less than 1×10^{-20} m^2/N (unless stated otherwise). For all optimisations run, except in some cases mentioned in Chapter 9, the GA was stopped due to the latter condition, i.e. convergence occurred within 5000 iterations.

Optimisation of both SA and NSA laminate variables described in Table 4.1 was performed by the GA in Chapters 4, 5 and just SA in Chapter 9. The ply percentage for each angle was allowed to vary continuously. NSA designs are described by integer angle variables (between 0°-180°), which allow for more defined design results and since manufacturing methods currently use a tolerance of ±5°, an angle step of less than ±1° is not feasible. Design rules, discussed in Section 3.6 are applied when appropriate.

3.5.3 Selection & Definition of Design Loads

Standard angle laminates are normally restricted to a fixed coordinate system about which laminates are balanced (for example, the 0° fibres are aligned from root to tip in a wing skin) [157]. In both standard and non-standard laminates, an equal number of positive and negative angle plies ensures all designs are balanced about the 0° laminate/manufacturing axes unless otherwise stated. All general load states in the laminate (balancing) axes can be described by their principal loading and a misalignment angle, η, from the balancing axes, shown in Fig 3.1. A special case

existed when $\eta = 0°$, where the principal loading axes are aligned with the balancing axes. This is generally not the case in design as the balancing axes are aligned with the laminate manufacturing axes. However, balance could potentially be achieved in different axes, thereby enforcing $\eta = 0°$. In order to assess the full range of possible loadings a spread of principal loading ratios, σ_I/σ_{II}, are considered. Each principal load ratio is also applied with a range of different misalignments, η.

3.5.4 Optimisation Process

The general laminate design optimisation process utilised to provide the designs described in Chapters 4, 5 and 9 is outlined in the flowchart in Fig. 3.4. The optimisation code takes input design loadings and the 'ga' manipulates values of design variables to find optimum laminates for minimum in-plane elastic energy subject to design constraints.
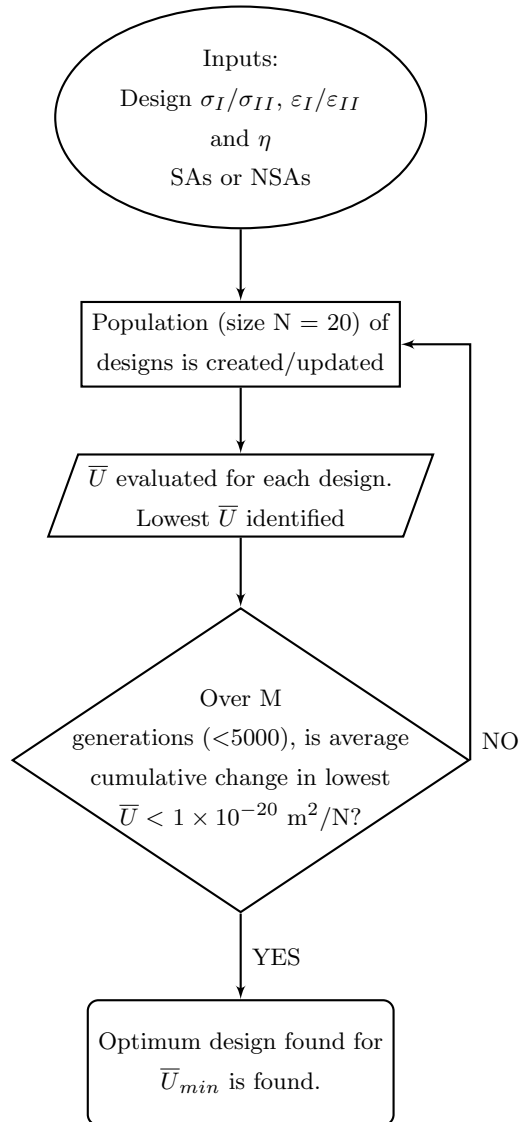
Figure 3.4: *General optimisation process.*

3.6 Laminate Design Rules Justification

The industry laminate design rules are applied during the initial design stage. They aim to generate laminates with the required performance aspects without having to proceed through a lengthy optimisation routine. However, scarce research has been conducted into whether these rules are precluding the selection of more optimal, suitable designs. These rules include [5–8]:

(i) Sole use of Standard Angles (SA), 0°, +45°, -45° and 90°.

(ii) At least 10% thickness of each SA.

(iii) Symmetry about the laminate mid-plane, enforcing $\mathbf{B} = 0$.

(iv) Balancing of angle plies in the manufacturing /geometric axis, enforcing A_{16}, A_{26} = 0 (no. of +45°s = no. of -45°s).

(v) Ply unblocking to ensure a maximum of 4-6 plies or 1 mm of the same orientation of plies in a row [5].

(vi) Reduced angular separation between plies, e.g. $\leq 45°$ angular separations between adjacent plies if possible for reduced interlaminar shear stress. A 90° switch from one ply to the next should be prevented if possible.

(vii) $\pm45°$ near the surface for damage tolerance and buckling performance.

These design rules can either applied to the optimisations or new techniques can be used to directly design for the laminate behaviour that the rules are trying to create, potentially saving weight.

3.6.1 Standard Angles and the 10% rule

Standard angles form the stacks in most current designs. Netting analysis [87], in which fibres only carry load in their longitudinal direction and the resin matrix is ignored, indicates that designs with fewer than three fibre directions produce mechanisms when subject to small disturbances in loading. Verchery [87] has shown that Netting analysis, can be treated as a limiting case of Classical Laminate Theory. This reveals the reasoning behind established aerospace laminate design practice of using four standard angles (SAs) (0°, +45°, -45° and 90°) and a design rule of a 10% minimum ply percentage to provide a level of redundancy against loading uncertainty [157]. Standard angle results were produced with the 10% design rule in Chapters 4 and 5, in which a minimum of 10% of each of the four SA plies is maintained. This rule is enforced by limiting the choice of ply percentages available to the GA.

Due to the greater design space of NSAs they are thought to offer greater performance benefits over SAs. From lamination parameters it has been shown that NSAs can produce in-plane stiffnesses that are not possible with SAs, hence the use of NSAs to improve design will be investigated [61, 158].

Designing laminates for the range of critical loads that could be applied from the flight envelope should allow the assumption that the laminate does not need to be designed for any loading uncertainty. All possible loads should already be designed for. This is potentially not the case if there is some uncertainty about the laminate loads derived from the aircraft critical flight envelope. Thus the 10% ply percentage rule is still applied in order to give the laminate some base stiffness and strength, which is conservative. The laminate stiffness mechanics are also more stable as Poisson's ratios are limited when fibres are spread in all directions [76,91,92,146,159], however this can instead be directly designed for.

Instead of the 10% rule laminates could be designed directly for:

(i) a critical loading with a base level of stiffness in all directions to provide some robustness to an uncertain loading

or

(ii) an uncertain critical loading to provide robustness to load uncertainty with a separate constraint for a Poisson's ratio limit if desired.

Option number (ii) was incorporated into the design in Chapter 5 and compared to the 10% rule to see if improvements could be made on the current practice. There exists no such rule for non-standard angles causing weakness in strength when non Quasi-Isotropic (QI) NSA laminates rely on the matrix under load [77]. Therefore an effective 10% rule is required for non-standard angles. Peeters and Abdalla [91] have been able to optimise non-standard angle designs for maximum stiffness to a load whilst having a constraint ensuring a certain level of stiffness in all directions. This cleverly mimics the robust performance characteristics the 10% rule creates. Abdalla [92] has been able to apply a base stiffness for NSAs in the in-plane lamination parameter space from which a design can be chosen that possesses a robust stiffness in all directions. Using approach (ii) will also allow NSA laminates to be made robust allowing a direct comparison to SA angles design as will be seen later in Chapter 5. This extends the literature since design is tailored to the specific loading uncertainties for different design cases instead of giving equal weighting by having an equal base stiffness in all directions.

3.6.2 Balance and Symmetry

Balancing laminates in the manufacturing axes (A_{16}, $A_{26} = 0$) is the common industry design approach, satisfied by having the same number of $+\theta$ and $-\theta$ angle plies. Balancing is used to ensure that in-plane loads are prohibited from creating an unbalanced shearing, and thus twisting of the wing box about the neutral-axis of the structure [5]. Twisting of the wing box may be favourable to reduce aerodynamic drag during a manoeuvre and so such coupling can be built-in to achieve such effects [97, 98]. Balancing also helps reduce unbalanced residual thermal stresses that form during cure [160]. If these thermal stresses could be removed, the rule could be relaxed and laminate design could potentially be improved as seen in Chapters 4 and 5. Tsai has also argued for the removal of the balancing rule and instead using the extension-shear coupling to aid the performance of the laminate in order to further reduce weight [99]. Balancing about the principal loading axis, η, shows the effect of this rule on optimality (see Chapters 4 and 5).

Symmetry in laminates ensures that $[B] = 0$, resulting in no out-of-plane bending effects from in-plane loads. Alongside balancing, an unpopulated B matrix creates a favourable homogenous mechanical behaviour. This lack of coupling ensures no warping during cure due to thermal stresses being symmetric [160]. Symmetry is not required to ensure $[B] = 0$ as seen with special types of unsymmetric orthrotopic laminates such as fully uncoupled stacks [93] ([+/-/-/+/-/+/+/-]) as well as a host of others classified by York [95]. These fully orthotropic laminates have no bend-twist coupling terms, D_{16}, $D_{26} = 0$, providing full metallic like mechanical properties reducing potentially unwanted effects during wing bending. This bend-twist coupling can potentially be favourable, again improving aerodynamic drag performance with wing twisting [97, 98]. York suggests straying from the design rules of symmetry and balance can give rise to useful coupling behaviours and greater flexibility in design [97]. Unsymmetric laminates that do not have $[B] = 0$ are suggested as possible in order to seek greater weight saving. The B matrix terms can be minimised by repeating the non-symmetric stacks many times and so the laminate behaviour is still homogeneous [99].

The enforcement of A_{16}, $A_{26} = 0$ is ensured in the optimised designs in this thesis by constraining designs to have the same number of + and - plies. $[B] = 0$ is ensured by either making the laminate symmetric or employing the use of fully uncoupled blocks [93].

3.6.3 Ply Unblocking and Ply Separation

Ply unblocking and ply separation is used to ensure reduced residual stresses and edge failure [5]. Modelling of the failure due to the inter-ply shear mechanism will suit the design process so that laminates can obtain the greatest weight saving instead of being constrained by a fixed design rule. This is not considered in this work and should be aimed for in future work. Instead a way to apply ply unblocking in laminates with continuous ply percentages is investigated in Section 5.3.4.

3.6.4 Surface Plies for Damage Tolerance and Buckling

Use of surface plies that are generally less load bearing and compliant, such as $\pm45°$, has provided increased damage tolerance and damage resistance performance [5, 101, 102]. Buckling performance is increased by improving the bending stiffness terms ($[D]$) with $\pm45°$, depending on loading and laminate geometry. NSAs have been shown to increase damage tolerance as well as buckling performance and so incorporation into laminate design is sought [9, 28, 147, 148].

3.7 Conclusions

A general design optimisation approach was formulated to allow new techniques to be compared to the current industry practice. This includes consideration of a general design loading described by the principal loading ratio, σ_I/σ_{II}, and a misalignment angle of the balancing axes from the principal loading axes, η. General designs are decided to be described by designer friendly angles and ply percentages that are independent of thickness, and easily optimised. The design objective of minimisation of in-plane elastic energy (compliance) to assess minimum weight potential was justified compared to more complex in-plane strength methods. The square root of the elastic energy was shown to represent the relative but not absolute weight of the laminate, allowing the possible weight comparison of different techniques. Discrete designs for individual design cases may lack the weight improvement that any new technique could provide due to inaccurate failure modelling or optimum deviation when discretising.

A MATLAB genetic algorithm was chosen to optimise these variables since the design space is not convex. The optimisation routine was set out to allow efficient and robust location of the optimum designs related to the objective of minimum elastic energy whilst meeting appropriate design rules. Justification of the composite aerospace design rules was discussed qualitatively. The scope for improvement over the current design practice was explored. Directly designing for the desired

laminate behaviour, and thereby scrapping certain design rules such as balance and the 10% rule, may lead to more optimal designs, and will be pursued in the following Chapters. Use of NSAs is suggested to offer significant scope for reducing laminate weight. These new design methodologies theoretically show potential and provide several different investigative avenues of research.

Chapter 4

Use of Non-Standard Angles

In this chapter, work is included that was carried out by colleagues Kevin Johnson, Richard Butler and Andrew Rhead looking at eigenvalues and eigenvectors of the uncured sublaminate stiffness matrix. These were used to describe compatibility between sublaminate modes of deformation during cure and thus indicate the ease of manufacture of laminates in their uncured state. The potential for non-standard plies to improve sublaminate deformation compatibility was also explored by these colleagues and a novel stiffness matching algorithm for finding non-standard angle designs that are equivalent to standard angle designs is created. All the work in this chapter formed part of a publication in the journal Composite Structures [161].

New structural efficiency diagrams are presented based on laminate in-plane normalised elastic energy, $\overline{U}$. Optimisations show that additional weight is incurred when (i) laminate balancing axes are not aligned with principal loading axes and (ii) principal loading ratios vary within a part with fixed ply percentages. This presents an opportunity for fibre steering and laminate tailoring in aerospace design. Moreover, from a manufacturing standpoint, standard ply angles (0°, +45°, -45° and 90°) have incompatible modes of deformation between adjacent sublaminates in their uncured state (during forming); such modes promote the occurrence of wrinkling defects during manufacture which reduces part strength significantly. Non-standard ply angles are shown to promote compatible modes of deformation and offer significant potential, in terms of formability, which could potentially increase production rates by reducing the need for so-called manufacturing knockdown factors. There is little in-plane stiffness advantage of non-standard plies, and have been shown to match standard angles with more design flexibility, both analytically and through optimisation investigations.

4.1 Introduction

Laminates for aerospace components are currently designed using standard ply angles whilst following established design rules [5]. These rules include: ply angle symmetry about the laminate mid-plane, equal numbers (balancing) of +45°, -45° angle plies, 10% thickness in each of the 4 ply angles, and ply blocks of identical angles must be a maximum of 1 mm. Additionally, ±45° plies are usually positioned at the outer surface for enhanced damage tolerance. The percentage of 0°/±45°/90° plies in a laminate is a function of the typical loading a component will carry; for example in wing skins, stiffeners and wing spars, target percentages are typically 44/44/12, 60/30/10 and 10/80/10, respectively.

Unfortunately, such rules do not account sufficiently for manufacturing processes and can also limit the possible laminate designs that have the required curvature-stable manufacturability and stiffness coupling [94, 162]. Restriction of ply orientations to the four standard fibre angles can also contribute to the development of manufacturing induced defects during the curved laminate forming process. This is because, in its pre-cured state, the resin matrix has an extremely low transverse modulus and so the unidirectional fibres within layers (predominantly) rotate in shear (scissor) to enable a change in geometry. The general scissoring behaviour of cross-plied UD can be modelled by using pin-jointed-net theory [163], originally created to analyse shearing of woven fabric. Limitations to formability arise in the fibre direction, where fibres cannot extend, nor can they resist compression without causing a buckling (wrinkling) defect.

The combination of all four standard angles within a laminate and their interaction make it difficult to form the laminate into a curved shape from flat. Indeed Hallender et al. [164] discovered that defects occurred during forming of a C-Section spar when +45° and -45° plies were separated by a 0° ply. In contrast wrinkling defects were not produced when ±45° and 0°/90° ply pairings were grouped separately, as these separate groups were able to deform independently, as shown in Figure 4.1. Here the ply groups can be seen to want to deform with different modes of deformation over the same spherical shape, contrast regions 1 and 2 (0°/90°) to 3 and 4 (±45°), respectively. Hence, the properties of ply groups within the laminate (sublaminates) were seen to be a critical feature of formability and can be linked to the compatibility of sublaminate modes of deformation. These ply pairings contain plies at 90° to each other and thus potentially pose a problem with interlaminar shear transfer and reducing the damage resistance during impact [5]. Relaxation of the stacking design rules of reduced adjacent ply angle changes is potentially viable to allow greater ease of manufacture up until the point at which interlaminar shear failure becomes weight critical.
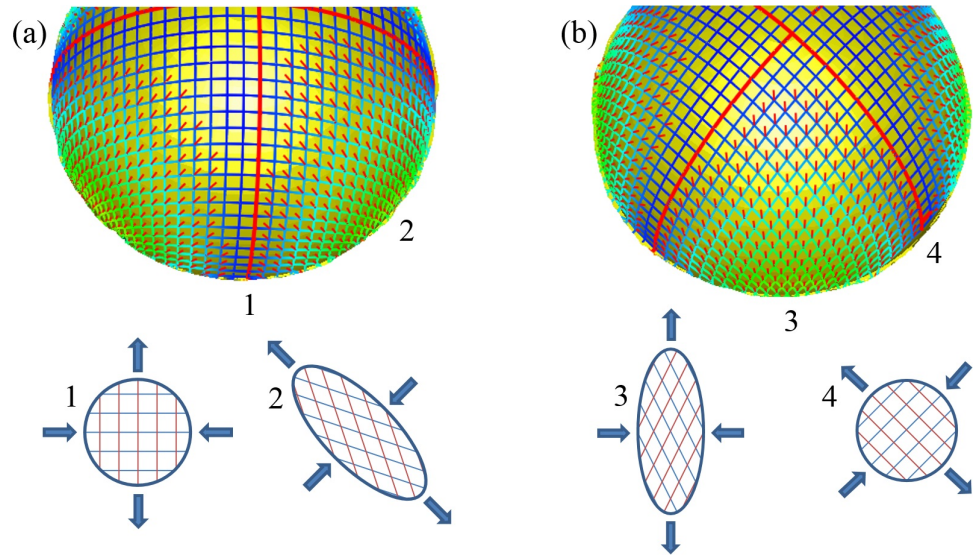
Figure 4.1: *Forming of (a) 0/90° and (b) ±45° plies over a sphere [165] and local modes in regions 1-4. The shearing of fibres is orthogonal in regions 1 (2) and 3 (4) and so forming needs to allow slip between 0°/90° and ±45° plies.*

Clearly, any shift in design practice toward non-standard angles cannot come at the cost of laminate performance, where laminate tailoring and tow-steering are pushing the boundaries of minimum weight composite structural design [166]. Efforts are also being made to make the composite laminate design process simpler and more accessible [23]. Thus, in combination with a method for finding non-standard ply angles that match the in-plane stiffness of standard ply angles, a simple strain energy (compliance) minimisation is used to compare performance of standard and non-standard laminates as explained in Chapter 3.

Minimisation of elastic strain energy allows laminates to be designed that store the least energy, creating the stiffest configuration for a given design loading, see Fig. 4.2. However, such design does not directly convert to minimum weight, as failure is nonlinear and complex; comprising damage to both resin and fibre, which is induced by mechanisms such as delamination, buckling, bearing, edge effects and manufacturing defects. Nevertheless, in this work elastic energy is considered to be an indication of performance to assess the potential of different design approaches to reduce laminate weight. Further to the above, manufacturing constraints mean that lay-up axes and principal loading axes are not necessarily aligned. Hence results are presented to illustrate the effect of aligning (and misaligning) the laminate balancing axes with the principal loading axes.

Figure 4.2 illustrates the conflict between manufacturing and performance in an energy landscape. The laminate manufacturing process imposes a fixed deformation on the uncured laminate arising from consolidation of complex parts or by forming

such parts from an initially flat state. The objective is both to minimise the strain energy U_{mn} for an imposed strain, and to avoid orthogonality in these low energy sublaminate modes to allow this energy to minimised by physically allowing ease of deformation. In contrast, improved performance requires minimisation of strain energy for an imposed stress, see U_p in Fig. 4.2.
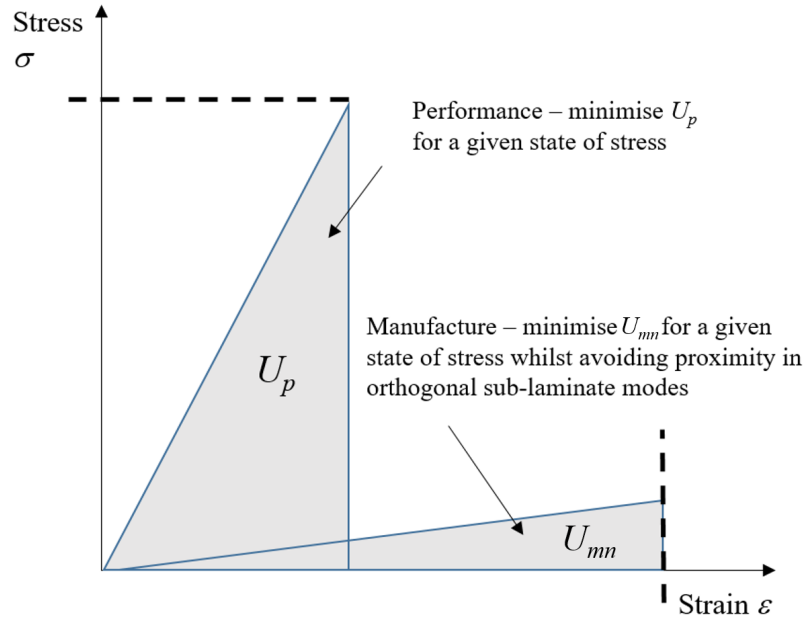
Figure 4.2: *Illustration of laminate strain energy relating to (cured) performance U_p and (uncured) manufacture U_{mn}. Note that minimisation of U_p maximises the load-carrying capacity of the fibres whilst minimisation of U_{mn} maximises deformation by resin-dominated modes.*

4.2   Theory

The following outlines the theory required (i) to create non-standard ply laminates with matching in-plane stiffness to standard ply laminates and (ii) to assess the comparative manufacturability and performance of standard and non-standard ply laminates, where performance is qualified by normalised in-plane elastic energy.

4.2.1   Equivalent representations of ply and laminate stiffness

The material specific in-plane stiffness of a single ply, linking in-plane stress components σ to in-plane strain ε, is given by Classical Laminate Theory as

$$\{\sigma\} = \begin{Bmatrix} \sigma_{11} \\ \sigma_{22} \\ \tau_{12} \end{Bmatrix} = [Q]\{\varepsilon\} = \begin{bmatrix} Q_{11} & Q_{12} & 0 \\ Q_{12} & Q_{22} & 0 \\ 0 & 0 & Q_{66} \end{bmatrix} \begin{Bmatrix} \varepsilon_{11} \\ \varepsilon_{22} \\ \gamma_{12} \end{Bmatrix} \qquad (4.1)$$

$$Q_{11} = \frac{E_{11}}{1 - \nu_{12}\nu_{21}} \qquad\qquad Q_{22} = \frac{E_{22}}{1 - \nu_{12}\nu_{21}}$$

$$\qquad (4.2)$$

$$Q_{12} = \frac{\nu_{12}E_{22}}{1 - \nu_{12}\nu_{21}} = \frac{\nu_{21}E_{11}}{1 - \nu_{12}\nu_{21}} \quad Q_{66} = G_{12}$$

Where E_{11} and E_{22} are longitudinal and transverse stiffnesses respectively, ν_{12} and ν_{21} are major and minor Poissons ratios respectively, and G_{12} is the shear modulus. Subscripts 1 and 2 relate to local ply axes as shown in Fig. 4.3.
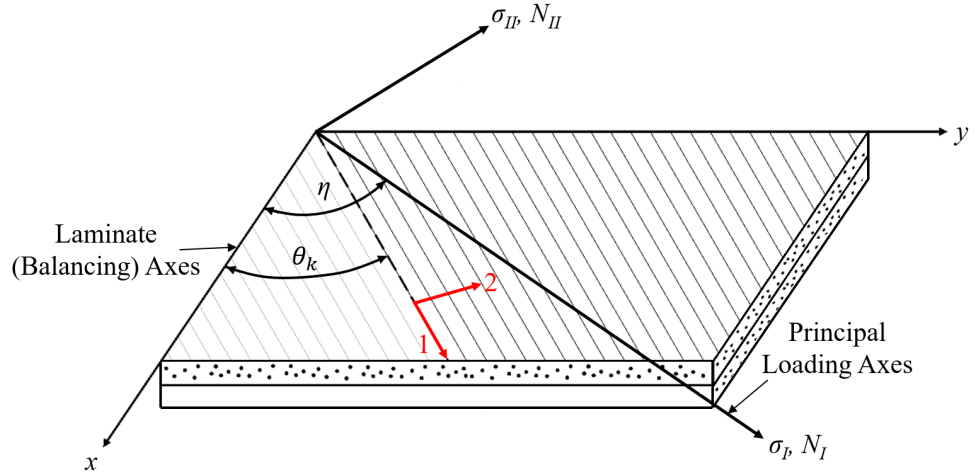
Figure 4.3: *Repeat of Fig 3.1. Local ply axes (1-2) and laminate (balancing) axes (x-y). The principal loading axes (σ_I-σ_{II}) and misalignment angle η of the balancing axes are also shown, allowing simplification of any general in-plane loading condition N_x, N_y and N_{xy}.*

The stacking sequence of a standard balanced laminate of total thickness T, consisting of ply pairs, is represented by

$$[(\pm\theta_1)_{\gamma 1}/(\pm\theta_2)_{\gamma 2}/.../(\pm\theta_n)_{\gamma n}]_S \qquad (4.3)$$

where $\gamma_1...\gamma_n$ refers to the proportion contribution of individual $\pm$ ply pairs to the total number of plies. A laminate stiffness matrix $\overline{[Q]}$ is formed by summing individual ply $[Q]$ matrices subject to associated transformation to align with ply orientations described by Eq. 4.3. Then assuming that (i) the laminate is balanced with zero in-plane to out-of-plane coupling (i.e. $\overline{Q}_{16}$, $\overline{Q}_{26} = 0$) and (ii) a state of plane stress (σ_z, τ_{xz}, $\tau_{yz} = 0$), exists. Classical Laminate Theory gives the in-plane laminate stress-strain relationship as

$$\{\sigma\} = \begin{Bmatrix} \sigma_x \\ \sigma_y \\ \tau_{xy} \end{Bmatrix} = \{N\}/T = \frac{1}{T} \begin{Bmatrix} N_x \\ N_y \\ N_{xy} \end{Bmatrix} = [\overline{Q}] \{\varepsilon\} = \begin{bmatrix} \overline{Q}_{11} & \overline{Q}_{12} & 0 \\ \overline{Q}_{12} & \overline{Q}_{22} & 0 \\ 0 & 0 & \overline{Q}_{66} \end{bmatrix} \begin{Bmatrix} \varepsilon_x \\ \varepsilon_y \\ \gamma_{xy} \end{Bmatrix}$$
(4.4)

where subscripts x and y refer to laminate axes in Fig. 4.3 and σ_x, σ_y, τ_{xy} (and ε_x, ε_y, γ_{xy}) are the applied laminate in-plane axial, transverse and shear stresses (and corresponding laminate strains), respectively. The $\overline{Q}_{ij}$ terms represent the individual in-plane stiffnesses and can be defined using lamination parameters and stiffness invariants [61, 158] as follows

$$\overline{Q}_{11} = U_1 + U_2\,\xi_1 + U_3\,\xi_2 \tag{4.5}$$

$$\overline{Q}_{12} = U_4 - U_3\,\xi_2 \tag{4.6}$$

$$\overline{Q}_{22} = U_1 - U_2\,\xi_1 + U_3\,\xi_2 \tag{4.7}$$

$$\overline{Q}_{66} = U_5 - U_3\,\xi_2 \tag{4.8}$$

where ξ_1 and ξ_2 are the in-plane lamination parameters, defined as follows

$$\xi_1 = \frac{1}{T} \int_0^T cos2\theta_k\,dz = \frac{1}{T} \sum_{k=1}^m cos2\theta_k t_k \tag{4.9}$$

$$\xi_2 = \frac{1}{T} \int_0^T cos4\theta_k\,dz = \frac{1}{T} \sum_{k=1}^m cos4\theta_k\,t_k \tag{4.10}$$

with m being the total number of plies in the laminate, t_k the ply thickness and θ_k the associated general ply angle within the stack of Eq. 4.3. U_i are stiffness invariants defined as,

$$
\begin{aligned}
U_1 &= \frac{1}{8}\left(3Q_{11} + 3Q_{22} + 2Q_{12} + 4Q_{66}\right) \\
U_2 &= \frac{1}{2}\left(Q_{11} - Q_{22}\right) \\
U_3 &= \frac{1}{8}\left(Q_{11} + Q_{22} + 6Q_{12} - 4Q_{44}\right) \\
U_4 &= \frac{1}{8}\left(Q_{11} + Q_{22} + 6Q_{12} - 4Q_{66}\right) \\
U_5 &= \frac{1}{8}\left(Q_{11} + Q_{22} - 2Q_{12} + 4Q_{66}\right)
\end{aligned}
\tag{4.11}
$$

A further representation of $[\overline{Q}]$ follows from its eigen decomposition,

$$[\overline{Q}] = [\varepsilon_\lambda][\lambda][\varepsilon_\lambda]^T = \begin{bmatrix} \varepsilon_{x,1} & \varepsilon_{x,2} & \varepsilon_{x,3} \\ \varepsilon_{y,1} & \varepsilon_{y,2} & \varepsilon_{y,3} \\ \gamma_{xy,1} & \gamma_{xy,2} & \gamma_{xy,3} \end{bmatrix} \begin{bmatrix} \lambda_1 & 0 & 0 \\ 0 & \lambda_2 & 0 \\ 0 & 0 & \lambda_3 \end{bmatrix} \begin{bmatrix} \varepsilon_{x,1} & \varepsilon_{y,1} & \gamma_{xy,1} \\ \varepsilon_{x,2} & \varepsilon_{y,2} & \gamma_{xy,2} \\ \varepsilon_{x,3} & \varepsilon_{y,3} & \gamma_{xy,3} \end{bmatrix} \tag{4.12}$$

where λ_i are eigenvalues and the ith column of $[\varepsilon_\lambda]$ is the eigenvector associated with the ith eigenvalue. Eigenvalues/vectors are determined from the solution of the equation,

$$([\overline{Q}] - \lambda_i[I])[V] = 0 \qquad (4.13)$$

where $[V]$ is any vector from the space of strain vectors and $[I]$ is the identity matrix.

4.2.2 Equivalent stiffness of laminates with standard and non-standard ply angles

A parametric study of the effect of ply angle and ply percentage on the in-plane lamination parameter design space was undertaken. The relative extent of design spaces for laminates made of (i) standard angle plies and (ii) two balanced non-standard angles $(\pm\psi)_\gamma/(\pm\phi)_{1-\gamma}$ are shown in Fig. 4.4. Note that γ defines the proportion of $\pm\psi$ plies and that standard angle designs are seen to be a subset of the non-standard angle stiffness design space [61, 158]. Example stiffness matched NSA laminates for a skin (44/44/12), stiffener (60/30/10) and spar (10/80/10) are shown. The procedure for this stiffness matching of standard angles with non-standard angles using lamination parameters is outlined below, with the general ply axes outlined in Fig. 4.3.
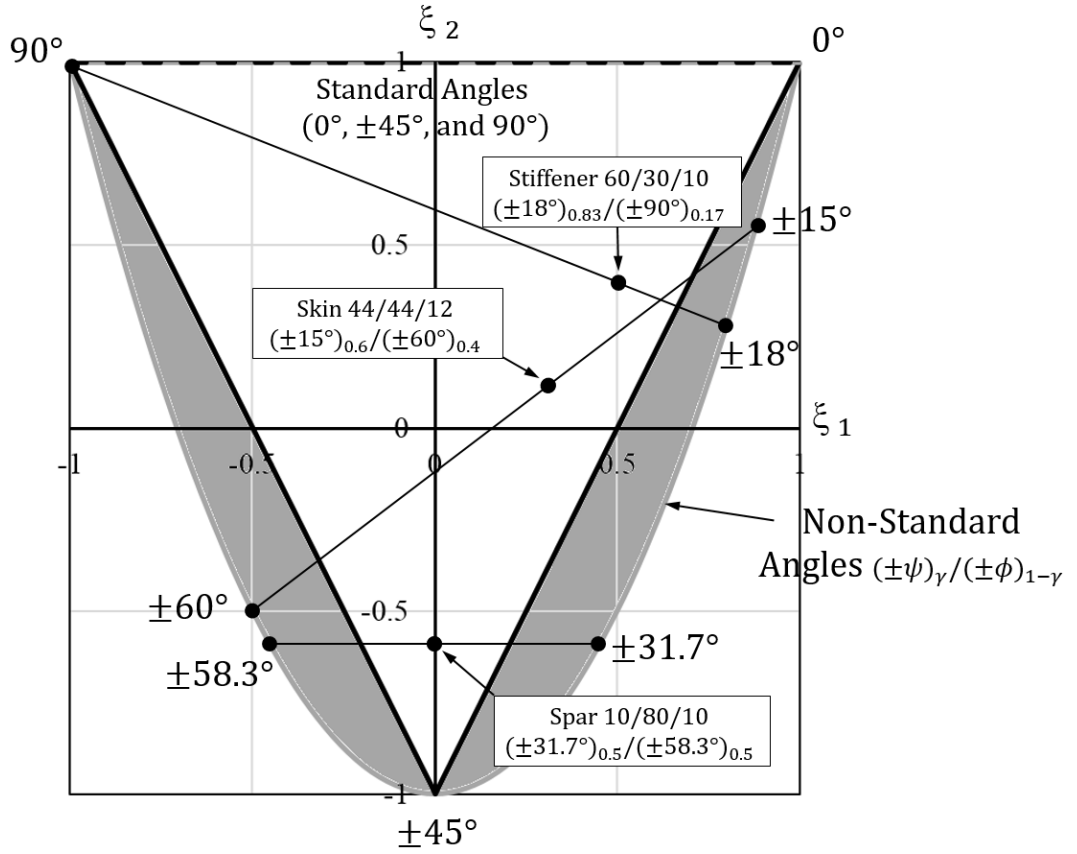
Figure 4.4: *Comparison of in-plane lamination parameter design space for standard and non-standard angle $(\pm\psi)_\gamma/(\pm\phi)_{1-\gamma}$ laminates with ply percentage variation permitted. The standard angle design space is a subset of the non-standard angle space. Examples NSA laminates are shown for a skin (44/44/12), stiffener (60/30/10) and spar (10/80/10).*

Assuming a given set of values for a standard angle laminate $\overline{Q}_{ij}^S$, (where superscript S indicates standard plies) values of in-plane lamination parameters are sort that reproduce $\overline{Q}_{ij}^S$ using non-standard angles. In order to isolate angle-dependent terms we rearrange Eq. 4.6 and Eq. 4.8 as

$$U_3\xi_2 = -\overline{Q}_{12}^S + U_4 \tag{4.14}$$

$$U_3\xi_2 = -\overline{Q}_{66}^S + U_5 \tag{4.15}$$

Substituting Eq. 4.14 into Eq. 4.5 we obtain

$$U_1 = \overline{Q}_{11}^S + \overline{Q}_{12}^S - U_4 - U_2\xi_1 \tag{4.16}$$

Similarly, substituting Eq. 4.15 into Eq. 4.7 gives

$$U_1 = \overline{Q}_{22}^S + \overline{Q}_{66}^S - U_5 + U_2\xi_1 \tag{4.17}$$

Setting Eq. 4.16 equal to Eq. 4.17 and rearranging we obtain

$$\xi_1 = \frac{\overline{Q}_{11}^S - \overline{Q}_{22}^S + \overline{Q}_{12}^S - \overline{Q}_{66}^S - U_4 + U_5}{2U_2} \tag{4.18}$$

Hence, from Eq. 4.18, any given proportion of standard angles within a laminate will have a certain value of ξ_1. In order to represent ξ_1 by two balanced non-standard angles $\pm\psi$ and $\pm\phi$ with proportion γ and 1-γ, respectively, we define the following parameters

$$\begin{aligned} \alpha &= cos\,2\psi, \quad \text{where } -1 < \alpha < 1 \\ \beta &= cos\,2\phi, \quad \text{where } -1 < \beta < 1 \end{aligned} \tag{4.19}$$

Therefore from Eq. 4.9 and Eq. 4.19 we obtain,

$$\xi_1^N = \gamma\alpha + (1-\gamma)\beta \tag{4.20}$$

where ξ_1^N and ξ_2^N are lamination parameters for non-standard angle layups. Hence

$$\gamma = \frac{\xi_1^N - \beta}{\alpha - \beta} \tag{4.21}$$

Rearranging Eq. 4.15 so that

$$\xi_2 = \frac{U_5 - \overline{Q}_{66}^S}{U_3} \tag{4.22}$$

As before, any given standard laminate will also have a certain value of ξ_2 creating a unique pair of values ξ_1 and ξ_2. Applying a similar process as Eqs. 4.19 and 4.20, by making the double angle substitution, gives

$$\xi_2^N = \gamma\,(2\alpha^2 - 1) + (1-\gamma)(2\beta^2 - 1) \tag{4.23}$$

Now rearranging and solving for β and substituting for γ from Eq. 4.21 we have

$$\beta = -\left(\frac{\xi_2^N + 1 - 2\alpha^2}{4(\alpha - \xi_1^N)}\right) \pm \sqrt{\left(\frac{\xi_2^N + 1 - 2\alpha^2}{4(\alpha - \xi_1^N)}\right)^2 - \left(\frac{2\alpha^2\xi_1^N - \alpha - \xi_2^N\alpha}{2(\alpha - \xi_1^N)}\right)} \tag{4.24}$$

If we choose any angle $\pm\psi$ and hence its corresponding value of α from Eq. 4.19, we can use Eqs. 4.18, 4.22 and 4.24 to define β, which can then be used to obtain the second angle $\pm\phi$. The thickness proportion of these two sets of angles is then given

by Eq. 4.21. A given standard angled laminate can therefore be fully matched by repeating this process for all values of $\pm\psi$, provided that solutions to Eq. 4.24 are in the range $-1 \leq \beta \leq 1$.

4.3 Laminate stacking sequence optimisation for minimum elastic energy

The performance of a laminate subject to a multi-axial state of stress is assumed to be represented by its Hookean strain energy or elastic energy; minimum energy indicates maximum performance. For each design loading, a Matlab genetic algorithm (GA) function 'ga [167] finds the laminate design that minimises the laminate in-plane normalised elastic energy in Eq. 3.11 thus creating designs with $\overline{U}_{min}$. It runs as described in Section 3.5 for a range of loads (17,408) described by η and σ_I/σ_{II}. $\eta = 0°$ is a special case where the principal loading axes are aligned with the balancing axes. This is generally not the case in design as the balancing axes are aligned with the laminate manufacturing axes. However, balance could potentially be achieved in different axes, or the principal axes, thereby enforcing $\eta = 0°$.

Optimisation of both standard (0°, $\pm$45°, and 90°) and non-standard angle ($\pm\psi_\gamma/\pm \phi_{1-\gamma}$) laminates was performed by the GA. Standard angle results were produced both with and without a 10% design rule in which a minimum of 10% of each of the four ply angles is maintained. This rule is enforced by limiting the choice of ply percentages available to the GA. The full optimisation process is detailed in Chapter 3, see the flowchart in Fig 3.4. In the results that follow material properties of E_{11} = 128 GPa, E_{22} = 10 GPa, G_{12} = 4.5 GPa, ν_{12} = 0.3 for AS4/8552 are assumed.

4.4 Results

4.4.1 Standard and non-standard laminates with equivalent in-plane stiffness

Laminates for stiffener, skin and spar wing components typically have standard angle (0°/$\pm$45°/90°) ply percentages of 60/30/10, 44/44/12 and 10/80/10 respectively. For each application Figs. 4.5 (a) and (b) show a matched stiffness design space for non-standard angles derived from the equations of Section 4.2.2. Note that, in order to satisfy the requirement of generating a identical in-plane stiffness $[\overline{Q}]$ to the original standard angle laminate, both values for the thickness proportion γ and angle ϕ vary with a change in initial angle ψ. Highlighted points in Fig. 4.5 represent

an arbitrary example for the spar laminate, where angle ψ is set at $\pm 31.7°$ and the second angle ϕ $\pm 58.3°$ is derived from Eqs. 4.19, 4.21 and 4.24. The thickness proportion $\gamma = 0.5$, indicates a 50/50 distribution of angle sets creating a non-standard double angle laminate ($\pm 31.7_{0.5}/\pm 58.3_{0.5}$). Converted to example 20 ply stacks gives $[45/-45/45/-45/90/45/-45/45/-45/0]_s$ for a SA layup and $[32/-32/-32/32/-58/58/58/-58/58/-32//32/-58/-58/58/58/-58/-32/32/32/-32]$ for a NSA layup. The NSA layup makes use of a fully uncoupled sequence [93]. It also has a small amount of extension-twist coupling near the centre which is not part of the fully uncoupled sequence. This coupling is minimised as the anti-symmetric plies are near the mid-plane. Other equivalent designs for a skin and stiffener are shown in Fig. 4.4.

4.4.2 Performance optimisation

Results in Fig. 4.6 were obtained using the procedure in Section 4.3 and show the envelope of minimum elastic energy with principal design load for both optimised standard angle (with and without the 10% rule) and non-standard angle designs. Radial variation indicates the magnitude of elastic energy. Angular variation specifies the ratio of principal loading σ_I/σ_{II}. The inner and outer limits (rings) of Fig. 4.6 indicate extent of the minimum elastic energy $\overline{U}_{min}$ for optimised designs when optimising for different η, the principal loading to balancing axes misalignment. Inner rings show the lowest (best) achievable minimum elastic energy from variation in η. This occurs for $\eta = 0°$ where the principal loading axes are aligned with the balancing axes. Outer rings show the upper bound of minimum elastic energy with variation in η. Laminate designs represented by the outer ring are optimised for minimum (best) energy whilst meeting the constraint of worst possible misalignment η_w. Non-optimised laminate designs may have energies that sit outside the outer ring. All optimised minimum elastic energy $\overline{U}_{min}$ results, for all values η, lie between the inner and outer rings. Note that non-zero misalignment indicates the optimised design is under both shear and direct load.
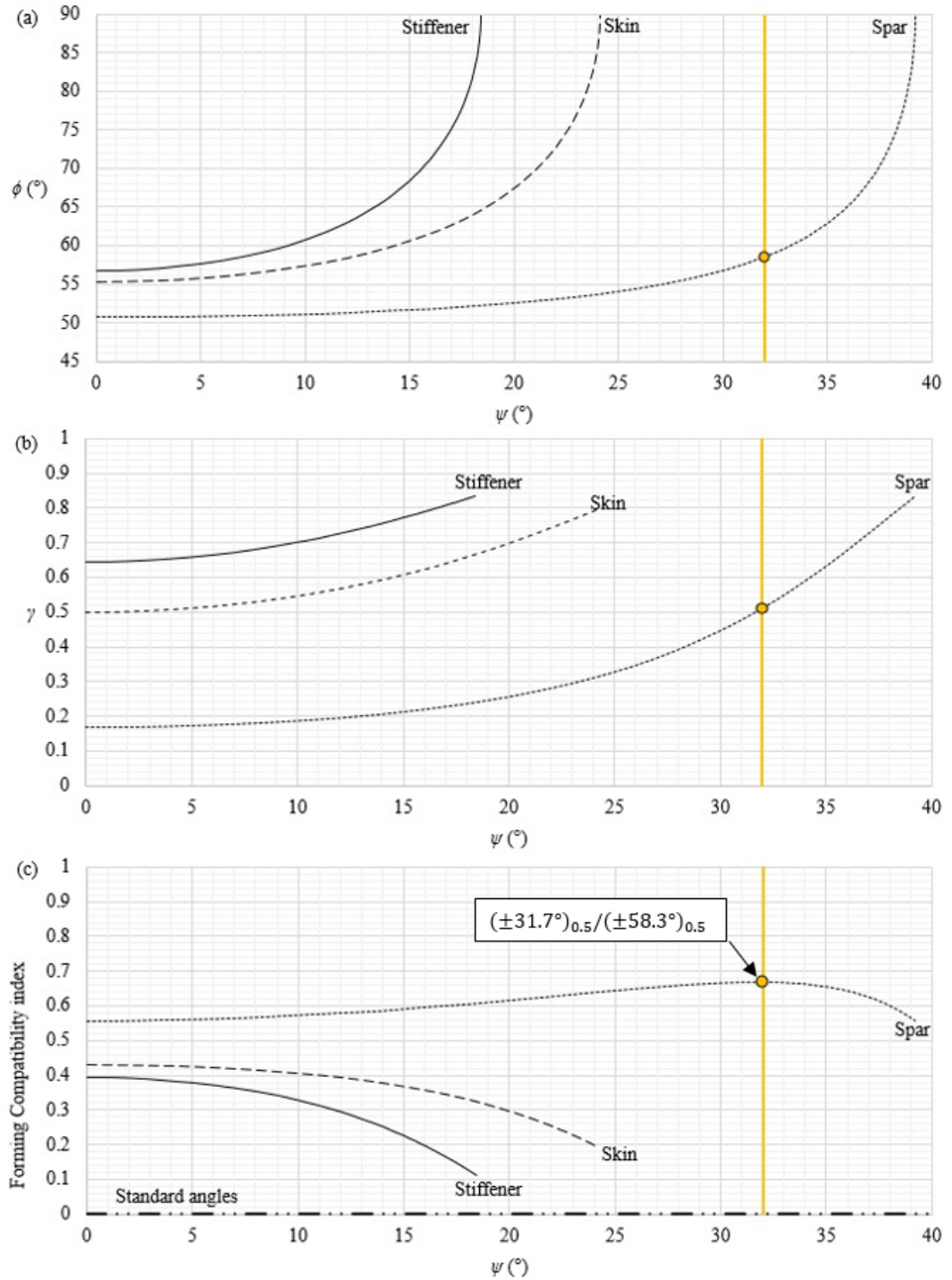
Figure 4.5: *(a) Non-standard ply angles $(\pm\psi)_\gamma/(\pm\phi)_{1-\gamma}$ for laminates with equivalent in-plane stiffness of standard angle stiffener (60/30/10), skin (44/44/12) and spar (10/80/10) laminates. (b) Contribution (γ) to laminate thickness of ply angle pair $\pm\psi$. (c) Compatibility of $\pm\psi$ and $\pm\phi$ uncured sublaminate eigenvectors associated with lowest energy mode of deformation, indicating forming compatibility. An index of 0 indicates orthogonal modes and no compatibility, 1 indicates parallel modes and full compatibility. As indicated 0/90° and $\pm45°$ sublaminates have incompatible modes. An example stiffness matched NSA design of $(\pm31.7°)_{0.5}/(\pm58.7°)_{0.5}$ is shown.*
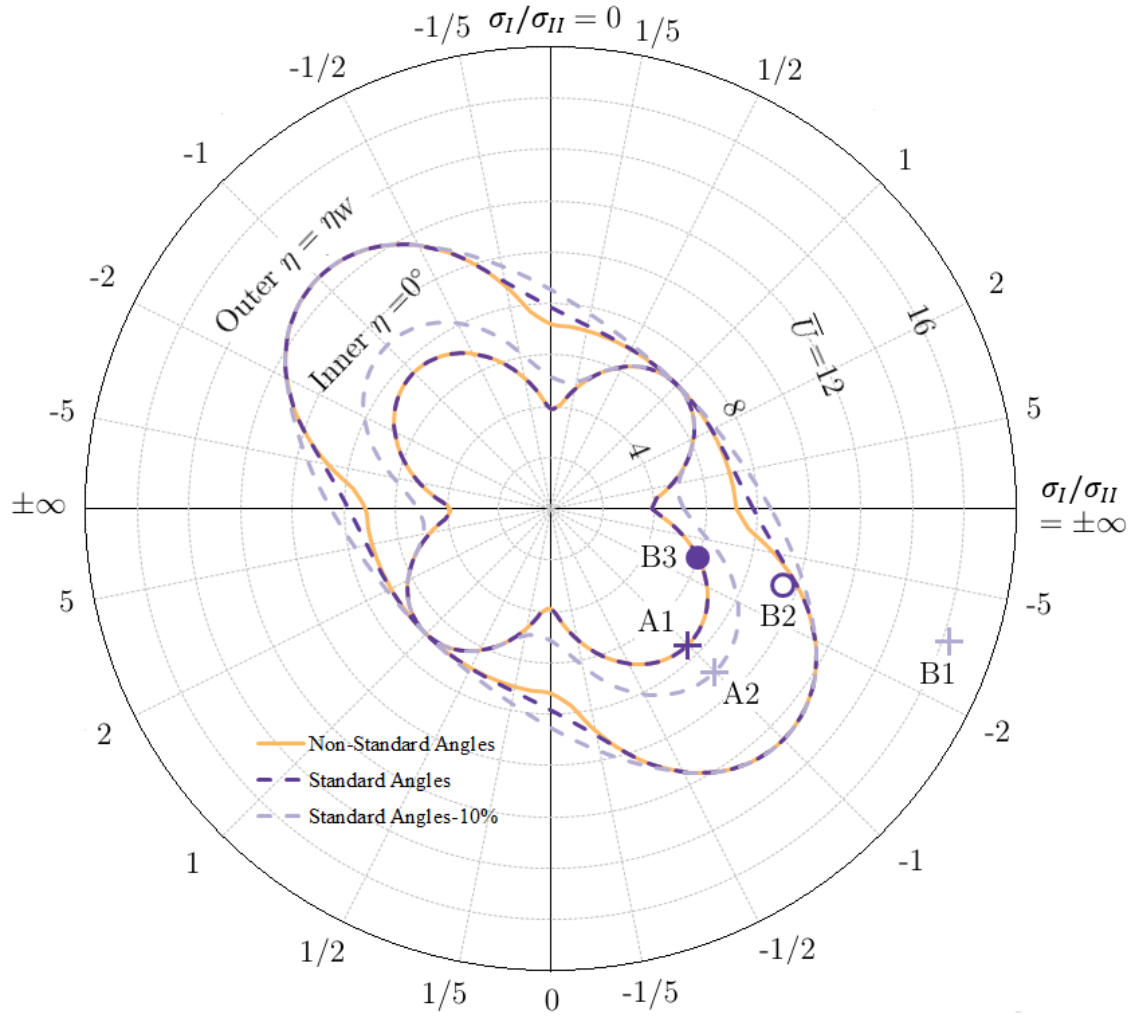
Figure 4.6: *Comparison of normalised elastic energy $\overline{U}$ (1×10^{-12} m^2/N) for optimised standard angle laminates (with and without the 10% rule) and non-standard angle laminates designed for angular variation in principal load ratios σ_I/σ_{II}. The inner and outer rings represent, respectively, the best and worst misalignment, η, of the principal loading with the balancing axes. Points A1-B3 refer to specific designs in Table 4.1.*

A spar design case is used to illustrate the effect of the misalignment angle η. Pure shear load may be expected near the centre of a spar web corresponding to, σ_I/σ_{II} = -1 and η = 45°, see Fig. 4.7. The design represented by point A1 in Fig. 4.6, consisting of ±45° plies only with η = 45°, is the minimum elastic energy laminate for this loading for both standard and non-standard angles and thus is represents the optimum stiffness design. Point A2 in Fig. 4.6 corresponds to the equivalent standard angle laminate design problem but with the 10% minimum ply percentage rule enforced. It is noted that for pure shear, despite $\eta \neq 0$, optimal plies are balanced about the principal loading axes. However, loading varies across the spar and a different design will be optimal at the spar caps where bending stresses are significant and $\sigma_I/\sigma_{II} \neq$ -1, see Fig. 4.7. If the same magnitude of shear that occurs

in the web is assumed to occur in the spar caps and $\sigma_I/\sigma_{II} = -3$, then from Mohrs circle, see Fig. 4.7(a), a multi-axial load state is created in the spar axes where $\eta = 15°$. Point B1, in Fig. 4.6 and Table 4.1, and Point A1* (in Table 4.1 only) indicate the energies achieved if this spar cap loading is applied to the designs for Points A2 and A1, respectively. This represents inferior performance at the spar cap if current manufacturing practice is followed and web laminate designs are maintained throughout the spar.
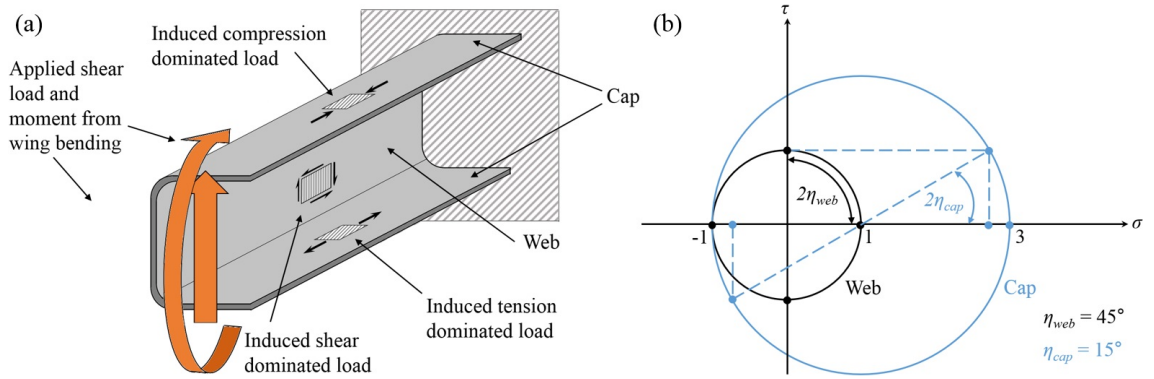
Figure 4.7: *(a) Schematic view of idealised loading of a spar section. Web and cap sections together with dominant loading type are identified. (b) Mohrs circle representation of the example spar web and spar cap loadings of $\sigma_I/\sigma_{II} = -1$ and $\eta = 45°$ (pure shear) and $\sigma_I/\sigma_{II} = -3$ and $\eta = 15°$, respectively, for the loading applied to design Points A and B in Table 1 and Fig. 4.6.*

Points B2 and B3 represent minimum elastic energy for standard angle laminates optimised for the cap loading whilst balancing in the spar manufacturing axes ($\eta = 15°$) and the principal loading axes ($\eta = 0°$), respectively. In this special case of point B3 the cap SA angles are rotated by 15° e.g. 0° fibres are aligned at 15°.

Variation in ply percentages of optimum standard angle designs with principal load ratio, corresponding to the inner and outer rings of Fig. 4.6, is shown in Fig. 4.8 (a) and (b), respectively. Figure 4.8 (a) shows that if axial (transverse) loading dominates, there are a larger proportion of 0° (90°) plies. The requirement for ±45° plies is seen to only exist for positive principal load ratios. However, optimum designs corresponding to the outer ring in Fig. 4.8(b), where the principal loading is not aligned with the balancing axes, require a combination of 0°, ±45° and 90° plies.

Design Point	% 0°	% ±45°	% 90°	Design Load σ_I/σ_{II}	η (°)	Applied Load σ_I/σ_{II}	η (°)	$\overline{U}$ $(1 \times 10^{-12}$ m^2/N$)$	Equivalent weight: $\sqrt{\overline{U}}$ (% Increase at Cap)
A1	0.0	100.0	0.0	-1(W)	45	-1 (W)	45	7.5	2.7
A1*	0.0	100.0	0.0	-1(W)	45	-3(C)	15	27.9	5.3 (+31%)
A2	10.0	80.0	10.0	-1(W)	45	-1(W)	45	9.0	3
B1	10.0	80.0	10.0	-1(W)	45	-3(C)	15	16.3	4 (datum)
B2	58.9	30.7	10.4	-3(C)	15	-3(C)	15	9.5	3.1 (-24%)
B3	78.1	0.0	21.9	-3(C)	0	-3(C)	0	6.0	2.5 (-39%)

Table 4.1: *Laminate designs, design loads and applied loads in spar web (W) and spar cap (C) for Points A1-B3, shown in Fig. 4.6. Note that design Point A1* is not shown in Fig. 4.6.*
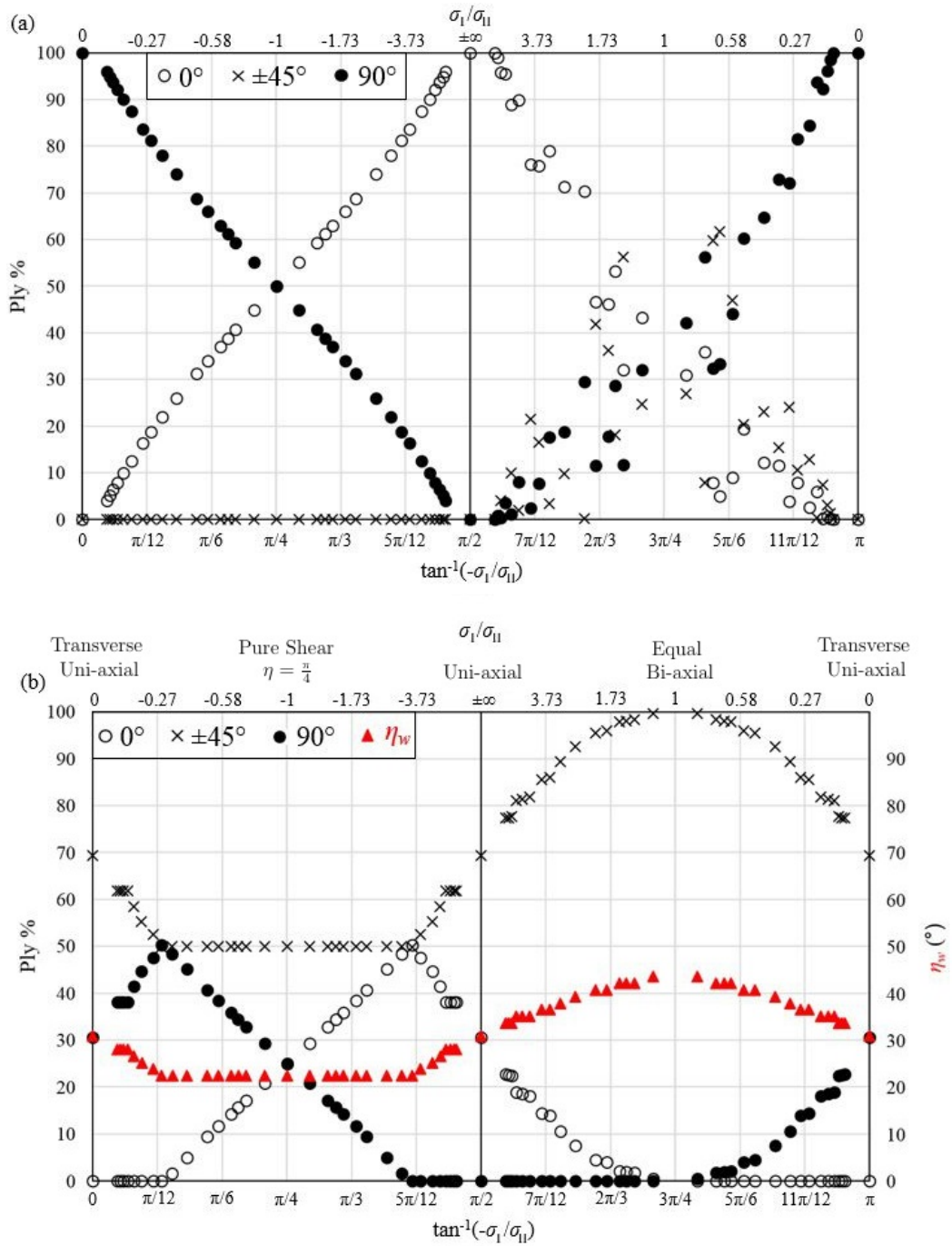
Figure 4.8: *Ply percentage variation of the optimum standard angle laminate designs for (a) the Fig. 4.6 inner ring and (b) the outer ring. The η_w shown in (b) corresponds to the worst case off-axis misalignment of the balancing axes from the principal loading to optimise for. Note designs are not presented for the special case of $\sigma_I/\sigma_{II} = 1$ (hydrostatic pressure) but are described in Section 4.5.2.*

4.4.3 Compatibility of pre-cure deformation

It is noted that the lowest eigenvalue, and its corresponding eigenvector derived from the $[\overline{Q}]$ of a sublaminate, describe its minimum energy mode of elastic deformation. During manufacturing processes such as Hot Drape Forming, where optimum operating temperatures reach 90°C [168], the resin influenced moduli E_{22} and G_{12} are over four orders of magnitude lower than fibre influenced modulus E_{11}, see Table 4.2. Therefore, it can be assumed that minimum energy modes of deformation during forming are resin dominated and that modes with eigenvalues of order 108 kPa will involve fibre stretching and thus will not occur during manufacture where stresses are low.

	E_{11} (kPa)	E_{22} (kPa)	G_{12} (kPa)	ν
Uncured (90°C)	1.28×10^8	100	338	0.12
Cured	1.28×10^8	10.3×10^6	6×10^6	0.3

Table 4.2: *AS4/8552 material properties at the ideal forming temperature and in cured state. The Poissons ratio at 90°C forming temperature was calculated using a Poissons ratio for carbon of 0.2 and a fibre volume content of 0.6, to give the resulting ratio of 0.12.*

The in-plane stiffness of an uncured sublaminate, represented by Eqs. 4.1 to 4.4 using uncured elastic properties (see Table 4.2), is used to determine sublaminate $[\overline{Q}]$. From these $[\overline{Q}]$ and following the theory of Section 4.2.1, eigenmodes for both standard and non-standard angled sublaminates can be determined and their compatibility assessed. Table 4.2 gives these eigenmodes for single ply orientations. Modes are also given for sublaminates, and their respective thickness proportions γ, that make up the standard and non-standard angle sublaminates from the spar example shown in Fig. 4.5. The scalar product of the eigenvectors of the minimum energy modes for each of the ψ and ϕ sublaminates can be used to assess the relative compatibility of the sublaminates in forming. Note that incompatible sublaminates with orthogonal eigenvectors such as [0°/90°] and [±45°] have a scalar product of 0. The most compatible sublaminates have parallel modes and thus the greatest scalar product value. Figure 4.5 (c) plots the scalar product of the minimum energy eigenmodes of all pairs of non-standard sublaminates that form the laminates defined in Figs. 4.5 (a) and (b).

Sublaminate	γ	λ_1 (kPa)	$\varepsilon_{x,1}$	$\varepsilon_{y,1}$	$\gamma_{xy,1}$	λ_2 (kPa)	$\varepsilon_{x,2}$	$\varepsilon_{y,2}$	$\gamma_{xy,2}$	λ_2 (10^7 kPa)	$\varepsilon_{x,3}$	$\varepsilon_{y,3}$	$\gamma_{xy,3}$
$0°$	1	100	0	-1	0	338	0	0	1	12.8	-1	0	0
$90°$	1	100	-1	0	0	349	0	0	1	12.8	0	1	0
$45°$	1	67	0.41	0.41	-0.82	676	0.71	-0.71	0	9.6	0.58	0.58	0.58
$-45°$	1	67	0.41	0.41	0.82	676	0.71	-0.71	0	9.6	-0.58	-0.58	0.58
Spar													
$0°/90°$	0.2	69	0	0	1	1.28×10^7	-0.71	0.71	0	12.8	-0.71	0.71	0
$\pm45°$	0.8	541	-0.71	-0.71	0	2.56×10^7	0	0	1	5.18	0.71	0.71	0
$\pm31.7°$	0.5	242	0.36	-0.93	0	1.28×10^7	0	0	1	3.84	-0.93	-0.36	0
$\pm58.3°$	0.5	242	-0.93	0.36	0	1.28×10^7	0	0	1	3.84	0.36	0.93	0

Table 4.3: *Sublaminate eigenvalues (λ) and eigenvectors for the first three modes of uncured AS4/8552 material for spar sublaminates, with standard and non-standard fibre orientations. All modes have been normalised to have unit magnitude.*

4.5 Discussion

4.5.1 Standard and Non-Standard Laminates with Equivalent In-Plane Stiffness

Figure 4.5 shows that stiffness matching of standard angle laminates with non-standard angle laminates can be achieved over a range of non-standard angles. While maintaining the exact stiffness properties of the original standard angle laminate, non-standard angles can be freely chosen to improve manufacturability and potentially other design requirements such as buckling resistance [9] or damage tolerance [28]. The three design examples explored in Fig. 4.5 carry very different loadings which limit the range of non-standard matched stiffness designs to a greater or lesser extent. Regions of stiffness matching can be seen in Fig. 4.4. The standard stiffener laminate, which has the highest proportion of 0° fibres, is the most restrictive offering the smallest range of ψ that can be paired with ϕ angles to generate a $[\overline{Q}]$ identical to the original standard laminate. In contrast, the standard spar laminate which is dominated by $\pm 45°$ plies, allows for twice the range in angle ψ. Similarly, this contrast in range applies for the thickness proportion γ.

It is noted that, despite having very different fibre proportions, all three design cases produce a non-standard fibre angle combination where ϕ always takes a value between 50° and 90°. The stiffener and skin laminates also produce a very similar angle for ϕ in the low regions of ψ. This creates the potential for a composite structure that has areas with different performance criteria, to incorporate one common ply angle. The common transition method between two areas, ply dropping, would therefore result in a much more uniform changeover in material properties.

4.5.2 Optimisation for Performance

The principal load ratio inherently affects the value of minimum elastic energy possible as seen by the variation in magnitude around the inner ring in Fig. 4.6. In Table 4.1, Points A1 and B3 show that to create the lowest achievable minimum elastic energies for the inner ring in Fig. 4.6, the principal load must be aligned with the balancing axes ($\eta = 0°$). However, it is uncommon for a principal loading to be aligned with the balancing axes. Therefore, realistically achievable energies will lie above the inner rings as there is an increase in the elastic energy stored due to extra shear deformation from the presence of a shear load when $\eta \neq 0°$.

No designs are plotted for $\sigma_I/\sigma_{II} = 1$ in Figs. 4.8 (a) and (b) as there are many optimum designs where any rotation of any combination of a π/n quasi-isotropic (QI) laminate (where n is an integer ≥ 2) is optimal.

Principal loading is essentially bi-axial if off-axis alignment of balancing in the principal axes is allowed ($\eta = 0°$) or if the principal load is already aligned to the laminate axes, which is an unlikely design scenario. Under such conditions, non-standard angle plies offer no elastic energy advantage over standard angle plies, even though the designs are potentially different, see inner rings in Fig. 4.6. The optimal laminate stiffness requirements for bi-axial design loads must then lie within the standard angle lamination parameter design space shown in Fig. 4.4. It is only when a multi-axial design load exists ($\eta \neq 0°$), equivalent to a misaligned principal loading to the balancing axes, which is often the case in practical design, that a small advantage appears for use of non-standard plies, as seen by the difference in elastic energy of the outer rings in the vicinity of $\sigma_I/\sigma_{II} = \pm\infty$.

Figure 4.6 shows that application of the 10% minimum ply percentage rule generally increases the minimum elastic energy achievable. This is especially true where entirely 0° or 90° designs are theoretically optimal, and for all compressive-tensile principal loadings ($-\infty < \sigma_I/\sigma_{II} < 0$, i.e. negative ratios), where optimal designs require a combination of 0° and 90° plies and no ±45° plies. However, the 10% rule creates robustness to variation in loading. For example, under the web design load of pure shear there is a small energy penalty at Point A2 compared to Point A1 due to the 10% rule but when applying the spar cap loading, the elastic energy is significantly less, see Point B1 compared to A1* in Table 4.1, since the 10% rule creates some robustness to variation in load. The 10% rule is, however, arbitrary and is not required for a deterministic loading condition. Point B2, which has a potential 24% reduction in weight over Point B1, is a realistic optimal design if the spar cap loading is assumed to be fixed and known, but also satisfies the 10% rule and represents the optimum design with the rule enforced, allowing robustness to load uncertainty. Going from the design Point A2 to Point B2 shows the potential to modify laminate ply percentages from a spar web to cap to account for variation in load ratios. If the 10% rule and the requirement to balance in the spar/laminate axes are also removed, further improvement is seen at Point B3 with a 39% potential weight reduction over Point B1, highlighting the potential benefit of steering fibres throughout the part from Point A1 at the web. Balancing in the principal axes is more worthwhile for $-\infty < \sigma_I/\sigma_{II} < 0$, where the addition of shear from the misalignment creates higher weight designs, shown by higher energies in the outer ring designs compared to $\infty > \sigma_I/\sigma_{II} > 0$, where greater proportions of ±45° plies are optimal and aid with efficiency under shear.

In Fig. 4.8 the optimum designs corresponding to the inner rings are unique for $\sigma_I/\sigma_{II} \leq 0$ and $\sigma_I/\sigma_{II} = \pm\infty$ when $\eta = 0°$. This is because 0° and 90° plies are able to provide optimal stiffness properties. A smooth variation in 0° and 90° ply percentage is seen in Fig. 4.8 (a) over these loadings adding evidence that no

other optimal laminates are possible. However for $0 < \sigma_I/\sigma_{II} < \infty$ optimal designs are not unique as shown in the scattered distribution of the standard angle ply percentages in Fig. 4.8 (a). This suggests that different optimal $[\overline{Q}]$ matrices exist for the same design loading, and is confirmed by the presence of different optimal $[\overline{Q}]$ matrices in the optimised non-standard angle laminates that provide the same minimum energies for the same design load.

In summary, minimum elastic energy is seen to be limited by (i) the principal loading ratio, (ii) the 10% ply percentage rule and (iii) the principal loading axes misalignment with the balancing axes, η. If the loading is known to be fixed and/or there is no requirement to balance in a fixed axis system, then there is potential to design lower weight laminates.

4.5.3   Manufacturing

Although eigenmode analysis based on $[\overline{Q}]$ matrices derived from uncured properties does not accurately describe the deformation of the uncured laminate nor any inter-ply slipping (sublaminate modes), it does enable assessment of whether the low energy in-plane modes of sublaminates are either compatible or incompatible (orthogonal). Such comparison can be used to assess laminate manufacturability. From Table 4.3, the lowest modes for individual plies are seen to be orthogonal and hence incompatible.

However, when $+45°$ and -45° plies are grouped together they become more compatible with the preferred individual 0° and 90° modes. This may be why Hallender et al. [164] discovered that wrinkling defects were not produced during forming of a C-Section spar when $\pm45°$ groups were enforced. Such defects did occur when $+45°$ and -45° plies were separated by a 0° ply. As is shown in Table 4.3 and Fig. 4.5(c) the sublaminates of standard angle spars generate initial modes that are orthogonal to each other, whereas the non-standard angle modes offer a greater compatibility. As demonstrated in Fig. 4.5(c), this similarity in modes is not only applicable for this example laminate but for every other configuration of stiffness matched non-standard angle design. Hence deformation of the non-standard designs appear to be more homogeneous and thus less likely to trigger wrinkling defects.

4.6   Conclusions

Elastic energy minimisation and eigenmode compatibility are applied to improve performance and manufacturability through the use of non-standard ply laminate designs and balancing of plies about an axes with variable misalignment from principal loading axes.

The performance of a laminated composite aircraft component, ignoring complex failures such as kink banding, buckling and compression after impact, is dependent on orientating plies such that load is carried predominantly by the fibres. The capacity of a laminate stacking sequence to direct a multi-axial in-plane load into the stiffer fibres can be measured by assessing its elastic energy under a specific design load. It was found that laminate designs for optimal performance occur when balancing axes are fully aligned with principal loading axes. Although in this configuration use of non-standard plies is shown to have no benefit. For positive biaxial loading ratios the design space available was significantly enlarged as multiple combinations of non-standard plies were available to match standard angle laminate stiffness.

Some limited performance benefit was found to be available from non-standard angles should, as is often the case in aerospace components, the balancing axes be misaligned from the principal loading axes. Example aerospace component loading scenarios demonstrated that if principal load axes vary across a component (e.g. web to cap in a spar) then significant benefit could be derived from stiffness tailoring through tapering and tow-steering to ensure balancing axes track the change in principal loading axes.

The repeatability of manufacturing processes which produce defect free laminates, is critical to structural performance. It is proposed that manufacturing defects can be minimised by creating compatible modes of deformation between sublaminates. Such compatibility is assessed via compatibility of the lowest energy mode of deformation of each sublaminate, assuming pre-cured material properties. Non-standard plies are shown to offer significant improvements in compatibility whilst maintaining identical post-cured stiffness. This can potentially improve performance by reducing the likelihood of fibre wrinkle defects, consequently increasing production rates and reducing the need for so-called manufacturing knockdown factors, which allow for the presence of small manufacturing defects.

Chapter 5

Appropriateness of the 10% rule

Work in this chapter formed part of a paper submitted to Composites: Part A. Here, minimisation of normalised elastic energy under an uncertain in-plane general loading is used to indicate laminate efficiency and by equivalence minimum weight in the absence of matrix failure. Results are the first to investigate the comparative robustness of standard and non-standard angles to uncertain loading and indicate that weight reductions of up to 8% can be achieved if optimum design using standard angles ($\theta = 0°$, $\pm45°$ or $90°$) and industry design rules is replaced by optimising non-standard angles ($0° \leq \theta \leq 180°$) directly for uncertain loading. However, greater reductions of up to 20% are possible through alignment of laminate balancing axes with principal loading axes As such, a non-standard angle design strategy is only shown to be warranted if the demonstrated non-uniqueness of optimum designs can be exploited to improve other performance drivers.

5.1 Introduction

Minimum weight aerospace laminate design is a multi-constraint problem. All relevant failure modes such as buckling, damage tolerance, bolt bearing and notched strength should be considered in order to produce a minimum weight design that delivers the required performance. However, such a complex approach is not justified in the initial design stage. Netting analysis, which ignores the support of the resin matrix and aligns fibres in principal directions to carry principal stresses, leads to laminate designs in which the stresses in fibres are limited to some value associated with failure i.e. fully-stressed fibre design. Verchery [87] has shown that Netting analysis, can be treated as a limiting case of Classical Laminate Theory. His approach indicates that designs with fewer than three fibre directions produce mechanisms when subject to small disturbances in loading. This reveals the reasoning behind established aerospace laminate design practice of using four standard

angles (SAs) (0°, +45°, -45° and 90°) and a design rule of a 10% minimum ply percentage to provide a level of redundancy against loading uncertainty [157]. In contrast, non-standard angle (NSA) designs permit the use of all possible fibre angles ($0° \leq \theta \leq 180°$) providing greater scope for stiffness tailoring. The advantages of further laminate tailoring has been demonstrated through use of lamination parameters and NSA layups compared to quasi-isotropic layups in optimisation procedures. This is seen for wing structure solutions in aero-elastic tailoring purposes [169, 170], increased panel buckling performance [9, 158] as well as enabling certain types of stiffness couplings [94]. NSAs have also been extensively studied for their use in winding angles for optimising pressure vessel strength [171, 172]. However, a lack of specific design rules for NSA laminates can lead to optimum aerostructure designs for specific loadings that, from Netting analysis, rely considerably on the matrix to prevent mechanism collapse if the load state is varied. In this work, to avoid this problem, both NSA and SA laminates are designed considering an uncertain in-plane loading. This has the potential to offer a replacement for the 10% minimum ply percentage rule in SA designs and allows the use of NSAs without an equivalent constraint.

In order to compare design approaches that use SAs and NSAs, laminate in-plane elastic energy under combined bi-axial and shear loading is used to assess laminate efficiency. Elastic energy minimisation or compliance energy minimisation is a computationally efficient technique that uses either topology or orientation of materials with directional properties, to produce the structures with maximum efficiency. Structures with optimum efficiency take advantage of directional material stiffness properties to produce a minimum global strain state. This requires the structure to have the greatest global stiffness for a given volume of material. Prager and Taylor [10] first outlined optimality criteria justifying the technique of minimisation of elastic energy (subject to given loads) to produce a structure with optimal efficiency. Pedersen [58] subsequently applied this technique to composite materials to find analytical solutions for orientation of a single ply angle subject to in-plane loading. Solutions for multi-layered anisotropic laminates are provided for multi-axial design loadings.

Minimisation of in-plane elastic energy in laminate design does not directly imply maximisation of in-plane strength of a composite material. Nevertheless, it is assumed to be sufficient to capture the in-plane strength relationship as fibres are aligned to best carry the applied multi-axial stresses, which is the case for maximum in-plane strength design in a Netting analysis regime [152, 153]. Thus the performance of a laminate under a vector of loading can be shown by the single attribute of in-plane elastic energy. Laminates are optimised using the techniques presented with a Genetic Algorithm and the results are presented in plots revealing

the potential benefits and drawbacks of new and current methodologies.

5.2 Minimum weight laminate design

In this section, a process is defined that minimises in-plane elastic energy under fixed and uncertain in-plane multi-axial loadings (axial, transverse, shear) in order to find distributions of SA and NSA plies that maximise laminate efficiency and thus minimise weight. Design constraints for both SA and NSA laminates, in the form of stacking sequence rules, are also derived.

The derivation of elastic energy is detailed in Chapter 3, see Section 3.4, and the key equation for normalised elastic energy per unit volume is given below

$$\overline{U} = \frac{(q_{11}\sigma_x^2 + 2q_{12}\sigma_x\sigma_y + q_{22}\sigma^2 + q_{66}\tau_{xy}^2)}{2(\sigma_x^2 + \sigma_y^2 + 2\tau_{xy}^2)} \tag{5.1}$$

The principal loads/stresses (σ_I & σ_{II}) are found using the following equation

$$\sigma_{I,II} = \frac{(\sigma_x + \sigma_y)}{2} \pm \sqrt{\left(\frac{(\sigma_x - \sigma_y)}{2}\right)^2 + \tau_{xy}^2} \tag{5.2}$$

The misalignment angle, η, of the balancing axes (about which $+\theta$ and $-\theta$ plies are evenly distributed to prevent extension-shear coupling) from the principal loading axes is shown in Fig. 5.3 and defined as

$$\eta = \frac{1}{2} tan^{-1} \frac{2\tau_{xy}}{(\sigma_x - \sigma_y)} \tag{5.3}$$

If the laminate is not balanced, either for all axes, or in the axes in which the elastic energy is calculated then $q_{16}\sigma_x\tau_{xy}$ and $q_{26}\sigma_y\tau_{xy}$ terms appear in the numerator of Eq. 5.1.

5.3 Optimisation

5.3.1 Problem Description

Current design techniques consider a fixed critical loading condition, relating to some worst case from various critical loads that could be applied to an aircraft structure. Any uncertainty in secondary loading is considered to be negated by enforcement of a 10% minimum ply percentage rule [157]. The new design strategy proposed here, optimises directly for maximum in-plane stiffness for a critical design load case in

which secondary loadings are uncertain. To provide a comparison of the current and proposed design practices, laminates are optimised for minimum normalised elastic energy (minimum weight) under either a fixed loading (current practice, 10% rule) or uncertain loading (proposed new strategy). The two strategies are compared under a worst case loading derived from the envelope of loadings created by a deviation in secondary loads of up to either $\pm 10\%$ or $\pm 20\%$ of the primary load. In reality the loading uncertainty will vary with different parts across the aircraft and thus the uncertainty considered is used only to discover potential benefits of the proposed methodologies.

5.3.2   Designing for an Uncertain Loading

Critical laminate design depends on the worst loading case that could be applied. Hence, the design concept here is to achieve maximum performance under the worst case loading taken from the loading envelope defined by $\pm 10\%$ or $\pm 20\%$ uncertainty. The worst loading case corresponds to the loading where a laminate has the highest normalised elastic energy, i.e. maximum weight. However, this is dependent on the range of loadings and the laminate design being considered. By keeping the value of primary loading fixed (e.g. σ_x), a three dimensional surface for normalised elastic energy as a function of the two secondary loading variables (e.g. σ_y and τ_{xy}) described by Eq. 5.1 can be created for each individual laminate design, see Fig. 5.1. The Extreme Value theorem [173] for two variables is used which finds the maxima of Eq. 5.1 (with fixed $[\overline{Q}]$) both within the interior of the allowed range of secondary loads and on its boundaries, and compares values of normalised elastic energy to find the worst loading and its corresponding normalised elastic energy ($\overline{U}_{WC}$).

5.3.3   Optimisation Strategies and Variables

Laminates to be optimised contain either SAs or NSAs, and are designed using a Matlab Genetic Algorithm (GA) 'ga' [153–156] for a fixed or an uncertain design loading (see Fig. 5.1 and Fig. 3.4 (a) and (b)) as shown in Table 5.1. Laminated aerospace structures are, in general, subject to a combination of in-plane axial, transverse and shear load. As described in Section 5.2 (and in detail in Chapter 3), optimal laminate designs will efficiently distribute fibres to meet these loads producing a laminate with minimum elastic energy.

Standard angle ply designs are assumed to be balanced and symmetric $\overline{Q}_{16} = \overline{Q}_{26}$ = $B_{ij} = 0$ (i = 1,2,6; j = 1,2,6) and are described by two independent (and one dependent) ply percentage variables. NSA designs are described by three integer angle variables (between 0°-180°) and two independent ply percentage variables
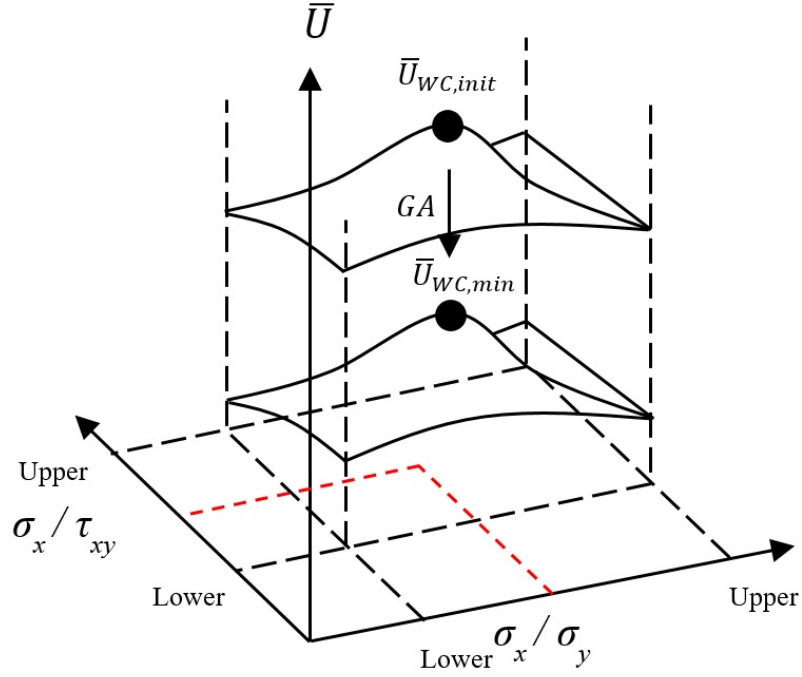
Figure 5.1: *Schematic of optimisation for an uncertain design loading using a Genetic Algorithm in combination with the Extreme Value theorem to find optimal designs under worst case loading.*

(γ_ψ and γ_ϕ) shown in Table 5.1. Each of the three main angles (ψ,ϕ,θ) within a NSA laminate is assumed to be made up of an infinite number of fully uncoupled blocks [93]. Each block [$+\theta/-\theta/$-$\theta/+\theta/$-$\theta/+\theta/+\theta/$-θ] is divided in half about the laminate mid-plane creating anti-symmetry. These blocks ensures $\overline{Q}_{16} = \overline{Q}_{26} = B_{ij} = 0$ (i = 1,2,6; j = 1,2,6) but are not a requirement as long as other stacking techniques can be used to maintain this condition. Note that variables are defined such that SA designs are a subset of NSA designs (excepting the symmetry of $\pm 45°$ plies for NSAs) and so an SA design could be returned in an NSA optimisation run if it is the optimal laminate design. Two pairs of $\pm$ non-standard angles, as seen in Chapter 4, will provide the same levels of optimal stiffness as per in-plane lamination parameters but was not considered due to a desire to compare similar SA and NSA stacks, which have three unique angle magnitudes [61,158]. To have a general view of design results, applicable to range of thicknesses, discrete ply stacking sequences are discarded in favour of continuous ply percentages. However, there is a disadvantage in that some designs will not be discretisable into standard ply thicknesses (depending on total laminate thickness) and thus realistic optimality and weight saving will be inconclusive for load cases where competing design strategies produce laminates with little difference in performance.
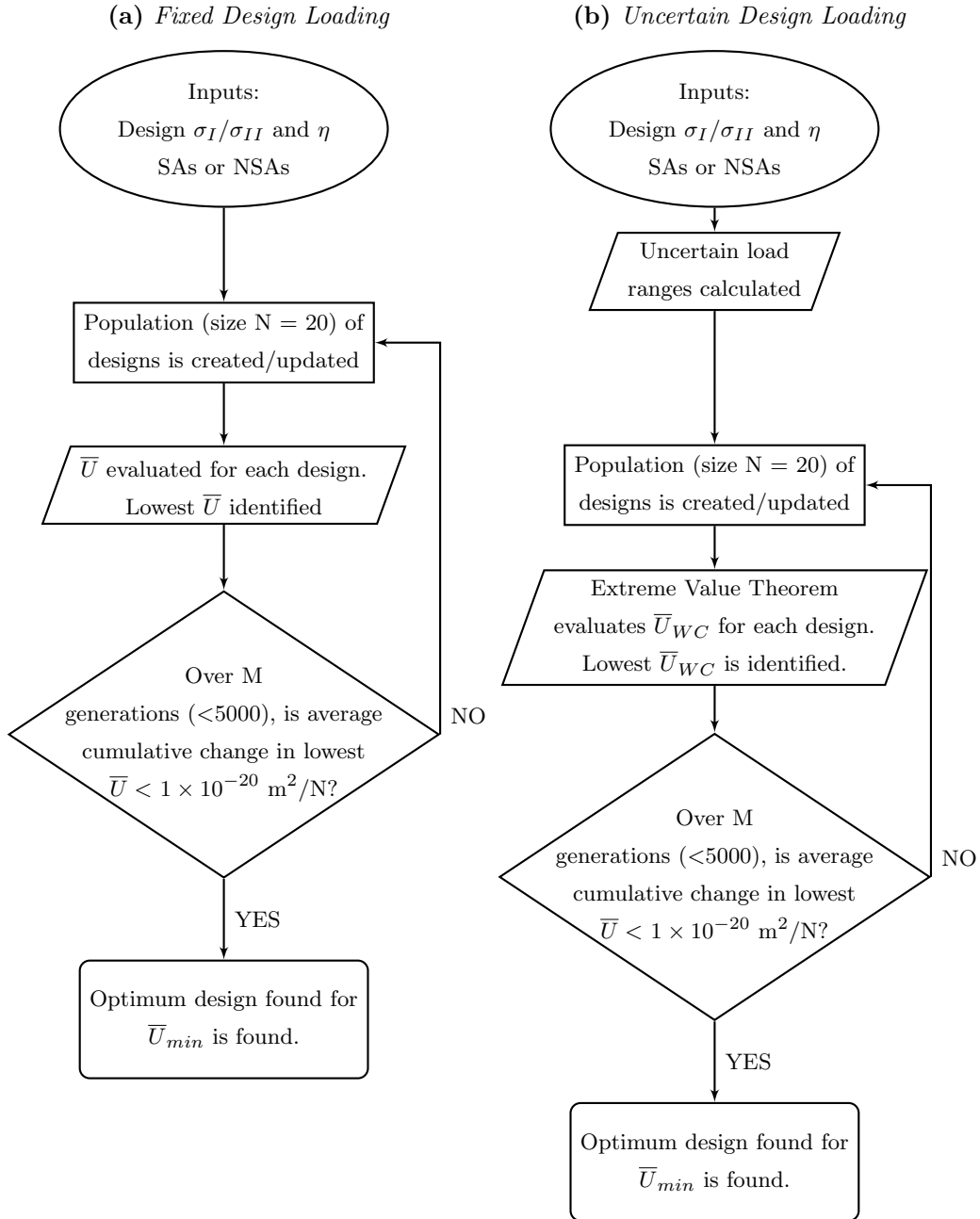
Figure 5.2: *Optimisation procedure for design of a laminate for minimum elastic energy under (a) a fixed design loading and (b) an uncertain design loading.*

Design strategy ID	Angles (integer °)	Ply %'s	Design Load	10% Rule	Ply Unblocking Rule
SA1	0, ±45, 90	γ_0, γ_{45}, 1-($\gamma_0 + \gamma_{45}$)	Fixed	✓	✓
NSA1	±ψ, ±φ, ±θ	γ_ψ, γ_ϕ, 1-($\gamma_\psi + \gamma_\phi$)	Fixed	✗	✓
SA2	0, ±45, 90	γ_0, γ_{45}, 1-($\gamma_0 + \gamma_{45}$)	Uncertain	✗	✓
NSA2	±ψ, ±φ, ±θ	γ_ψ, γ_ϕ, 1-($\gamma_\psi + \gamma_\phi$)	Uncertain	✗	✓

Table 5.1: *Details of four design strategies considered in the laminate design optimisation, angle variables, ply percentages variables and active design rules.*

5.3.4 Laminate Design Rules

Design rules are applied to laminates in order to account for failure mechanisms not directly optimised for and to ensure favourable deformation which may not be taken care of during the optimisation [157]. The two extra design rules, in addition to the requirement of $\overline{Q}_{16} = \overline{Q}_{26} = B_{ij} = 0$, are:

(i) Ply unblocking: To prevent the formation of large interlaminar shear stresses that may drive free-edge failure, and thermal stresses that could cause premature failure, a maximum of 4-6 or 1mm of contiguous plies of the same/similar orientation is allowed [157]. In SA designs, compliance is ensured by requiring that the ply percentages of the non-dominant 0° or 90° plies summed with the ±45° plies, equal at least one quarter of the dominant 0° or 90° ply percentage, e.g. for every four dominant plies there is one ply that differs by at least 45°. In NSA designs, ply groups of similar angles are assumed to be unblocked by an angular separation of at least 22.5°. The GA can choose between two techniques to find an optimal design:

   (a) Use of higher angles (| ±θ | ≥ 22.5°) to unblock dominant lower angles (| ±θ | < 22.5°) and vice versa (| ±θ | ≤ 67.5° unblock | ±θ | > 67.5°). As for SAs, a maximum ratio of 4:1 for dominant to non-dominant ply angles is maintained. The angles used to unblock are assumed to be placed in a fashion that is symmetric and balanced, maintaining $\overline{Q}_{16} = \overline{Q}_{26} = B_{ij}$ = 0.

   (b) Where ply percentages of the two non-dominant angles are too low to meet unblocking requirements in (a) all plies with | ±θ | < 22.5° or > 67.5° associated with the maximum ply percentage are swapped for ±22.5° or ±67.5° as appropriate.

(ii) 10% minimum ply percentage: In current SA laminate design practice, a 10% minimum of each of 0°, +45°, -45° and 90° ply angles safeguards against uncertainty in loading (SA1, Table 5.1). This rule is enforced for SA1 designs by limiting the choice of ply percentages available to the GA. No convention for enforcing this rule on NSA designs exists. Instead, here, the optimisation procedure in Section 5.3.6 designs directly for uncertainty in loading. This procedure is applied in both SA and NSA design strategies, see SA2 and NSA2 in Table 5.1.

5.3.5 Design Loading and Principal Loading Misalignment

SA laminates are normally restricted to a fixed manufacturing (x, y) coordinate system about which laminates are balanced (for example, 0° fibres are aligned from root to tip in a wing skin) [157]. In both SA and NSA laminates, an equal number of positive and negative angle plies ensures designs are balanced about the (x,y) axes, see Fig. 5.3. All general load states can be described by their principal loading and a misalignment angle, η, from the (x,y) balancing axes, see Fig. 5.3. For example, $\eta = \pi/4$ indicates a state of pure shear is applied in the balancing axes. $\eta = 0$ is also a special case where the principal loading axes are aligned with the balancing axes, see Fig. 5.3 (b). This is generally not the case in design as balancing axes are usually aligned with the laminate manufacturing axes. However, balance can theoretically be achieved in axes other than the manufacturing axes, such as the principal axes, thereby achieving $\eta = 0$. In the results that follow 257 principal loading ratios, σ_I/σ_{II} (from ∞ to -∞), and 513 principal axes misalignments, η (from $\pi/2$ to -$\pi/2$), are considered creating 131,841 different design loading scenarios.

A designer with a given design loading in the laminate axes (x,y), described by the ratios between, or magnitudes of, the three stresses σ_x, σ_y and τ_{xy}, can, using Eq. 5.2 and Eq. 5.3 respectively, convert this loading into the principal loading ratio σ_I/σ_{II} and misalignment angle η. To convert any (x, y) design load or ratio into a principal design load (and a value of η) arbitrary values of (x, y) stress in the correct ratio (the absolute values are irrelevant) should be input into Eqs. 5.2 and 5.3 and the quotient of the result taken to produce σ_I/σ_{II}.
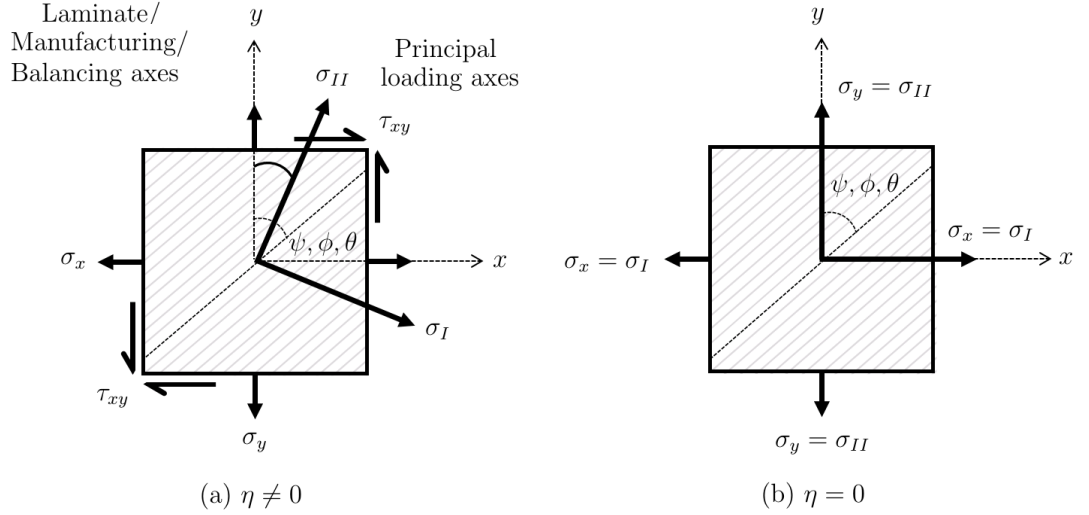
Figure 5.3: (a) Diagram showing laminate (x, y) axes (from which ply angles (ψ, ϕ, θ) are defined and balanced) and principal loading axes offset from balancing axes by angle η. For (b) $\eta = 0$ and thus the balancing axes are aligned with the principal loading axes.

When considering the results that follow in Section 5.4, it may help the reader to know the design loading in the laminate axes (x, y) for a given σ_I/σ_{II} and η, as these latter variables form the plot axes. The (x, y) stresses can determined using Eqs. 5.4-5.6 with arbitrary values of σ_I and σ_{II} in the correct ratio.

$$\sigma_x = \frac{(\sigma_I + \sigma_{II})}{2} + \frac{(\sigma_I - \sigma_{II})}{2} \cos 2\eta \tag{5.4}$$

$$\sigma_y = \frac{(\sigma_I + \sigma_{II})}{2} - \frac{(\sigma_I - \sigma_{II})}{2} \cos 2\eta \tag{5.5}$$

$$\tau_{xy} = -\frac{(\sigma_I - \sigma_{II})}{2} \sin 2\eta \tag{5.6}$$

5.3.6 Optimisation using Genetic Algorithm

A Genetic Algorithm (GA) which optimises either (i) two thicknesses or (ii) two thicknesses and three ply angle variables, describing the SA and NSA designs (see Table 5.1) respectively, was used to obtain minimum normalised elastic energy under multiple fixed ($\overline{U}_{min}$) and uncertain ($\overline{U}_{WC,min}$) multi-axial design loadings (σ_I/σ_{II} and η), see Fig 5.1. The GA creates an initial random population (of size N = 20) of candidate design variables and calculates a scored fitness value for each (all meet design constraints as per Section 5.3.4). The lowest energy designs are chosen and used to determine the next generation/population of design variables. Eliteness, crossover and mutation all feature in 'ga' [153]. Iteration continues until the stopping criteria of (i) a maximum number of iterations reaches 5000 or (ii) the change in

the normalised elastic energy value between iterations is less than 1×10^{-20} m^2/N. (Note that none of the results below were derived as a consequence of the maximum number of iterations limit being reached). Runs for all 131,841 different design loadings considered took approximately 2-3 hours.

5.4 Results

In the results that follow material properties of $E_{11} = 128$ GPa, $E_{22} = 10$ GPa, $G_{12} = 4.5$ GPa, $\nu_{12} = 0.3$ for AS4/8552 are assumed. General design loadings (σ_x, σ_y and τ_{xy}) are represented by the ratio of principal stresses, σ_I/σ_{II}, and the misalignment of the balancing axes from the principal loading axes, η, (established from σ_x, σ_y and τ_{xy} via Mohrs Circle, see Eqs. 5.2 and 5.3). However, initially in Figs. 5.4 and 5.5, to aid the reader in understanding the results, η is given two fixed values (0 and $\pi/8$ rad) with later results showing a continuous variation in η. $\eta = \pi/8$ radians describes the loading conditions of equal magntiude in N_x, N_y and N_{xy}. This is the least optimal loading condition to design for as fibres must be evenly spread to carry this load, reducing the efficiency of fibres in any one direction. Figures 5.4 (a) and (b) show ply percentages for optimum SA designs under a fixed loading i.e. 0% uncertainty of input loading is considered. Similarly, Figs. 5.4 (c) and (d) show optimum designs related to the NSA1 design configuration in Table 5.1. Figures 5.4 (e) and (f) demonstrate the effect of design rules using SAs or NSAs on the normalised elastic energy of optimised laminates under their design loadings including the energy of designs presented in Figs. 5.4 (a-d). Low energy is indicative of more efficient use of material.

(a) $\eta = 0$

(b) $\eta = \pi/8$

(c)

(d)

Uni-axial   Pure   Transverse   Equal   Uni-axial

Shear   Uni-axial   Bi-axial

$\eta = \frac{\pi}{4}$ σ_I/σ_{II}
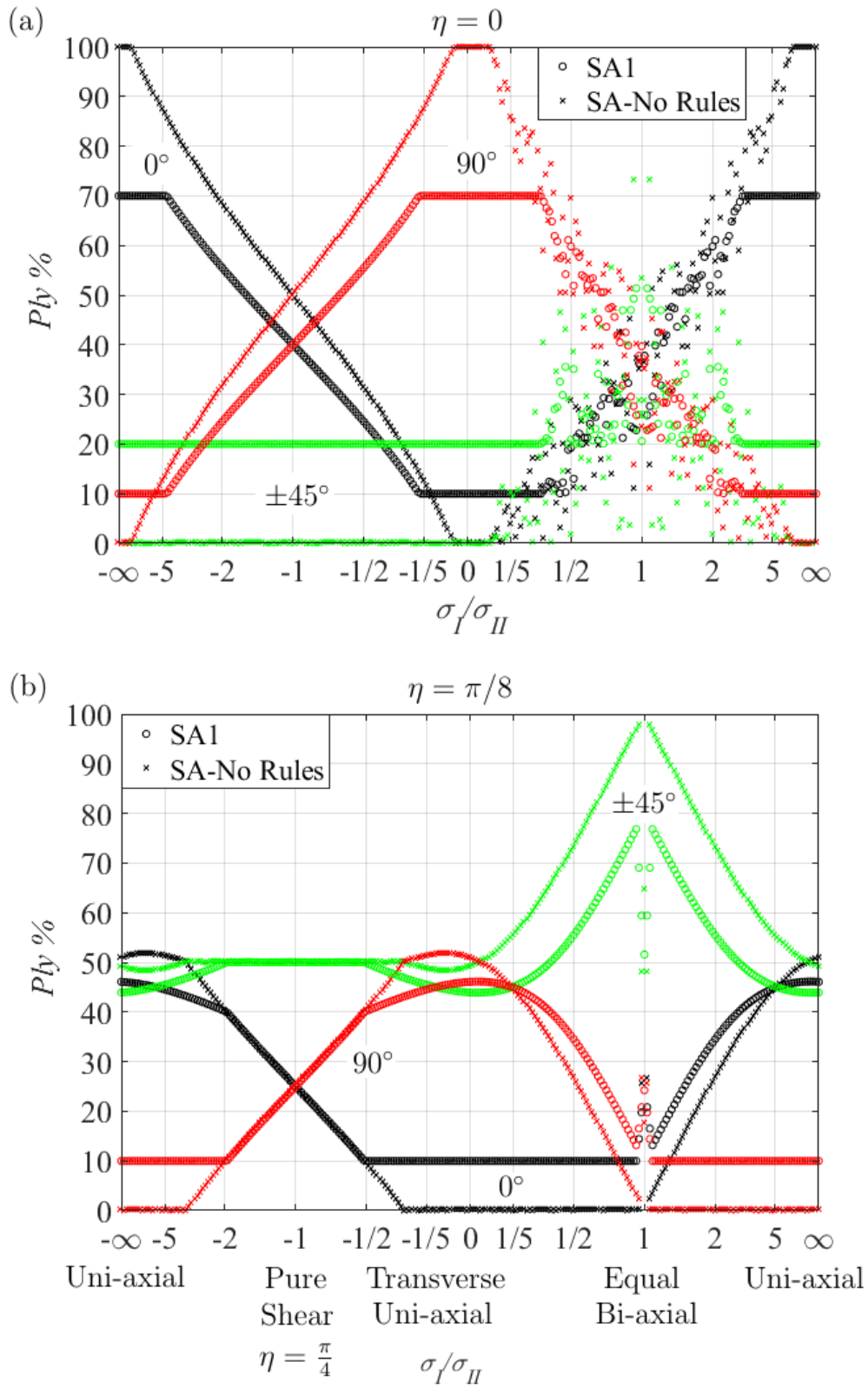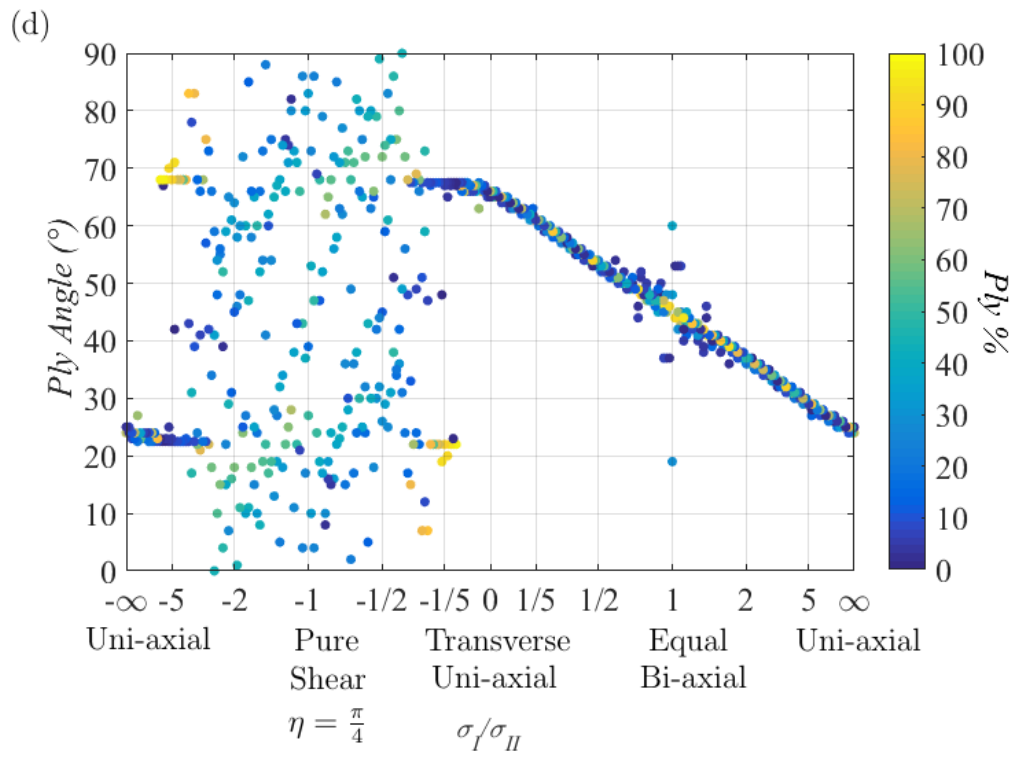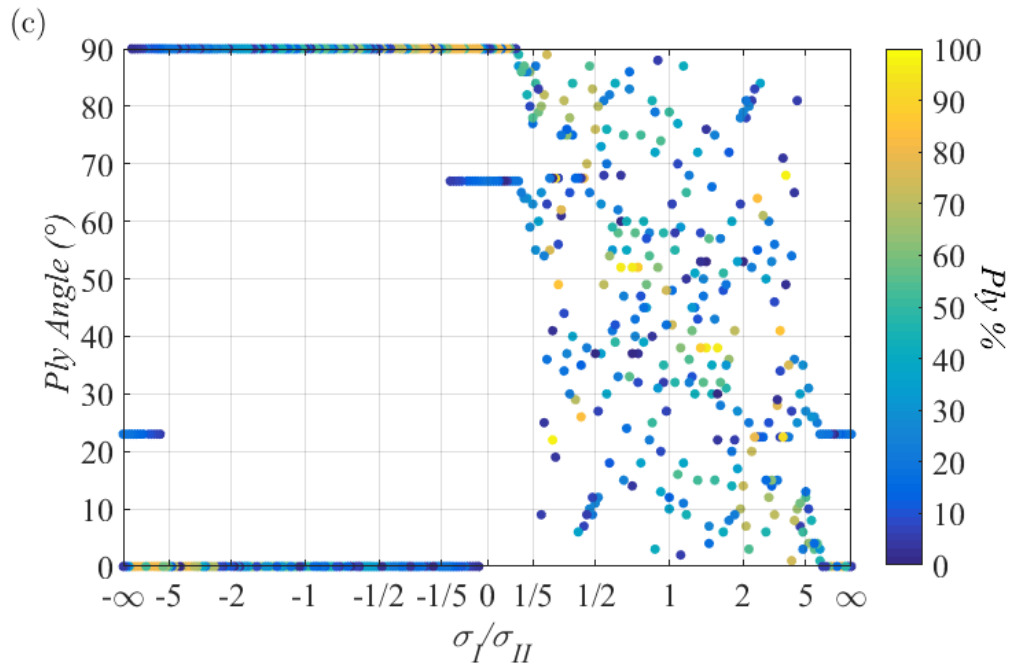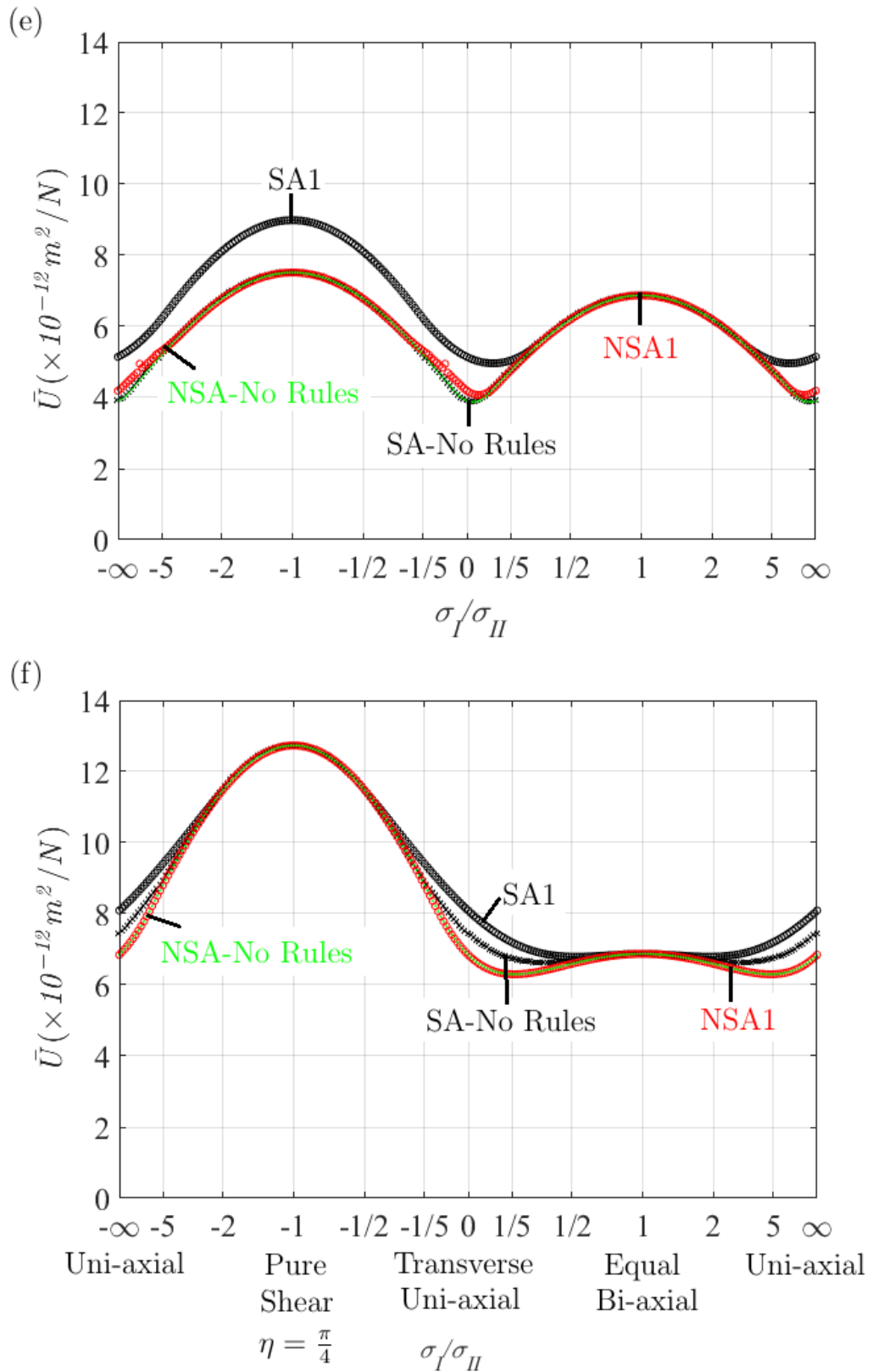
Figure 5.4: *SA ply percentages for optimum minimum elastic energy designs under a fixed loading are given for (a) η= 0 and (b) η = π/8. Cross (circle) markers indicate unconstrained (constrained SA1) laminates. NSA ply angles and percentages for optimum NSA1 designs are given for (c) η= 0 and (d) η = π/8. Normalised elastic energy of minimum elastic energy laminates, $\overline{U}$, with standard and non-standard ply angles for loadings with (e) η = 0 and (f) η = π/8.*

Figures 5.5 (a), (b), (c) and (d), show, respectively, the normalised elastic energies of optimised laminates, for each of the four design strategies SA1, NSA1, SA2 and NSA2 (see Table 5.1), under a worst case loading applied within the range of loading uncertainty that exists for each design loading ($\pm 10\%$ or $\pm 20\%$).
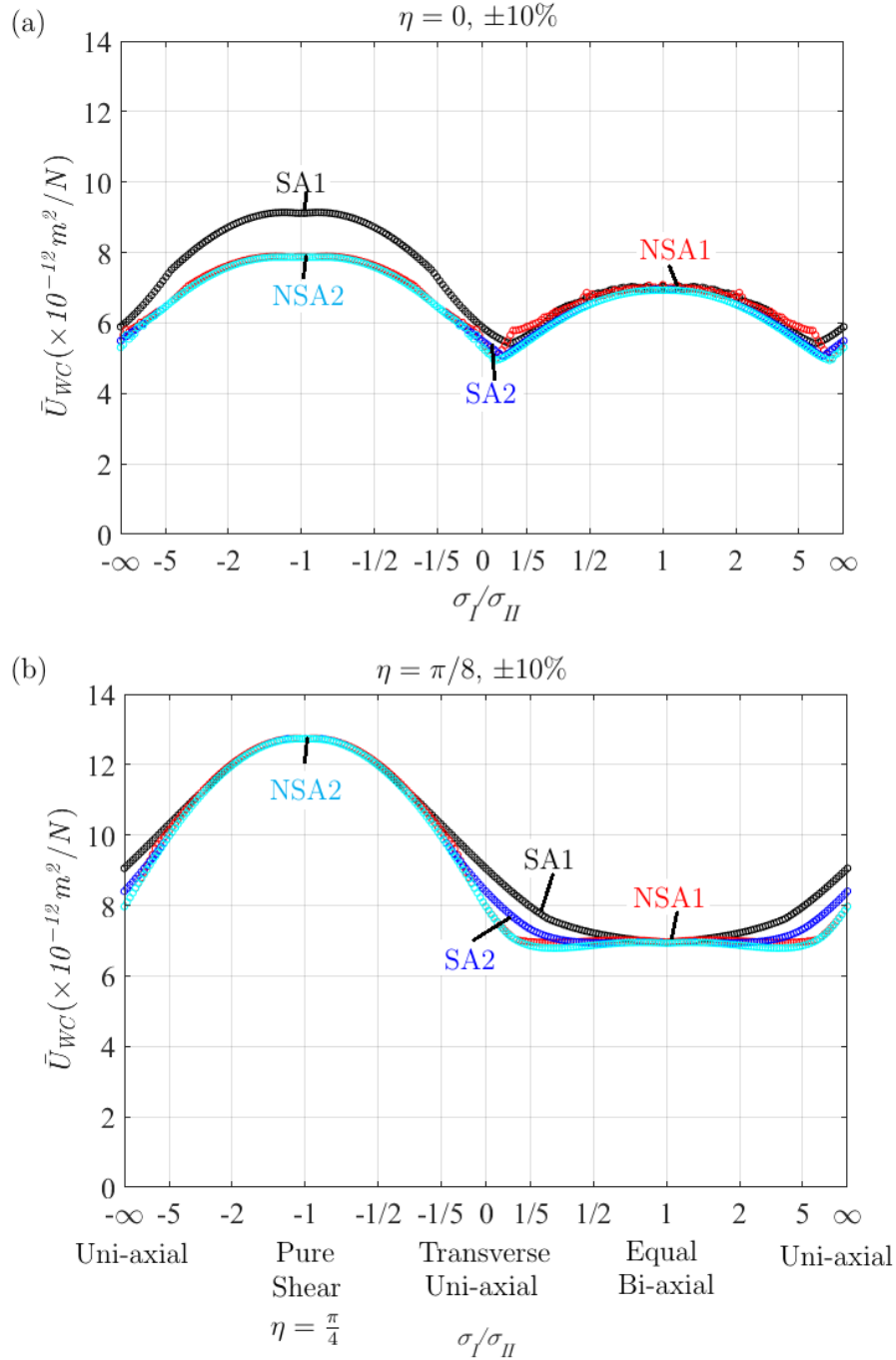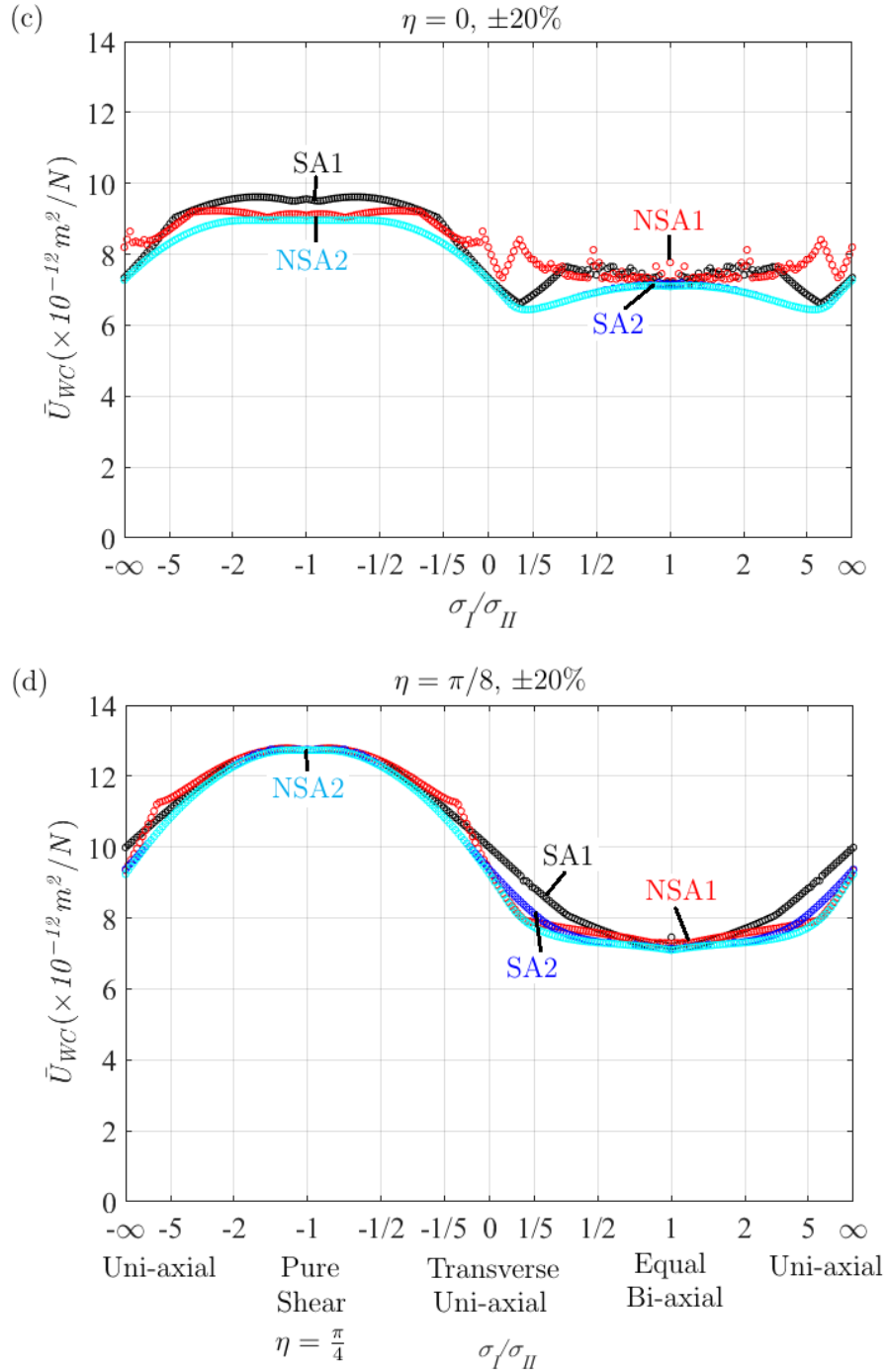
Figure 5.5: *(a-d) Variation in the worst case normalised elastic energy,* $\overline{U}_{WC}$ *designs subject to* $\pm 10\%$, *(a-b) or* $\pm 20\%$ *(c-d) uncertainty in design load (see Section 5.3) for* $\eta = 0$ *or* $\pi/8$.

In Figs. 5.6 (a)-(d), η is allowed to vary continuously. Individual points represent an optimised laminate design and are coloured according to the normalised elastic energy produced when the worst case loading derived from an uncertainty of $\pm 10\%$ is applied. Figures 5.6 (a), (b), (c) and (d) provide results for design strategies SA1, NSA1, SA2 and NSA2 (see Table 5.1) respectively.
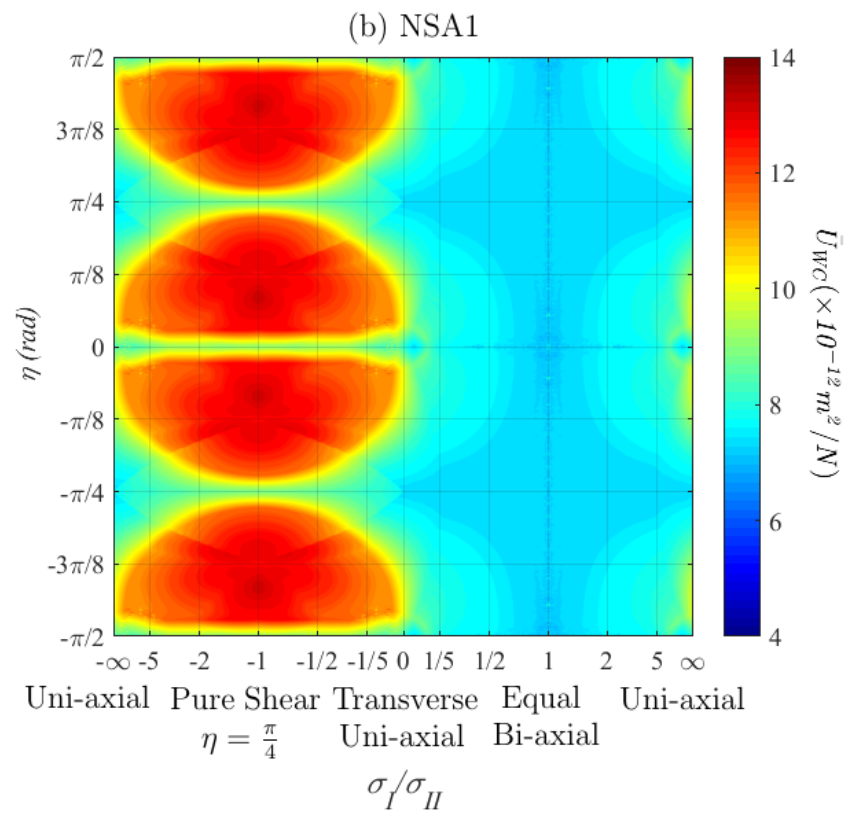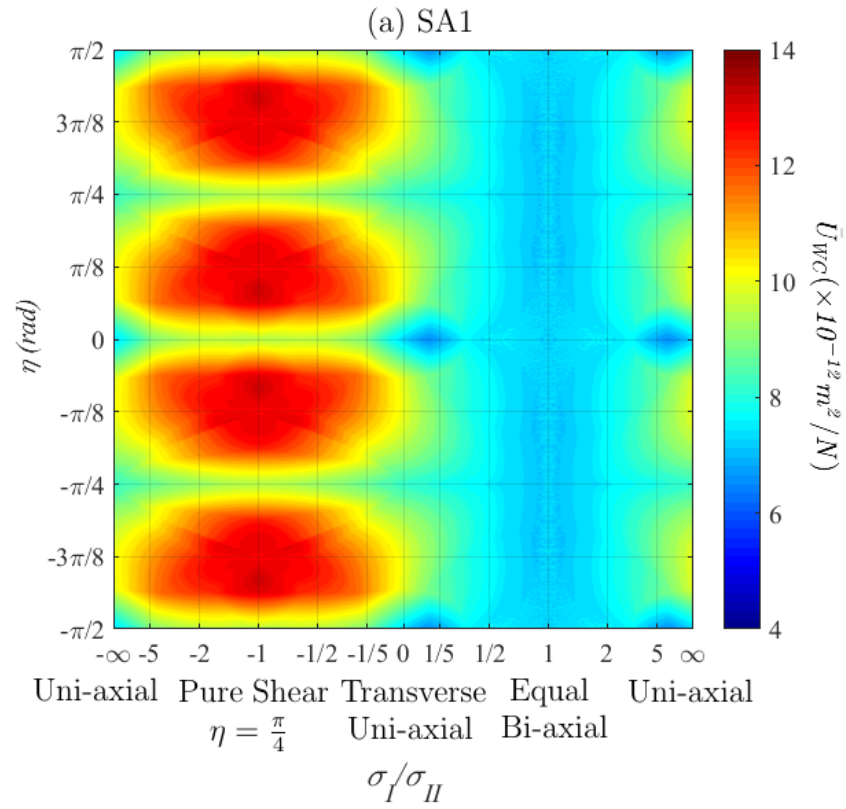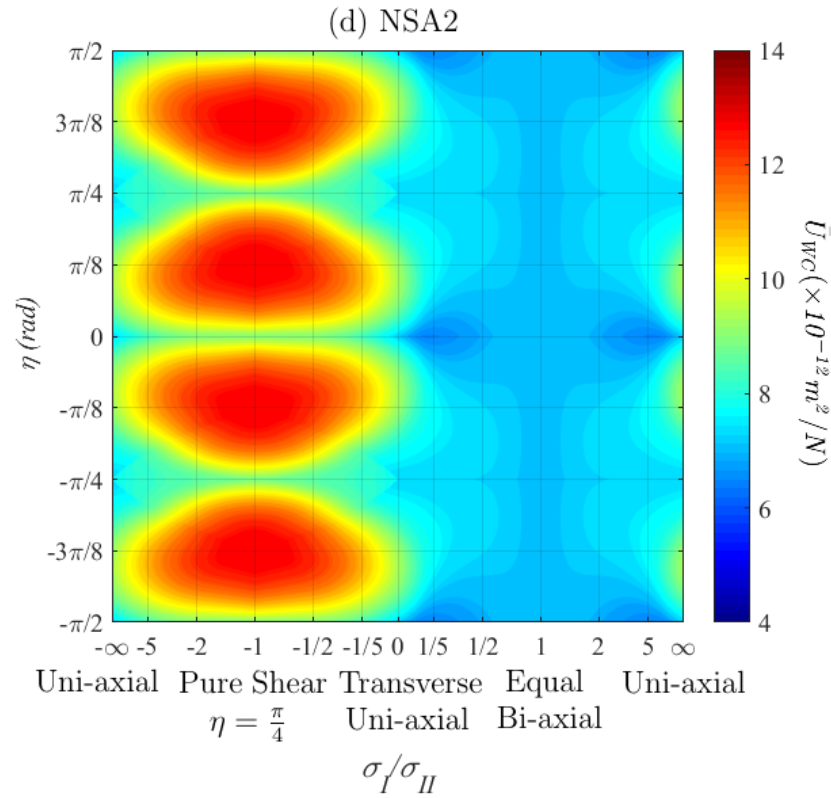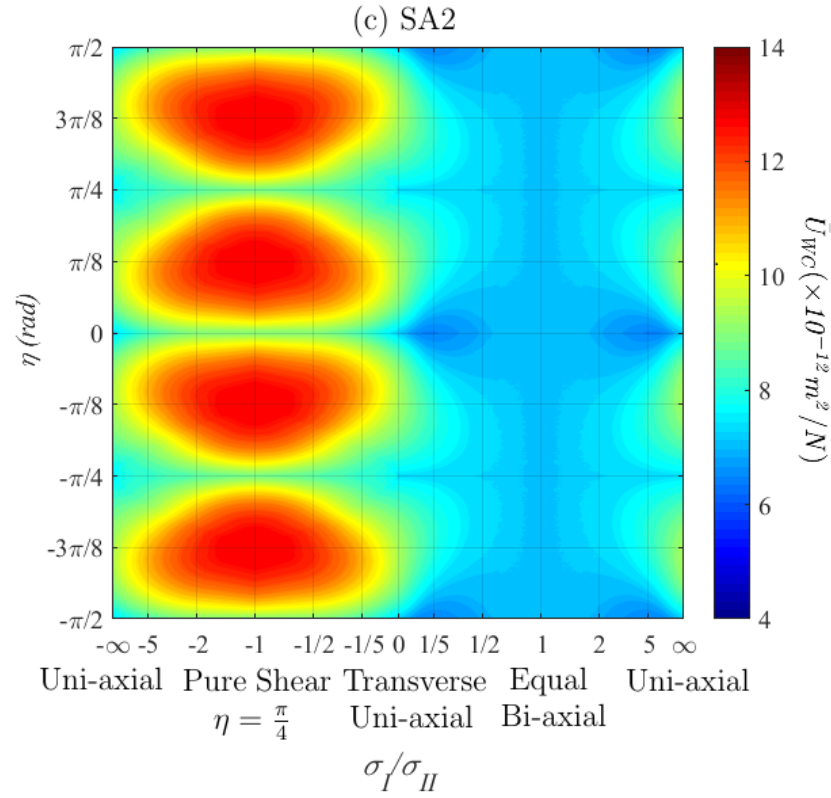
(a) SA1

(b) NSA1

Figure 5.6: *Laminate normalised elastic energies (Eq. 5.1) under worst case loading for a range of general design loadings described by σ_I/σ_{II} and η eith $\pm 20\%$ uncertainty. (a) SA1: 10% minimum ply percentage rule accounts for load uncertainty. (b) NSA1: no load uncertainty considered. (c) SA2: no 10% rule, designed directly for load uncertainty. (d) NSA2: designed directly for load uncertainty.*

(a) 0°

(b) ±45°

(c) 90°

Uni-axial   Pure Shear   Transverse   Equal   Uni-axial
           $\eta = \frac{\pi}{4}$ Uni-axial   Bi-axial

σ_I/σ_{II}

(d) ψ

(e) ϕ

(f) θ
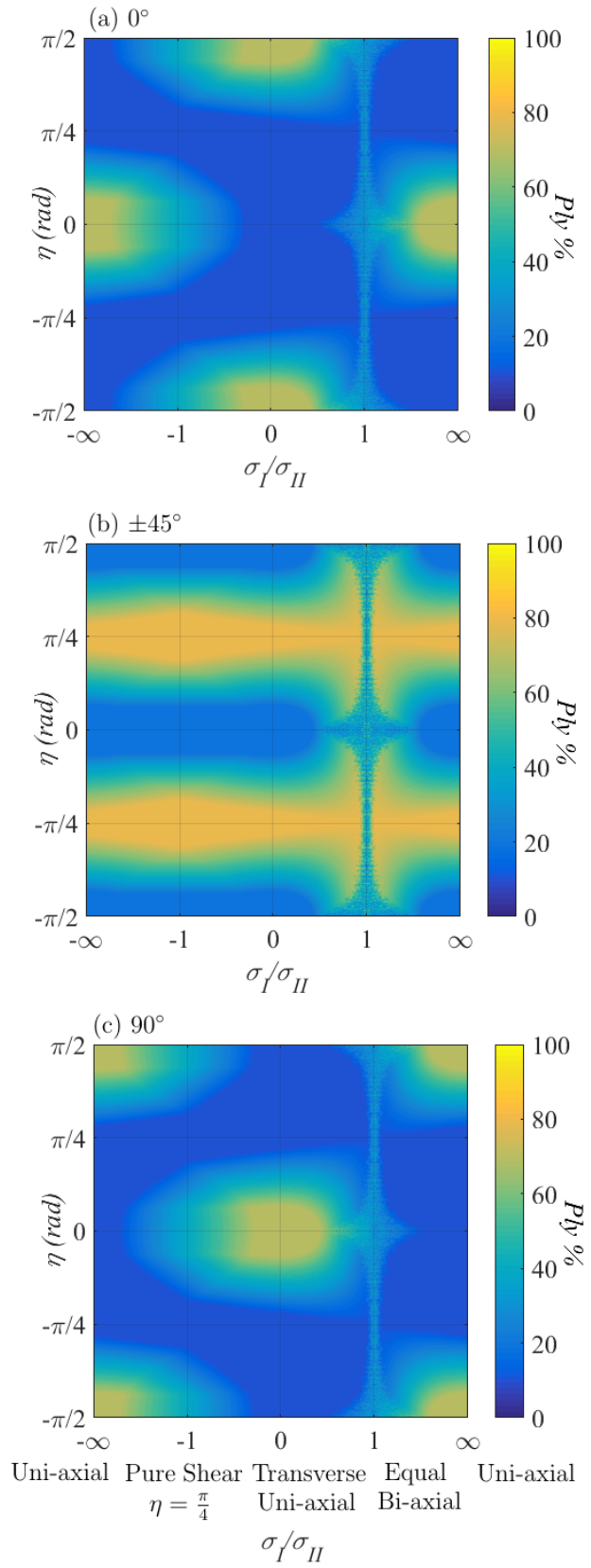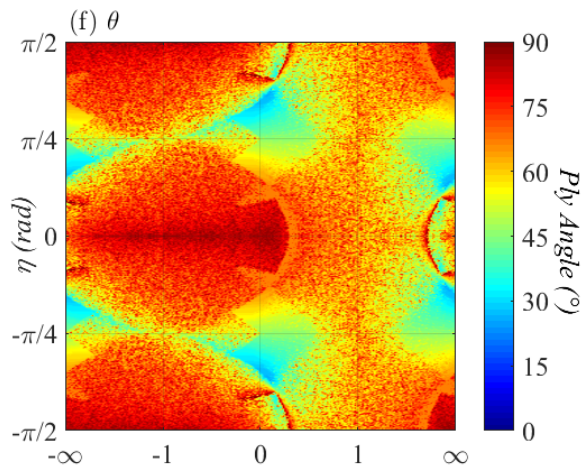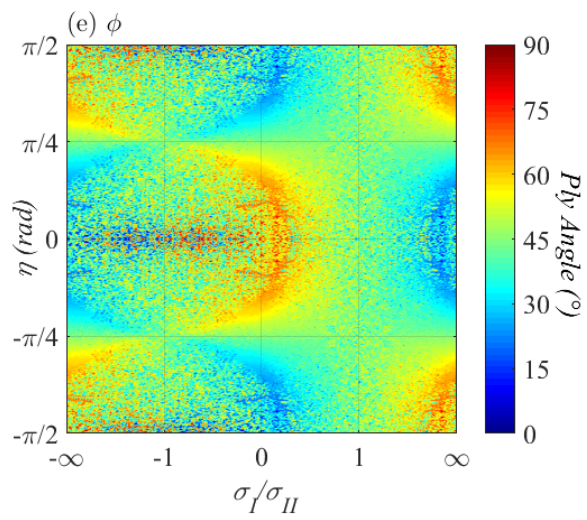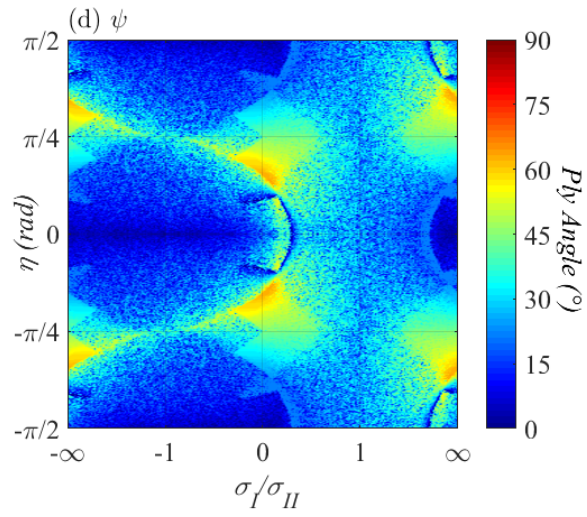
Uni-axial   Pure   Transverse   Equal   Uni-axial
             Shear   Uni-axial   Bi-axial
$\eta = \frac{\pi}{4}$

σ_I/σ_{II}
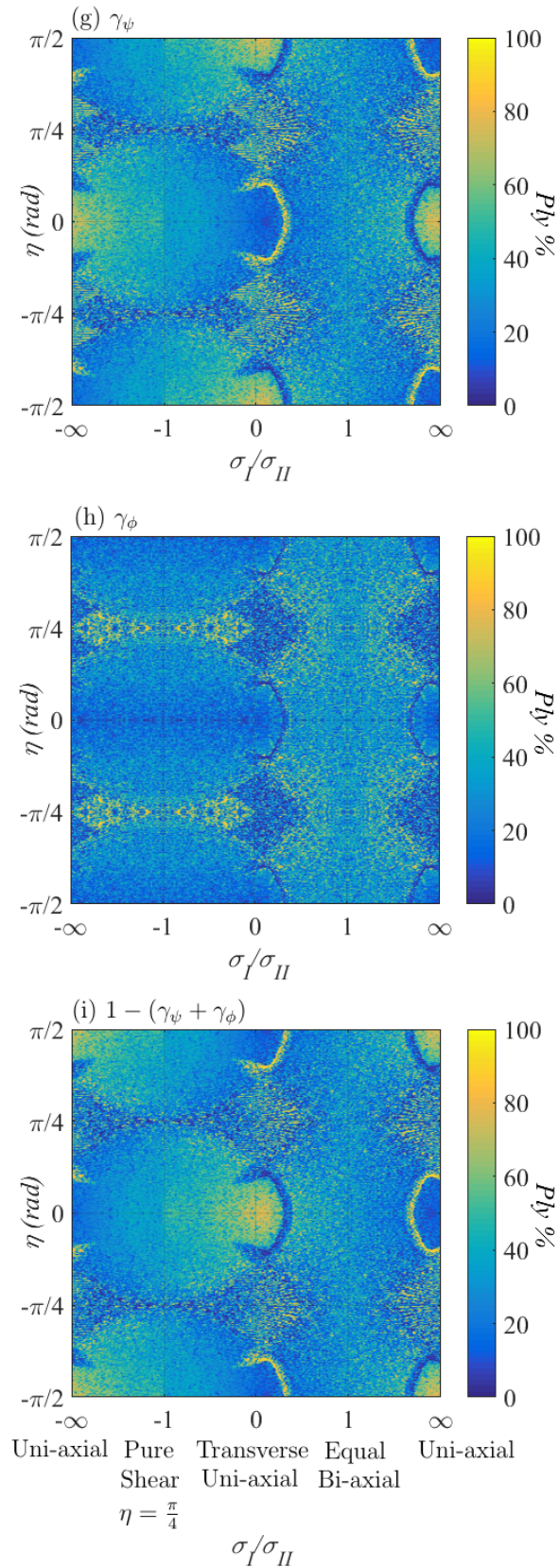
Figure 5.7: *Percentages of (a) 0°, (b) ±45° and (c) 90° plies in SA1 design of Figure 5.6 (a) where a 10% minimum ply percentage rule accounts for load uncertainty. Ply angles lowest to highest (d-f) and related ply percentages (g-i) respectively for NSA2 designs of Figure 5.5 (d) where ±20% uncertainty in loading is designed for, see Section 5.3.*

Figure 5.7 shows ply angles and ply percentages for optimum laminate designs derived from the SA1 (current practice) and NSA2 (strategy with greatest potential) design strategies under the worst case loadings seen in Figs. 5.6 (a) and (d) respectively. Angle variables for NSA2 designs are ordered such that the lowest magnitude of angle (e.g. 0°) is associated with the uppermost plots Fig. 5.7 (d) and (g), and the highest (e.g. 90°) with the lowermost plots Fig. 5.7 (f) and (i).

(a) SA2 vs SA1
±10% Load Uncertainty

(b) SA2 vs SA1
±20% Load Uncertainty

(c) NSA2 vs SA1
±10% Load Uncertainty

(d) NSA2 vs SA1
±20% Load Uncertainty
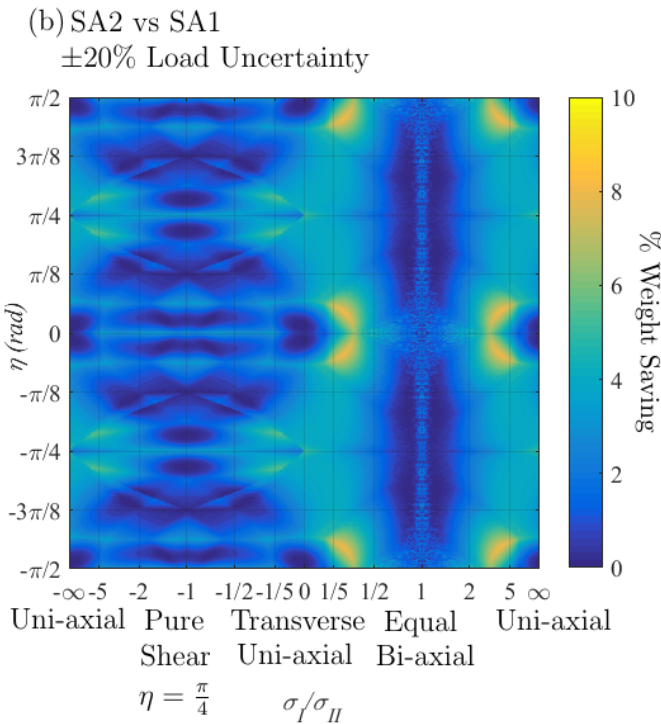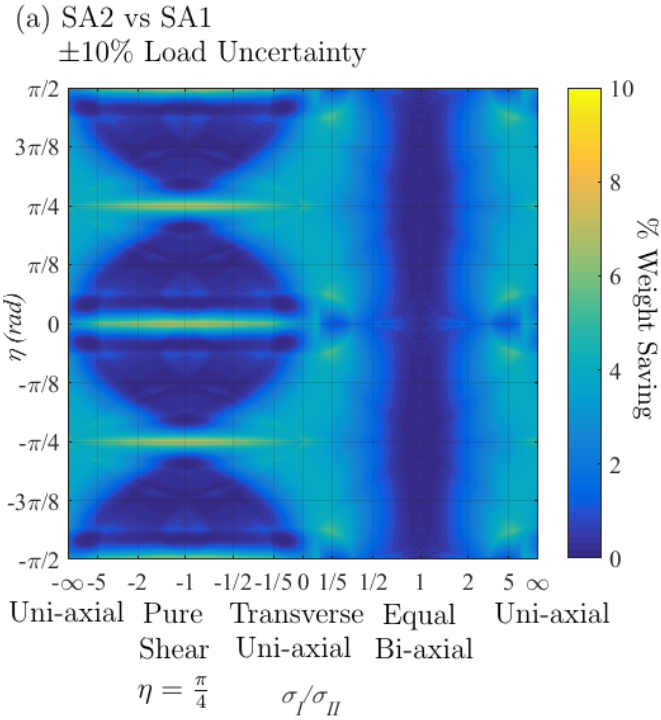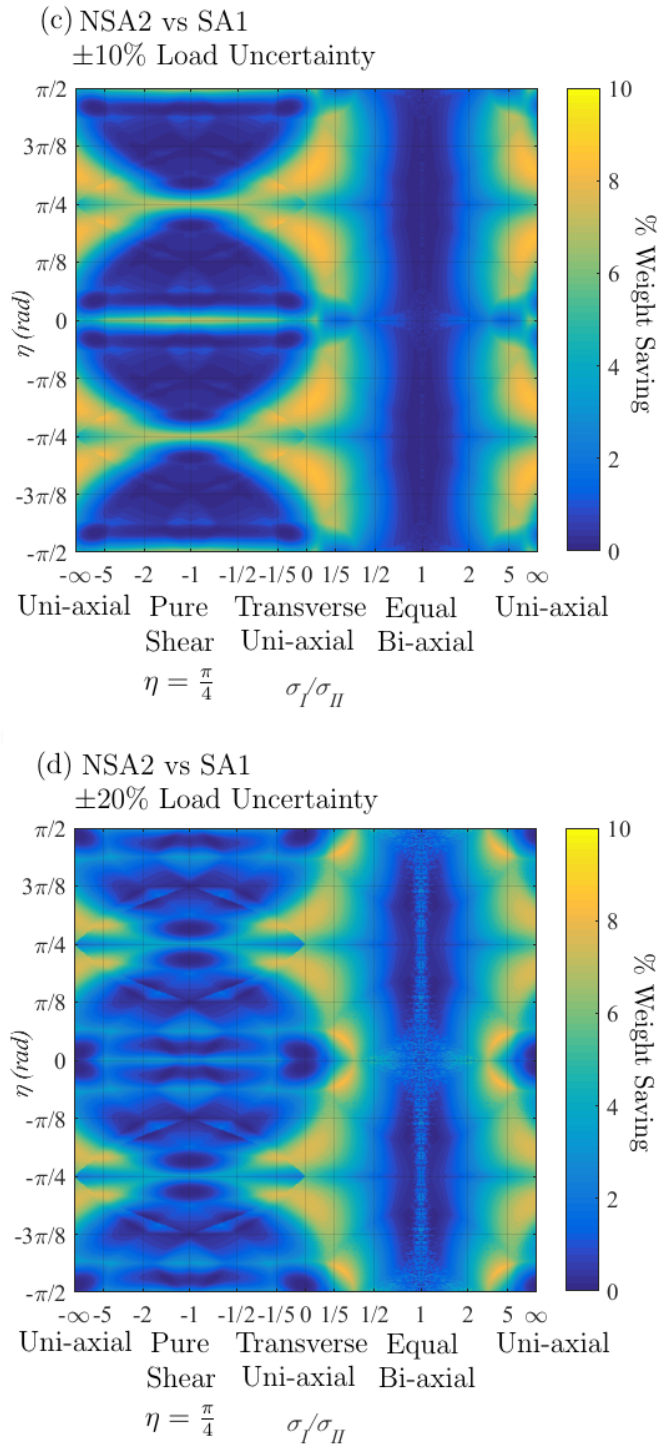
Figure 5.8: *Weight savings derived from different design strategies for variable η and design loadings described by σ_I/σ_{II} with an uncertainty of ±10% or ±20%. (a) and (b) percentage weight saving of an SA2 strategy over an SA1 strategy, (c) and (d) percentage weight saving for an NSA2 strategy over an SA1 strategy. (e) and (f) percentage weight saving for an NSA2 strategy over an SA2 strategy.*

Figure 5.8 shows weight saving plots illustrating differences in $\sqrt{\overline{U}_{WC}}$ for different design strategies. Plots are derived for both ±10% and ±20% uncertainty by subtraction of values for one design strategy from another. SA2 is compared to

SA1, NSA2 to SA1 and NSA2 to SA2 shown in Figs. 5.8 (a-b), (c-d) and (e-f), respectively.

Figure 5.9 is constructed by plotting the percentage difference between maximum and minimum values for $\sqrt{\overline{U}_{WC}}$ that fall on any vertical line in Fig. 5.6 (a). Minimum $\sqrt{\overline{U}_{WC}}$ occurs for $\eta = 0$ and maximum values occur for some worst case value of η. Thus Fig. 5.9 indicates maximum weight savings that can be obtained for an SA1 and NSA2 design strategy if, in a notional design problem, balancing axes were realigned from some worst case alignment to the principal loading axes.
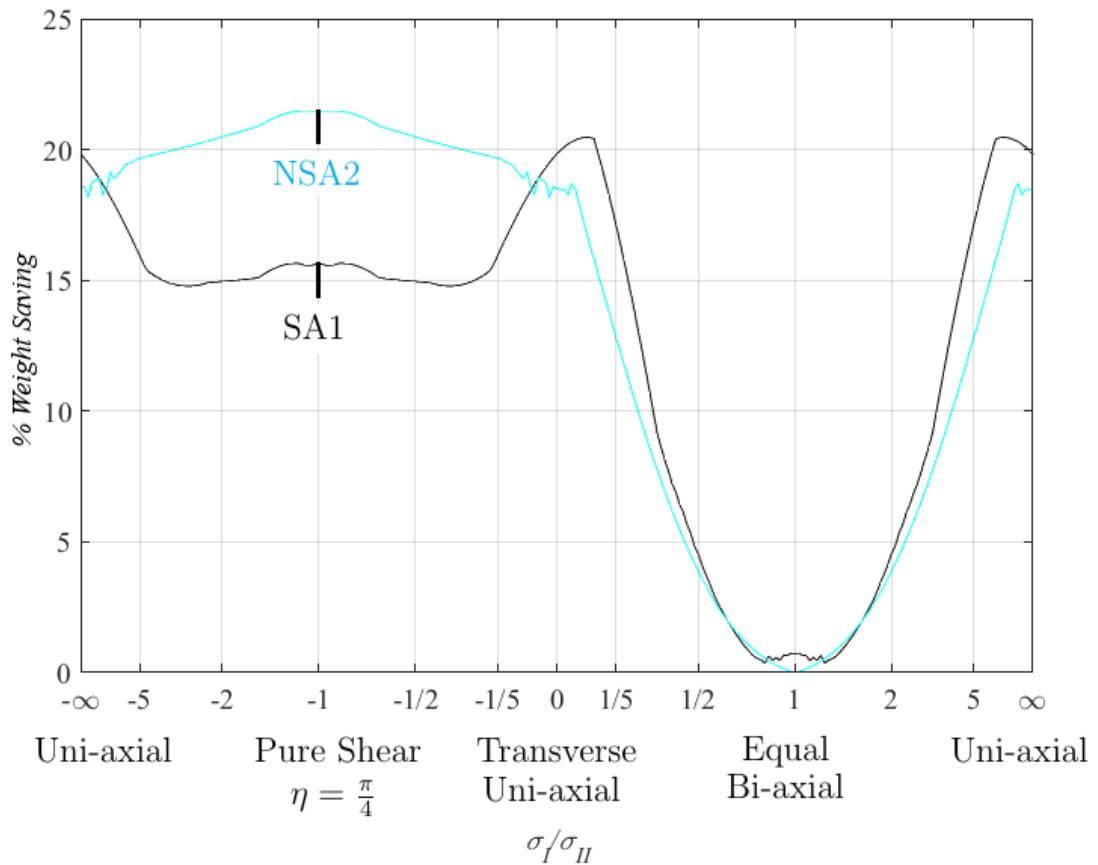
Figure 5.9: *Weight saving from balancing laminates in the principal loading axes, $\eta = 0$, compared to balancing at the worst misalignment from the range of possible η, for all σ_I/σ_{II} design loading ratios using the SA1 and the NSA2 strategies when a loading uncertainty of $\pm 10\%$ is applied.*

5.5 Discussion

It is noted that the approach of equating minimum in-plane energy with improved performance/minimum weight is only applicable to laminates that fail via in-plane fibre based mechanisms. No attempt is made to account for damaged based failures or structural failures such as buckling. Furthermore, designs presented are formed from continuous ply percentages and thus results are more representative of thick laminates (or those made with thin plies) where a greater range of ply percentages is more achievable. This is compounded for NSA designs which rely on a fully uncoupled laminate structure [93] that might constrain the design space.

5.5.1 Energy extrema and the effect of misalignment of balancing and principal loading axes

Single axis loading and thus single axis optimal fibre orientations create energy minima, e.g. at $\sigma_I/\sigma_{II} \approx 0$ and ∞ in Fig. 5.4 (e). Minimum energy for all load ratios in Fig. 5.6 lies on lines of $\eta = 0 \pm \frac{n\pi}{2}$. This indicates that laminate design can be improved significantly by balancing laminates in the principal loading axes. Indeed, in Fig. 5.9 a maximum weight saving of 20% is possible at $\sigma_I/\sigma_{II} = 10.15$ or 0.99 when using the current, SA1, design practice and balancing laminates in the principal loading axes. As the variation in energy with η across the loadings in Fig. 5.6 is nonlinear, the realistic weight saving from employing this technique will highly depend on the original misalignment η, the σ_I/σ_{II} design load ratio and the uncertainty in loading considered. For example, near $\sigma_I/\sigma_{II} = 1$ the energy shows little variation with η in comparison to those near $\sigma_I/\sigma_{II} = $ -1, see also Fig. 5.9. Previous work has shown the effect of principal load ratio on potential weight saving when balancing about the principal loading axes [161]. Weight savings of up to 22% are possible when employing this technique when designing directly for the uncertainty using NSAs ($\sigma_I/\sigma_{II} = $ -1, NSA2).

Energy maxima or high weight designs for $\eta = 0$ (Fig. 5.4 (e)) occur where orthogonal principal stresses with equal magnitude ($\sigma_I/\sigma_{II} \approx 1$ and $\sigma_I/\sigma_{II} \approx $ -1) create the greatest difference in requirements for optimal stiffness. Indeed, Fig. 5.6 indicates that maxima continue to occur at $\sigma_I/\sigma_{II} \approx 1$ for any fixed η.

As is evident in Figs. 5.4 and 5.6, maxima in the vicinity of $\sigma_I/\sigma_{II} = $ -1 are larger than $\sigma_I/\sigma_{II} = 1$. This is a consequence of the sign of $2\,q_{12}\,\sigma_I\,\sigma_{II}$ in Eq. 5.1. The value of $2\,q_{12}\,\sigma_I\,\sigma_{II}$ is positive for $\sigma_I/\sigma_{II} < 0$ and thus is additive to the energy stored. Physically this is due to the softer laminate response to the compression-tension loading acting in the same direction as the laminate Poissons ratio deformation. Conversely for $\sigma_I/\sigma_{II} > 0$, the $2\,q_{12}\,\sigma_I\,\sigma_{II}$ term is negative resulting in lower en-

ergies and a stiffer laminate response due to loading acting against Poissons ratio deformation.

Comparison of Figs. 5.4 (e) and (f) shows that an increase in η from 0 to $\pi/8$ increases energy for all σ_I/σ_{II} ratios with the exception of hydrostatic ratios. For hydrostatic ratios alignment of principal load has no effect on loading present in the laminate axes due to equal loads being present in all directions. This increase is also seen in Fig. 5.6 as $\eta \to \pi/8$, and is a consequence of the $q_{33}\tau_{xy}$ term in Eq. 5.1 becoming non-zero with the introduction of a shear load component. Global maxima occur at $\eta = \pi/8, 3\pi/8$ where all design loads are the same magnitude and the axial and transverse loads have opposite sign ($\sigma_x = -\sigma_y = \tau_{xy}$). For these load ratios, design traits required to efficiently carry the three load components are in greatest conflict.

5.5.2 Minimum Energy design strategies and non-uniqueness of designs

Comparison of ply angles derived under $\pm 10\%$ loading uncertainty, using SA1 (Fig. 5.7 (a)-(c)) and NSA2 (Fig. 5.7 (d)-(i)) strategies indicate, irrespective of design strategy, $0°$, $90°$, $\pm 45°$ plies dominate if the loading is axially, transverse or shear dominated, respectively. For example, for $\sigma_I/\sigma_{II} = 0$ and $\eta = 0$ in Fig. 5.7 (c), (f) and (i) laminates with high proportions of $90°$ plies are optimal. Similarly, a comparison of Figs. 5.4(a) and (c) shows $0°$ and $90°$ plies are optimal in both SA and NSA designs when $\sigma_I/\sigma_{II} < 0$ and $\eta = 0$. This is a consequence of (i) a positive $2q_{12}\sigma_I\sigma_{II}$ term in Eq. 5.1 penalising the use of other angles with higher Poissons ratios (which produce large negative q_{12} terms) and (ii) $0°$ and $90°$ plies minimising the energy storage associated with a softer laminate response. In Fig. 5.4 (c) and (d), regions where straight horizontal lines appear at angles of $22.5°$ and $67.5°$ show clearly the effect of the ply unblocking rule from Section 5.3.4 preventing laminates from having too high a proportion of low ($|\pm\theta| < 22.5°$) or high ($|\pm\theta| > 67.5°$) angles that would normally be desired from an energy minimisation standpoint. When $\sigma_I/\sigma_{II} < 0$ plots in Figure 5.7 show that as η tends from 0 to $\pi/4$, and thus loading in the balancing axes moves from purely bi-axial to including large proportions of shear, optimum plies transition from purely $0°$ and $90°$ to mostly $\pm 45°$ for both SA and NSA designs.

In contrast to the above, for $\sigma_I/\sigma_{II} > 0$ in Fig. 5.4 (a) and (c) and $\eta = 0$ in Fig. 5.7 (d-i), the optimality of designs with $\pm 45°$ and $\pm\theta$ angles can be seen. The Poissons ratio increases brought about by these ply angles result in larger negative q_{12} and act to increase the effective laminate stiffness for $\sigma_I/\sigma_{II} > 0$ thereby decreasing the energy stored. This is not true when $\eta = \pi/8$ near $\sigma_I/\sigma_{II} = 0$ and ∞ in

Fig. 5.4 (f). Here $q_{33} \tau_{xy} \neq 0$ in Eq. 5.1, as shear appears in the design loading, and optimal laminate stiffnesses are achieved by NSAs but not SAs which can only seek to minimise energy with non-optimal $\pm 45°$ angles (contrast Figs. 5.4 (b) and (d)). For example, $\pm 30°$ and $\pm 60°$ designs seen in Fig. 5.4 (d) produce laminate stiffnesses that are unachievable by SAs in Figs. 5.4 (b) [61].

Taking an example for close to maximum weight saving of 7.71% at $\sigma_I/\sigma_{II} = -1/5$ and $\eta = 7\pi/32$ in Fig. 5.8 (c) of the NSA2 technique over SA1, the current practice, the general loading can be found: $N_x/N_y = 0.55$ and $N_x/N_{xy} = -0.48$. For this loading the optimal NSA layup is 100% $\pm 54°$ and the SA layup is a 10/80/10. These would create 20 ply stacks of $[54/-54/-54/54/-54/54/54/-54/54/-54//54/-54/54/-54/-54/54/-54/54/54/-54]$ for a NSA layup and $[45/-45/45/-45/90/45/-45/45/-45/0]_s$ for a SA layup. The NSA stack has minimal extension-twist coupling with some anti-symmetric plies about the centre, with the rest of the stack having a fully uncoupled stacking sequence. This NSA laminate is not feasible as it is made up from just two ply angles, which does not provide robust stiffness or strength performance [73]. These $\pm\theta$ plies exist on boundary of the in-plane lamination parameter design space where there is an advantage of NSAs. However if these laminates are not feasible then NSAs do not offer a benefit in terms of in-plane performance.

Another example with a 8.39% weight saving at $\sigma_I/\sigma_{II} = 0$ and $\eta = 3\pi/16$ in Fig. 5.8 (c) gives a general loading: $N_x/N_y = 0.45$ and $N_x/N_{xy} = -0.67$. The NSA layup is 100% $\pm 58°$ and the SA layup is a 10/67/23. The SA design for a 16 ply layup assuming discretisation to 12.5/62.5/25, $[45/-45/90/90/45/-45/0/45//-45/0/-45/45/90/90/-45/45]$, which is symmetric except for the $\pm 45°$ pair at the midplane, creating a small amount of extension-twist coupling. The NSA layup is fully uncoupled $[58/-58/-58/58/-58/58/58/-58//58/-58/-58/58/-58/58/58/-58]$ but again consists of just two plies and so is not feasible.

Regions of scattered points in Figs. 5.4 (a) and (c) for $\sigma_I/\sigma_{II} > 0$ and Fig 5.4 (d) for $\sigma_I/\sigma_{II} < 0$, are a consequence of non-uniqueness of optimum laminate designs. Similarly, regions where colouring is noisy in Figs. 5.7 (d)-(i) are a result of non-uniqueness of solution and indicate that significant regions of the NSA loading space have multiple optimum solutions and thus offer a less constrained design space than the SA designs in Figs 5.7 (a)-(c). For Figs. 5.4 (a) and (c) this is a consequence of a negative $2 q_{12} \sigma_I \sigma_{II}$ term in Eq. 5.1. This negative term allows minimum energies to be met via different stiffness designs that either increase q_{12}, or decrease q_{11} and q_{22} (or a combination of the two). For $\sigma_I/\sigma_{II} < 0$ in Fig. 5.4 (d), non-uniqueness in designs occurs as a consequence of the capacity of NSAs to provide multiple optimal solutions; three $\pm$ angles are available and thus provide additional redundancy for a given stiffness (energy). This gives scope for optimising NSA solutions for a different

purpose whilst maintaining the optimal laminate stiffness, potentially presenting an advantage over SA solutions.

5.5.3 Industrial design rules versus designing for uncertainty

Contrasting Figs. 5.5 (c) and (d) with 5.5 (a) and (b) shows that absolute values of energies for all design techniques increase with a $\pm 20\%$ load uncertainty as the potential applied loads can be more severe. Comparison of plots in Figs. 5.5 and 5.8 shows that reductions in energy/weight when designing directly for uncertainty are smaller for 20% loading uncertainty than for 10% uncertainty. This implies that, although there is a greater uncertainty in loading, there is less of an advantage (depending on the value of η) in designing directly for this uncertainty.

Both the 10% rule and ply unblocking rule are detrimental to optimum designs under many load scenarios and comparison of plots in Figs 5.4 (e) and (f) shows that design rules have a stronger effect for SAs than for NSAs. This is both a consequence of the fact that $\pm 22.5°$ and $\pm 67.5°$ plies are available for unblocking in NSA designs (compared to only $\pm 45°$ in SA designs) which allows for better alignment of fibre and loading axes but mainly due to the fact that the 10% rule is not applied to NSAs and ensures $\geq 30\%$ of the angles in SA designs are accounted for i.e. at least 10% of 0° and 90° and 20% of $\pm 45°$ plies. The effect of design rules is most apparent when either loading is dominated by one component, and thus where plies of a single angle (0° or 90°) are optimal (e.g. $\sigma_I/\sigma_{II} \approx 0, \infty$, for $\eta = 0$) or where designs are prevented from reaching the more optimal 0% of $\pm 45°$ unconstrained solutions (e.g. $\sigma_I/\sigma_{II} < 0$, $\eta = 0$) see Figs 5.4 (a) and (e) and Fig. 5.5 (a). Figure 5.8 (a) shows that for 10% uncertainty designing directly for an uncertain loading using standard angles (SA2) instead of using the 10% rule (SA1) creates a weight saving $> 5\%$ for only 3.0% of design loadings. This rises to 4.9% of design loadings when a $\pm 20\%$ loading uncertainty is considered with a peak weight saving of 8.2%, see Fig. 5.8 (b). The difference in the weights of SA1 and SA2 designs indicate the current practice of designing for a fixed design loading using SAs with the 10% minimum ply percentage rule has merit, even when subject to an uncertain loading not directly designed for.

In Fig. 5.8 (c) and (d) NSA laminates are designed for an uncertain loading (NSA2) and the largest weight saving over the current industrial practice (SA1) is seen to be 8.5%. In this comparison $< 26\%$ loadings allow $> 5\%$ weight saving for both $\pm 10\%$ and $\pm 20\%$ loading uncertainty. If uncertainty is designed for directly using both SA (SA2) and NSA (NSA2) then 100% of the weight savings from using NSAs compared to SAs are $< 5\%$ and at least 70% provide $< 1\%$ weight saving, see Figs. 5.9 (e) and (f). Hence, for a significant proportion of load cases, results indicate designing directly for uncertainty using SAs may reduce weight by the same amount

as designing directly for uncertainty using NSAs. Considering the cost associated with change and development of manufacturing processes required, the use of NSAs may not be worthwhile. However, as NSAs can match SA performance and for many load cases offer multiple equally optimal, but different, designs. Their use may therefore be viable when designing for competing constraints e.g. manufacturing, damage tolerance or buckling resistance where the properties and design flexibility of NSAs allow a lower weight design. The technique of designing directly for the uncertainty in loading also allows NSA laminates to be robust considering the lack of an equivalent 10% rule.

5.6 Conclusions

The normalised elastic energy derived from subjecting composite laminates to uncertain loading is used to compare design strategies for achieving minimum weight under the assumption of a fibre based failure. Designs employing non-standard angles ($0° \leq \theta \leq 180°$) are compared with standard angle ($0°$, $\pm 45°$ and $90°$) designs and the use of the industrially applied 10% minimum ply percentage rule is compared to designing directly for an uncertainty in secondary loads of up to $\pm 20\%$ of the primary load.

Results from this study are the first to investigate the comparative robustness of standard and non-standard angles designs to an uncertain loading and indicate the potential for use of non-standard angles to reduce weight of future aircraft. It is shown that designing with non-standard angles for an uncertain design loading offers weight savings of up to 8.5%, compared to the current industry standard angle design rule strategy. However, if design rules are ignored and standard angle laminates are also designed to carry uncertain loading directly, weight reduction through the use of non-standard angles is limited to $< 5\%$ and is $< 1\%$ for a significant proportion of potential design loads. The small amount of non-standard laminates that have stiffness advantage are also not feasible since they are only formed of two ply angles. Therefore there is no real advantage of non-standard angles for in-plane performance. Laminate balancing about the principal loading axes, which effectively introduces non-standard angles in the manufacturing axes, is shown to allow up to $\sim 20\%$ weight saving for both standard and non-standard laminates and is particularly effective in dealing with the inefficiencies of laminate designs under shear.

Given the additional cost and complexity of manufacture, for most load cases, a non-standard angle design is unwarranted. Indeed, in many cases balancing about principal loading axes is sufficient to convey the majority of any weight saving. Similarly, the widely used 10% rule is found to be effective in mitigating deleterious effects

of uncertain loading especially when greater uncertainty is applied. Nevertheless, such conclusions only hold where laminate strength is not limited by resin dominated or structural (e.g. buckling) failure. In these cases, or where other design aspects become important, e.g. minimising manufacturing defects, non-standard ply angles may offer an advantage. For instance, the considerable non-uniqueness of minimum weight non-standard angle designs, demonstrated in this study indicates non-standard angles offer enhanced scope for providing optimal stiffness properties whilst concurrently tailoring for other laminate requirements.

Chapter 6

Damage Tolerance Modelling

The minimum weight potential of composites is being limited by the conservative damage tolerance strain allowables used in industry. This is driving the need for fast and accurate analytical models that predict the point of damage propagation. Current models use SERR methods for uni-axial load cases applied to standard angle laminates. A novel multi-axial model is presented, using SERR techniques that consider the full laminate energy for 1D propagation for any multi-axial loading regime.

Correlation to experimental tests is shown and discussed. Tension and shear after impact tests were designed and then investigated and tested by a Masters project student. Unconservatism in the model is due to behaviour not accounted for, including sublaminate coupling and post-buckled stiffness. This is discussed and the model requirements to provide accurate predictions are explored. Model conservatism is included in the modelling assumptions by using a worst case buckling strain and a Mode I critical straine energy release rate. The reduced version of the model is analytical and can be applied to optimisation methods for general laminate design, as seen in the preliminary work in Chapter 9.

6.1   Introduction

The minimum weight potential of composite laminates is limited by their weak through thickness strength. Critical BVID damage from low-velocity impacts is desired not to propagate before the ultimate design loading in order to satisfy airworthiness regulations [21]. However such damage has been shown to reduce the residual strength by up to 80% [11]. Thus damage tolerance often becomes the critical weight limiting aspect of laminate design [5]. Current industry use of empirically derived conservative strain limits is driving the need for more accurate modelling,

prediction and design of the effects of impact damage on the residual strength of the laminate.

BVID creates sublaminates above delaminations that, if near to the surface, can potentially buckle under compressive loading and under further loading propagation of the delamination can occur. This propagation failure mechanism called sublaminate-buckle-driven delamination propagation is summarised in Fig. 6.1. Compressive loading on the sublaminate is required in order to allow this mechanism to occur. Whether the delamination will open or close, is dictated by the delamination depth and its effective strut length, with laminates at depths lower than 25% thickness unlikely to buckle [131]. However around 25% depth a delamination was shown to switch from an opening buckling mode to a closing mode and failure of the global laminate would occur through other means. Data from Melin and Schön [133] showed the transition from opening to closing typically occurred in the 10-20% depth range. BVID would generally be seen around this range.

(a)   (b)   (c)
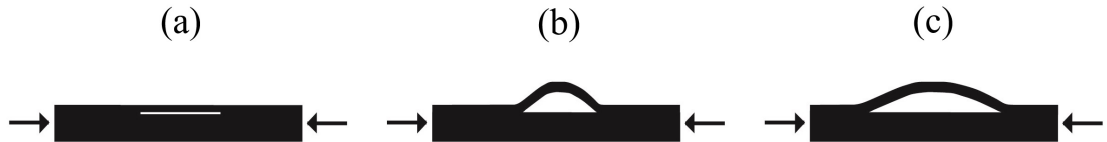
Figure 6.1: *The mechanism for sublaminate buckle-driven delamination propagation in 1D. (a) Near surface delamination damage present, (b) sublaminate buckles under compression and (c) delamination growth occurs under further compression.*

Consideration of global laminate buckling failure is required since it is coupled with the local sublaminate buckling. The three possible compressive buckling failure types are shown below in Fig. 6.2, where interaction in Fig. 6.2 (b) exaggerates the effects of the local buckle leading to the greatest reduction in compressive strength [129]. This mechanism is not being accounted for in this thesis although is noted for future work.

(a)   (b)   (c)
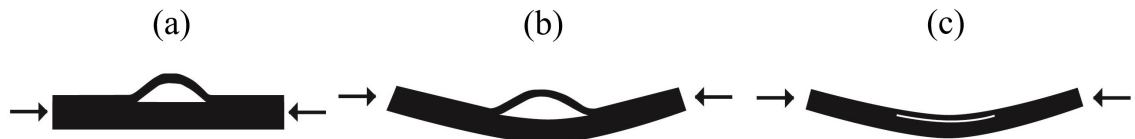
Figure 6.2: *Possible buckling failure from (a) local sublaminate buckling (b) local-global buckling interaction (delamination opening) and (c) global buckling (delamination closing).*

Open-hole and soft inclusion modelling techniques have shown good correlation with CAI tests [13,137,144]. However these techniques are limited as they do not directly

model the sublaminate-buckle driven delamination propagation failure mechanism and are likely to falter when the behaviour becomes more complex, as is the nature of multi-axial laminate loading states.

SERR models using linear elastic fracture mechanics (LEFM) have been successfully able to predict the point of delamination propagation in quasi-isotropic SA laminates using 1D SERR techniques relating to the sublaminate-buckle driven delamination propagation mechanism for circular and elliptical delaminations under uni-axial loading [16–18, 102, 107, 146]. The propagation mechanism has been shown to be mainly Mode I and Mode II dominated [102, 118, 134], with conservative Mode I assumptions showing good correlations to coupon tests [102].

Models have been shown to have problems with high sublaminate Poisson's ratios and large amounts of sublaminate coupling that complicate the post-buckled sublaminate behaviour. Nonlinear pre and post-buckling effects associated with buckling mode shape and sublaminate coupling, such as extension-twist coupling, can produce non-conservative predictions with such models [140, 146].

There is a lack of accurate prediction for multi-axial loadings that better represent a realistic laminate loading scenario. In this chapter a multi-axial loading SERR damage model for prediction of delamination propagation strains is produced to be used as a quick analytical tool for initial laminate design optimisations.

6.2 Behaviour to be Modelled

Assuming there is a given delamination and sublaminate that buckles under load then modelling of the sublaminate buckle-driven delamination propagation mechanism can take place. Fracture mechanics modelling indicates propagation failure, when the laminate SERR reaches a critical SERR value, G_C, determined by the fracture toughness values of the material and the mode-mixity of the crack front. The materials with the highest interlaminar fracture toughness display the greater compressive residual strength [11], and so creating materials with improved properties is a viable strategy to improve damage tolerance. The mode-mixity of the G_C is determined by the relative contributions of the three modes, shown in Fig. 6.3, with Mode I and II found to dominate [102, 118, 134]. The contributions of the modes is complicated, being influenced by a wide range of factors such as delamination morphology, buckled shape, sublaminate stiffness/coupling and laminate strain state [142]. In order to accurately predict propagation, G_C must be accurately determined. The SERR is defined by the rate of change of total laminate strain energy, δU, with new area of crack growth, δA, see Eq. 6.1. This is evaluated by comparing the internal strain energy before (Fig. 6.1(b)) and after propagation (Fig. 6.1(c)).

The most accurate change in energy with delamination growth (SERR) is desired. All behaviour that affects this energy should be ideally designed for.

$$G = \frac{\delta U}{\delta A} \qquad (6.1)$$

Mode I	Mode II	Mode III
Peeling, G_{IC}	Sliding Shear, G_{IIC}	Tearing, G_{IIIC}
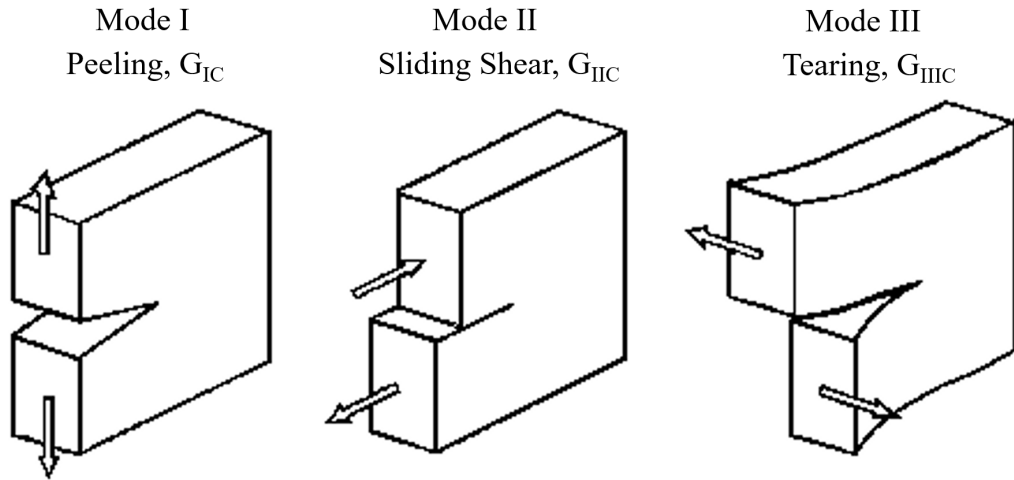
Figure 6.3: *The three modes of fracture*

Therefore the modelling requirements for accurate damage tolerance prediction rely on just two aspects:

(i) G_C evaluation through modelling of the mode-mixity.

(ii) SERR, G evaluation through modelling the strain energy change with propagation.

Only (ii) is modelled. For (i) the mode-mixity is assumed to be unknown and a conservative Mode I critical strain energy release rate, G_{IC}, is assumed ($G_C = G_{IC}$). Justification of this is discussed in Chapter 9.

6.2.1 SERR Modelling

Sublaminate Buckling

The strain energy state of the sublaminate buckle is related to its stiffness and shape, which is interlinked with the buckling strain magnitude. Thus the sublaminate buckling stress/strain is found to be vital in the accurate prediction of the CAI strength [137], and consequently evaluation of the SERR. Premature or delayed buckling, when compared to the predicted buckling strain, is shown to have little effect on the CAI strength. This is suggested to be due to similar amounts of energy (and thus SERR) in the post-buckled state, related to the theoretical

buckling strain, irrespective of the actual buckling [102]. It has been shown that simple approximations of no stiffness in the post-buckled sublaminate can produce predictions close to the experimental results for onset of propagation, even when using a rectangular buckled shape for the sublaminate [136]. Whereas in practice the buckle may represent more of an ellipse shape as is assumed by a number of researchers [16, 108, 137, 138]. Anisotropy in circular or elliptical buckles is problematic. A closed form solution using the Rayleigh Ritz method for sublaminates with some asymmetry is possible [137]. To account for any possibility of sublaminate stiffness coupling, techniques for fully general buckling analysis using efficient buckling analysis software can be used such as that of the infinite strip software VICONOPT [139]. This is used by Butler et al. [102] on a circular sublaminate and by representing the sublaminate by a finite number of same width strips whilst assuming a shape for periodic buckling of these strips. The buckling shape equations for each strip can be solved exactly and the software can combine the strips to form a transcendental eigenvalue problem. Only 6 strips are needed to find a sufficiently accurate buckling strain and thus is extremely efficient, and therefore suit initial stage design use. The problem of CAI modelling does not seem to be limited by the calculation of the correct buckling strain.

Delamination

CAI strength is dictated by the maximum near-surface delamination area, with a larger delamination area causing a lower strength and buckling strain [101, 129, 132]. Tafreshi and Oswald [130] considered the delamination size as a proportion of overall panel area, increasing proportional delamination area decreased the damage tolerance. Amaro et al. [124] showed from experimental tests that the CAI strength is mainly related to delamination size as well as the number of delaminations. The effect of multiple delaminations was found to reduce the damage tolerance of laminates more than just a single delamination.

Stacking Sequence and Loading

Ignoring the effect on damage resistance, the stacking sequence has been shown to affect the buckling and subsequent CAI strength greatly [124], with NSA designs suggested to improve damage tolerance performance over current techniques [28]. In Rhead et al. [146], $\pm30°$ fibre angles were placed in the sublaminate above an artificial delamination in uni-axial CAI tests. Strip model and the FEA predictions for delamination propagation were found to be non-conservative. It is suggested this may be due to large Poissons ratio mismatches present with $\pm30°$ having close to maximum Poissons ratio inducing further transverse compression after buckling.

Another possible reason is the large extension-twist coupling of $\pm 30°$ causing more energetic post-buckled behaviour, both creating an increased SERR. Such transverse compression loading is not usually seen in compressive uni-axial coupon tests and suggests the need to account for the whole range of strain and loading states.

Propagation Direction

It has been shown in Greenhalgh and Singh [135] that at the interface of a buckled delamination, the growth mostly occurs in the direction of the fibres of the sub-laminate if they are in the direction more transverse to the applied load. Cairns et al. [18] noted delaminations generally grow perpendicular to the applied load. The direction depends on the strength of the anisotropy where, for example, Mode I peeling fracture in the sublaminate fibre direction (or Mode II shearing in the tensile sublaminate fibre direction) may offer the direction of least resistance in which propagation can occur . A preferred direction of crack propagation will exist where the SERR will reach a critical value associated with the mode-mixity that exists at the delamination front in this direction.

A model that searches for the direction of lowest propagation is likely to produce more accurate predictions and is desired. The main variables affecting the laminate SERR are as follows:

   (i) Sublaminate buckling strain

  (ii) Post-buckled shape

 (iii) Delamination size/area

 (iv) Number of delaminations

  (v) Sublaminate stacking sequence

 (vi) Sublaminate stiffness coupling

(vii) Post-buckled stiffness

(viii) Applied strain/loading state

 (ix) Direction of crack growth

6.2.2   Other Considerations

Modelling in this chapter focuses on the extension of the strip model [102]. A semi-analytical 1D strut propagation model, in two directions x and y, incorporating the use of the efficient buckling analysis in VICONOPT [139], discussed previously. Propagation strain predictions were made for uniaxial coupon tests with anisotropic

sublaminates above artificial circular delaminations with predictions within 10% of the experimental values. Laminates were balanced and symmetric standard angle (SA) quasi-isotropic stacks. The model effectively approximates the extent of any through-thickness delamination damage morphology as a circular delamination. A conservative Mode I critical SERR is assumed to predict damage growth. The results agree well with the behaviour remaining within the assumptions of the model. The laminate must remain flat (thin-film assumption) and not have too large full elastic coupling in the sublaminate which can cause global buckling interaction with the base laminate and non-linear post-buckled effects altering the SERR. The strip model has been shown to predict non-conservatively for $\pm 30°$ sublaminates with large extension-twist coupling ($B_{16}, B_{26} \neq 0$) and high Poisson's ratios as can be seen by coupons 9-14 in Table 6.3 [140, 146], which affects the energy in the post-buckle.

From the strip model it can be seen that the sublaminate stiffness coupling effects, post-buckling, and any post-buckled stiffness is ignored, along with effects of multiple delaminations. It can be seen that the energy associated with strains other than the axial strain is not accounted for, with $\varepsilon_y = \gamma_{xy} = 0$. For a multi-axial loading model, the whole strain state is likely to become more important. This could either decrease or increase the damage tolerance depending on how much the full 2D energy affects the SERR. The strip model does not evaluate the SERR around the full delamination perimeter and so does not predict a critical direction of propagation.

The strip model does attempt to account for behaviour related to variables (i),(ii),(iii), (v) and (vi) specified in the list for SERR considerations above ((vi) not accounted for after buckling). It also applies conservatism with regards the critical SERR. Models that account for the real physical behaviour are more likely to provide a better prediction of damage tolerance performance. If behaviour is too complex to model, then a conservative outlook should be taken if possible, see Fig. 6.4. An abstract view of the reality of the damage tolerance modelling problem is shown, where the aim is to produce a model that captures the relationship for a variety of cases. A less conservative but not non-conservative model is desired in order to improve on the use of strain allowables.
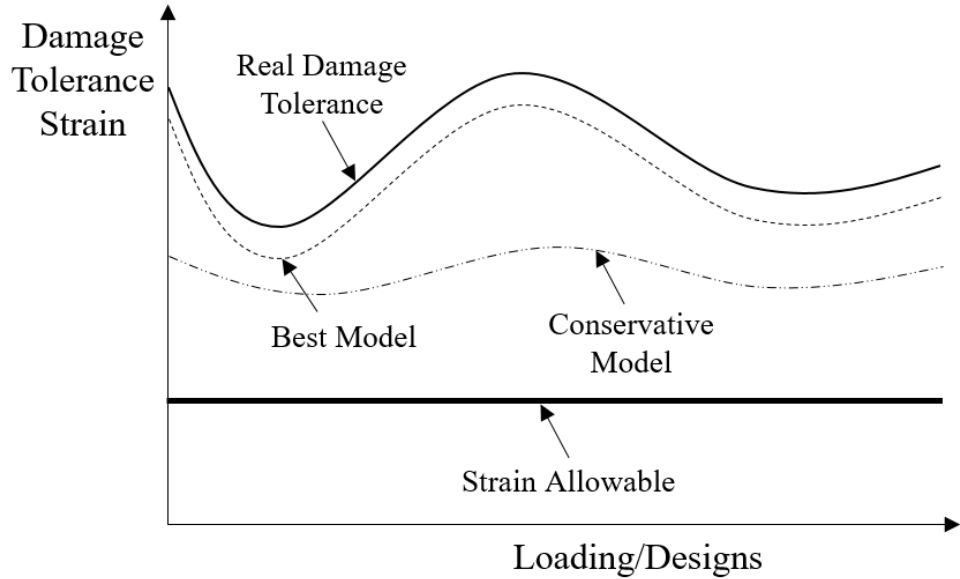
Figure 6.4: *Abstract diagram showing the goal of the best model over conservative strain allowables.*

6.3 Multi-Axial Model

Modelling of the sublaminate-buckling delamination propagation mechanism for multi-axial loading is undertaken using LEFM for 1D propagation. The laminate is assumed to contain a circular delamination (see Fig. 6.5) at a depth where sublaminate buckling is able to occur. Assuming CLT, and plane stress assumptions the laminate and sublaminate pre-buckled mechanical properties can be described.

$$N = A\,\varepsilon \tag{6.2}$$
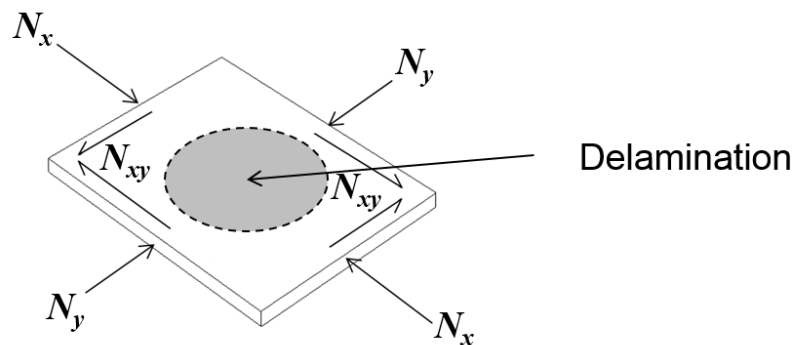
Figure 6.5: *Loading on the laminate, with a circular central delamination.*

The strain state at the sublaminate boundary, ε_{SL} throughout is assumed to be the same as the laminate, ε_L, from CLT. The length, width and thickness of the laminate

are assumed to be significantly larger than the sublaminate (thin-film assumption) so as to not effect the CLT behaviour.

The laminate strain energy is evaluated before and after delamination propagation in order to calculate a SERR or G, the rate of change of energy with new crack area, see Eq. 6.3. Following the 1D strip model derivation [102, 107] and accounting for the difference between energies before and after propagation in Fig. 6.6 the multi-axial model can be derived. The original sublaminate as well as the new length of material that the crack propagates over are the only elements of the laminate where any energy change occurs and thus only these elements will be considered. The energy, U, contained in these elements can be split up into membrane and bending energy components.
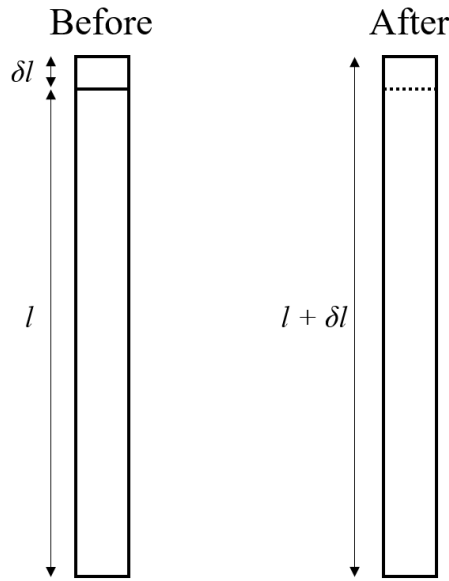
Figure 6.6: *Infinitesimal length change δl of a unit width buckled sublaminate strut l, representing 1D propagation of a delamination.*

$$\Delta U = \Delta \text{ Membrane Energy} + \Delta \text{ Bending Energy} \qquad (6.3)$$

for unit width

$$\Delta U = \Delta N \Delta \varepsilon + \Delta M \Delta \kappa \qquad (6.4)$$

therefore the SERR can be defined as

$$G = \frac{\Delta U}{\Delta A} = \frac{\Delta U}{\delta l} \qquad (6.5)$$

where ΔA in this instance is the change in area of the delaminated region due to propagation.

Membrane Energy

The membrane energy of the original sublaminate is only stored up to the point of buckling, after which the assumption of no post-buckled stiffness means the membrane energy remains constant. Thus all the membrane energy in the sublaminate is assumed to be from initial buckling, as decsribed by Eq. 6.6. This is the same as Eq. 3.6 but for unit width. Subscript 1 or 2 refers to the energy state before or after propagation respectively.

$$U_{m,1}(l) = \frac{1}{2} \int_0^l N_{SL,C} \, \varepsilon_C \, dx \tag{6.6}$$

where $N_{SL,C}$ is the critical buckling load vector applied to the sublaminate. Substituting in Eq. 6.2 for $N_{SL,C}$ and integrating

$$U_{m,1}(l) = \frac{1}{2} \, l \, \varepsilon_C^T \, A_{SL} \, \varepsilon_C \tag{6.7}$$

where $[A_{SL}]$ is the sublaminate in-plane stiffness matrix in the assumed direction of propagation.

The membrane energy in the unbuckled element δl in Fig. 6.6, which lies outside the buckle, stores membrane energy up to point of propagation after which it forms part of the buckled sublaminate.

$$U_{m,1}(\delta l) = \frac{1}{2} \int_0^{\delta l} N_{SL} \, \varepsilon \, dx \tag{6.8}$$

If F is the strain factor on the buckling strain vector dictating the strain applied to the laminate/sublaminate.

$$F = \frac{\varepsilon}{\varepsilon_C} \tag{6.9}$$

substituting N_{SL} from Eq. 6.2 and F from Eq. 6.9 into Eq. 6.8 gives

$$U_{m,1}(\delta l) = \frac{1}{2} \, \delta l \, \varepsilon^T \, A_{SL} \, \varepsilon = \frac{1}{2} \, \delta l \, F^2 \, \varepsilon_C^T \, A_{SL} \, \varepsilon_C \tag{6.10}$$

After propagation the membrane energy per unit width of the larger sublaminate is

$$U_{m,2}(l + \delta l) = \frac{1}{2} \int_0^{l+\delta l} N_{SL,C} \, \varepsilon_C \, dx = \frac{1}{2} \, (l + \delta l) \, \varepsilon_C^T \, A_{SL} \, \varepsilon_C \tag{6.11}$$

therefore the ΔU contribution from the difference in sublaminate membrane energy before and after propagation is

$$\Delta U_m = U_{m,1}(l) + U_{m,1}(\delta l) - U_{m,2}(l + \delta l)$$
$$= \frac{1}{2} \delta l \left(F^2 - 1 \right) \varepsilon_C^T A_{SL} \, \varepsilon_C \tag{6.12}$$

6.3.1 Bending Energy

The post-buckled stiffness of the sublaminate is assumed to be zero, with solely bending energy being stored post-buckling as the laminate strain is increased. The bending energy is assumed to be equal to the equivalent membrane energy that would be stored as the strain (but not load) is increased at the sublaminate boundary. Thus the bending energy increases linearly above the buckling strain as the laminate continues to strain under load.

The bending energy per unit width in the original sublaminate of length l is as follows,

$$U_{b,1}(l) = \int_0^l N_{SL,C} \left(\varepsilon - \varepsilon_C \right) dx \tag{6.13}$$

where $\varepsilon - \varepsilon_C$ represents the applied strain state after buckling since no bending energy is stored until buckling occurs. Eq. 6.13 can be simplified to

$$U_{b,1}(l) = l \left(F - 1 \right) \varepsilon_C^T A_{SL} \, \varepsilon_C \tag{6.14}$$

There exists no initial bending energy for the flat element δl.

Rhead [174] showed that as the sublaminate gets larger through propagation there is a new imaginary buckling strain, ε_{AC}, that better represents the energy state within the now larger sublaminate. The relationship can be assumed to follow

$$\varepsilon_C = \frac{K}{l^2} \tag{6.15}$$

where K is a constant that will depend on the material properties and other sublaminate dimensions. The new buckling strain, ε_{AC}, can then be expressed as

$$\varepsilon_{AC} = \frac{K}{(l + \delta l)^2} \tag{6.16}$$

using ε_{AC} for the buckling strain term related to the buckling load, the bending energy after propagation may be expressed as

$$U_{b,2}(l + \delta l) = (l + \delta l) \left(F - 1 \right) \varepsilon_{AC}^T A_{SL} \, \varepsilon_C \tag{6.17}$$

$(F - 1)$ still appears since it represents the applied strain above the buckling strain which is the same before and after the instant of propagation. The contribution of the bending energy to ΔU is evaluated by subtracting the bending energy state after propagation from before propagation:

$$\Delta U_b = U_{b,1}(l) - U_{b,2}(l + \delta l) = (l\, \varepsilon_C^T - (l + \delta l)\, \varepsilon_{AC}^T)\,(F - 1)\, A_{SL}\, \varepsilon_C \tag{6.18}$$

Substituting in the buckling relationships from Eqs. 6.15 and 6.16 gives

$$
\begin{aligned}
\Delta U_b &= \left(l\frac{K}{l^2} - (l + \delta l)\frac{K}{(l + \delta l)^2} \right)(F - 1)\, A_{SL}\, \varepsilon_C \\
&= \left(\frac{K}{l} - \frac{K}{(l + \delta l)} \right)(F - 1)\, A_{SL}\, \varepsilon_C
\end{aligned}
\tag{6.19}
$$

As in previous work by Rhead [174], the binomial theorem is used to approximate $(l + \delta l)^{-1}$, where terms of second or higher order are ignored

$$(l + \delta l)^{-1} = \frac{1}{l} - \frac{\delta l}{l^2} \tag{6.20}$$

substituting in Eq. 6.15

$$
\begin{aligned}
\Delta U_b &= \left(\frac{K}{l} - \frac{K}{l} + \frac{K\delta l}{l^2} \right)(F - 1)\, A_{SL}\, \varepsilon_C \\
&= \delta l\,(F - 1)\, \varepsilon_C^T\, A_{SL}\, \varepsilon_C
\end{aligned}
\tag{6.21}
$$

6.3.2 SERR and Model

The SERR, G, for the multi-axial model is now developed from the addition of the change in membrane and bending energies divided by the change in length δl, as $\delta l \to 0$.

$$
\begin{aligned}
G &= \frac{\Delta U}{\delta l} \\
&= \lim_{\delta l \to 0}\{\Delta U_m + \Delta U_b\}\frac{1}{\delta l} \\
&= \lim_{\delta l \to 0}\left\{ \frac{1}{2}\delta l\,(F^2 - 1)\,\varepsilon_C^T\, A_{SL}\, \varepsilon_C + \delta l\,(F - 1)\,\varepsilon_C^T\, A_{SL}\, \varepsilon_C \right\}\frac{1}{\delta l} \\
&= \frac{1}{2}(F^2 + 2F + 3)\,\varepsilon_C^T\, A_{SL}\, \varepsilon_C
\end{aligned}
\tag{6.22}
$$

$$G = \frac{1}{2}(F - 1)(F + 3)\,\varepsilon_C^T\, A_{SL}\, \varepsilon_C \tag{6.23}$$

Due to the uncertainty associated with predicting the mode-mixity correctly, (discussed in Chapter 9) it is not attempted here. Instead it is assumed that if the SERR can be calculated correctly then the Mode I critical SERR can be used to provide conservatism within the model. Therefore at the crack front, a strip of unit width is assumed to propagate in Mode I when $G = G_{IC}$ at an applied strain threshold factor F_{th} (factor applied to the buckling strain).

$$G_{IC} = \frac{1}{2}(F_{th} - 1)(F_{th} + 3)\, \varepsilon_C^T\, A_{SL}\, \varepsilon_C \qquad (6.24)$$

Rearranging Eq. 6.24 and solving for F_{th} using the quadratic formula gives

$$F_{th} = \sqrt{4 + \frac{2G_{IC}}{\varepsilon_C^T\, A_{SL}\, \varepsilon_C}} - 1 \qquad (6.25)$$

F can be a factor applied to any magnitude of strain state ($\varepsilon^T\, [A_{SL}]\, \varepsilon$) used in the denominator (in this case the buckling strain state, ε_C, defines the magnitude of the strains). The threshold strain in any direction (θ), ε_θ, can then be evaluated since $\varepsilon_{\theta,th} = F_{th}\varepsilon_\theta$.

$$\varepsilon_{\theta,th} = \varepsilon_{\theta,C} \left(\sqrt{4 + \frac{2G_{IC}}{\varepsilon_{\theta,C}^T\, A_{SL}\, \varepsilon_{\theta,C}}} - 1 \right) \qquad (6.26)$$

The denominator term $\varepsilon_{\theta,C}^T\, A_{SL}\, \varepsilon_{\theta,C}$ is the same formulation for elastic energy in the sublaminate under strain. This term is independent of θ and is the same in all transformed strain directions, since it is an energy per unit area.

This is similar to the strip model [102, 107].

$$\varepsilon_{x,th} = \varepsilon_{x,C} \left(\sqrt{4 + \frac{2G_{IC}}{\varepsilon_{x,C}^2\, A_{SL,NN}}} - 1 \right) \qquad (6.27)$$

where $A_{SL,NN}$ is the larger of $A_{SL,11}$ or $A_{SL,22}$.

6.3.3 Modelling independent of buckling strain

The strip model sublaminate buckling strain is evaluated using the infinite strip buckling software VICONOPT [175]. As the severity of an individual impact is unknown, a priori, and will result in uncertain delamination sizes and depths, conservative worst case (minimum) threshold strains, $\varepsilon_{th,min}$, must be assumed at all interfaces. Taking this into consideration, a reduced version of the strip model was created and used in initial damage tolerance design work included in Appendix

A [152]. The derivation of the reduced multi-axial model follows in a similar manner. The buckling strain vector, ε_C, is the only variable dependent on delamination size in Eqs. 6.24 and 6.26. Hence, the uncertainty in damage morphology can be mitigated by finding the minimum value (with respect to ε_C) of ε_{th} in Eq. 6.26. First Eq. 6.24 will be written as follows:

$$G_{IC} = \frac{1}{2}(F_{th} - F_C)(F_{th} + 3F_C)\,\varepsilon^T A_{SL}\,\varepsilon \tag{6.28}$$

where F_C is now the strain buckling factor on a base strain vector ε which can have any magnitude, on which F_{th} is now a factor.

Then differentiation of Eq. 6.28 with respect to F_C gives

$$\frac{dG_{IC}}{dF_C} = (2F_{th} - 6F_C)\varepsilon^T A_{SL}\,\varepsilon \tag{6.29}$$

As $d\varepsilon_{th}/d\varepsilon_C = 0$ is sought and G_{IC} is constant (and thus $dG_{IC}/dF_C = 0$) rearrangement of Eq. 6.29 gives

$$F_C = \frac{F_{th,min}}{3} \tag{6.30}$$

and thus

$$\varepsilon_C = \frac{\varepsilon_{th,min}}{3} \tag{6.31}$$

According to the model, this means that the lowest threshold strain performance occurs for a buckling strain state that is three times less.

Plotting the full model F_{th} vs F_C reveals this minimum in Fig. 6.7.
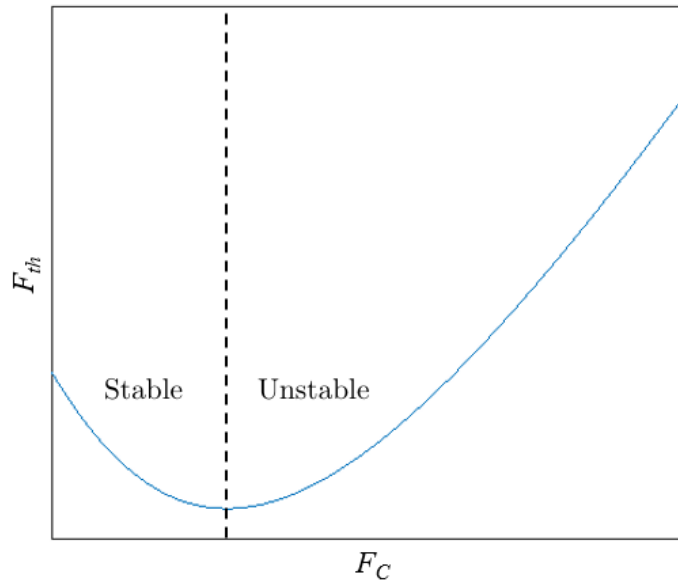
Figure 6.7: *Example F_{th} variation with F_C.*

Substitution of Eq. 6.30 into Eq. 6.28 gives

$$G_{IC} = \frac{1}{2}\left(F_{th,min}^2 + 2F_{th,min}\frac{F_{th,min}}{3} - 3\frac{F_{th}^2}{9}\right)\varepsilon^T A_{SL}\,\varepsilon = \frac{2}{3}F_{th}^2\,\varepsilon^T A_{SL}\,\varepsilon \qquad (6.32)$$

and rearranging for the minimum value of F_{th}

$$F_{th} = \sqrt{\frac{3G_{IC}}{2(\varepsilon^T A_{SL}\,\varepsilon)}} \qquad (6.33)$$

or if ε_C is used as the base strain

$$F_{th} = \sqrt{\frac{3G_{IC}}{2(\varepsilon_C^T A_{SL}\,\varepsilon_C)}} \qquad (6.34)$$

Multiplying by the buckling strain in direction θ, since $\varepsilon_{\theta,th} = F_{th}\varepsilon_{\theta,C}$, gives the reduced multi-axial model.

$$\varepsilon_{\theta,th} = \varepsilon_{\theta,C}\left(\sqrt{\frac{3G_{IC}}{2(\varepsilon_{\theta,C}^T A_{SL}\,\varepsilon_{\theta,C})}}\right) \qquad (6.35)$$

An equation able to predict the propagation strain in any direction for any multi-axial strain state. Note that the reduced model is not dependent on the buckling strain $\varepsilon_{\theta,C}$, but a base strain state of any magnitude (in this case the magnitude of the buckling strain), used in the denominator. It can be written more generally as

$$\varepsilon_{\theta,th} = \varepsilon_{\theta}\left(\sqrt{\frac{3G_{IC}}{2(\varepsilon_{\theta}^T A_{SL}\,\varepsilon_{\theta})}}\right) \qquad (6.36)$$

This is similar to the reduced strip model version from Nielsen et al. [152]

$$\varepsilon_{x,th} = \sqrt{\frac{3G_{IC}}{2A_{SL,NN}}} \qquad (6.37)$$

where $A_{SL,NN}$ is the larger of $A_{SL,11}$ or $A_{SL,22}$.

As Eq. 6.36 is independent of ε_C, minima may correspond to unrealistically large delamination diameters and thus can be a conservative lower bound on ε_{th} for realistic damage e.g. (BVID). It also removes the need for a buckling calculation of circular or other shaped sublaminate. Note that Eqs. 6.30 and 6.31 guarantee that delamination growth will be stable i.e. propagation will only occur with increasing strain (see Rhead et al [176] for full details and derivation). The derivation of Eq. 6.36 includes the following simplifying assumptions: (1) loading has a compressive component; (2) energy for propagation is only available from the thin sublaminate and unbuckled element δl (thin-film assumption); (3) delaminations at each interface and their subsequent propagation under compressive load can be treated in isolation with the

lowest of the derived propagation strains ε_{th} taken as the overall laminate residual strength. If Mode I fracture does not dominate propagation, then results are expected to be conservative.

Eq. 6.36 shows that the propagation strain now only depends on the sublaminate in-plane stiffness matrix, $[A_{SL}]$. $[A_{SL}]$ is always larger with increasing thickness, irrespective of sublaminate arrangement. Therefore the lowest and most critical propagation strains occur for the largest thickness of sublaminate that can possibly open. This creates a conservative modelling assumption.

The multi-axial model can offer predictions of threshold strain in any direction θ. However the model results in a SERR that is constant around the perimeter. Therefore the threshold strain at which propagation occurs, when translated back to the axial direction, is always constant. Figure 6.8 shows this, strains in different directions are due to translations from Mohr's circle of strain only. Therefore the multi-axial model does not reveal a preferred direction of propagation. The strip model on the other hand produces a variation in axial threshold strain to cause propagation at different directions around the perimeter, see Fig 6.9. The model does not include strains in any other direction other than the direction in which it is applied. It is only designed to be applied in the compressive loading direction for a uni-axial test. The axial direction is seen to be predicted as the preferred direction of propagation due to the lowest axial threshold strain. The drop off in axial threshold strain from the axial direction is due to the change in strain and stiffness components in the new directions. In most experimental tests where propagation is predicted well by the model, propagation does not occur in the compressive direction in which it is applied. Thus the strip model does not account for the full strain state around the delamination correctly.
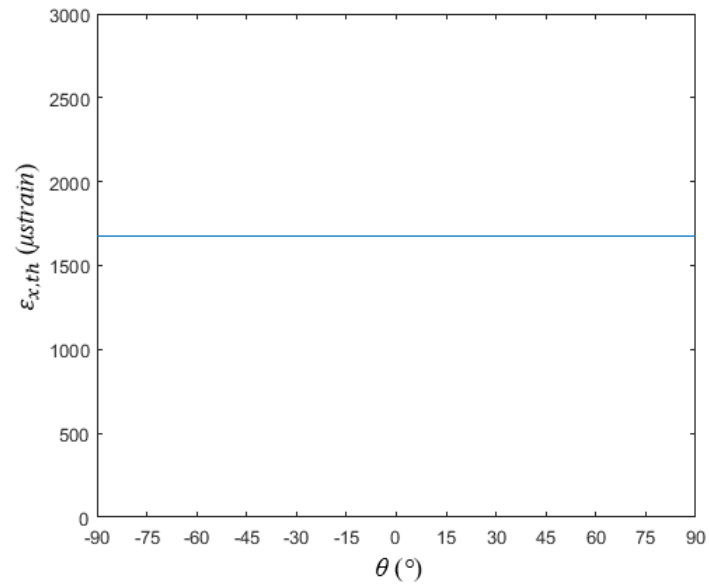
Figure 6.8: *Effect on the resultant threshold strain in the x direction when changing the direction in which the multi-axial model is applied, assuming the [0/0] sublaminate and buckling strains from Test 1 in Table 6.2.*
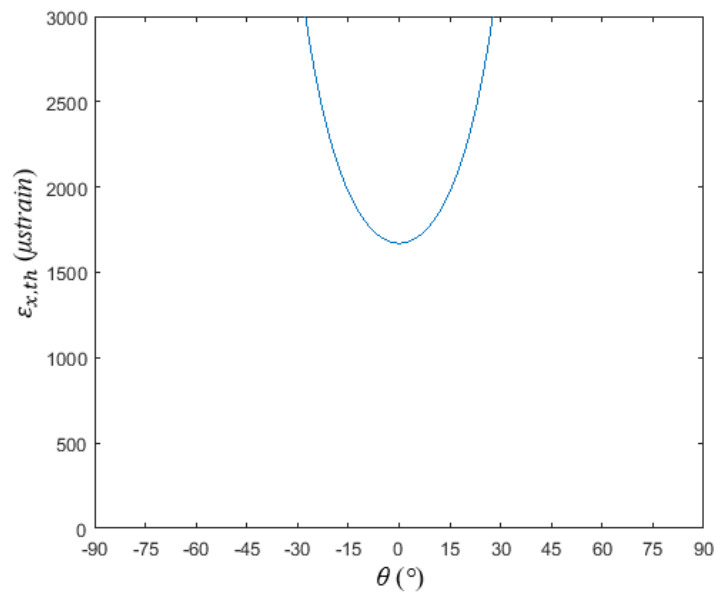
Figure 6.9: *Effect on the resultant threshold strain in the x direction when changing the direction in which the strip model is applied, assuming the [0/0] sublaminate and buckling strains from Test 1 in Table 6.2.*

6.4   Experimental Comparison

A range of damage tolerance experimental results were taken from the literature to be compared against predictions from the new multi-axial model (Eq. 6.26), the strip model [102] (Eq. 6.27), the reduced multi-axial model (Eq. 6.36) and reduced strip model [152] (Eq. 6.37).

Experimental results from 4 separate data sets have been amalgamated in Tables 6.1, 6.2 and 6.3. Note that compressive strains are recorded as positive values and tensile, negative values, as is the standard for CAI test results. The specifics of each testing regime, and the details of the authors and papers are given in the following paragraphs. They include uni-axial compression (CAI) and tension (TAI) coupon tests featuring artificial delaminations in order to reduce the complexities associated with the damage, fitting to the behaviour of the models. The delaminations were created by inserting a PTFE (Polytetrafluoroethylene) circular insert between layers pre-cure. A combination of Digital Image Correlation (DIC), strain gauge and Instron load-displacement data were used to evaluate the loading, strain and 3D displacements of the coupons.

CAI tests used an anti-buckling guide to prevent global laminate buckling behaviour, so as to isolate the failure to the sublaminate buckle-driven propagation mechanism. A range of SA sublaminates were investigated by Butler et al. [102] through variation of a QI SA laminate stacking sequence with sublaminate angle and stiffness coupling varying as seen in Table 6.1. The strip model was found to allow predictions of delamination propagation within 10% of experimental values. Further work by colleagues Rhead et al. [146] showed that the use of a NSA, specifically $\pm 30°$, in the sublaminate produced non-conservative strip model propagation predictions compared to the experiment. This was thought to be due to $\pm 30°$ plies having a maximised Poisson's ratio inducing a large amount of transverse compressive load post-buckling causing earlier propagation. Extension-twist coupling present in the laminate was also thought to be a potential reason, with nonlinear twisting behaviour post-buckling creating a greater SERR to reach the critical SERR and a lower threshold strain.

Further Masters work carried out by Nielsen [140] was set out to isolate the effect of Poisson's ratio mismatch and extenion-twist coupling on the buckling and propagation performance of $\pm 30°$ sublaminates in CAI. The base laminate was altered to remove as well as provide a Poisson's ratio mismatch. The extension-twist coupling was removed by employing fully uncoupled stacks in the surface ensuring $[B] = 0$. Delamination depths were on the limit of the 25% thickness depth where delaminations may no longer open [131]. These results confirmed the influence of large Poisson's ratio mismatch on the SERR and lowering of the threshold strain. However

extension-twist coupling was seen to aid in delaying propagation, unexpectedly.

Tension After Impact (TAI) tests were designed by the thesis author to be used as part of a final year Masters project. Culliford [177] tested and analysed these coupons, summarised in the report. This work introduces the novel concept of using TAI tests to apply bi-axial strain states to the artificially created sublaminate. By designing the base laminates with NSAs, this created a high laminate Poisson's ratio (≥ 0.5) that applied a specific strain loading to the sublaminate when loaded uni-axially. This included a pure shear strain state, termed Shear After Impact (SAI). This was produced by creating a bi-axial strain ratio of 1:-1 in a uni-axial tension test. Therefore the shear strain would be established at $45°$ to the coupon. Tension induces a transverse compressive strain state which was used in order to apply compression to cause the buckling and thus allow the sublaminate buckle-driven delamination propagation mechanism to occur. Only designs with sublaminates that had a Poisson's ratio less than that of the full laminate were designed as there would otherwise be no transverse compressive loading on the sublaminate and no buckling or propagation could occur ($\nu_L > \nu_{SL}$, thus $N_{SL,y}$ is compressive). Tension tests automatically avoid the problem of global buckling behaviour and allow a much faster testing procedure compared to CAI. SA sublaminates were considered with angles and stacks, creating different stiffness coupling behaviours summarised in Table 6.1.

Figure 6.10 displays the difference between model predictions and experiment for increasing amounts of compression inducing Poisson's ratio mismatch. Negative mismatches apply tension transversely. Figure 6.11 indicates the difference between model predictions and experiment for increasing magnitudes of extension-twist coupling.
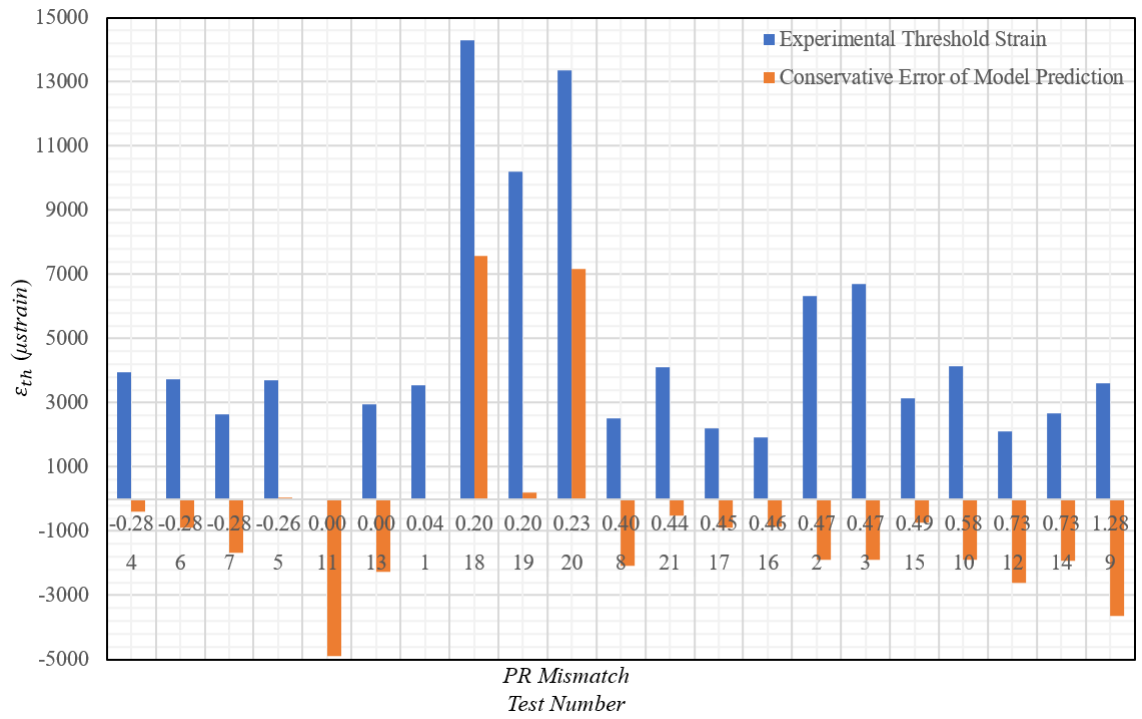
Figure 6.10: *Experimental propagation results in the compressive direction and multi-axis model predictions with increasing Poisson's ratio mismatch of Tests from Table 6.1.*
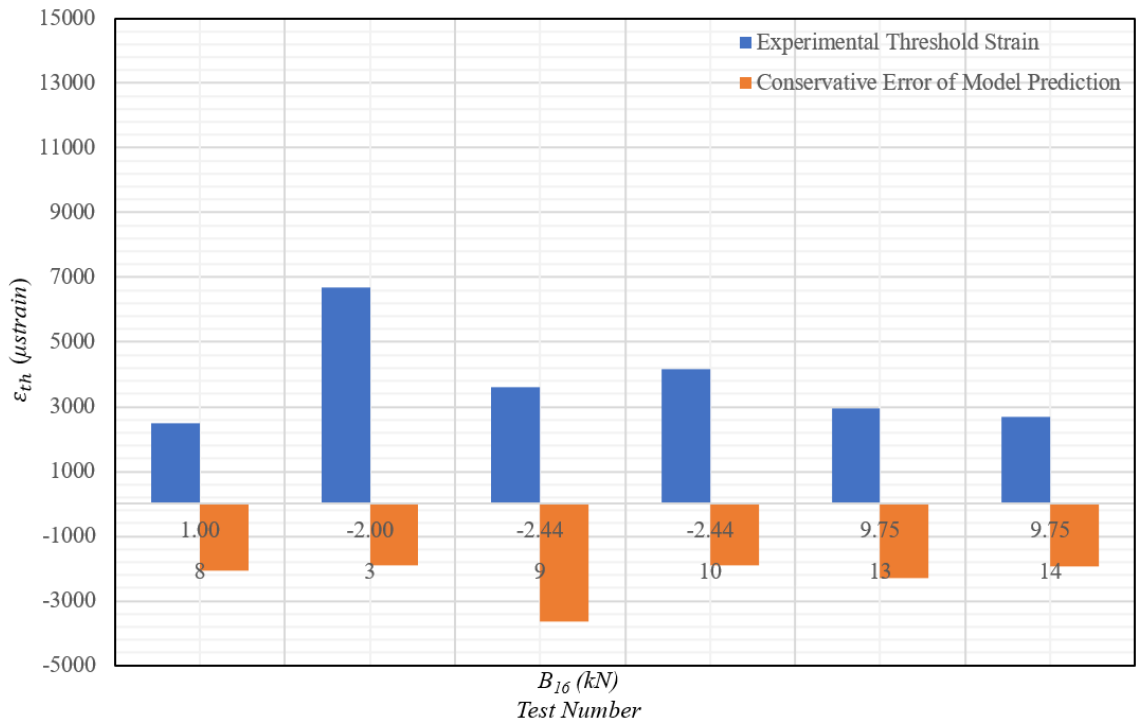
Figure 6.11: *Experimental propagation results in the compressive direction and multi-axial model predictions with increasing dominant sublaminate extension-twist coupling (B_{16}) of Tests from Table 6.1.*

Table 6.1

	Sublaminate Layup	Material	G_{IC} (J/m²)	E_{xx} (GPa)	Delam. Diameter (mm)	Sublaminate Thickness T_{SL} (mm)	Laminate Thickness T (mm)
Butler *et al.* [102]	1 0_2					0.5	4
	2 45_2						
	3 ± 45						
	4 $90/0/90$	M21/T700C	550	51.9	39		
CAI	5 $0/90/90$					0.75	
	6 $90/90/0$						
	7 $0/0/90$						
	8 $0/45$					0.5	
Rhead *et al.* [146]	9 ± 30	M21/T700C	550	74.0	39	0.5	4
CAI	10 ± 30			70.7			
Nielsen [140]	11 $\pm 30/\mp 30/\mp 30/\pm 30$			50.4			
	12 $\pm 30/\mp 30/\mp 30/\pm 30$	HTA/913	225	47.5	55	1	4
CAI	13 $-30_4/30_4$			50.4			
	14 $30_4/-30_4$			47.5			
Culliford [177]	15 90_2			53.9			
	16 $0/90$			55.5			
TAI	17 $0/90/0$	M21/T800S	550	114.8	50	0.524	4.192
[a]SAI Induced	18 -45_2^a			46.0			
[b]Altered coupon	19 $-45_2^{a,b}$			46.0			
dimensions	20 $45/-45^a$ (woven)	AS4/8552	261	38.1		0.2795	5.963
	21 $0/90$ (woven)	(WAMS51 sub)		46.3			

Table 6.1: *Experimental damage tolerance test coupon specifications from literature [102, 140, 146, 177]*

#	Sublaminate Layup	Laminate Strain Ratio ($1/\nu_L$:1)	$\nu_{sL} - \nu_L$	Sublaminate Coupling	Experimental Buckling Strains $\varepsilon_{x,C}$ (μstrain for all)	$\varepsilon_{y,C}$	VICONOPT Buckling Strains $\varepsilon_{x,C}$	$\varepsilon_{y,C}$
1	0_2	3.15	0.038	-	1250	-	682	-2166
2	45_2	3.15	0.471	A_{16}, A_{16}	1200-1620	-	1617	-514
3	±45	3.15	0.471	B_{16}, B_{26}	3010	-	807	-256
4	90/0/90	3.15	-0.28	-	2630-3250	-	1898	-603
5	0/90/90	3.15	-0.256	B_{11}, B_{22}	2340/1250	-	2164	-687
6	90/90/0	3.15	-0.284	B_{11}, B_{22}	2800/3730	-	2164	-687
7	0/0/90	3.15	-0.284	B_{11}, B_{22}	1060-1470	-	1262	-401
8	0/45	3.15	0.396	[B], A_{16}, A_{26}	400-600	-	511	-162
9	±30	6.70	1.279	B_{16}, B_{26}	1000-1460	-	444	-66
10	±30	1.18	0.580	B_{16}, B_{26}	1700-2000	-	622	-528
11	$\pm30/\mp30/\mp30/\pm30$	0.86	0	-	No Buckling		369	-428
12	$\pm30/\mp30/\mp30/\pm30$	2.34	0.732	-	2100	-	2251	-963
13	$-30_4/30_4$	0.87	0	B_{16}, B_{26}	2570	-	2181	-2528
14	$30_4/-30_4$	2.38	0.732	B_{16}, B_{26}	2510	-	1346	-576
15	90_2	1.99	-0.49	-	-687	405	-1062	535
16	0/90	2.01	-0.465	B_{11}, B_{22}	-1504/-2828	652/1157	-2127	1059
17	0/90/0	2.00	-0.453	-	-2114/-3933	986/1709	-5332	2667
18	-45_2	1.00	-0.200	A_{16}, A_{26}	0	0	6347	-6391
19	-45_2	1.00	-0.200	A_{16}, A_{26}	0	0	-6347	6391
20	45/-45 (woven)	1.00	-0.226	-	-3611	3735	-2650	2653
21	0/90 (woven)	2.01	-0.443	-	-1777	1058	-1252	622

Table 6.2: *Experimental vs VICONOPT Strip Model sublaminate buckling strains (given in μstrain) for coupons described in Table 6.1.*

145

Table 6.3 — Experimental Threshold Strains (μstrain for all)

	Sublaminate Layup	Experimental Threshold Strains $\varepsilon_{x,th}$ (μstrain for all)	Experimental Threshold Strains $\varepsilon_{y,th}$	Strip Model $\varepsilon_{x,th}$	Strip Model $\varepsilon_{y,th}$	Reduced Strip Model $\varepsilon_{x,th}$	Reduced Strip Model $\varepsilon_{y,th}$	Multi-Axial Model $\varepsilon_{x,th}$	Multi-Axial Model $\varepsilon_{y,th}$	Reduced Multi-Axial Model $\varepsilon_{x,th}$	Reduced Multi-Axial Model $\varepsilon_{y,th}$
1	0_2	3540	-	3551	-1128	3470	-1102	3566	-1133	3485	-1107
2	45_2	6310-7050	-	6263	-1990	6224	-1977	8209	-2608	8036	-2553
3	±45	6700	-	6559	-2083	6224	-1977	8611	-2735	8036	-2553
4	90/0/90	3950-4260	-	3574	-1135	3414	-1084	4361	-1385	4310	-1370
5	0/90/90	3700-4280	-	3690	-1172	3414	-1084	3646	-1158	3357	-1066
6	90/90/0	3730	-	3690	-1172	3414	-1084	4617	-1467	4521	-1436
7	0/0/90	2650	-	3419	-1086	3414	-1084	4318	-1372	4310	-1369
8	0/45	2500-2700	-	4543	-1443	4287	-1362	4570	-1451	4310	-1369
9	±30	3600	-	4805	-717	4480	-668	7230	-1079	6602	-985
10	±30	4150	-	4699	-3988	4480	-3803	6052	-5137	5678	-4820
11	$\pm30/\mp30/\pm30/\mp30/\pm30$	No Propagation		4047	-4692	2007	-2327	4906	-5688	3815	-4423
12	$\pm30/\mp30/\pm30/\mp30/\pm30$	2100	-	2813	-1203	2007	-859	2977	-1274	2302	-985
13	$-30_4/30_4$	2940	-	2759	-3198	2007	-2327	3107	-3601	2588	-3000
14	$30_4/-30_4$	2680	-	2206	-944	2007	-859	2437	-1043	2302	-985
15	90_2	-5991	3129	-6173	3110	-7970	4015	-7689	3873	-7352	3704
16	0/90	-4272	1927	-8393	4179	-6061	3018	-5630	2803	-5616	2796
17	0/90/0	-5214	2207	-7352	3677	-8294	4149	-6182	3092	-3760	1881
18	-45_2	-12840	14280	-7822	7876	-2954	2975	-6653	6699	-2430	2447
19	-45_2	-10010	10210	-7822	7876	-5452	5489	-9943	10012	-8841	8902
20	45/-45 (woven)	-12090	13360	-6196	6203	-5483	5489	-6173	6180	-6109	6115
21	0/90 (woven)	-7237	4095	-10025	4981	-12360	6140	-9323	4632	-8897	4420

Table 6.3: *Experimental vs analytical models for delamination propagation strains, all in μstrain, for coupons described in Tables 6.1 & 6.2.*

6.5 Discussion

The findings from these tests and model comparisons are discussed in terms of the new insight into how damage behaviour affects the modelling requirements. The full test results are discussed in their individual papers or reports [102,140,146,177], and each attempts to understand and describe the instances where the modelling is ineffective at predicting the propagation strains. The discussion of individual tests has not been attempted in this chapter.

6.5.1 Modelling of Experimental Behaviour

From the literature it was established that in order to predict the point of delamination propagation correctly then both the (i) magnitude of the critical SERR, G_C, around the delamination perimeter as well as the (ii) SERR, G, of the buckled sublaminate with delamination propagation, must be modelled accurately.

If the conservative Mode I critical fracture toughness is assumed in the model, as is the case for the multi-axial and strip models, then the only non-conservatism must lie in the evaluation of the sublaminate SERR.

Modelling predictions are seen to be non-conservative when predicting threshold strain in a few instances (Tests 7-10, 12, 16, 17, 21, see Table 6.3), confirming that the SERR is not modelled correctly in those instances. The following sub-sections explore the reasons for these poorly predicted results.

Buckling strain

The VICONOPT buckling software can be seen to predict experimental buckling strains closely. Discrepancies however appear when there is a number of phenomena present, such as: delayed buckling through adhesion (Tests 1, 3, 4, 6); global buckling interaction (Tests 2, 7, 8); gradual bending/buckling (in-plane to out-of-plane coupling) (Tests 15, 18, 19); different buckled mode prediction (Tests 5, 9, 10, 13); buckle formed from cure (Tests 15, 18, 19).

The buckling strain is a fundamental property of the sublaminate. It is known to be very important for the prediction of delamination propagation and so the accuracy of buckling prediction is critical. The SERR is directly related to buckling strain, due to the fact the buckling strain relates to the stiffness and shape of the buckle. This indicates the magnitude of the energy the buckle stores in bending, and thus how much can be relaxed and released with growth of that delamination. Delayed buckling due to adhesion has been shown to have little effect on strip model

predictions, since it is likely not the point of buckling that is important, but the energy state of the buckle, which relates to the theoretical and not real buckling strain [102].

Global bending/buckling is not accounted for in the models but will clearly reduce the buckling strain due to an eccentricity of loading applied to the sublaminate. The SERR will be increased in such a scenario if the eccentricity of load remains. Accounting for this significant laminate behaviour is important if it is likely to occur, as is the case for wing bending. It is not accounted for in these predictions and should be accounted for in future work.

Gradual bending/buckling is caused by the presence of a non-zero in-plane to out-of-plane stiffness coupling matrix $[B]$. At the onset of loading, this coupling causes out of plane displacement of the laminate with a complete buckle forming with no bifurcation. VICONOPT does not account for gradual bending scenarios due to coupling but this may not be problematic if the buckled energy is still captured correctly by the theoretical buckling strain.

VICONOPT predictions do not model the contact surface of the laminate under the sublaminate buckle and so buckling strains can relate to certain modes that displace into the buckle, which cannot happen in reality. Accounting for this contact should allow accurate predictions to be made, and thus the SERR to be captured accurately. This could be carried out by modelling the area which does buckle in VICONOPT. Otherwise the energy associated with asymmetric buckles in Tests 9 and 10 ($\pm 30°$ sublaminates) will not be evaluated correctly. However this was not carried out in this thesis and is part of the future work.

In Tests 15, 17 and 18, sublaminate buckling is caused by the thermal stresses built up during cure leaving a buckle which exists before any load is applied. The presence of already buckled sublaminates means the energy in the buckle must be considered differently to an energy related to a VICONOPT buckling strain that assumes a flat sublaminate after cure. Energy must be stored in bending both before the coupon is loaded and from the start of load application. The predictions are not adjusted to account for this fact but should be in the future.

If the worst case buckling strain is assumed, as is the case in the reduced models, then the prediction is only non-conservative due to miscalculation of the energy of the post-buckled state and SERR (still assuming a Mode I critical SERR).

Propagation Strain

There are a variety of behaviours that affect the energy in the buckle before and after propagation as well as the mode-mixity at the crack tip and thus critical SERR. From the range of experimental results considered, there are a few aspects that the models cannot account for relating to the point of propagation failure. These include; intra-ply cracks forming during the test or from cure; sublaminate post-buckled coupling (as detailed in Table 6.1; post-buckled stiffness (Test 7) and crack jumps to alternative (and preferential) delamination interfaces (Tests 4, 7, 16).

Intra-ply cracks can form in sublaminates with solely one angle due to the thermal stresses in cure or due to the mechanical loading during the test (Tests 15, 18 and 19). These cracks will change the strain that can be applied across the crack and thus generally reduce the energy within the buckle. This is perhaps likely to cause an increase in conservatism of the model due to the lower SERR, although the strip model predicts the propagation strains for these tests well since the strip model does not account for the energy from transverse strains. These cracks are difficult to model but is not problematic if only conservative propagation prediction is desired. The greatest weight saving will be achieved if these complex intra-ply cracks can be predicted and propagation models account for the drop in SERR.

Increasing extension-twist coupling (only present in Tests 3, 8-10, 13 and 14) does not positively correlate with reduced predictions, an inverse correlation may be more appropriate (see Fig. 6.11). This is despite the extra twisting moments that will be applied post-buckling that should theoretically raise the SERR due to the greater energy in the buckle to be relaxed with propagation. Other in-plane to out-of-plane coupling do not seem to have an effect on the threshold strain predictions. It is suggested that the bending stiffness dominates the energy in a circular buckle, reducing the effects of B_{11} and B_{22} couplings that would otherwise cause similar deflection patterns to that of the buckled shape, more directly than any twist couplings.

Poisson's ratio mismatch seems to have some correlation to the non-conservative failure predictions most notably for $\pm 30°$ sublaminates in Tests 8, 9, see Fig. 6.10. If the sublaminate had no post-buckled stiffness then there would be no increased transverse compressive force applied to the sublaminate. Therefore the modelling assumption of no post-buckled stiffness is suggested not to be adequate [102, 136, 146, 176]. It is likely sublaminates have a post-buckled stiffness that increase the SERR further. The post-buckled stiffness is assumed to be zero and any energy stored in bending is not related to a post-buckled shape, or bending stiffness, but an in-plane stiffness. Therefore accounting for the energy by trying to model these aspects correctly is likely to provide more accurate predictions.

6.5.2 Models

The multi-axial model presented accounts for the full in-plane strain behaviour and thus is a step change in the strip model. However it still has the same problems associated with not capturing the SERR correctly as well as the Mode-mixity of the crack front. Assuming the worst case mode mixity of Mode I, and the use of a worst case buckling strain (reduced multi-axial model), non-conservatism of the model must be a problem with evaluating the post-buckled energy state. The SERR is not elevated to the degree required to cause conservative predictions with such a theoretically conservative model. Past work has shown good predictions with the assumption of zero post-buckled in-plane stiffness [102, 136, 146, 176]. However the problem still exists where the post-buckled effects and stiffness must be accounted for in future models to correctly capture the SERR. The reasons for using the reduced multi-axial model with a Mode I critical SERR for design is discussed in Chapter 9.

The modelling considered does not account for the mode-mixity of the crack front, any post-buckling sublaminate stiffness/coupling effects and any effects changing the theoretical buckling strain (laminate contact mode shapes, global buckling, buckles from manufacture and any intra-ply cracks). Accounting for these behaviours will allow better prediction. The multi-axial model shows no change in SERR around the perimeter of the model due to all expressions being based off of in-plane energy, which is unrealistic.

It is worth noting that the strip model and multi-axial model both predict that very large area delaminations with low buckling strains can have high propagation strains compared to smaller delaminations, as can be seen be seen in Fig. 6.7. This opposes experimental results from the literature [129, 130], suggesting a larger size of damage will reduce the CAI strength. The suggestion that greater damage equals lower residual strength seems logical but if the SERR is lower in reality for larger buckles then CAI strength should increase accordingly.

The stability of the crack growth can be seen on Fig. 6.7 with delaminations to the right of the minimum having unstable propagation, since, as the crack grows, the theoretical buckling strain state decreases (assuming a similar buckling relationship with the new buckled shape). This causes the sublaminate to move further left along the curve where there is a lower threshold strain and so further crack growth occurs. This is the case up until the minimum where stable crack growth occurs and the buckling strain decreases. If the applied strain to the sublaminate is already high enough, propagation will continue to occur until the original level of strain to the right of the minimum is reached. If this is true, then crack growth will always become stable where increasingly greater strains are required to cause propagation. A new design method of allowing stable delamination growth may therefore be suggested.

This could work in a similar fashion to metals where stable crack growth is allowed up to critical length for the limit load [178]. Therefore a massive reduction in weight of composite structures can be produced by reducing the safety factor assuming stable crack growth. Whether or not stable crack growth is realistic for all cases is still unknown as the crack behaviour is complicated with crack jumps and intra-ply cracks making the proposed design strategy uncertain.

One drawback of these types of models, highlighted in Davies and Olsson [118], is that they are verified under conditions that allow buckling-driven delamination failure to occur whilst suppressing other failure mechanisms. The use of anti-buckling guides, for example, suppresses any global buckling interaction that can occur. They do not account for any interaction between different failure behaviours that have the possibility to reduce the CAI strength. It is important to understand the mechanics of the entire problem so that a more realistic model can be produced. It is acknowledged that the behaviour modelled in isolation does allow understanding of the parameters affecting the strength and does facilitate further work and understanding, which has been the main product of exploring these models and their drawbacks.

6.6   Conclusions

The requirements for the accurate modelling of the sublaminate buckle-driven delamination propagation mechanism are discussed. A novel multi-axial propagation prediction model is derived along with a more conservative reduced model that is independent of buckling strain. New models and older strip model variants are contrasted and compared to experimental CAI and TAI results from the literature. Reasons for non-conservative predictions are explored leading to further discussion of the important behaviour that need to be modelled.

The two main aspects affecting accurate predictions are the evaluation of critical SERR and the SERR of the post-buckled sublaminate.

The aspects that affect the SERR are looked into only with a conservative Mode I critical SERR assumed. Realistic mode-mixity is not modelled.

The theoretical buckling strain was suggested to be a fundamental property affecting the energy of the buckle with the actual buckling strain having little effect on the SERR.

Assuming a worst case buckling strain, the reduced model still provides non-conservative predictions despite this model being theoretically conservative. A large amount of test behaviour not specifically accounted for in the model is present. The behaviours

correlating to non-conservative predictions are related to the post-buckled stiffness and coupling effects including large Poisson's ratio mismatches between the laminate and sublaminate. The models assume zero post-buckled stiffness. Non-conservatism comes from problems with evaluating too low a post-buckled SERR. SERR is directly related to the shape, stiffness and post-buckled residual stiffness. Future models that account for the reality of the physical behaviour affecting the SERR are more likely to provide a better prediction of damage tolerance performance. If behaviour is too complex to model, then a conservative outlook should be taken if possible.

The reduced multi-axial model suits fast laminate optimisation due to its analytical nature. This is seen in the preliminary optimisation work in Chapter 9.

Chapter 7

Discussion

The objective of improving on the current design practice for minimum weight design by employing new design techniques is undertaken. New modelling capability and the formulation of new design techniques alongside relaxation of conservative design rules produced promising results. The techniques are based off of the concept that it is more optimal to design directly for a laminate requirement by modelling it correctly instead of using conservative and somewhat arbitrary design rules and allowables.

7.1 Method for General Laminate Optimisation

In order to assess the minimum weight potential of new design techniques over the current practice, a general outlook over a large range of design conditions is desired, avoiding the isolated improvements in weight that may be specific to only a few design cases. Therefore a general laminate design framework that can be used to optimise laminates using different techniques and a way to compare techniques in a general fashion was created.

General design loading inputs are described by just two variables the principal loading ratio σ_I/σ_{II} and the misalignment angle of the balancing axes from the principal loading axes, η. These variables are independent of thickness and can be quickly calculated by a designer from any given design loading. General designs formed of easily understandable ply angles and ply percentages are preferred. The problems associated with discrete stacking sequence design discretisation [33, 34, 45–48] is removed since ply percentages are continuous and so a MATLAB genetic algorithm finds optimal designs robustly for the objective of minimum in-plane elastic energy, despite the non-convex design space [43, 44]. The convex design space of lamination parameters that aid optimisation with gradient-based methods is not required and

any problems to do with discretisation avoided [26, 43].

The performance marker chosen to allow weight comparison of design techniques and to assess minimum weight potential is the in-plane elastic energy described by Eq. 3.11. It is used as an easily applied in-plane strength performance marker, where energy aligns with strength in a Netting analysis regime deemed to be the limit of CLT [87]. This is justified since failure criteria are notoriously poor at general failure predictions even when more accurate and complex micro, meso and macro models are applied [159]. The main goal is being able to rank designs sufficiently in order to correctly pick the optimal laminate designs. It follows that the closer the model to the real failure behaviour, the better the ability to rank designs as seen by the abstract plot in Fig. 7.1. Therefore future work will look into using more accurate models that will provide a more realistic insight into optimum design for in-plane strength. The caveat of elastic energy performance showing minimum weight potential is that weight is likely to be limited by other performance characteristics that are generally more critical, such as buckling and damage tolerance. These aspects must be incorporated in a full design scenario in order to realise any suggested weight savings in reality.
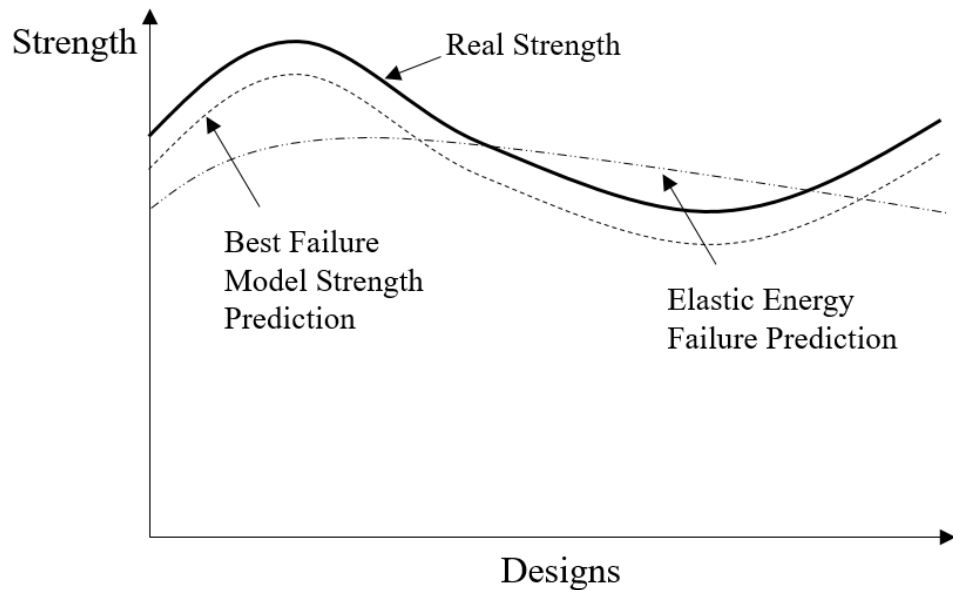
Figure 7.1: *Abstract diagram showing the idea of having the best strength predictor to allow design ranking.*

There are numerous suggestions for improvement on the laminate design rules that generally act as constraints on optimisations (discussed in depth in 3.6). The ideas for improving upon these rules include; removal of the 10% rule and instead designing directly for laminate robustness [91, 92]; use of coupling and removal of coupling constraints [96–100]; use of NSAs instead of SAs for increased performance [9, 28, 147, 148]; modelling and specific damage tolerance design instead of using conservative

strain allowables.

7.2   Laminate Balancing and Non-Standard Angles

The principal load ratio σ_I/σ_{II} inherently affects the value of minimum in-plane elastic energy, and thus in-plane performance, as stiffness must must either be inefficiently shared in the directions of bi-axial load or efficiently used in just one direction for a uni-axial load. η the misalignment angle of the balancing axes from the principal loading axes also inherently affects the in-plane performance. The greatest in-plane performances are found when the laminates are balanced about the principal loading axes (η), as plies do not orientate themselves asymmetrically about the symmetric loading, as is the case for any non-zero misalignments. Balancing affects the performance of designs the greatest for compression-tension ($\sigma_I/\sigma_{II} < 0$) as designs desire to be solely 0° and 90° to minimise the inefficiency of having a high q_{12} in the positive cross term in Eq. 3.11, which allows the laminate to strain more with perpendicular loadings being applied in each other's Poisson's ratio deformations. For positive principal loading ratios ($\sigma_I/\sigma_{II} > 0$) laminates can increase the in-plane performance by increasing q_{12}, as the cross term is now negative. Therefore $\pm 45°$ plies can be used in optimal designs that better cope with shear and reduce the inefficiency of balancing away from the principal axes. Weight savings of up to 22% are possible through increased in-plane performance when relaxing the balancing rule and instead balancing in the principal loading axes. It is uncommon for a principal loading to be aligned with the balancing axes and so there is scope for weight reduction through using this technique. Balancing in the principal loading axes should allow maintenance of no unequal shear or warping during cure, as the shear stresses are balanced, just not in the typical x-y directions. Twisting of the wing box and/or unequal in-plane shearing will not be seen if the principal loading remains in the balancing axes directions during flight. Although it may be desired to have unbalanced laminates, or laminate with extension-twist and bend-twist coupling in order to improve the aerodynamic drag characteristics [97, 98].

Stiffness matching of standard angle laminates with non-standard angle laminates can be achieved over a range of non-standard angle designs. While maintaining the exact stiffness properties of the original standard angle laminate, non-standard angles can be freely chosen to satisfy design requirements for improved manufacturability or laminate performance such as buckling resistance or damage tolerance. It is possible to have a common ply angle in different parts of the structure that have different performance criteria. The common transition method between two areas, ply dropping, would therefore result in a much more uniform changeover in material properties. Non-standard angles are shown to have minor benefits over standard

angles for in-plane performance when a large amount of shear loading is present. If laminates balance in the principal loading axes ($\eta = 0$), the loading is essentially bi-axial and there is no in-plane performance benefit of standard angles. The large non-uniqueness in the NSA design space gives rise to increased flexibility in design to allow better performance in all design requirements, as optimal SA designs are a subset of NSA designs. NSA designs could potentially offer increased in-plane performance for low ply numbers where large variations in the SA ply percentage cannot create the optimum stiffness performance. Optimum designs are unique for $\sigma_I/\sigma_{II} \leq 0$ and $\sigma_I/\sigma_{II} = \pm\infty$ when $\eta = 0°$. For $0 < \sigma_I/\sigma_{II} < \infty$ optimal designs are not unique due to different optimal [Q] stiffness matrices that exist for the same design loading to minimise the elastic energy, therefore there is greater flexibility in the design landscape for in-plane performance. Ply percentage variation through a part is useful to follow the loading variation through a part, and leads to in-plane performance increases and potential reductions of laminate weight. Steering fibres throughout a part and maintaining balance about the principal loading axes can increase the in-plane performance of laminates even more, offering the greatest weight savings.

7.3 Manufacturing

Ease of laminate formability can bot increase the manufacturing rate by ensuring faster cure cycles still form parts with no defects, as well as reduce knockdown factors due to increased part quality. Although eigenmode analysis based on [Q] derived from uncured properties does not accurately describe the deformation of the uncured laminate nor any inter-ply slipping (sublaminate modes), it does enable assessment of whether the low energy in-plane modes of sublaminates are either compatible or incompatible (orthogonal). Such comparison can be used to assess laminate manufacturability. $\pm45°$ grouping becomes more compatible with individual $0°$ and $90°$ ply modes. This may be why Hallender et al. [164] discovered that wrinkling defects were not produced during forming of a C-Section spar when $\pm45°$ plies were grouped together. Such defects did occur when $+45°$ and $-45°$ plies were separated by a $0°$ ply. Non-standard angle angle design modes offer a greater parallelity, which exist for every other configuration of stiffness matched non-standard angle design. Hence deformation of the non-standard designs appear to be more homogeneous and thus less likely to trigger wrinkling defects.

7.4   The 10% Ply Percentage Rule

The 10% minimum ply percentage rule generally increases the minimum elastic energy achievable reducing the in-plane performance for a fixed design loading due to the stiffness penalties incurred by enforcing plies to be present that are non-optimal for the design loading. Optimal stiffness designs may satisfy the ply percentage requirements of the 10% rule and thus the rule itself does not reduce the in-plane performance of the laminate. However for a defined uncertain loading applied to the secondary loads of $\pm 10\%$ or $\pm 20\%$ of the primary load, thought to represent a standard variation in load seen for a laminate, the 10% rule is seen to perform admirably despite being somewhat arbitrary. This design technique was compared to directly designing for the uncertainty using the extreme value theorem for worst case elastic energy performance over the range of loads defined by the uncertainty. Less than 5% of design loadings provide a weight savings over 5% compared to the standard industry practice. It is always more optimal to design directly for the uncertainty in loading but the advantage is small. NSAs offer $< 5\%$ weight saving over SAs, again showing the little benefit provided for in-plane performance, seen only for loadings with a significant shear component. Even in this case, designs are not feasible since they only contain two ply angles.

However, the full range of design loads that could be applied should be known from the range of flight loads that appear in the flight envelope. Therefore it does not make complete sense to design for an uncertain loading if the loading is known. Uncertainty exists in the knowledge of the actual load a laminate can experience from these known flight loads, which maintains the presence of uncertainty in the problem. Robust design is sensible to allow a certain base stiffness in all directions, constraining the Poisson's ratio and providing a more stable stiffness response. The techniques presented should use the defined range of loadings that could possibly be applied, from within statistical bounds, as inputs to the optimisation, finding the worst case in-plane performance for a laminate under these loads and attempt to alter the laminate design to raise the worst case performance as in Chapter 5 (min-max optimisation). The technique of designing directly for the uncertainty in loading also allows NSA laminates to be robust considering the lack of an equivalent 10% rule, and thus the technique is viable. The advantage of designing for a defined range of loads is that your design will be tailored to the uncertainty about these loads instead of equating the importance of all directions of load as the 10% rule accomplishes.

Both the 10% rule and ply unblocking rule are detrimental to optimum designs under many load scenarios and design rules have a stronger effect for SAs than for NSAs. This is both a consequence of the fact that $\pm 22.5°$ and $\pm 67.5°$ plies are available

for unblocking in NSA designs (compared to only ±45° in SA designs) which allows for better alignment of fibre and loading axes but mainly due to the fact that the 10% rule is not applied to NSAs and ensures $\geq 30\%$ of the angles in SA designs are accounted for i.e. at least 10% of 0° and 90° and 20% of ±45° plies. The effect of design rules is most apparent when either loading is dominated by one component.

7.5 Damage Modelling

A fracture mechanics based analytical model for the sublaminate buckle-driven delamination propagation mechanism for multi-axial loading was derived. This model allows prediction of a global stress or strain propagation state

Experimental test results from the literature revealed the areas where the modelling capacity needed to be improved, with non-conservative predictions being made.

From the literature it was established that in order to predict the point of delamination propagation correctly then both the magnitude of the critical SERR, G_C around the delamination perimeter as well as the SERR, G of the buckled sublaminate with delamination propagation, must be modelled accurately.

If the conservative Mode I critical fracture toughness, G_{IC}, is assumed in the model, as is the case for the multi-axial and strip models, then the only unconservatism must lie in the evaluation of the sublaminate SERR, G. Future work to understand the mode-mixity at the crack front should be carried out also. Although for design purposes it is very much an unknown value due to the uncertainty of the impact and damage that could be present, therefore a conservative outlook is preferred at present.

The buckling strain is a fundamental property of the sublaminate and for prediction of delamination propagation. The SERR is directly related to buckling strain, due to the fact the buckling strain relates to the stiffness and shape of the buckle giving a value of how much energy the buckle stores in bending, and thus how much can be relaxed with growth of that delamination. Delayed buckling due to adhesion has been shown to have little effect on strip model predictions, since it is likely not the point of buckling that is important, but the energy state of the buckle, which relates to the theoretical and not real buckling strain [102].

The VICONOPT buckling software [139] can be seen to predict experimental buckling strains closely. Discrepancies appear when there is: delayed buckling through adhesion; global buckling interaction; gradual bending/buckling from the start (inplant to out-of-plane coupling); different buckled mode prediction; buckle from cure. However these behaviours are future complexities to model, the modelling does not

predict correctly for other fundamental reasons discussed. Even if the worst case buckling strain is assumed, as is the case in the reduced models, predictions are still found to be non-conservative due to assumptions not capturing the correct energy of the post-buckled state and SERR (still assuming a Mode I critical SERR).

There are a variety of behaviours that affect the energy in the buckle before and after propagation. From the range of experimental results considered, there are a few aspects that the models cannot account for relating to the point of propagation failure. These include; intra-ply cracks forming during the test or from cure; sublaminate post-buckled coupling; post-buckled stiffness; crack jumps.

Intra-ply cracks across the buckle generally increase the damage tolerance performance, increasing the conservatism of predictions since less energy is contained in the buckle, lowering the SERR.

Extension-twist coupling, does not noticeably correlate with reduced predictions, as is true for other coupling types but theoretically the SERR should be increased in the post-buckle. It is, however, not accounted for in the model.

Poisson's ratio mismatches between the sublaminate and laminate seem to have some correlation to the non-conservative failure predictions most notably for $\pm30°$ sublaminates, see Fig. 6.10. If the sublaminate had no post-buckled stiffness then there would be no increased transverse compressive force applied to the sublaminate due to this mismatch. This reasons that the sublaminate may not be infinitely soft in-plane as modelled [102, 136, 146, 176] and is likely to have a post-buckled stiffness that can increase the SERR beyond that accounted for. Therefore future models should attempt to account for the post-buckled stiffness and these Poisson's mismatches.

The drawbacks of the simplified failure mechanisms modelled is that other failure mechanisms such as global buckling are ignored. It is important to understand the mechanics of the entire problem so that a more realistic model can be produced.

7.6   Damage Tolerance Optimisation

Preliminary work carried out in Chapter 9 uses a new general damage tolerance optimisation method for multi-axial loads using the reduced multi-axial model from Chapter 6. It is applied when designing SA laminates independent of thickness and so offers the ability to design for all possible loading directions and magnitudes. The reduced model is described by Eq. 6.36 which makes the conservative assumptions of a Mode I critical SERR, a worst case buckling strain and a 25% depth sublaminate.

Initial results suggest NSAs are likely to offer no improvement over standard angles

for damage tolerance since the performance of these laminates relate directly to the stiffness of the laminate and sublaminate which can be approved minimally with NSAs (see Chapters 4 and 5), mainly for shear loading. Although for a small number of plies greater stiffnesses can be achieved with NSAs.

The general design philosophy for increased damage tolerance stress is to place stiff plies in the core (to maximise the stiffness and reduce the straining of the laminate) and to place soft plies in the surface (to reduce the sublaminate energy).

The damage tolerance capability depends on the loading ratios applied, with uni-axial loadings offering greater performance as more of the stiffness can be used to ensure one direction has a higher failure stress/strain than another. For more combined multi-axial load,s stiffness has to be shared in all directions and so a lower but more global failure stress/strain is created.

Damage tolerance depends on the thickness of the sublaminate being considered. Thinner sublaminates increase the damage tolerance performance. For thick laminates the sublaminates that are able to open are likely to be at depth percentages of less than 25% in reality, since the maximum BVID creates small sublaminate length to thickness ratios that will not allow buckling under load.

Damage tolerance stress is the weight limiting requirement as the laminate is limited by a maximum load and not strain. Improvement is also shown over the use of conservative strain allowables, with higher magnitudes of propagation strain for an example 1 mm sublaminate ranging from 5000-10000 μstrain, and 200-800 MPa, which is above some in-plane ply failure limits of around 5000 μstrain. Therefore damage tolerance is theoretically increased to the level of in-plane strength. This is unlikely in reality but if possible removes the drawbacks of damage tolerance requirements creating overweight laminates. Other failure mechanisms such as transverse micro-cracking of the optimal sublaminate plies, found to be orthogonal to the maximum strain load, would likely prevent such a performance from being achievable.

The designs presented may be non-conservative because the reduced multi-axial propagation model, derived in Chapter 6 was used. Although it assumes conservatively for possible buckling strain and damage morphology (sublaminate of 25% depth), it does not account for post-buckled sublaminate coupling and stiffness that can act to increase the SERR to non-conservative levels, as discussed in Chapter 6.

Chapter 8

Conclusions

A design optimisation framework was introduced to establish a general view of the minimum weight potential of new design techniques. This includes using multi-axial loading inputs independent of magnitude, described by just two variables, the principal loadings ratios σ_I/σ_{II} (stress loading) or $\varepsilon_I/\varepsilon_{II}$ (strain loading) and η, the misalignment angle of the balancing axes from the principal loading axes. Minimum in-plane elastic energy is used as an optimisation objective for in-plane performance, replacing weight. A general way to formulate and present designs that are independent of thickness is created, where just angles and ply percentages are variables. Optimisations are carried out using a MATLAB genetic algorithm with results presented in novel energy and design diagrams for all possible in-plane loading combinations. Standard and non-standard design variables are incorporated.

New design techniques were investigated for greater minimum weight potential compared to the current industry design practice. Focus was placed on improvement on the use the of the 10% ply percentage rule, laminate balancing, standard angles and conservative damage tolerance strain allowables. Directly designing for a certain laminate behaviour will always provide greater minimum weight potential compared to the use of somewhat arbitrary design rules.

Minimum elastic energy is seen to be limited by (i) the principal loading ratio, (ii) the 10% ply percentage rule and (iii) the principal loading axes misalignment with the balancing axes, η. If the loading is known to be fixed and/or there is no requirement to balance in the manufacturing axes, then there is potential to design lower weight laminates.

Relaxing the balancing rule in the x-y axes and balancing laminates in principal loading axes ($\eta = 0$) can increase the in-plane performance of laminates, with weight savings up to 22% for certain loadings. Assuming weight is dependent on the in-plane performance. Non-standard angles have no in-plane performance benefit under such conditions and offer little benefit when a shear loading is incorporated ($\eta \neq 0$). The

non-uniqueness of the non-standard angle designs for the same laminate stiffness and energy creates an extended design space which is useful for design flexibility in order to meet the many laminate performance requirements. Ply percentage variation and steering of fibres through a part have been shown to increase the in-plane performance by tracking the change in load and principal loading axes.

Improvement in manufacturability is suggested by creating compatible modes of deformation between sublaminates. Non-standard plies are shown to offer significant improvements in compatibility whilst maintaining identical post-cured stiffness. This can potentially improve performance by reducing the likelihood of fibre wrinkle defects, consequently increasing production rates and reducing the need for so-called manufacturing knockdown factors, which allow for the presence of small manufacturing defects.

The 10% ply percentage rule performs close to the performance of directly designing for an assumed realistic uncertain loading. Robust NSA designs are created that lack specific design rules. The new design technique created is useful for ensuring maximisation of the worst case performance over a range of possible loadings or variables, tailoring the design to the uncertainty.

A fracture mechanics based sublaminate buckle-driven delamination propagation mechanism model for a multi-axial loading is derived, improving on models for only uni-axial loadings. The model was compared to experimental results from the literature. The modelling challenges were highlighted. The theoretical buckling strain was suggested to be a fundamental property affecting the energy of the buckle with the actual buckling strain having little effect on the SERR. The two main aspects affecting accurate predictions are the evaluation of the critical SERR via mode-mixity at the crack front and evaluation of the SERR of the post-buckled sublaminate with propagation. Non-conservative predictions are reasoned and evidenced to be due to lack of consideration of post-buckled sublaminate coupling and stiffness, that miss out on the sublaminate coupling and Poisson's ratio mismatches which influence the SERR.

Future models that account for the reality of the SERR mechanics are more likely to provide a better prediction of damage tolerance performance. If behaviour is too complex to model, then a conservative outlook should be taken if possible.

Adaptation of the model for conservative damage tolerance design, independent of thickness and buckling strain, was undertaken. A fully general damage tolerance optimisation method was created. A conservative Mode I critical SERR, and conservative damage that can open up to a depth of 25% laminate thickness, is assumed. The model is applied in design using standard angles. This reduced multi-axial model suits fast initial laminate optimisation due to its analytical nature.

Preliminary optimisation work has suggested that laminate damage tolerance stress or load, and not strain, is an appropriate performance property limiting the weight of the laminate. The general design philosophy for increased damage tolerance stress is to place stiff plies in the core and to place soft plies in the surface.

All designs optimised are continuous in their ply percentages and advantages of new techniques are presented in a general fashion. Therefore discrete designs for individual design cases, in reality, may lack the weight improvement suggested by any new technique due (i) a specific design loading not offering any improvement with a new design technique, (ii) inaccurate assumptions of the design technique, (iii) optimum deviation when discretising or (iv) other failure mechanisms are weight limiting.

Chapter 9

Future Work and Preliminary Damage Tolerance Design

9.1 Future Objectives

The aim of improving on the current industry design techniques is still pertinent beyond the work conducted in this thesis. The techniques presented showing improvement in design need to be validated in a full laminate design scenario taking into account all laminate requirements in order to evaluate if the weight savings suggested are available in reality. More accurate in-plane strength models will be used to ensure the laminates can be optimised fully and laminate weight should be related to the most critical performance aspect for the range of loadings that could be placed in service.

Improvement on the analytical damage tolerance propagation model will be undertaken to improve prediction and the ability to find safe optimal laminates in design optimisations. Better evaluation of the strain energy release rate is required, accounting for post-buckling sublaminate stiffness and coupling behaviour. Interaction of other potentially non-conservative aspects such as global bending/buckling and multiple delaminations are also need in order to make the modelling represent a real laminate design scenario. Preliminary work using the reduced multi-axial model (see Chapter 6) for damage tolerance design optimisations is presented in the following sections.

9.2 Damage Tolerance Optimisation Summary

Laminate optimisation using models that more accurately predict damage tolerance failure are needed to allow weight improvement over current conservative design tech-

niques. Models have been developed for uni-axial loading but have not previously been developed for multi-axial load cases. The reduced multi-axial model derived in Chapter 6, is applied to the design optimisation conservatively for multi-axial loadings. An assumed sublaminate of 25% laminate thickness enforces conservatism and damage tolerant standard angle designs are produced that are independent of thickness and general for any given loading. Optimisations either (i) maximise the damage tolerance performance or (ii) minimise laminate in-plane elastic energy to ensure sufficient in-plane performance with a damage tolerance constraint applied. Damage tolerance performance is found to be inversely proportional to the square root of the sublaminate thickness, assuming the modelling assumptions are valid. For a given design stress loading, maximum damage tolerance stress is stated as the important performance metric. Laminate damage tolerance stress, is altered by changing (i) the laminate stiffness and thus strain state under load (increasing the stiffness can increase the stress), (ii) the strain state (ratios of strain effecting the strain at which propagation occurs), and (iii) the sublaminate stiffness/stack (a more compliant sublaminate gives higher propagation strain performance). The strain state has the largest effect on the strain at which propagation occurs. This can be varied via stiffness tailoring but is less viable in design scenarios where laminate constraints prevent the option of flexibility in the laminate stiffness. If the strain state is fixed, the only way to alter the damage tolerance performance is through the sublaminate stack. Optimum surface plies are found to be orthogonal to the direction of required damage tolerance, which has been shown to be unfeasible in the literature, revealing the need for other failure mechanisms to be modelled.

9.3   Introduction

Composite damage tolerance design has typically used empirically derived conservative strain limits of 4000-5000 μstrain to stop BVID propagation from occurring up to the ultimate load [5, 12]. Accurate analytical modelling of the sublaminate-buckle driven delamination propagation failure is desired to reduce the conservatism of design. Such models can then be applied in the form of quick initial analysis tools to allow a reduction in weight to be realised [102, 178].

Damage tolerance models have been applied to SA design optimisations including the strip model [33–35, 152, 174] showing improved experimental damage tolerance. Ply dispersion models have been applied to NSA design optimisations to ensure sufficient ply angle change between interfaces [28]. This increases the fibre bridging between plies acting as a protective mechanism to damage propagation. Haftka et al. [29] modelled sublaminate buckling to represent failure due to delamination damage. Design using such a model provided a weight saving compared to the use

of structural redundancies in parts that allow areas to fail. Models used for global design have been based on simple techniques, with the more accurate models only being applicable to uni-axial loading states [35]. There is currently no general solution to improving upon the current conservative strain allowables used in industry for damage tolerance design. In this chapter a model derived in Chapter 6 for any multi-axial loading state, predicting the point of delamination failure, is used in optimisations to create general damage tolerant SA designs that are independent of thickness for a range of general loadings.

9.4   Design Modelling

9.4.1   Conservative Damage Modelling

Worst Case Depth and Buckling Strain

Impact damage generally forms delaminations that exist at several interfaces, in a conical shape, increasing in size towards the back-face away form the impact surface [112]. The uncertainty of the low-velocity impact with variation in weight, size, speed, direction and location can create BVID damage morphology that is similarly uncertain. This includes both shape, size and depth of delamination, which heavily depend on the laminate properties including stacking sequence [118], and are not known at the initial design stage. Since accurate impact damage predictions models only exist with FE modelling [118,119,122], any quick analytical design tools capable of initial design optimisations must assume a conservative damage outlook. The most critical damage must therefore be assumed at all interfaces, see Fig. 9.1.
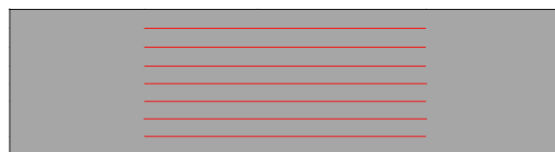
Figure 9.1: *Figure showing maximum damage throughout the laminate thickness. Maximum BVID delaminations are marked.*

The maximum BVID delamination length is observed to be just over 9 times the laminate thickness [107]. An accurate buckling strain prediction is seen to be vital for evaluation of the SERR and thus propagation strain prediction [102,137]. However even if the worst size delamination is assumed, the shape of such a delamination is unknown and therefore an accurate buckling strain calculation using VICONOPT is not possible [179]. Therefore a worst case buckling strain must be assumed. As per

the modelling in Chapter 6, Fig. 6.7, for any given depth of delamination there will be a worst case buckling strain related to the minimum propagation performance. Fig. 6.7 also suggests larger delamination sizes are not always more critical, opposing that of the literature [101, 124, 127, 129, 130]. This supports the reasoning for using a worst case buckling strain for conservative damage tolerance design, rather than maximum BVID damage for each interface.

$$\varepsilon_{\theta,th} = \varepsilon_\theta \left(\sqrt{\frac{3G_{IC}}{2(\varepsilon_\theta^T A_{SL} \varepsilon_\theta)}} \right) \tag{9.1}$$

The reduced multi-axial model derived in Chapter 6, seen in Eq. 9.1, can be used assuming a worst case buckling strain for each interface. For delamination damage at each interface to cause failure it must first be able to open through sublaminate buckling, otherwise the damage propagation mechanism cannot occur. Ignoring any global buckling and bending interaction effects, the maximum depth of delamination that can still open is found to be around 25% thickness [131], any deeper delaminations assumed not to be able to open.

The reduced multi-axial model, in Eq. 9.1, predicts the propagation strain, ε_{th}, and is dependent upon the sublaminate thickness (delamination depth/interface) included in the in-plane stiffness matrix $[A_{SL}] = \overline{Q}_{SL}T_{SL}$ (which can have full population of the stiffness matrix). The $[A_{SL}]$ matrix is always larger with increasing thickness hence for any sublaminate arrangement this means that, according to the model, the lowest and most critical propagation strain (highest SERR) will occur at the largest thickness that can open, assumed to be the 25% thickness limit. Effects of multiple delaminations present at other interfaces inside the sublaminate are ignored, which could be an non-conservative assumption due to interaction of sublaminate buckles [124–126] generally lowering CAI strength. On the other hand the presence of delaminations in the core below the buckled sublaminate is shown to not effect the CAI strength [127].

Therefore the worst buckling strain at the most critical depth is assumed in order to make the model conservative for design when the damage size, depth and morphology are unknown.

Uncertainty in Mode-Mixity at the crack front

Due to the uncertainty in the damage (and thus the post-buckled behaviour), the mode-mixity and critical SERR (G_C) at the crack tip around the delamination perimeter, is unknown. A square shaped delamination gives different mode-mixities and SERRs around the crack tip compared to a circular shape [180]. The reduced

model predicts the same SERR in all directions, as per Fig. 6.8. Since the mode-mixity is not modelled, a conservative Mode I critical SERR, G_{IC}, is employed, with no G_C being below this value. This ensures that any non-conservatism in the model must come from the evaluation of the SERR, G, which already includes conservative assumptions. As explained in Chapter 6, with comparison to experimental results, non-conservatism in the model exists through not accounting for post-buckled sub-laminate coupling and stiffness. Therefore designs produced using this model in optimisations have the possibility of possessing lower damage tolerance performance than suggested.

9.4.2 Modelling for Damage Tolerance Strength

Laminate damage tolerance failure stress is thought to be more appropriate as the structure is generally weight limited by loads and not strains. Therefore if the laminate level damage tolerance stress (load) is required to be evaluated in one of the x, y or xy directions then it can be carried out by multiplying the damage tolerance strains in these directions by the laminate stiffness matrix $\left[\overline{Q}\right]$.

$$
\begin{Bmatrix} \sigma_{x,th} \\ \sigma_{y,th} \\ \tau_{xy,th} \end{Bmatrix} = \begin{bmatrix} \overline{Q}_{11} & \overline{Q}_{12} & 0 \\ \overline{Q}_{12} & \overline{Q}_{22} & 0 \\ 0 & 0 & \overline{Q}_{66} \end{bmatrix} \begin{bmatrix} \varepsilon_{x,th} \\ \varepsilon_{y,th} \\ \gamma_{xy,th} \end{bmatrix}
\tag{9.2}
$$

The damage tolerance stress then depends on both the threshold strain state and the laminate stiffness, which are not independent. Therefore a balance of both must be achieved in order to maximise the damage tolerance stress in a given x, y or xy direction.

9.4.3 Design Independent of Thickness

The propagation strain ε_{th} of the reduced model, in Eq. 9.1, is dependent on the sublaminate thickness through $[A_{SL}] = Q_{SL}T_{SL}$. Therefore if the sublaminate at one surface is always 25% thickness of the laminate (25% on both sides), then ε_{th} depends on the thickness of the laminate as well. Designing laminates independent of thickness is thus not straight forward.

In order to design independent of thickness the laminates can be evaluated not for a propagation strain but instead for a thickness normalised damage tolerance, $\varepsilon_{th}\sqrt{T_{SL}}$. By rearranging Eq. 9.1, the sublaminate stiffness matrix $\overline{Q}_{SL}$ can be separated from the thickness component, and a critical $\varepsilon_{th}\sqrt{T_{SL}}$ can be calculated.

$$\varepsilon_{\theta,th}\sqrt{T_{SL}} = \varepsilon_\theta \left(\sqrt{\frac{3G_{IC}}{2(\varepsilon_\theta^T \overline{Q}_{SL}\,\varepsilon_\theta)}} \right) \tag{9.3}$$

Therefore designs are optimised with either $\varepsilon_{th}\sqrt{T_{SL}}$ or $\sigma_{th}\sqrt{T_{SL}}$ as the thickness normalised damage tolerance performance, making damage tolerant design independent of thickness.

Optimum designs will have a given $\varepsilon_{th}\sqrt{T_{SL}}$ or $\sigma_{th}\sqrt{T_{SL}}$. Therefore a designer can input the laminate total thickness, and thus sublaminate thickness, to produce the actual value of ε_{th} or σ_{th}. For minimum weight design that is assumed to always be limited by damage tolerance the largest value of $\varepsilon_{th}\sqrt{T_{SL}}$ or $\sigma_{th}\sqrt{T_{SL}}$ should be picked and then ε_{th} and σ_{th} can be scaled to give the required damage tolerance by changing the thickness. This will ensure minimum weight design. Increasing the thickness of the sublaminate reduces the damage tolerance performance.

This ε_{th} (and σ_{th}) and T_{SL} relationship for a given design with a certain $\varepsilon_{th}\sqrt{T_{SL}}$ clearly shows that a larger sublaminate thickness, and thus laminate thickness, reduces the ε_{th}, see Fig. 9.2.
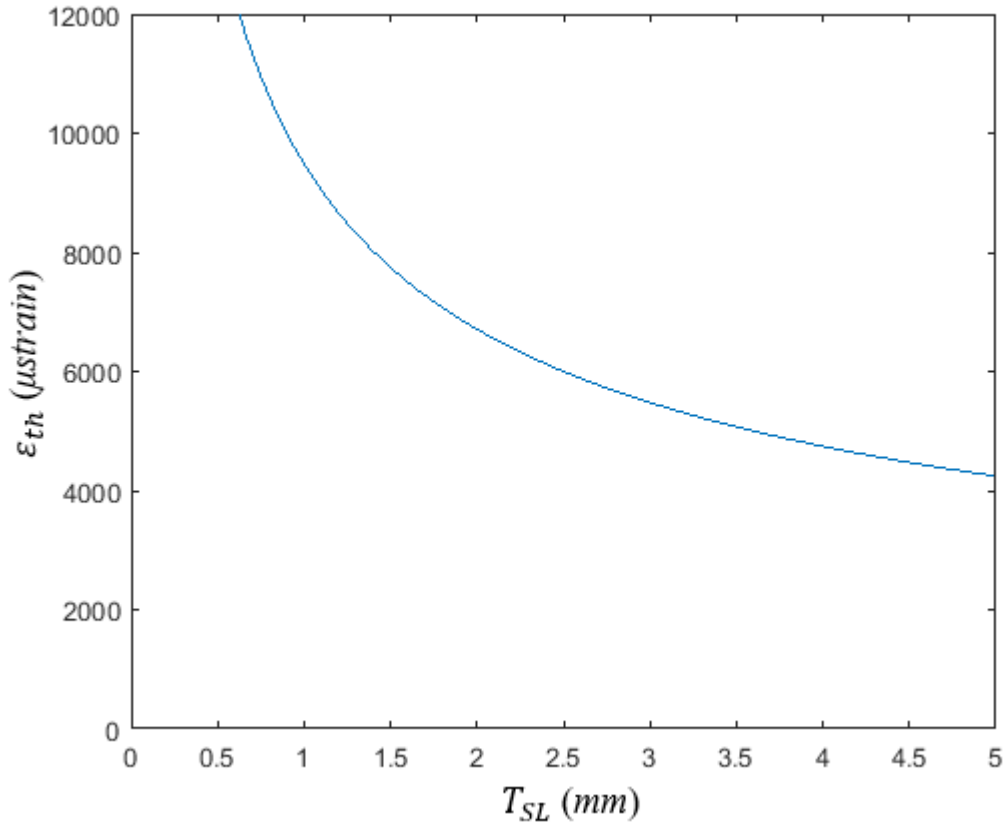

Figure 9.2: ε_{th} vs T_{SL}, for a $\varepsilon_{th}\sqrt{T_{SL}}$ of 300 μstrain $m^{\frac{1}{2}}$

9.5 Optimisation Overview

Optimisations are carried out using two different damage tolerance philosophies:

1. Damage tolerance stress, σ_{th}, for a design stress loading

2. Damage tolerance strain, ε_{th}, for a design strain loading

For each philosophy, optimisations are run for two different objectives:

(i) Maximum damage tolerance performance for all multi-axial loadings

(ii) Minimum/Maximum in-plane elastic energy, $\overline{U}$, with damage tolerance constraint for all bi-axial loadings

The optimisation technique described in Section 3.5, using a MATLAB GA, is adapted to include the reduced multi-axial damage tolerance model. The stress and strain formats, from Section 9.4.1, act as constraints as well as objectives for maximisation. Only loadings that have at least some compressive component are considered, since the sublaminate buckle-driven delamination propagation mechanism cannot occur otherwise. Therefore loading ratios, described generally by the principal load ratio σ_I/σ_{II} (or $\varepsilon_I/\varepsilon_{II}$) and the misalignment angle η, are either compression-compression or compression-tension. Damage tolerance is optimised for (1) the dominant stress or (2) dominant strain direction, either being x, y or xy for the design stress/strain loading considered (for strain loadings magnitudes of ε_x, ε_y and ε_{xy}, and not γ_{xy}, are compared due to the Mohr's circle of strain).

Optimisation objective (i), maximum damage tolerance, runs two different optimisations, with no constraints, for all possible multi-axial loads described by σ_I/σ_{II} (or $\varepsilon_I/\varepsilon_{II}$) and η. GA optimisation is halted if either the maximum number of iterations reaches 5000 or for (1) if the change in $\sigma_{th}\sqrt{T_{SL}}$ value between iterations is less than 1×10^{-11} MPa m$^{\frac{1}{2}}$, or for (2) if the change in $\varepsilon_{th}\sqrt{T_{SL}}$ value between iterations is less than 1×10^{-8} μstrain m$^{\frac{1}{2}}$.

Optimisations for objective (ii), minimum/maximum in-plane elastic energy (Eqn. 3.11), are carried out to maintain in-plane laminate performance whilst meeting constraints for all bi-axial loads described by σ_I/σ_{II} or $\varepsilon_I/\varepsilon_{II}$, respectively. Bi-axial loadings are chosen for this optimisation as they allow optimal designs to be seen without adding a fourth dimension to the design space. Designs are also applicable to all multi-axial design loadings if balance is allowed in the principal loading axes $\eta = 0$ (see Chapters 4 and 5). 101 variations in the damage tolerance constraints for all bi-axial loadings were applied. The maximum value of these damage tolerance constraints were decided by running initial optimisations to see what maximum performance could be created. A maximum constraint of 40 MPa m$^{\frac{1}{2}}$ for $\sigma_{th}\sqrt{T_{SL}}$ and 350 μstrain m$^{\frac{1}{2}}$ for $\varepsilon_{th}\sqrt{T_{SL}}$, is used. For a 4 mm thick laminate ($T_{SL} = 1$ mm),

with a damage tolerance considered in the x direction, this gives a maximum $\sigma_{x,th}$ = 1265 MPa and maximum $\varepsilon_{x,th}$ = 11068 μstrain. These are unrealistic values since composite in-plane failure tends to be less than half these values. Damage tolerance models for use in design may be more appropriate for ranking of designs rather than predicting the actual failure magnitude.

Damage tolerance strain optimisations, (2), are only considered for fixed strain ratios. Thus if the thin-film assumption holds and the base laminate remains flat, the rest of the laminate has no bearing on the damage tolerance performance. It can no longer fundamentally alter the strain the sublaminate experiences. Therefore the sublaminate only is designed in this case. Thus the design optimisation objective in (ii), of minimum elastic energy, translates to a maximisation of sublaminate energy for a given applied strain. Since for a given strain loading, global stiffness is maximised by maximising the energy (equivalent to minimising energy for a given stress), as per the load-strain relationship, see Fig. 3.3. The energy only refers to the strain normalised energy of the sublaminate seen in Eq. 9.4, a similar format to Eq. 3.11. If $\overline{Q}_{SL,16}$ and $\overline{Q}_{SL,26}$ exist, they should be incorporated into the numerator of Eq. 9.4.

$$\overline{U}_{SL} = \frac{\overline{Q}_{SL,11}\varepsilon_x^2 + 2\overline{Q}_{SL,12}\varepsilon_x\varepsilon_y + \overline{Q}_{SL,22}\varepsilon_y^2 + \overline{Q}_{SL,66}\gamma_{xy}^2}{2\left(\varepsilon_x^2 + \varepsilon_y^2 + 2\left(\frac{\gamma_{xy}}{2}\right)^2\right)} \tag{9.4}$$

This optimisation is carried out in order to investigate the fundamental nature of the strain state and what happens to damage tolerant design when there is lack of flexibility in this variable.

Designs are optimised using SAs ($0°$, $\pm45°$ and $90°$) with a total of 6 ply percentages, 3 ply percentage variables for the sublaminate (25% thickness on both sides) and 3 for the core laminate (50% in the centre). This creates 4 independent variables to be optimised, the second 2 being deduced by the remaining ply percentage. The 4 main optimisation techniques investigated are shown in Table 9.1.

The material properties used for this optimisation study are taken from Butler et al. [102] for Hexcel T700GC/M21. The CFRP properties are as follows; E_{11}= 136 GPa, E_{22}= 8.9 GPa, ν_{12}= 0.35, G_{12}= 4.5 GPa and G_{IC}= 550 J/m^2.

Damage Tolerance	Objective	Constraint	Loading	Variable
(1) $\sigma_{th}\sqrt{T_{SL}}$	(i) Max. $\sigma_{th}\sqrt{T_{SL}}$	N/A	σ_I/σ_{II} η	Laminate: 3 angles ($0°$, $\pm45°$ & $90°$) 2 proportions (γ_0, $\gamma_{\pm45}$, 1-($\gamma_0+\gamma_{\pm45}$))
	(ii) Min. $\overline{U}$	$\sigma_{th}\sqrt{T_{SL}}$	σ_I/σ_{II} $\eta=0$	
(2) $\varepsilon_{th}\sqrt{T_{SL}}$	(i) Max. $\varepsilon_{th}\sqrt{T_{SL}}$	N/A	$\varepsilon_I/\varepsilon_{II}$ η	Sublaminate: 3 angles ($0°$, $\pm45°$ & $90°$) 2 proportions (γ_0, $\gamma_{\pm45}$, 1-($\gamma_0+\gamma_{\pm45}$))
	(ii) Max. $\overline{U}_{SL}$	$\varepsilon_{th}\sqrt{T_{SL}}$	$\varepsilon_I/\varepsilon_{II}$ $\eta=0$	

Table 9.1: *Optimisation techniques for damage tolerance design. All 4 damage tolerance optimisation combinations performed in this Chapter are presented here; described by 2 damage tolerance philosophies and 2 optimisation objectives.*

These techniques are employed to investigate the effects of loading and laminate design on damage tolerance performance, as well as to present a potential method that improves upon the current industry practice.

The optimisation logic for the 4 optimisations carried out are shown in the flowchart in Fig. 9.3.
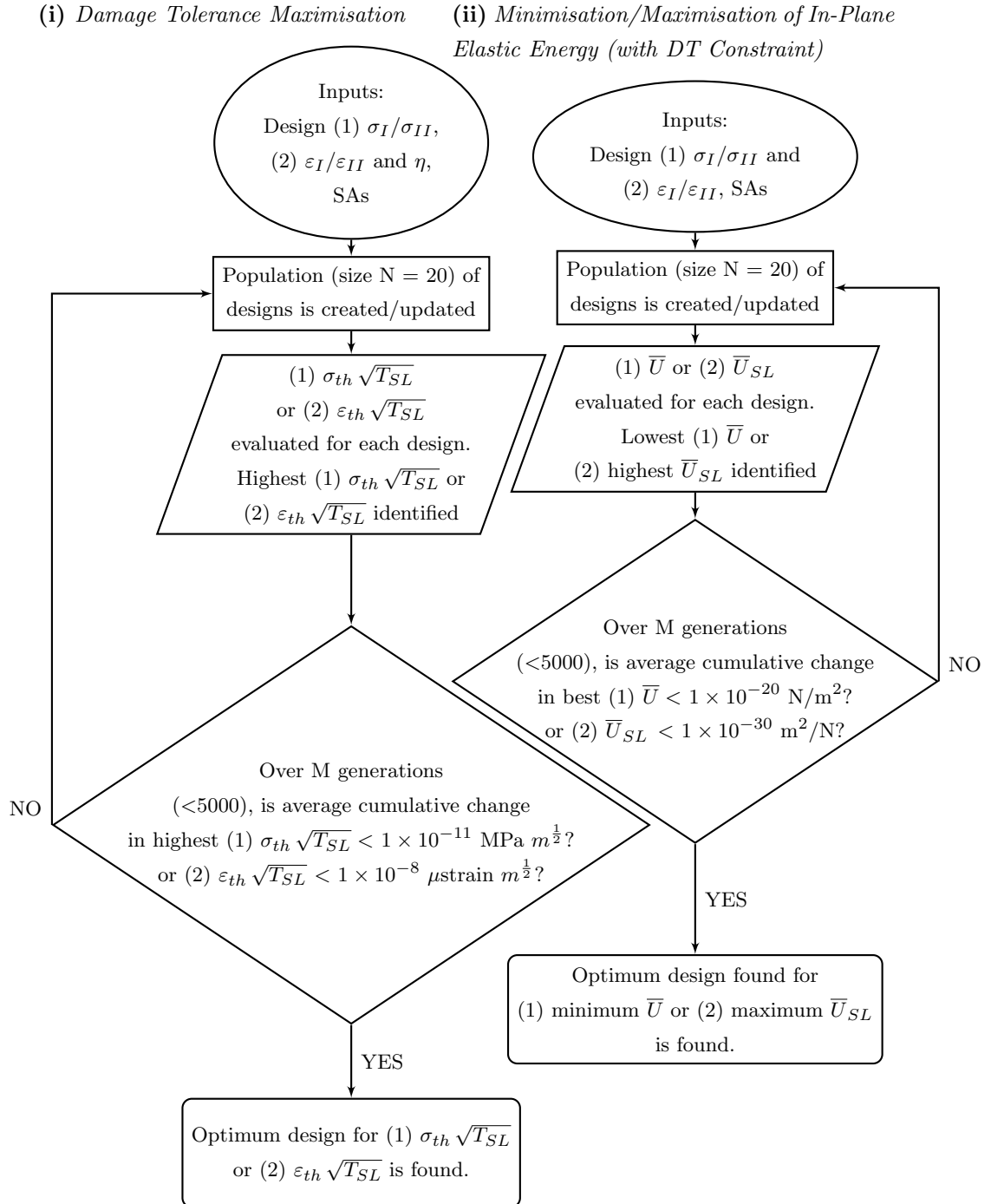

Figure 9.3: *Flowcharts summarising the optimisation steps for all four (1)i)(ii)-(2)(i)(ii) optimisations run for damage tolerant designs.*

9.6 Results and Discussion

Thickness independent laminate design optimisations were completed, as described in Section 9.5, culminating in a total of four optimisation investigations, including damage tolerance performance as objectives and constraints for a wide range of multi-axial stress and strain loading scenarios. The reduced multi-axial model from Chapter 6 was used conservatively, assuming a worst case buckling strain and damage that is able to open up to 25% laminate depth. The results are presented and discussed in order, with a general conclusions section that follows.

9.6.1 (1) Laminate optimisation for damage tolerance stress

Optimisation (1) considers results using optimisations for damage tolerance stress under multi and bi-axial stress loadings described by σ_I/σ_{II} and η.

(1)(i) Maximisation of damage tolerance stress for multi-axial loadings

2D plots for $\eta = 0$ are used to ease the reader into the results and to aid in the understanding of the 3D plots that follow. Positive and negative ratios represent a compression-compression and compression-tension loading respectively. $\eta = 0$ and $\eta = \pi/4$ represent horizontal lines on the 3D plots seen in the following subsections.

Fig. 9.4 shows the variation in the thickness normalised maximum damage tolerance stress, $\sigma_{th} \sqrt{T_{SL}}$, in the dominant laminate stress directions for all σ_I/σ_{II} loading ratios for when $\eta = 0$, i.e. bi-axial loadings, and for $\eta = \pi/4$. For $\eta = 0$, maximum damage tolerance stress performance varies gradually and by a large magnitude between the sharp peaks for uni-axial loadings ($\sigma_I/\sigma_{II} = 0$ or $\pm\infty$) and the sharp troughs towards equal bi-axial loadings ($\sigma_I/\sigma_{II} = \pm1$).

For $\eta = \pi/8$ the opposite is true, where peak performance is seen for equal bi-axial loadings ($\sigma_I/\sigma_{II} = \pm1$), with a more gradual peak with a small variation in damage tolerance performance for all loadings. The maximum possible damage tolerance stress performance for $\eta = \pi/4$ is seen to be generally lower than for $\eta = 0$, being 4x lower for the uni-axial load case. Overall the comparison shows that for problems with shear and bi-axial loading, there is a lower damage tolerance performance compared to uni-axial loading. This is due to stiffness having to be spread in more directions to meet the load.
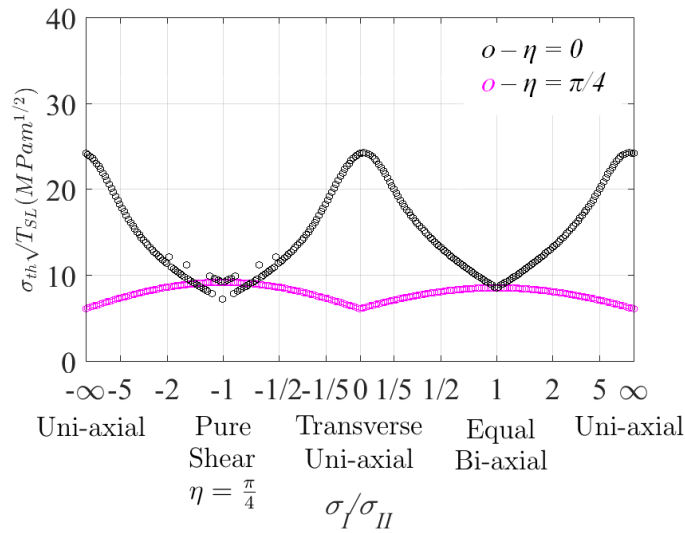
Figure 9.4: *Maximum $\sigma_{th} \sqrt{T_{SL}}$ variation of optimum designs for $\eta = 0$ and $\pi/4$.*
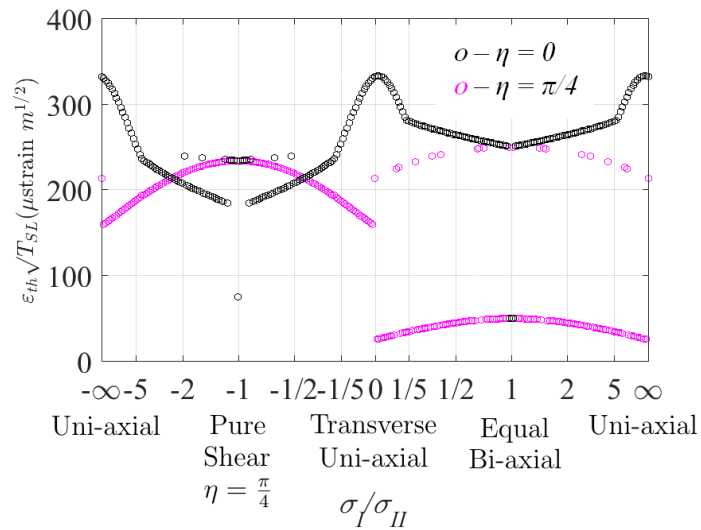

Figure 9.5: *$\varepsilon_{th} \sqrt{T_{SL}}$ variation of optimum designs for $\eta = 0$ and $\pi/4$.*
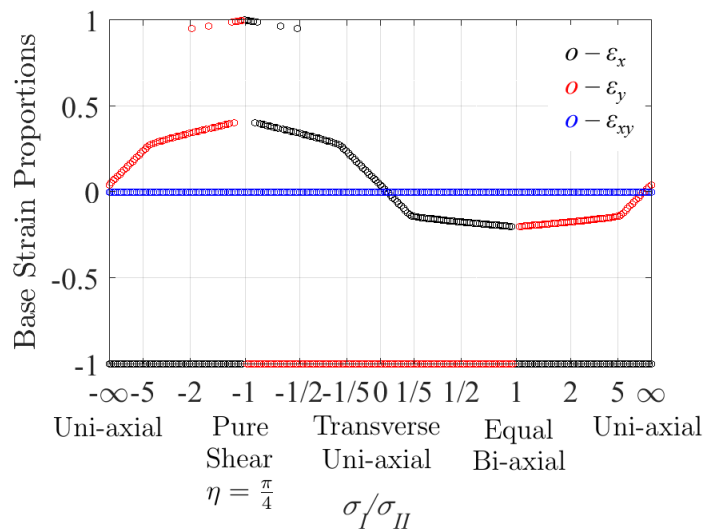

**Figure 9.6:** *Strain state proportions for optimal laminates when $\eta = 0$.*

Maximisation of $\sigma_{th}\sqrt{T_{SL}}$ in the dominant load direction results in the global stress state at failure being maximised, as the design stress loading ratios are fixed. Only the $\sigma_{th}\sqrt{T_{SL}}$ in the dominant stress direction, x, y or xy is plotted. Maximum damage tolerance stress performance of optimal laminates varies with the design stress loading since for more uni-axial loads a dominating stiffness exists alongside an increased $\varepsilon_{th}\sqrt{T_{SL}}$ through the sublaminate having the softest response to the load, minimising the SERR, see Eq.s 9.4.2 and 9.3. The stress in other directions will be lower at failure, due to the defined design loading, and consequently a lower stiffness is used in these directions. Whereas for a combined loading state stiffness must be shared in other directions to ensure the global failure stress is higher. The appropriate stiffness is placed in the loading directions in order to maximise the global stress applied at failure.

Fig. 9.5 shows the thickness normalised damage tolerance strain, $\varepsilon_{th}\sqrt{T_{SL}}$, in the dominant stress direction for the designs optimised for maximum $\sigma_{th}\sqrt{T_{SL}}$. For $\eta = 0$, $\varepsilon_{th}\sqrt{T_{SL}}$ still peaks for uni-axial loadings but is seen to approximately linearly vary from $\sigma_I/\sigma_{II} = \pm1/5$ or ±5 to the equal bi-axial loadings, $\sigma_I/\sigma_{II} = \pm1$. For $\eta = \pi/8$ peaks are still found for equal bi-axial loadings ($\sigma_I/\sigma_{II} = \pm1$). Discrepancies for positive loading ratios are seen with high and low $\varepsilon_{th}\sqrt{T_{SL}}$ being apparent.

Small dispersion in performance around $\sigma_I/\sigma_{II} = -1$ in Fig. 9.4 and Fig. 9.5 for $\eta = 0$, conicides with the strain state variation seen in Fig. 9.6. The proportions of the strain components for each optimal design at each σ_I/σ_{II} for $\eta = 0$ are plotted in Fig. 9.6. The largest strains are given a magnitude value of 1 and their compressive or tensile nature is maintained. The shear strain is zero as expected, with variation of bi-axial strains only for $\eta = 0$. The magnitude of the bi-axial strain ratios of optimal designs do not coincide with the design stress loading ratio. Therefore a stress loading condition is not the same as a strain loading condition. This is because placing stiffness proportionally in directions proportional to the stress ratio (i.e. minimising in-plane elastic energy) does not maximise damage tolerance stress performance.

Eq. 9.4.2 shows that there is a trade-off between increasing the propagation strain state, $\varepsilon_{th}\sqrt{T_{SL}}$, and the laminate stiffness $[\overline{Q}]$ in order to increase the laminate stress state $\sigma_{th}\sqrt{T_{SL}}$, which has fixed design load ratios in x, y and xy. Therefore the stress ratios and stiffnesses dictate the strain ratios the laminate is placed under. The design variables that the optimisation can vary affect the stiffness of the full laminate and sublaminate directly. The $\varepsilon_{th}\sqrt{T_{SL}}$, as per Eq. 9.3, is affected only by the laminate strain state and the sublaminate stiffness, both of which are co-dependent, culminating in the expression $\varepsilon_\theta^T\,\overline{Q}_{SL}\,\varepsilon_\theta$ in Eq. 9.3, being double that of the sublaminate in-plane elastic energy. In order to provide a large enough $\varepsilon_{th}\sqrt{T_{SL}}$ that balances with $[\overline{Q}]$ to provide maximum $\sigma_{th}\sqrt{T_{SL}}$, the $\varepsilon_\theta^T\,\overline{Q}_{SL}\,\varepsilon_\theta$ must be sufficiently

minimised. However, minimising the sublaminate $\left[\overline{Q}_{SL}\right]$ obstructs the minimisation of the laminate strain state since reducing the stiffness in 50% of the laminate (sublaminate) results in the strain under load being increased as the laminate is less stiff. Therefore a compromise must be made between sufficiently minimising $\left[\overline{Q}_{SL}\right]$ and minimising the strain state to provide a sufficiently maximised $\varepsilon_{th}\sqrt{T_{SL}}$.
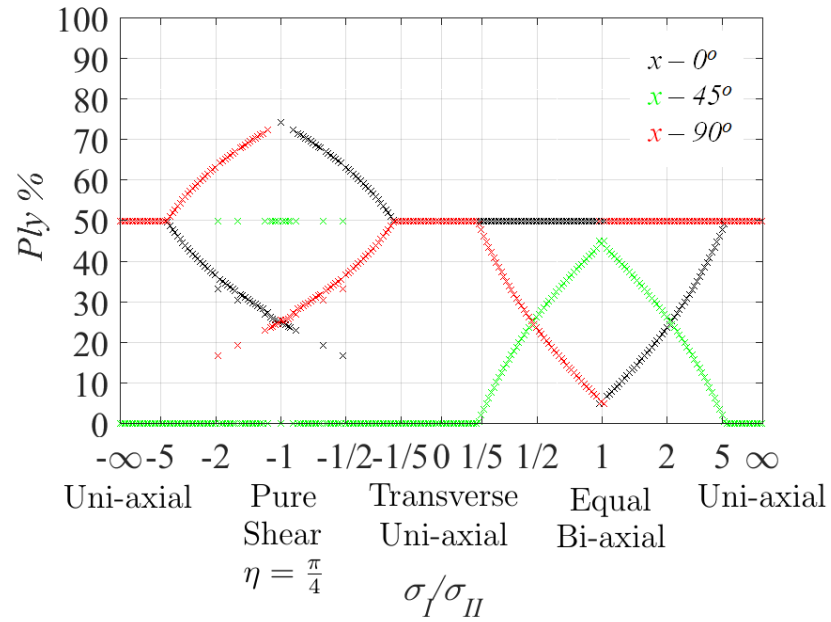
(a) *Laminate.*
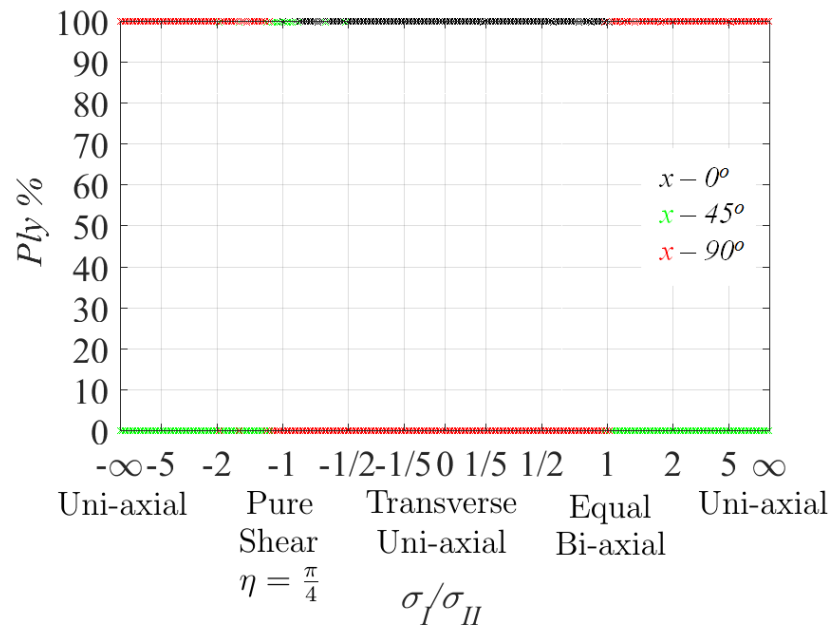
(b) *Sublaminate.*

Figure 9.7: *Optimal (a) laminate and (b) sublaminate ply percenatges for $0°$, $\pm45°$ and $90°$ plies for maximisation of $\sigma_{th}\sqrt{T_{SL}}$.*

Fig. 9.7 (a) and (b) show the variation in optimal laminate and sublaminate ply percentages using standard angles, respectively, for $\eta = 0$. The sublaminate designs contain 100% of one angle type for all loadings, despite the large range of ply percentages and combinations of angles to choose from. The sublaminate plies always align orthogonal to the dominant strain loading, which must be the most important aspect in reducing the $\varepsilon_\theta^T \overline{Q}_{SL} \varepsilon_\theta$ expression to provide a sufficiently large $\varepsilon_{th}\sqrt{T_{SL}}$ to maximise the $\sigma_{th}\sqrt{T_{SL}}$. This will come at the detriment to the maximising of the stiffness (for maximising $\sigma_{th}\sqrt{T_{SL}}$) and the minimising of the strain (for maximising $\varepsilon_{th}\sqrt{T_{SL}}$, to maximise $\sigma_{th}\sqrt{T_{SL}}$). Nonetheless $\sigma_{th}\sqrt{T_{SL}}$ is maximised with these singular ply angles. For $\sigma_I/\sigma_{II} \approx -1$ solely $\pm 45°$s offer the softest response to the load ($0°/90°$ in shear). For dominant axial(transverse) loads solely $90°(0°)$ plies are optimal for the respective cases, again being less stiff in the direction of load. These angles may not provide as large a strength as shown since compression failure in the matrix direction will occur. These angles minimise the in-plane elastic energy in the sublaminate for a given bi-axial strain loading, thus reducing the SERR. The energy expression seen in the dominator of Eq. 9.5, can be expanded to:

$$\varepsilon_\theta^T \overline{Q}_{SL} \varepsilon_\theta = 2\,U_{SL} = \overline{Q}_{SL,11}\,\varepsilon_x^2 + 2\overline{Q}_{SL,12}\,\varepsilon_x\,\varepsilon_y + \overline{Q}_{SL,22}\,\varepsilon_y^2 + \overline{Q}_{SL,66}\,\gamma_{xy}^2 \qquad (9.5)$$

If sublaminates are not balanced then $\overline{Q}_{SL,16}$ and $\overline{Q}_{SL,26}$ terms will be present in Eq. 9.5. Since all $\left[\overline{Q}_{SL}\right]$ terms are positive values, energy is only taken away from this expression when the $2\overline{Q}_{SL,12}\,\varepsilon_x\,\varepsilon_y$ term features opposite sign strains, as is generally the case for negative σ_I/σ_{II} load ratios. However in Fig. 9.5 it can be seen that for $\sigma_I/\sigma_{II} < 0$ the laminate has a lower $\varepsilon_{th}\sqrt{T_{SL}}$ generally. This is due to the laminate straining more under load in this region, as it is softer under perpendicular loads which act in the directions of each other's Poisson's deformation.

The optimal laminate designs shown in Fig. 9.7(a) can be seen to contain 50% sublaminate angles, dominated by one ply. The core of the laminate is left, which attempts to increase the $\sigma_{th}\sqrt{T_{SL}}$ by providing maximum stiffness and reducing the strain magnitudes, which also consequently reduces the $\varepsilon_{th}\sqrt{T_{SL}}$ and thus $\sigma_{th}\sqrt{T_{SL}}$. As in Chapter 5, $0°$ and $90°$ plies dominate in the core for $\sigma_{th}\sqrt{T_{SL}} < 0$, giving the greatest stiffness under load due to the positive cross term, $2q_{12}\,\sigma_I\sigma_{II}$ in Eq. 3.11.

The results for the full range of multi-axial loadings are now presented and all the results are discussed together. The dominant stress directions, dictating the plotted values of $\sigma_{th}\sqrt{T_{SL}}$ and $\varepsilon_{th}\sqrt{T_{SL}}$, are shown in Fig. 9.8 for the range of design stress loadings. Fig. 9.8 shows $\sigma_{th}\sqrt{T_{SL}}$ for all σ_I/σ_{II} and η. Damage tolerance stress performance can be seen to peak at a value of 25 MPa m$^{\frac{1}{2}}$ for uni-axial loadings. As discussed previously for Fig. 9.4, this is due to stiffness being placed in the appropriate direction to maximise the stress and minimise the strain state in order

to reduce the $\varepsilon_{th} \sqrt{T_{SL}}$ from Eq. 9.3. The loading state repeats every $\eta = \pi/2$ and so surrounding areas of blue show where the laminate has a less dominant loading state; where stiffness is required in all directions, minimising the maximum $\sigma_{th} \sqrt{T_{SL}}$ that can be achieved.
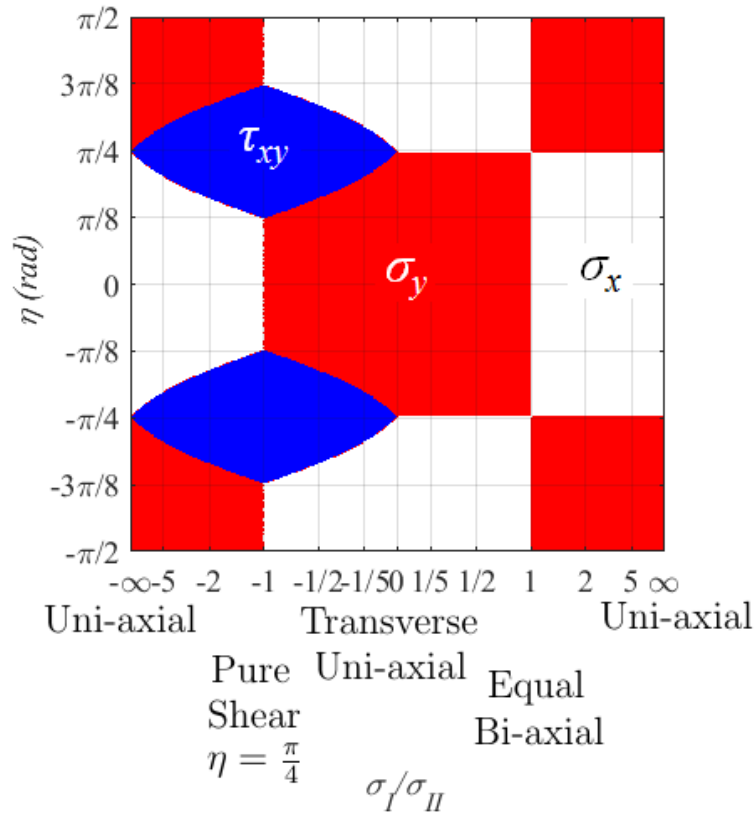
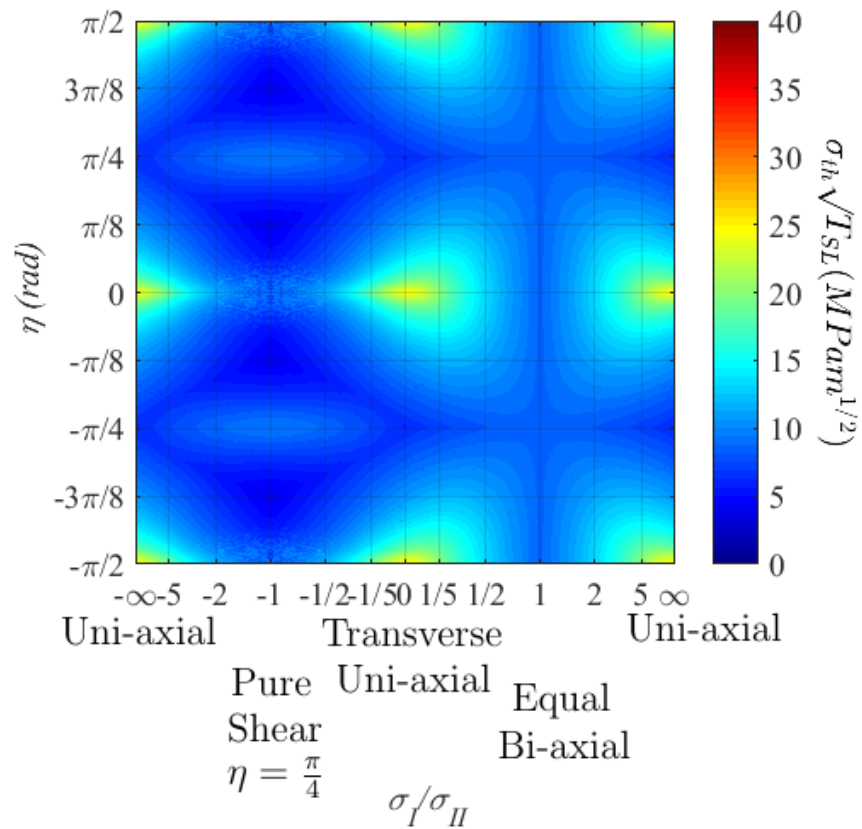**Figure 9.8:** *Dominant stress directions for the design stress loading landscape.*

Figure 9.9: *Maximum $\sigma_{th}\sqrt{T_{SL}}$ for optimal laminates for design stress loadings.*

The dominant strain loadings for the range of design stress loadings are shown in Fig. 9.10. They can be seen to match the dominant stress loadings seen in Fig. 9.8, with discrepancies shown around the shear components due to optimal laminate stiffnesses creating slightly greater or less shear strain under load. In Fig. 9.11 the damage tolerance strain performance, $\varepsilon_{th} \sqrt{T_{SL}}$, for the designs optimised for maximum $\sigma_{th} \sqrt{T_{SL}}$ are plotted. For $\sigma_I/\sigma_{II} < 0$, $\varepsilon_{th} \sqrt{T_{SL}}$ is lower compared to $\sigma_I/\sigma_{II} > 0$, due to the laminate straining more for these negative stress ratios. For a 1 mm sublaminate (4 mm laminate) the propagation strain ranges from 4700-10500 μstrain, and the propagation stresses from 200-750 MPa, depending on the loading state. For thinner or thicker sublaminates these values will increase or decrease respectively (see Fig. 9.2). This generally predicts greater damage tolerance performance than the industry strain allowables allow but some values are unrealistically high. This technique potentially allows greater weight savings due to being able to capture the fundamental damage tolerance relationship.
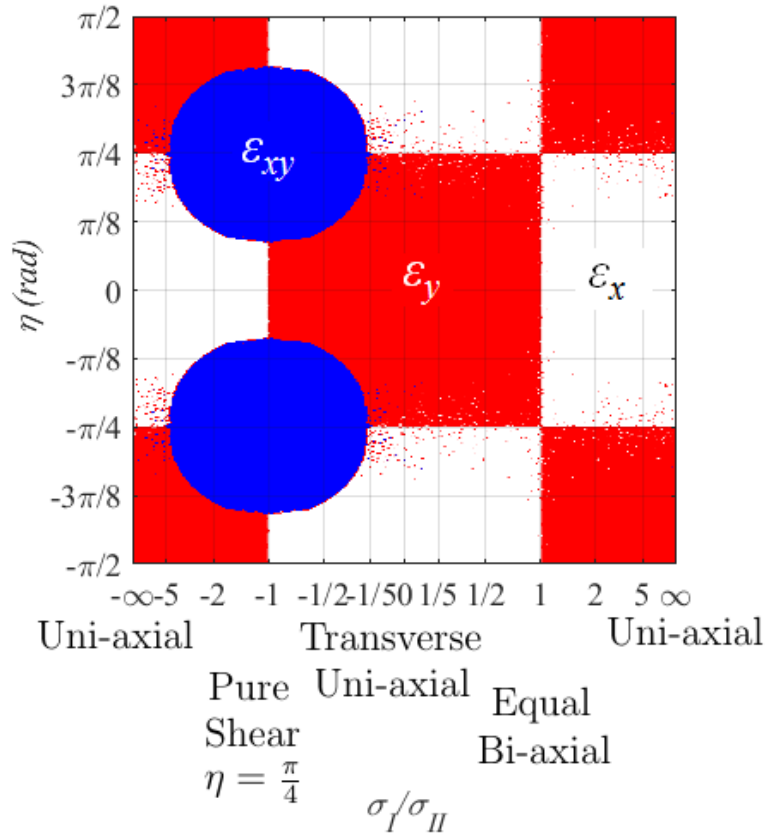
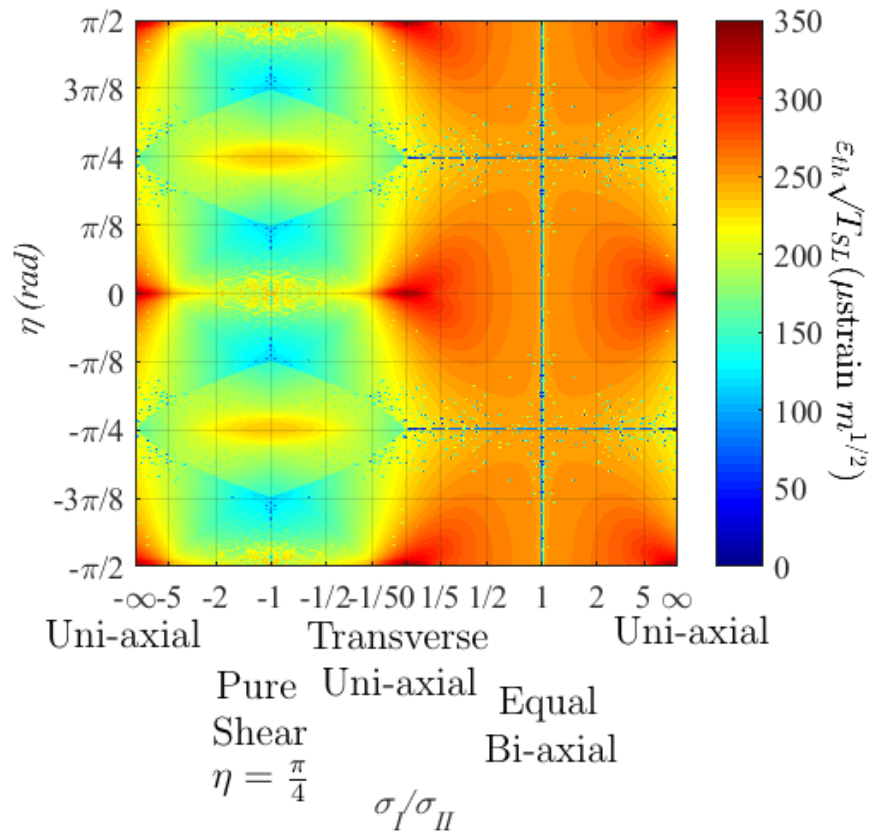**Figure 9.10:** *Dominant strain directions for the design stress loading landscape.*

Figure 9.11: $\varepsilon_{th}\sqrt{T_{SL}}$ *for optimal laminates for design stress loadings.*

The optimal laminate and sublaminate ply percentages for 0°, ±45° and 90° are shown in Figs. 9.12 (a,c,e) and (b,d,f) respectively. Observing the ply percentages of the SAs in the sublaminates of the optimum designs show that, again 100% of one angle type is seen in the sublaminates throughout. ±45° appear around the σ_I/σ_{II} = -1, for small values of η (which repeats near $\eta = \pi/2$). From Eq. 9.4, the in-plane energy in the sublaminate is theoretically reduced via reducing $\overline{Q}_{SL,11}$ and $\overline{Q}_{SL,22}$, this decrease can instead be directly exchanged for a decreased $\overline{Q}_{SL,12}$. Therefore either ±45° or a 0°/90° designs can be placed in the sublaminate for minimisation of this energy, maximising $\varepsilon_{th}\sqrt{T_{SL}}$. ±45° designs are likely favoured for η just above zero as they help increase the stiffness to a shear load, increasing $\sigma_{th}\sqrt{T_{SL}}$. For the remainder of the design loading, optimal sublaminate designs are all 0° or all 90° as they minimise the sublaminate energy by being orthogonal to the strain loading, which helps to provide sufficient $\varepsilon_{th}\sqrt{T_{SL}}$ to maximise $\sigma_{th}\sqrt{T_{SL}}$. Laminate designs (see Figs. 9.12 (a,c,e)) use the remaining 50% of the laminate (core) to maximise the laminate stiffness under load in order to maximise $\sigma_{th}\sqrt{T_{SL}}$, and so for axially, transverse and shear dominated loading, more 0°, ±45° and 90° plies are included, respectively.

(a) *Laminate* 0°.

(b) *Sublaminate* 0°.

(c) *Laminate* ±45°.

(d) *Sublaminate* ±45°.
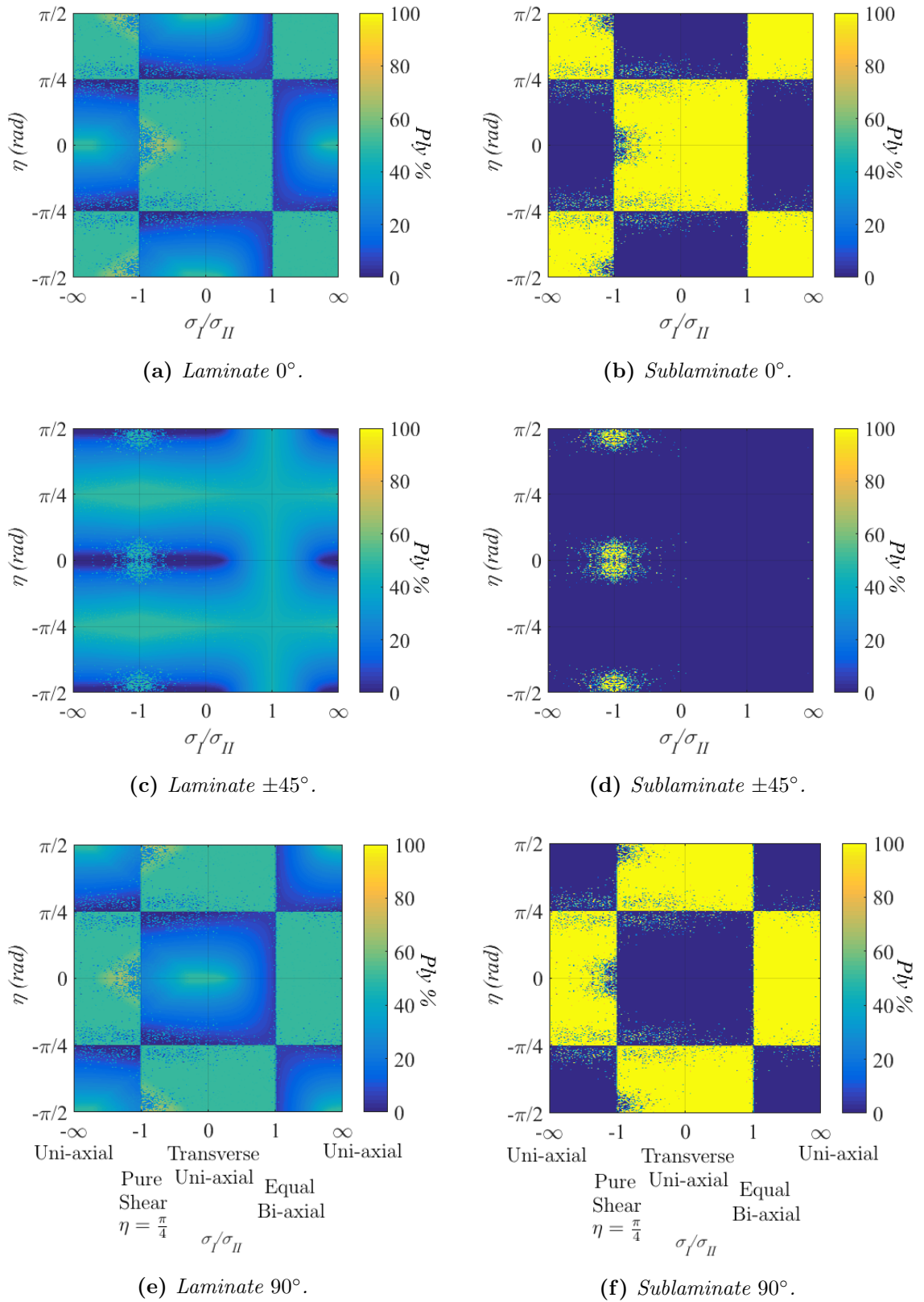

(e) *Laminate* 90°.

(f) *Sublaminate* 90°.

Figure 9.12: *Optimal laminate (a,c,e) and sublaminate (b,d,f) ply percentages for 0°, ±45° and 90° plies, for (1)(i) optimisation regime.*

(1)(ii) Minimum in-plane laminate energy with damage tolerance stress constraint

Results are for laminates optimised for minimum in-plane elastic energy with a damage tolerance stress constraint for all bi-axial loadings ($\eta = 0$). 2D plots are again introduced first for clarity.

Fig. 9.13 shows the optimum laminate damage tolerance stress performance before any damage constraint is applied and after the maximum constraint is applied. $\sigma_{th}\sqrt{T_{SL}}$ increases towards uni-axial loadings even without designing for the damage tolerance, due to the ability of dominant stiffness to increase $\sigma_{th}\sqrt{T_{SL}}$. The maximum damage tolerance performance curve is also shown in Fig. 9.4, as $\eta = 0$, from the separate maximisation optimisation. The maximum constraint doubles the damage tolerance performance, seen for uni-axial loadings, and at worst increases it by a $\frac{1}{3}$.

The sublaminate and laminate of designs with the maximum constraint applied are identical to that seen in Fig. 9.7. Fig. 9.14 shows the optimal laminate designs without the constraint, which match the designs for minimum elastic energy using SAs in Chapter 5. The sublaminate of these laminates has similar ply percentages as it is not influenced by any constraint.
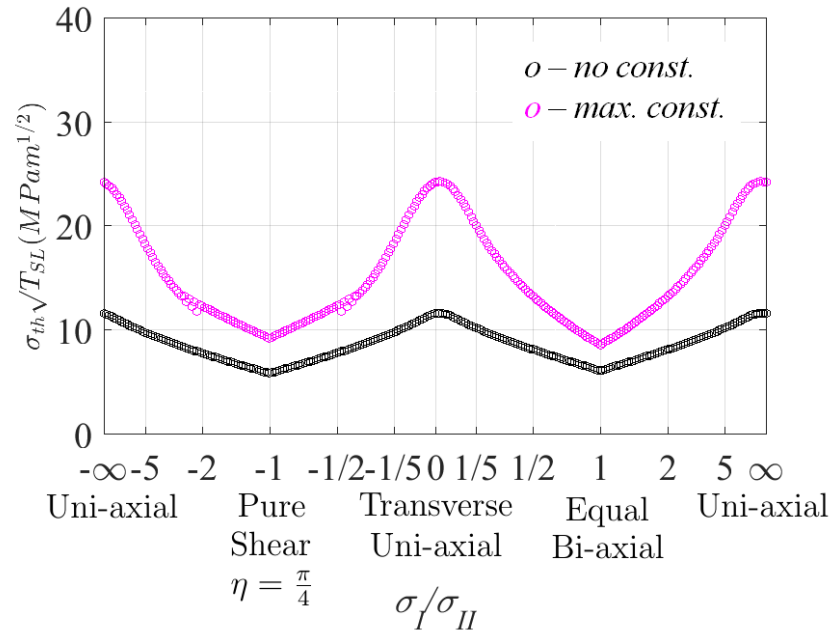
Figure 9.13: *Laminate $\sigma_{th} \sqrt{T_{SL}}$ for $\sigma_{th} \sqrt{T_{SL}}$ constraint = 0 and 40 MPa $m^{\frac{1}{2}}$*
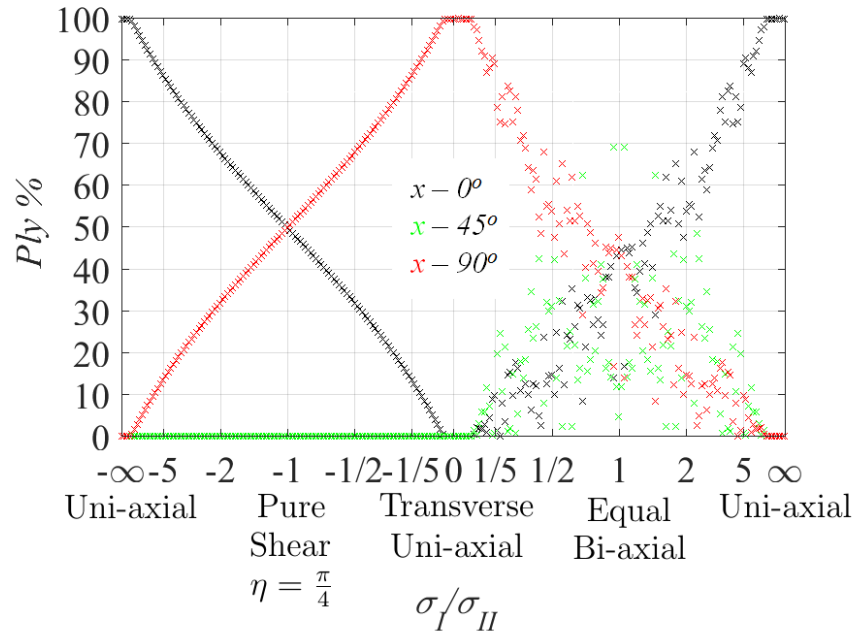
Figure 9.14: *Optimal laminate and sublaminate ply percentages for $0°$, $\pm 45°$ and $90°$ plies, for (1)(ii) optimisation regime when no constraint is applied.*

$\sigma_{th} \sqrt{T_{SL}}$ performance of the optimal laminates as the $\sigma_{th} \sqrt{T_{SL}}$ constraint is increased is shown in Fig. 9.15. Fig. 9.16 shows the constraint values for when the laminate optimisation could no longer meet the damage tolerance constraint. The laminate is seen to have the same $\sigma_{th} \sqrt{T_{SL}}$ performance up until the point a greater damage tolerance design is needed, this limit is dictated by the initial $\sigma_{th} \sqrt{T_{SL}}$ per-

formance seen in Fig. 9.13. To increase the damage tolerance performance, optimal designs must change. A sudden switch from the least damage tolerant design to the much higher damage tolerant design is seen, shown by the same bands of $\sigma_{th}\sqrt{T_{SL}}$ running vertically as the constraint is increased. This suggests that even though the damage tolerance value of $\sigma_{th}\sqrt{T_{SL}}$ is not required to meet the constraint, it is the most efficient way to increase $\sigma_{th}\sqrt{T_{SL}}$ whilst keeping the in-plane elastic energy to a minimum.

The in-plane elastic energy is plotted in Fig. 9.17. The general inefficiencies towards equal bi-axial loads are shown, as discussed in Chapter 5. There is a loss in in-plane efficiency, an approximation of in-plane strength, as the laminate becomes maximally damage tolerant. The energy shows that the maximum damage tolerant design is switched to immediately as a higher damage tolerant constraint is applied, with a more transitional area for $\sigma_I/\sigma_{II} \approx -1$. This sudden switch in design reveals the reasons for why optimal sublaminate plies that are all orthogonal to the dominant strain, coincide with maximum $\sigma_{th}\sqrt{T_{SL}}$ performance. If these plies offer the least penalty to the in-plane energy then the in-plane stiffness must be as large as possible, maximising $\sigma_{th}\sqrt{T_{SL}}$.

Laminate and sublaminate designs are shown in Figs. 9.18 (a,c,e) and (b,d,f) respectively. As the laminates are forced from the original designs with no constraint, to having a requirement of greater $\sigma_{th}\sqrt{T_{SL}}$ applied, the sublaminates designs are seen to vary. This includes designs having a variety of all angles present, up to 100% of one angle. $\pm45°$s dominate for $\sigma_I/\sigma_{II} \approx -1$ once the initial all 0° or all 90° plies (depending on σ_I/σ_{II}) are removed (initially present since they improve on $\sigma_{th}\sqrt{T_{SL}}$). They minimise the energy in the sublaminate by producing the softest response to a given strain state. This thus increases $\varepsilon_{th}\sqrt{T_{SL}}$ and the $\sigma_{th}\sqrt{T_{SL}}$. The same is true for the optimal sublaminate designs created of entirely all 0° and 90° plies for loadings that are transversely and axially dominant respectively.
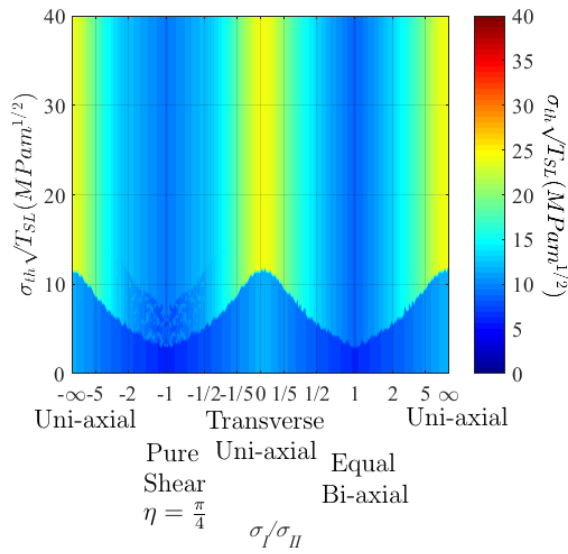
Figure 9.15: *Laminate $\sigma_{th}\sqrt{T_{SL}}$ as the $\sigma_{th}\sqrt{T_{SL}}$ constraint is increased.*
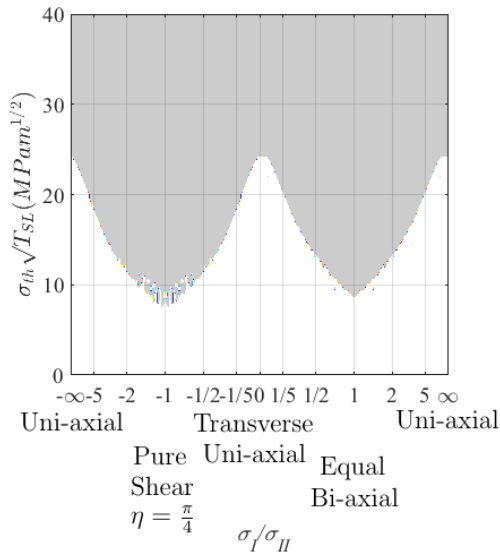
Figure 9.16: *The stress $\left(\sigma_{th}\sqrt{T_{SL}}\right)$ constraints vs. bi-axial loading, indicating in grey where the constraint is not satisfied.*
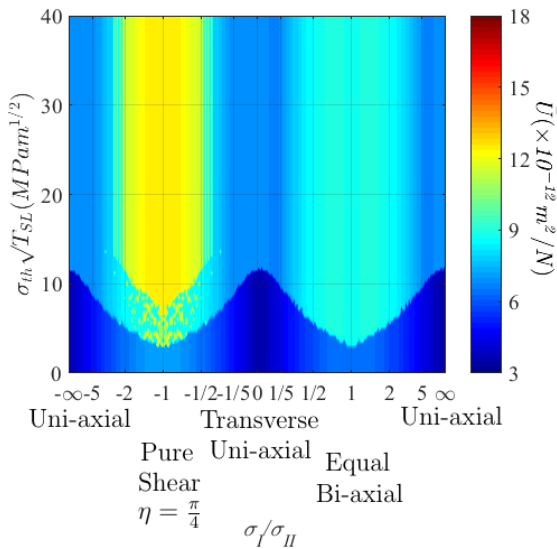
Figure 9.17: *Laminate $\overline{U}$ as the $\sigma_{th}\sqrt{T_{SL}}$ constraint is increased.*

(a) *Laminate* $0°$.

(b) *Sublaminate* $0°$.

(c) *Laminate* $\pm 45°$.

(d) *Sublaminate* $\pm 45°$.

(e) *Laminate* $90°$.

(f) *Sublaminate* $90°$.

Figure 9.18: *Optimal laminate (a,c,e) and sublaminate (b,d,f) ply percentages for* $0°$, $\pm 45°$ *and* $90°$ *plies, for the (1)(ii) optimisation regime.*

189

9.6.2 (2) Sublaminate optimisation for damage tolerance strain

Designing for damage tolerance strain under design strain loadings removes the added complexities with laminate stiffness creating variable strains for the same stress loading. The point of propagation is also dictated by the strain state applied to the sublaminate and so a closer view of the variables that influence damage tolerance can be investigated using this technique. The use of these techniques allows the designer to ensure a certain level of damage tolerance failure strain whilst knowing the strain ratio that the laminate will be placed under.

(2)(i) Maximisation of damage tolerance strain for multi-axial loadings

Results are shown for the maximisation of sublaminate $\varepsilon_{th}\sqrt{T_{SL}}$ for all strain loadings described by $\varepsilon_I/\varepsilon_{II}$ and η.
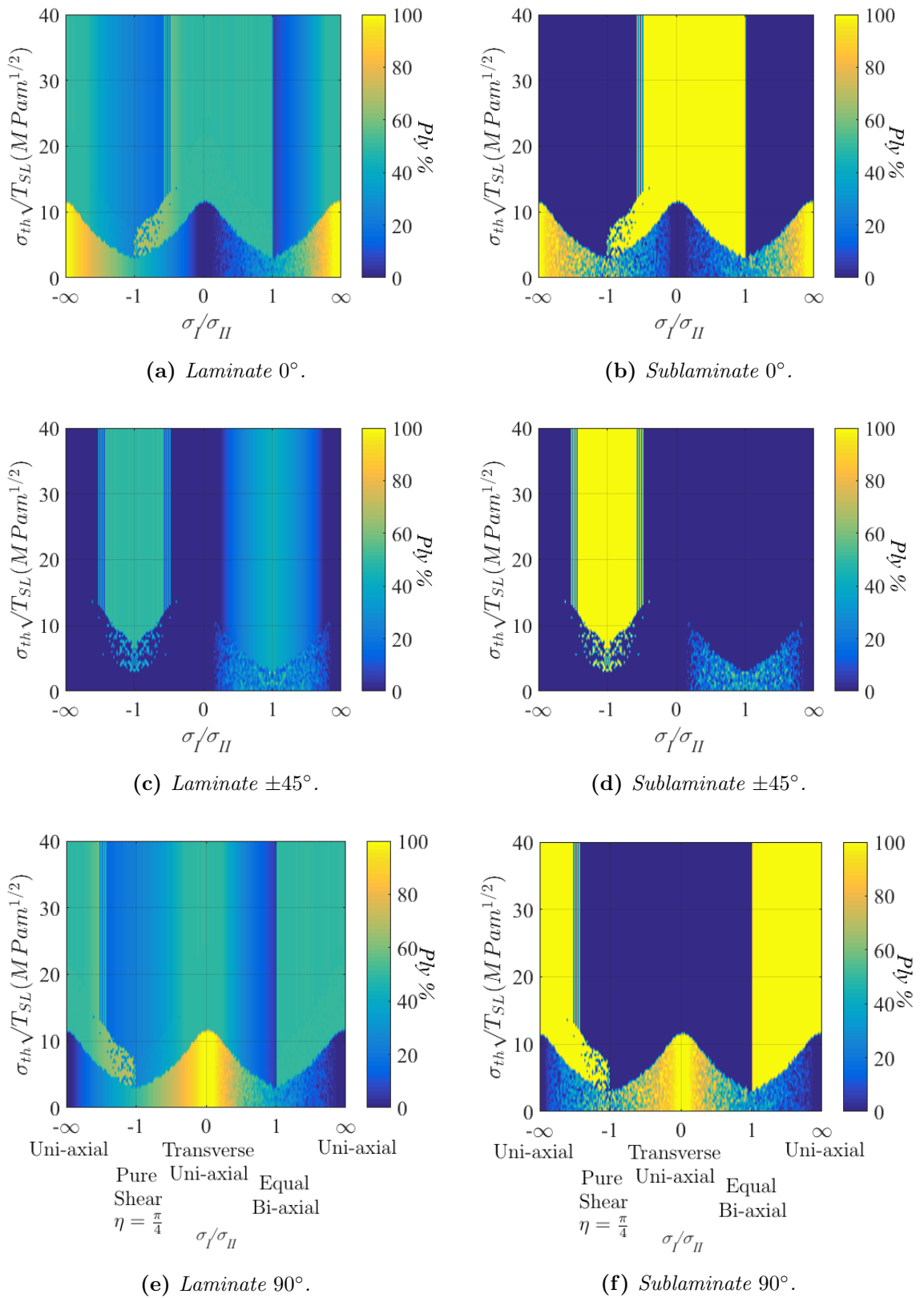
Fig. 9.19 shows that for $\varepsilon_I/\varepsilon_{II} < 0$, larger $\varepsilon_{th}\sqrt{T_{SL}}$ are possible, with peaks occurring at uni-axial loadings due to the softer sublaminate response when the plies are 100% orthogonal to the maximum strain direction as shown by all designs in Fig. 9.20. This shows that uni-axial loads maximise $\varepsilon_{th}\sqrt{T_{SL}}$ by having the softest response to the load, minimising the SERR in Eq. 9.3.

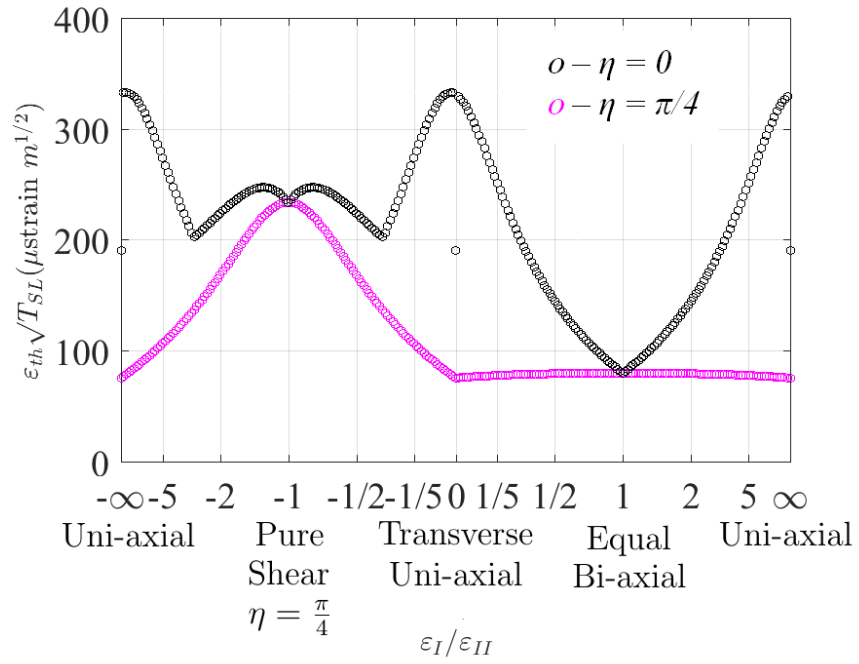**Figure 9.19:** *Maximum $\varepsilon_{th}\sqrt{T_{SL}}$ variation of optimal sublaminate designs for $\eta = 0$ and $\eta = \pi/4$*
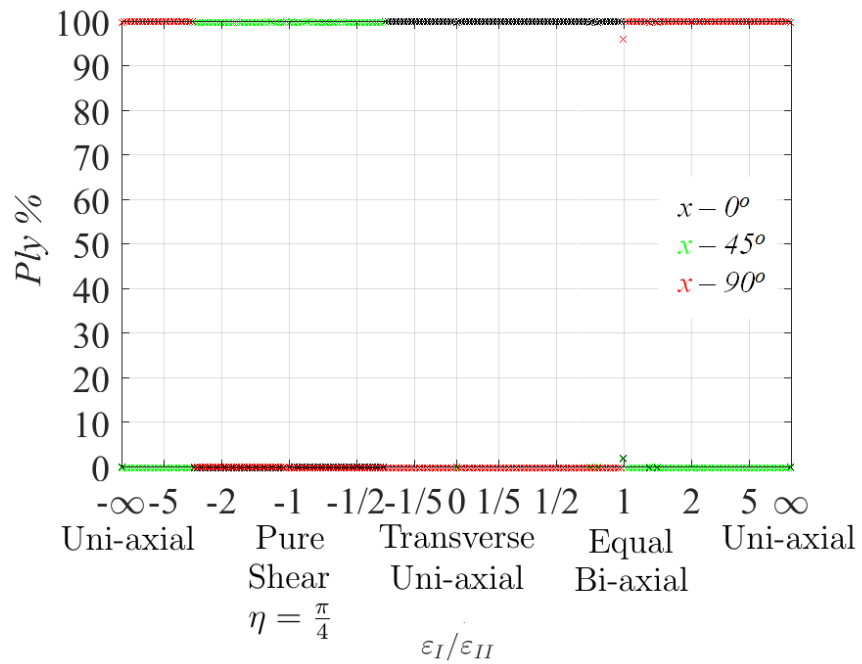

Figure 9.20: *Optimal sublaminate ply percentages for $0°$, $\pm 45°$ and $90°$ plies for $\eta = 0$.*

The dominant strain loadings for all possible design strain loadings are shown in Fig. 9.21. This shows the direction of the $\varepsilon_{th} \sqrt{T_{SL}}$ plotted for the optimal designs in Fig. 9.22. A complex pattern is seen showing the fundamental variation in $\varepsilon_{th} \sqrt{T_{SL}}$ for all possible strain loading scenarios that could exist when a laminate is loaded. Greater variation in performance is seen for $\varepsilon_I/\varepsilon_{II} < 0$ due to the greater design variation and the ability of the sublaminate SERR to be minimised with the cross-term $2\overline{Q}_{SL,12}\, \varepsilon_x\, \varepsilon_y$ in Eq. 9.5 being negative, maximising Eq. 9.3 for $\varepsilon_{th} \sqrt{T_{SL}}$. The optimal sublaminate designs plotted in Figs. 9.23(a-c) show 100% of one angle type is again always seen in the sublaminate. Plies always align most orthogonal to the maximum strain direction minimising the in-plane sublaminate energy in Eq. 9.5, and thus minimising the SERR, by creating stiffness components that compliment a given strain state maximising $\varepsilon_{th} \sqrt{T_{SL}}$. For $\varepsilon_I/\varepsilon_{II} < 0$, around $\eta = 0$, $\pm\frac{n\pi}{2}$ $\pm45°$s are seen where the loading is close to shear rotated by $45°$. For other loadings, axial dominant strains produce $90°$ optimal plies, and transverse, $0°$ plies.

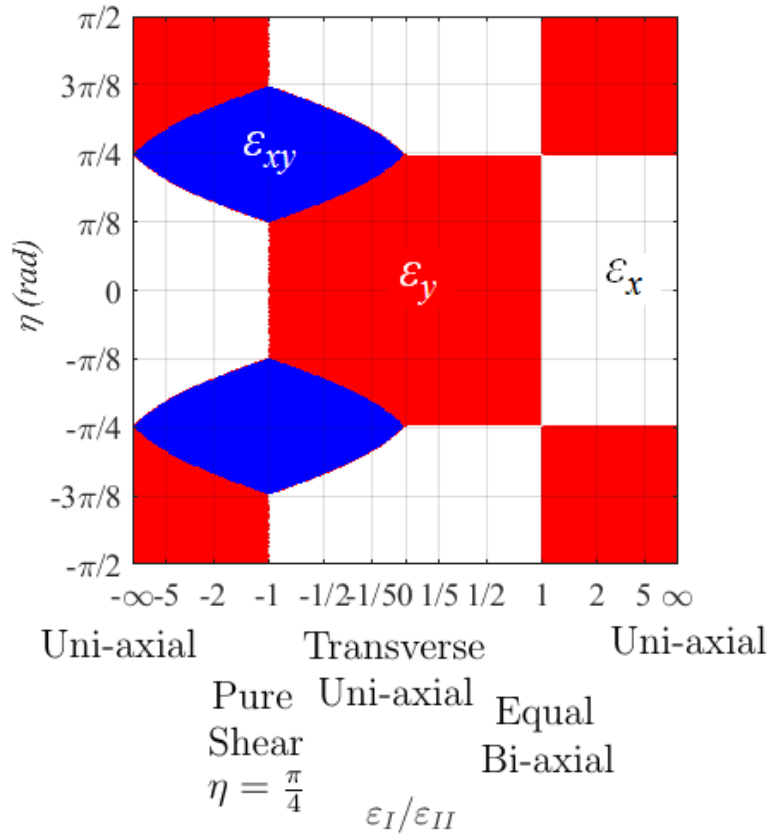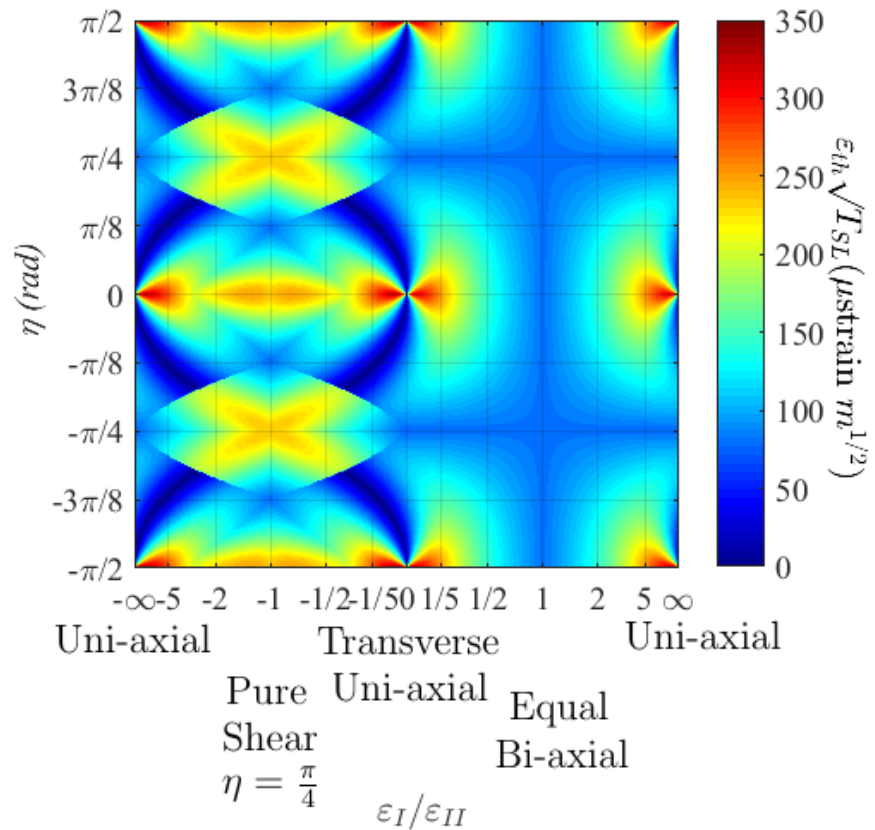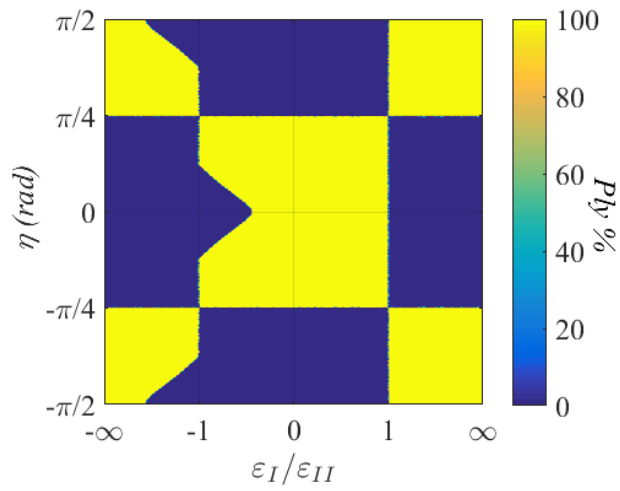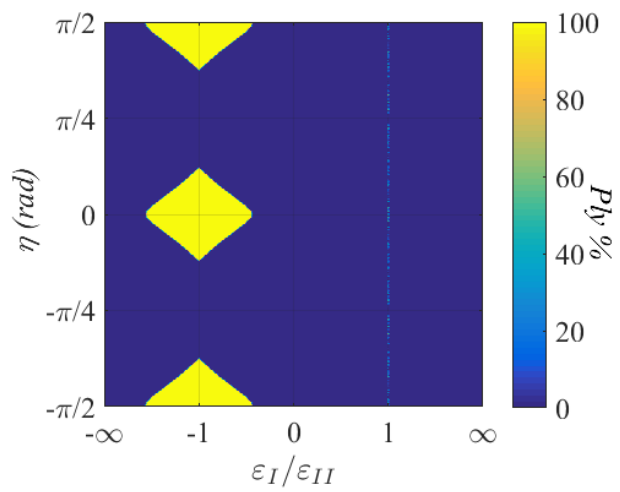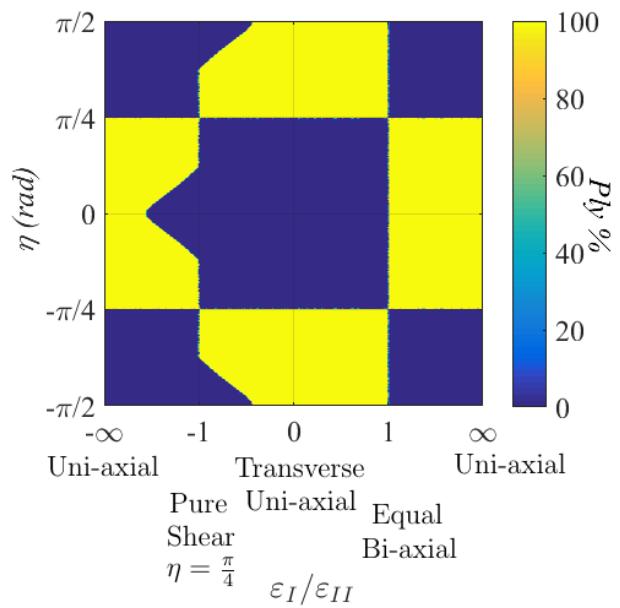**Figure 9.21:** *Dominant strain directions for the design strain loading landscape.*

Figure 9.22: *Maximum $\varepsilon_{th}\sqrt{T_{SL}}$ for optimal laminates for design strain loadings.*

(a) *Sublaminate* $0°$.

(b) *Sublaminate* $\pm45°$.

(c) *Sublaminate* $90°$.

Figure 9.23: *Optimal sublaminate ply percentages for* $0°$*,* $\pm45°$ *and* $90°$ *plies for design strain loadings.*

(2)(ii) Maximum in-plane sublaminate energy with damage tolerance strain constraint

The sublaminate in-plane elastic energy was attempted to be maximised whilst placing damage tolerance strain constraints for a range of bi-axial strain loadings. For a strain loading this maximisation would drive the design towards a global stiff configuration (minimisation is the equivalent for a stress loading) so that the in-plane performance could be maintained. However problems with the GA meeting constraints became apparent even though better damage tolerance designs were available. The GA tended to prefer settling for large energies (high stiffnesses) with no sacrifice in energy to meet the constraints. Therefore the maximisation objective was removed and the optimisation was ran with only the requirement of the strain constraint, with the energy of the laminate artificially made to not affect the GAs choice of designs. Unfortunately this creates the possibility that over designed laminates may be found as optimal.

Fig. 9.24 clearly shows that the initial laminate has higher normalised damage tolerance strain performance compared to the design with the maximum constraint applied. This seems illogical, however as the constraint was increased there became a point at which the constraint could not be met and in the attempts of the GA to find a better design it ends up settling in a sufficiently local optima where the stopping criteria is met. This becomes clear when viewing Figs. 9.27 and 9.28 after the laminates can no longer meet the constraints, the sublaminate damage tolerance performance is reduced even though the GA desires a higher performance when attempting to meet the constraint.

In Fig. 9.25, the initial sublaminate design, selected before a constraint is met, is shown. This figure sheds some light on how the optimiser works, with almost 100% of one angle for all loadings being the chosen design, despite a constraint of 0 damage tolerance performance. Plies are also orthogonal to the dominant strain loading which is known to maximise the normalised damage tolerance strain $\varepsilon_{th} \sqrt{T_{SL}}$. The creation of optimum damage tolerant designs before when a constraint on performance is set to zero suggests a constraint has been followed in some capacity. The GA works as follows: it knows a constraint is applied but does not know the magnitude of this constraint, and so it attempts to meet this as best it can without incurring penalties. Since nothing limits the GA from doing this, as this is it's only design objective for all design loadings, the sublaminates become over designed and have maximum performance from the beginning until the constraint is unfeasible. The non-optimal designs seen past the maximum constraint have sublaminates created of less than 100% of one angle type as shown in Fig. 9.26 for the maximum applied constraint and in Figs. 9.29 (a), (b) and (c). This shows there is a difference between no constraint and a constraint of value zero, which are used interchange-

ably in this thesis as there is generally no difference for laminate design that is constrained by an objective.

For a given strain loading there exists non-optimal and optimal sublaminate plies which vary the damage tolerance strain performance three-fold, close to uni-axial loadings, shown fully in Fig. 9.27. This figure clearly shows the large effect sublaminate stacking has on increasing the damage tolerance performance and thus why plies orthogonal to the dominant strains always seem to be optimal.
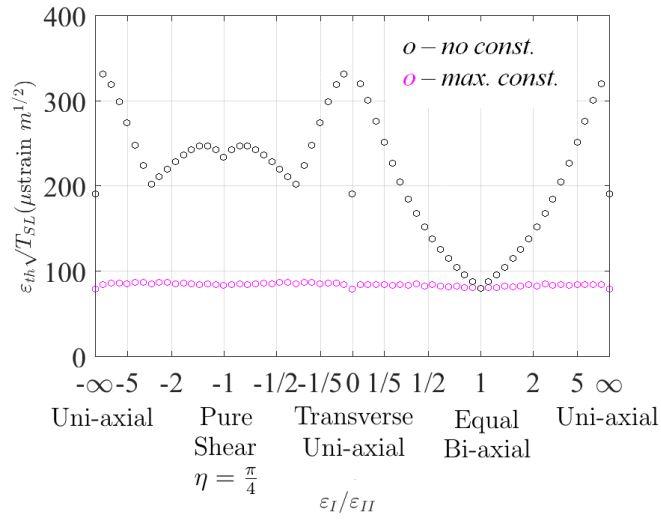
Figure 9.24: *Laminate $\varepsilon_{th}\sqrt{T_{SL}}$ for $\varepsilon_{th}\sqrt{T_{SL}}$ constraint = 0 and 350 μstrain $m^{\frac{1}{2}}$.*
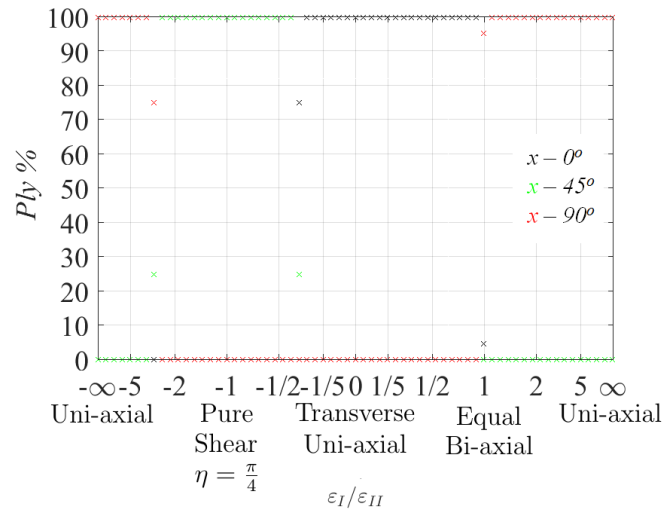
Figure 9.25: *Optimal sublaminate ply percentages for 0°, ±45° and 90° plies for bi-axial loadings, with no constraint applied.*
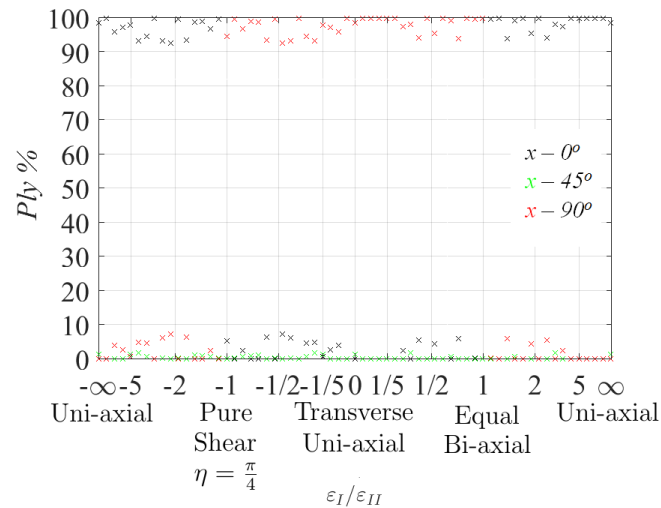
Figure 9.26: *Optimal sublaminate ply percentages for 0°, ±45° and 90° plies for bi-axial loadings, with maximum constraint applied.*
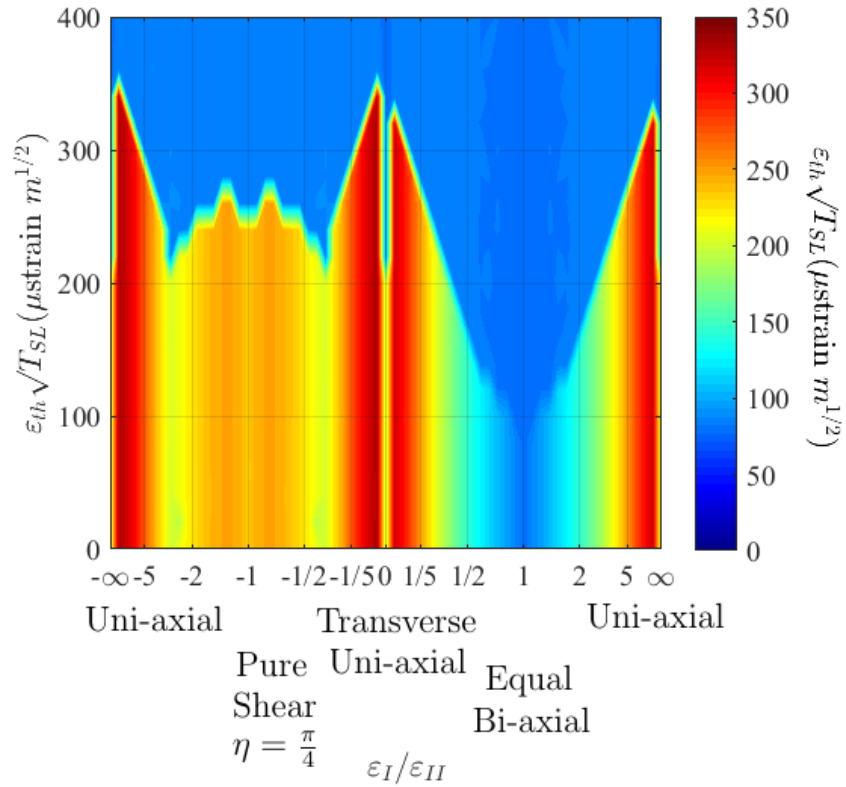
Figure 9.27: *Laminate $\varepsilon_{th}\sqrt{T_{SL}}$ as the $\varepsilon_{th}\sqrt{T_{SL}}$ constraint is increased.*
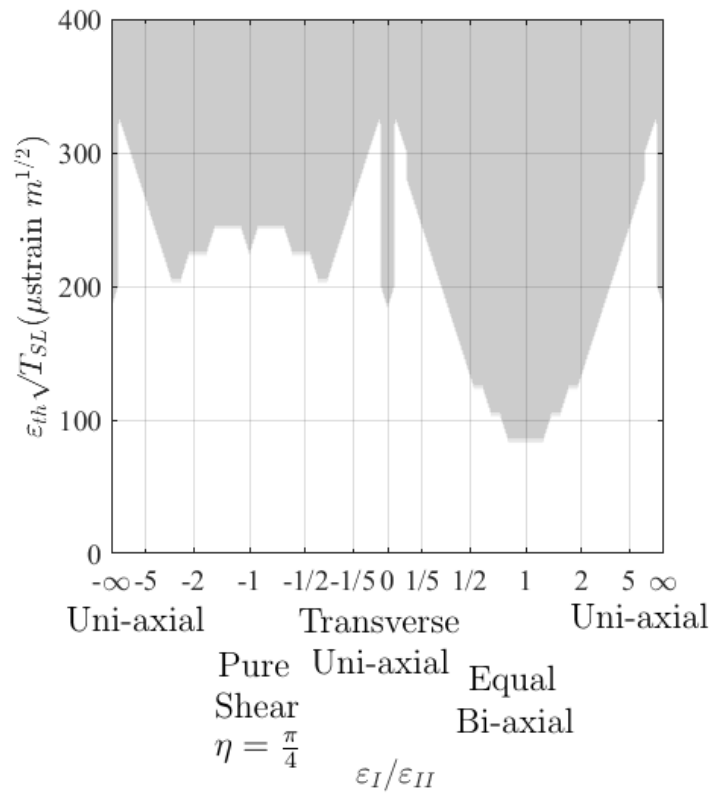
Figure 9.28: *The strain $(\varepsilon_{th}\sqrt{T_{SL}})$ constraints vs. bi-axial loading, indicating in grey where the constraint is not satisfied.*
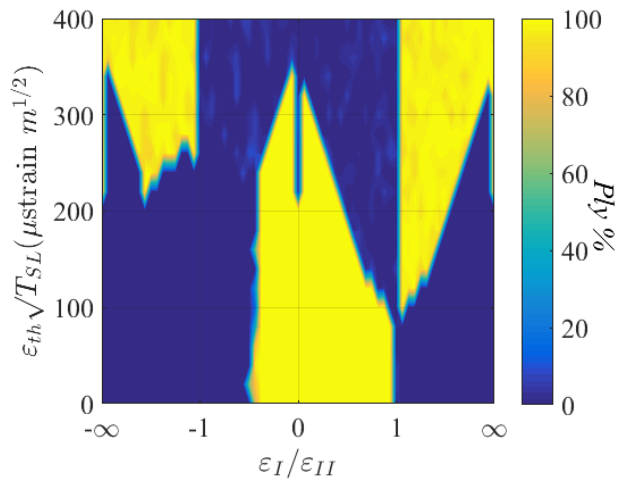
(a) *Sublaminate* $0°$.
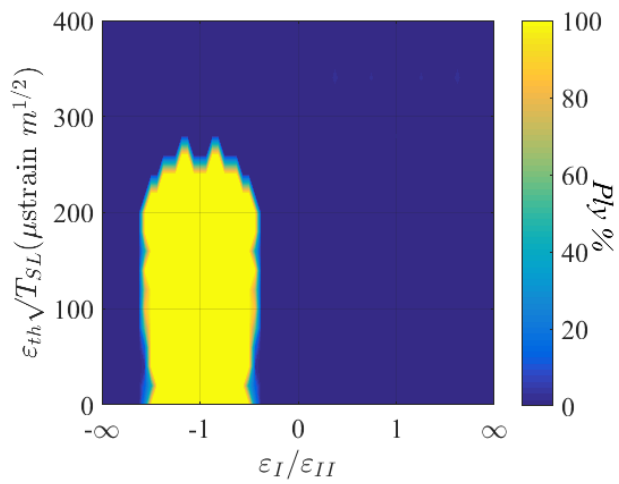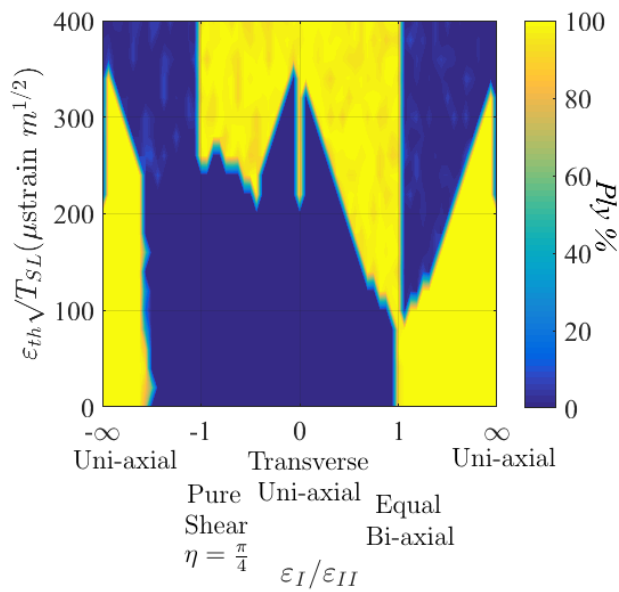
(b) *Sublaminate* $\pm 45°$.

(c) *Sublaminate* $90°$.

Figure 9.29: *Optimal sublaminate ply percentages for $0°$, $\pm 45°$ and $90°$ plies for design strain loadings in Optimisation 2(ii).*

9.6.3 General Discussion

All the behaviour seen in the results can be explained by understanding the role of laminate and sublaminate stiffness and strain on the damage tolerance performance of $\sigma_{th}\sqrt{T_{SL}}$ or $\varepsilon_{th}\sqrt{T_{SL}}$. These relationships are described fully by the Eqs. 9.1 and 9.4.2. Designs that are optimal can be better understood by considering the in-plane energies of the laminate and sublaminate seen in Eqs. 3.11 and 9.4 respectively.

$\varepsilon_{th}\sqrt{T_{SL}}$ is dictated by the sublaminate in-plane energy. This energy is affected by the laminate strain and the sublaminate stiffness, as per Eq. 9.5, which are co-dependent. The laminate strain depends on the laminate stiffness and thus sublaminate stiffness. Maximum $\varepsilon_{th}\sqrt{T_{SL}}$ is accomplished through minimisation of the in-plane sublaminate energy, which directly relates to the assumed SERR from the reduced multi-axial model in Chapter 6. This is achieved by reducing the laminate strain components in Eq. 9.5 (stiffer laminate in general) and reducing the sublaminate stiffness under strain (softer sublaminate). Maximum $\varepsilon_{th}\sqrt{T_{SL}}$ has only been investigated for a fixed strain loading and thus only sublaminate stiffness affected the performance. Plies orthogonal to the dominant strain load, minimise the SERR, maximising the $\varepsilon_{th}\sqrt{T_{SL}}$.

$\sigma_{th}\sqrt{T_{SL}}$ is dictated by the laminate stiffness and the $\varepsilon_{th}\sqrt{T_{SL}}$ value. Therefore maximum $\sigma_{th}\sqrt{T_{SL}}$ depends on (i) increasing the laminate stiffness, which reduces the laminate strain terms in Eq. 9.5, and (ii) reduction of the sublaminate stiffness. These are conflicting requirements and thus a compromise should generally be made. However, maximum $\sigma_{th}\sqrt{T_{SL}}$ is seen to coincide with placing plies orthogonal to the dominant strain direction, which may be maximising $\varepsilon_{th}\sqrt{T_{SL}}$. This is always true and seems to be the most in-plane efficient way to create designs with enough damage tolerance even for lower $\sigma_{th}\sqrt{T_{SL}}$ requirements. Once these orthogonal plies dominate, $\sigma_{th}\sqrt{T_{SL}}$ is increased by optimising the strain state and stiffness by changing the core design, which helps to decrease the SERR, increasing $\sigma_{th}\sqrt{T_{SL}}$ from both the stiffness and $\varepsilon_{th}\sqrt{T_{SL}}$ perspective. NSAs are likely to offer no improvement over standard angles for damage tolerance since the performance of these laminates relate directly to the stiffness of the laminate and sublaminate which can be approved minimally with NSAs (see Chapters 4 and 5), mainly for shear loading.

Increasing the damage tolerance constraints whilst designing for maximum global stiffness (minimisation/maximisation of in-plane laminate/sublaminate elastic energy under stress/strain loading), causes a sudden jump in damage tolerance performance where sublaminate plies are aligned orthogonal to the loading, which must also represent the greatest global stiffness under load at the increased damage tolerance level, as other designs will be chosen otherwise if they represent a more efficient

energy state. If this is untrue then there must be a problem with the optimisation set-up in terms of the ability of the GA to find optimum designs.

The general design philosophy for increased damage tolerance stress is to place stiff plies in the core (to maximise the stiffness and reduce the straining of the laminate) and to place soft plies in the surface (to reduce the sublaminate energy).

The damage tolerance capability depends on the loading ratios applied, with uni-axial loadings offering greater performance as more of the stiffness can be used to ensure one direction has a higher failure stress/strain than another. For more combined multi-axial loads stiffness has to be shared in all directions and so a lower but more global failure stress/strain is created.

Thickness independent laminate design optimisations were optimised using these techniques but the absolute magnitudes of the damage tolerance stress and strain are proportional to $\frac{1}{\sqrt{T_{SL}}}$. Therefore the sublaminate thickness and thus laminate thickness influence how high the laminate damage tolerance stress is; larger laminate thicknesses reduce the damage tolerance. There is likely to be an artificial lowering of the damage tolerance capability of thick laminates. This is because in thick laminates the absolute maximum BVID size is not increased but the absolute depth at which they are assumed to open is, as per the 25% thickness sublaminate. However in reality the sublaminate is unlikely to buckle over small length/thickness ratios. Therefore the sublaminate thickness that could buckle in reality will be less than the 25% sublaminate depth considered, with this percentage decreasing incrementally as the laminate gets thicker. Therefore the damage tolerance performance can be reasoned to depend on the sublaminate thickness only.

Damage tolerance stress is the weight limiting requirement as the laminate is limited by a maximum loading and not strain. Improvement is also shown over the use of conservative strain allowables, with higher magnitudes of propagation strain, for example a 1 mm sublaminate ranging from 5000-10000 μstrain, and 200-800 MPa. These values fall above that of most in-plane failure values and so suggest damage tolerance could be made less weight limiting. The results herein are not reliable absolute values of stress and strain and so they are questionable. Optimal plies are orthogonal to the loading which contradicts the literature with $\pm45°$ offering greater performance. This is perhaps due to the transverse cracking of orthogonal plies causing premature failure in reality.

The designs presented may be non-conservative because the reduced multi-axial propagation model, derived in Chapter 6. was used. Although it assumes conservatively for possible buckling strain and damage morphology (sublaminate of 25% depth), it does not account for post-buckled sublaminate coupling and stiffness that can act to increase the SERR to non-conservative levels, as discussed in Chapter 6.

The assumption was made that delaminations in the sublaminate above the buckled interface do not affect the propagation strain, however CAI has been shown to be lowered in the literature due to the presence of multiple delaminations [124–126]. Therefore this assumption may also be non-conservative and a future model should account for such behaviour.

9.7 Conclusions

A new multi-axial loading fracture mechanics based propagation model was incorporated in optimal design of damage tolerant composite laminates containing standard angles. The model was applied assuming conservative damage that can open up to a depth of 25% laminate thickness.

Novelty is shown in production of damage tolerant designs that are independent of thickness for a wide range of loadings.

Damage tolerance stress, and not strain, was investigated as an appropriate performance property limiting the weight of the laminate. The effect of the sublaminate strain state was investigated due to its fundamental effect on damage tolerance performance.

Four optimisations were carried out using two damage tolerance approaches, (1) damage tolerance stress for a design stress loading and (2) damage tolerance strain for a design strain loading, and two optimisation objectives (i) maximisation of damage tolerance and (ii) minimisation/maximisation of laminate/sublaminate elastic energy with damage tolerance constraints.

The sublaminate thickness is shown to affect the damage tolerance performance; decreased thicknesses increase damage tolerance. The techniques presented thus offer improvement over the current conservative strain allowables used in industry but is likely unreliable, since the model overestimates the performance and does not account for other failure mechanisms. Damage tolerance can be seen to vary with the input stress or strain loading applied, more multi-axial loading states will be more damage tolerance critical, such as shear compared to uni-axial.

Investigation of the damage tolerance design behaviour showed that, for a given thickness of sublaminate, propagation stress is dependent upon the co-dependent laminate propagation strain and laminate stiffness. The propagation strain is dependent on the in-plane strain energy of the sublaminate; lower energies, decreasing the SERR and increasing performance. The sublaminate strain energy depends on the laminate strain state and the sublaminate stiffness/stacking sequence. Therefore plies will align themselves to a soft configuration under a given strain state in order

to reduce the SERR and energy in the sublaminate. Plies orthogonal to the maximum strain direction minimise the energy and maximise damage tolerance stress. The general design philosophy for increased damage tolerance stress is to place stiff plies in the core and to place soft plies in the surface.

Appendix A

Reduced Damage Tolerance Strip Model

This Appendix is composed of work that was part of a conference publication at ECCM16 [152].

The reduction in strength of compressively loaded structures containing multiple, impact-damage-derived delaminations is currently limiting weight reduction in aerospace composite structures. Under compressive loading, layers above such delaminations (sublaminates) can buckle, driving delamination growth and ultimately causing failure. Hence it is necessary to account for this failure mechanism when deriving optimal laminate designs.

The Strip model [102] is an analytical method based on this sublaminate-buckling-driven delamination propagation mechanism and is used to calculate a laminate axial threshold stress σ_{th} below which delamination propagation will not occur. The strip model compares membrane and bending energy before and after propagation in the post-buckled system to calculate a Mode I SERR G_I,

$$G_I = \frac{A}{2}(\varepsilon - \varepsilon_C)(\varepsilon + 3\varepsilon_C) \tag{A.1}$$

Here A is the sublaminate axial stiffness and is equal to A_{11} if $A_{11} \geq A_{22}$ and A_{22} otherwise, ε_C is the sublaminate axial buckling strain and ε is the applied uniaxial strain. Delamination propagation is assumed to occur when there is sufficient applied strain ε_{th} to make G_I equal to the Mode I fracture toughness of the resin matrix (G_{IC});

$$G_{IC} = \frac{A}{2}(\varepsilon_{th} - \varepsilon_C)(\varepsilon_{th} + 3\varepsilon_C) \tag{A.2}$$

As the severity of an individual impact is unknown *a priori* and will result in uncertain delamination sizes and depths, the worst case (minimum) ε_{th} must be assumed at all interfaces. The depth of delamination considered to be at risk of propagation is limited to 25% of the laminate thickness as the thicker sublaminates associated with deeper delaminations will not buckle open and allow propagation to occur. ε_C is the only variable dependent on delamination size in Eqs. A.1 and A.2. Hence, the uncertainty in damage morphology can be mitigated by finding the minimum value (with respect to ε_C) of ε_{th} in Eq. A.2. Implicit differentiation of Eq. A.2 with respect to ε_C gives

$$\frac{dG_{IC}}{d\varepsilon_C} = \frac{A}{2}\left[2\varepsilon_{th}\left(\frac{d\varepsilon_{th}}{d\varepsilon_C}\right) + 2\varepsilon_C\left(\frac{d\varepsilon_{th}}{d\varepsilon_C}\right) + 2\varepsilon_{th} - 6\varepsilon_C\right] \tag{A.3}$$

As $(d\varepsilon_{th}/d\varepsilon_C) = 0$ is sought and G_{IC} is constant (and thus $(dG_{IC}/d\varepsilon_C) = 0$ rearrangement of Eq. A.3 gives

$$\varepsilon_C = \frac{\varepsilon_{th}}{3} \tag{A.4}$$

Substitution into Eq. A.2 then gives the minimum value of ε_{th} and multiplication by the laminate modulus E_{xx} gives the required minimum laminate threshold stress,

$$\sigma_{th,min} = E_{xx}\sqrt{\frac{3G_{IC}}{2A}} = \frac{1}{T_L}\left(A_{11} - \left(\frac{A_{12}^2}{A_{22}}\right)\right)\sqrt{\frac{3G_{IC}}{2A}} \tag{A.5}$$

As Eq. A.5 is independent of ε_C, minima may correspond to unrealistically large delamination diameters and thus can be a conservative lower bound on ε_{th} for realistic damage e.g. (BVID). Note that Eq. A.4 guarantees that delamination growth will be stable i.e. propagation will only occur with increasing strain (see [176] for full details and derivation). The derivation of Eqs. A.1 and A.2 includes the following simplifying assumptions: (1) loading is uni-axial and compressive; (2) energy for propagation is only available from the thin sublaminate (thin-film assumption); (3) Mode I fracture dominates propagation; (4) delaminations at each interface and their subsequent propagation under compressive load can be treated in isolation with the lowest of the derived propagation stresses σ_{th} taken as the overall laminate residual strength.

Appendix B

Failure Criteria

B.1 Tsai-Hill 2D Failure Criterion

Assuming plane stress conditions $(\sigma_3, \tau_{13}, \tau_{23} = 0)$

$$\left(\frac{\sigma_1}{X}\right)^2 + \left(\frac{\sigma_2}{Y}\right)^2 - \left(\frac{\sigma_1\sigma_2}{X^2}\right) + \left(\frac{\tau_{12}}{S}\right)^2 \geq 1 \tag{B.1}$$

where X, Y and S are the in-plane axial, transverse and shear failure strengths of the ply; σ_1, σ_2 and τ_{12} are the in-plane ply level stresses; and σ_3, τ_{13} and τ_{23} are the out-of-plane ply level stresses. Failure of a ply is assumed to occur when the failure index reaches 1 [181–183].

B.2 Tsai-Wu 2D Failure Criterion

This assumes both (i) plane stress and (ii) transverse isotropy [184].

$$F_i\sigma_i + F_{ij}\sigma_i\sigma_j \geq 1 \tag{B.2}$$

where i, j= 1, 2 and F_i and F_{ij} are strength tensors. Fully expanded, and accounting for any interaction terms and shear stress, Eq. B.2 becomes

$$F_1\sigma_1 + F_2\sigma_2 + F_{11}\sigma_1^2 + F_{22}\sigma_2^2 + F_{66}\sigma_6^2 + 2F_{12}\sigma_1\sigma_2 \geq 1 \tag{B.3}$$

where the strength tensors are described by the following equations. The ultimate strength for each mode of failure and the direction of failure is considered. The terms X_t and X_c are the tensile and compressive failure strengths in the axial direction; Y_t and Y_c are for the transverse direction respectively. The ultimate shear strength is represented by S. Failure of the ply is again assumed to occur when the failure index reaches 1.

$$F_1 = \frac{1}{X_t} - \frac{1}{X_c} \tag{B.4}$$

$$F_2 = \frac{1}{Y_t} - \frac{1}{Y_c} \tag{B.5}$$

$$F_{11} = \frac{1}{X_t X_c} \tag{B.6}$$

$$F_{22} = \frac{1}{Y_t Y_c} \tag{B.7}$$

$$F_{66} = \frac{1}{S^2} \tag{B.8}$$

$$F_{12} = F_{12}\sqrt{F_{11}F_{22}} = \frac{F_{12}}{\sqrt{X_t X_c Y_t Y_c}} \tag{B.9}$$

Bibliography

[1] IATA, "IATA Forecasts Passenger Demand to Double Over 20 Years," 2016. [Online] [Accessed: 31st May 2017.].

[2] ATAG, "Historic Aviation Climate Agreement Reached at ICAO," 2016. [Online] [Accessed: 31st May 2017.].

[3] ICAO, "Carbon Offsetting and Reduction Scheme for International Aviation (CORSIA)," 2016. [Online] [Accessed: 31st May 2017.].

[4] R. D. Adams, "50 years in carbon fibre, 60 years in composites," in *The Structural Integrity of Carbon Fibre Composites*, pp. 3–28, Elsevier Ltd., 2016.

[5] M. C. Y. Niu, *Composite Airframe Structures, Practical Design, Information and Data*. Hong Kong: Conmilit Press Ltd., 1992.

[6] M. M. Abdalla, S. Setoodeh, and Z. Gürdal, "Design of variable-stiffness composites panels of maximum fundamental frequency using lamination parameters," *Compos Struct*, vol. 81, pp. 283–291, 2007.

[7] J. A. Bailie, R. P. Ley, and A. Pasricha, "A summary and review of composite laminate design guidelines," Tech. Rep. NAS1-19347, Northrop Grumman Military Aircraft Systems Division, NASA, 1997.

[8] "Military handbook: Polymer matrix composites," 2002.

[9] P. M. Weaver and M. W. Bloomfield, "On the potential for elastic tailoring in layered composites buckling considerations," in *Proceedings of the 17th International Conference on Composite Materials*, (Edinburgh, UK), July- Aug 2009.

[10] W. Prager and J. E. Taylor, "Problems of optimal structural design," *J Appl Mech*, vol. 35, no. 1, pp. 102–106, 1968.

[11] B. A. Byers, "Behavior of damaged graphite/epoxy laminates under compressive loading," tech. rep., NASA Contractor Report, 159293, 1980.

[12] P. D. Mangalgiri, "Design allowable considerations for use of laminated composites in aircraft structures," *J Indian I Sci*, vol. 93, no. 4, pp. 571–592, 2013.

[13] F. Esrail and C. Kassapoglou, "An efficient approach to determine compression after impact strength of quasi-isotropic composite laminates," *Compos Sci Tech*, vol. 98, no. 27, pp. 28–35, 2014.

[14] L. Kärger, J. Baaran, A. Gunnion, and R. Thomson, "Evaluation of impact assessment methodologies. Part I: Applied methods," *Composites Part B*, vol. 40, no. 1, pp. 65–70, 2009.

[15] L. Kärger, J. Baaran, A. Gunnion, and R. Thomson, "Evaluation of impact assessment methodologies. Part II: Experimental validation," *Composites Part B*, vol. 40, no. 1, pp. 71–76, 2009.

[16] H. Chai and C. D. Babcock, "Two-dimensional modeling of compressive failure in delaminated laminates," *J Compos Mater*, vol. 19, no. 1, pp. 67–98, 1995.

[17] G. Flanagan, "Two-dimensional delamination growth in composite laminates," *Compos Mater: Testing and Design*, vol. 8, pp. 180–190, 1988.

[18] D. S. Cairns, P. J. Minguet, and M. G. Abdallah, "Theoretical and experimental response of composite laminates loaded in compression," *Compos Struct*, vol. 27, no. 4, pp. 431–437, 1994.

[19] EASA, "Certification Specifications and Acceptable Means of Compliance for Large Aeroplanes," 2013. [Online] [Accessed: 14th July 2014.].

[20] FAA, "Part 25- Airworthiness Standards: Transport Category Airplanes," 2014. [Online] [Accessed: 14th July 2014.].

[21] EASA, "AMC 20-29," 2010. [Online] [Accessed: 14th July 2014.].

[22] FAA, "AC 20-107B," 2010. [Online].

[23] S. W. Tsai and J. D. D. Melo, "An invariant-based theory of composites," *Compos Sci Tech*, vol. 100, no. 21, pp. 237–243, 20014.

[24] Z. Gürdal, R. T. Haftka, and P. Hajela, *Design and Optimization of Laminated Composite Materials*. Wiley, 1999.

[25] R. T. Haftka and J. L. Walsh, "Stacking sequence optimization for buckling of laminated plates by integer programming," *AIAA J*, vol. 30, no. 3, pp. 814–819, 1992.

[26] M. Autio, "Determining the real lay-up of a laminate corresponding to optimal lamination parameters by genetic search," *Struct Multidiscip Opt*, vol. 20, pp. 301–310, 2000.

[27] E. Reissner and Y. Stavsky, "Bending and stretching of certain types of heterogeneous isotropic elastic plates," *ASME J Appl Mech*, vol. 28, pp. 402–408, 1961.

[28] S. Gyan, R. Ganguli, and G. N. Naik, "Damage-tolerant design optimization of laminated composite structures using dispersion of ply angles by genetic algorithm," *J Reinf Plast Compos*, vol. 31, pp. 799–814, 2012.

[29] R. T. Haftka, J. H. Starnes, and S. Nair, "Design for global damage tolerance and associated mass penalties," *J Aircraft*, vol. 20, no. 1, pp. 83–88, 1983.

[30] L. A. Schmit and B. Farshi, "Optimum laminate design for strength and stiffness," *Int J Num Meth in Eng*, vol. 7, pp. 519–536, 1973.

[31] L. A. Schmit and B. Farshi, "Optimum design of laminated fibre composite plates," *Int J Num Meth in Eng*, vol. 11, pp. 623–640, 1977.

[32] U. Topal and U. Uzman, "Maximization of buckling load of laminated composite plates with central circular holes using mfd method," *Struct Multidiscip Opt*, vol. 35, pp. 131–139, 2008.

[33] N. Baker, A. T. Rhead, and R. Butler, "Optimisation of aerospace laminates for damage tolerance," in *Proceedings of the 7st ASMOUK/ISSMO International Conference of Engineering Design Optimisation*, (Bath, UK), 2008.

[34] N. Baker and R. Butler, "Compression after impact modeling of damage tolerant composite laminates," in *Proceedings of the 51st AIAA/ASME/ASCE/AHS/ASC structures, structural dynamics and materials conference*, (Orlando, Florida), 2010. AIAA-2010-2868.

[35] N. Baker, *Techniques for optimisation and analysis of composite structures for damage tolerance and buckling stiffness*. PhD thesis, University of Bath, 2012.

[36] J. H. Park, J. H. Hwang, C. S. Lee, and W. Hwang, "Stacking sequence design of composite laminates for maximum strength using genetic algorithms," *Compos Struct*, vol. 52, no. 2, pp. 217–231, 2001.

[37] U. Topal and U. Uzman, "Strength optimization of laminated composite plates," *J Compos Mater*, vol. 42, no. 17, pp. 1731–1746, 2008.

[38] T. R. Tauchert and S. Adibhatla, "Design of laminated plates for maximum stiffness," *J Compos Mater*, vol. 18, pp. 58–69, 1984.

[39] N. L. Pedersen, "Topology optimization of laminated plates with prestress," *Compos Struct*, vol. 80, no. 78, pp. 559–570, 2002.

[40] N. Zehnder and P. Ermanni, "A methodology for the global optimization of laminated composite structures," *Compos Struct*, vol. 72, pp. 311–320, 2006.

[41] R. Lipton and M. Stuebner, "Optimal design of composite structures for strength and stiffness: An inverse homogenization approach," *Struct Multidiscip Opt*, vol. 33, pp. 351–362, 2007.

[42] F. O. Sonmez, "Optimum design of composite structures: A literature survey (1969–2009)," *J Reinf Plas Compos*, vol. 36, no. 1, pp. 3–39, 2016.

[43] H. Fukunaga, H. Sekine, and M. Sato, "Optimal design of composite laminates for fundamental frequency," *J Sound Vibr*, vol. 171, no. 2, pp. 219–229, 1994.

[44] S. W. Tsai, J. C. Halpin, and N. J. Pagano, *Composites Material Workshop*. Westport, CT: Technomic, 1968.

[45] D. Muelas, J. M. Pena, and V. Robles, "Optimizing the design of composite panels using an improved genetic algorithm," in *Proceedings of the International Conference on Engineering Optimization*, (Brazil), 2008.

[46] G. Soremekun, Z. Gürdal, and R. T. Haftka, "Composite laminate design optimization by genetic algorithm with generalized elitist selection," *Comput Struct*, vol. 79, pp. 131–143, 2001.

[47] C. H. Park, W. Lee, and W. S. Han, "Improved genetic algorithm for multidisciplinary optimization of composite laminates," *Comput Struct*, vol. 86, pp. 1894–1903, 2008.

[48] R. L. Riche and R. T. Haftka, "Optimization of laminate stacking sequence for buckling load maximization of genetic algorithm," *AIAA J*, vol. 31, no. 5, pp. 951–956, 1993.

[49] D. E. Goldberry, *Algorithms in search, optimisation and machine learning*. Addison Wesley, 1989.

[50] A. R. M. Rao and N. Arvind, "Optimal stacking sequence design of laminate composite structures using tabu embedded simulated annealing," *Struct Eng Mech*, vol. 25, no. 2, pp. 239–268, 2007.

[51] A. Akbulut and F. O. Sonmez, "Optimum design of composite laminates for minimum thickness," *Comput Struct*, vol. 86, pp. 1974–1982, 2008.

[52] A. Todoroki and M. Sekishiro, "New iteration fractal branch and bound method for stacking sequence optimizations of multiple laminates," *Compos Struct*, vol. 81, pp. 419–426, 2007.

[53] J. Chen, R. Ge, and J. Wei, "Probabilistic optimal design of laminates using improved particle swarm optimization," *Eng Optim*, vol. 40, no. 8, pp. 695–708, 2008.

[54] J. Sedyono, H. Hadavinia, D. Venetsanos, and D. R. Marchant, "Enumeration search method for optimisation of stacking sequence of laminated composite plates subjected to buckling," *Open Eng*, vol. 5, pp. 190–204, 2015.

[55] R. L. Riche, A. Sauab, and J. Breard, "Coupled compression RTM and composite layup optimization," *Compos Sci Technol*, vol. 63, pp. 2277–2287, 2003.

[56] G. Marannano and G. V. Mariotti, "Structural optimization and experimental analysis of composite material panels for naval use," *Meccanica*, vol. 43, pp. 251–262, 2008.

[57] P. Pedersen, "On sensitivity analysis and optimal design of specially orthotropic laminates," *Eng Optim*, vol. 11, pp. 305–316, 1987.

[58] P. Pedersen, "On optimal orientation of orthotropic materials," *Struct Optim*, vol. 1, no. 2, pp. 101–106, 1989.

[59] P. Pedersen, "A note on design of fiber-nets for maximum stiffness," *J Elast*, vol. 73, pp. 127–145, 2003.

[60] M. Miki, Y. Murotsu, and N. M. et al., "Application of lamination parameters to reliability-based stiffness design of composites," *AIAA J*, vol. 31, no. 10, pp. 1938–1945, 1993.

[61] M. Miki and Y. Sugiyama, "Optimum design of laminated, composite plates using lamination parameters," *AIAA J*, vol. 31, no. 5, pp. 921–922, 1993.

[62] S. Setoodeh, M. M. Abdalla, and Z. Gürdal, "Design of variable-stiffness laminates using lamination parameters," *Composites Part B*, vol. 37, pp. 301–309, 2006.

[63] B. Liu, R. T. Haftka, and P. Trompette, "Maximization of buckling loads of composite panels using flexural lamination parameters," *Struct Multidiscip Opt*, vol. 26, pp. 28–36, 2004.

[64] C. G. Diaconu and H. Sekine, "Flexural characteristics and layup optimization of laminated composites plates under hygrothermal conditions using lamination parameters," *J Therm Stress*, vol. 26, pp. 905–922, 2003.

[65] D. Liu, V. V. Toropov, O. M. Querin, and D. C. Barton, "Bilevel optimization of blended composite wing panels," *J Aircraft*, vol. 48, no. 1, pp. 107–118, 2011.

[66] J. E. Herencia, P. M. Weaver, and M. I. Friswell, "Optimization of long anisotropic laminated fibre composite panels with t-shaped stiffeners," *AIAA J*, vol. 45, no. 10, pp. 2497–2509, 2007.

[67] J. E. Herencia, R. T. Haftka, P. M. Weaver, and M. I. Friswell, "Lay-up optimization of composite stiffened panels using linear approximations in lamination space," *AIAA J*, vol. 46, no. 9, pp. 2387–2391, 2008.

[68] P. Pedersen, L. Tobiesen, and S. H. Jensen, "Shapes of orthotropic plates for minimum energy concentration," *Mech Struct Mach*, vol. 20, no. 4, pp. 499–514, 1992.

[69] A. Muc, "Choice of design variables in the stacking sequence optimization for laminated structures," *Mech Compos Mater*, vol. 52, no. 2, pp. 211–224, 2016.

[70] P. Pedersen, "On thickness and orientational design with orthotropic materials," *Struct Optim*, vol. 64, pp. 68–78, 1991.

[71] R. E. Rowlands, *Strength (Failure) Theories and Their Experimental Correlation*. Elsevier Science Publishers B.V., 1985. Handbook of Composites.

[72] A. Puck and A. Schürmann, "Failure analysis of FRP laminates by means of physically based phenomenological models," *Compos Sci Technol*, vol. 58, no. 7, pp. 1045–1067, 1998.

[73] A. Puck and H. Schürmann, "Failure analysis of FRP laminates by means of physically based phenomenological models," *Compos Sci Technol*, vol. 62, no. 12–13, pp. 1633–1662, 2002.

[74] R. G. Cuntze, "The predictive capability of failure mode concept-based strength criteria for multi-directional laminates," *Compos Sci Technol*, vol. 64, pp. 487–516, 2004.

[75] R. G. Cuntze and A. Freund, "The predictive capability of failure mode concept-based strength criteria for multi-directional laminates," *Compos Sci Technol*, vol. 64, pp. 343–377, 2004.

[76] M. J. Hinton, A. S. Kaddour, and P. D. Soden, *Failure criteria in fibre reinforced polymer composites: the World-Wide Failure Exercise*. Oxford, UK: Elsevier Science Ltd, 2004.

[77] A. S. Kaddour, M. J. Hinton, and P. D. Soden, "Failure of 55 filament wound glass/epoxy composite tubes under biaxial compression," *J Compos Mater*, vol. 32, pp. 1618–1647, 1998.

[78] A. S. Kaddour and M. J. Hinton, "Evaluation of theories for predicting failure in polymer composite laminates under 3-D states of stress: Part A in the 2nd World-Wide Failure Exercise," *Special Issue of J. Compos. Mater.*, vol. 46, no. 19–20, 2012. Editors.

[79] A. S. Kaddour, M. J. Hinton, P. A. Smith, and S. Li, "Damage, matrix cracking criteria for fibre reinforced polymer composites, Part A of the 3rd World-Wide Failure Exercise," *Special Issue of J. Compos. Mater.*, vol. 47, no. 20–21, 2013. Editors.

[80] A. S. Kaddour, M. J. Hinton, S. Li, and P. A. Smith, "The World-Wide Failure Exercises: How can composites design and manufacture communities build their strength," in *Proceedings of the 16th European Conference on Composite Materials*, (Seville, Spain), June 2014.

[81] R. Butler, T. J. Dodwell, T. Kim, S. Kynaston, R. Scheichl, R. T. Hafkta, and N. H. Kim, "Uncertainty quantification of composite structures with defects using multilevel Monte Carlo simulations," in *Proceedings of the 17th AIAA Non-Deterministic Approaches Conference*, 2014.

[82] S. Sriramula and K. M. Chryssanthopoulos, "Quantification of uncertainty modelling in stochastic analysis of FRP composites," *Composites Part A*, vol. 40, pp. 1673–1684, 2009.

[83] S. Dey, S. Mukhopadhyay, and S. Adhikari, "Metamodel based high-fidelity stochastic analysis of composite laminates: a concise review with critical comparative assessment," *Compos Struct*, vol. 171, pp. 227–250, 2017.

[84] Y. Murotsu, M. Miki, and S. Shao, "Reliability design of fiber reinforced composites," *Structural Safety*, vol. 15, no. 1, pp. 35–49, 1994.

[85] M. Lombardi and R. T. Haftka, "Anti-optimization technique for structural design under load uncertainties," *Comp Meth App Mech Eng*, vol. 157, no. 1, pp. 19–31, 1998.

[86] X. Guo, W. Bai, W. Zhang, and X. Gao, "Confidence structural robust design and optimization under stiffness and load uncertainties," *Comp Meth App Mech Eng*, vol. 198, no. 41–44, pp. 3378–3399, 2009.

[87] G. Verchery, "The netting analysis as a limit case of the laminated structure theory," in *Proceedings of the 19th International Conference on Composite Materials*, (Montreal, Canada), pp. 1724–1731, 2013.

[88] V. V. Toropov, R. Jones, T. Willment, and M. Funnell, "Weight and manufacturability optimization of composite aircraft components based on a genetic algorithm," in *Proceedings of the 6th World Congresses of Structural and Multidisciplinary Optimization*, (Rio de Janeiro, Brazil), 2005.

[89] D. H. Bassir, F. X. Irisarri, and J. F. M. et al., "Incorporating industrial constraints for multiobjective optimization of composite laminates using a GA," *Int J Simul Multidiscip Des Optim*, vol. 2, no. 2, pp. 101–106, 2008.

[90] M. Miki and Y. Sugiyama, "Optimum design of laminated composite plates using lamination parameters," *AIAA J*, vol. 31, no. 5, pp. 921–922, 1993.

[91] D. Peeters and M. Abdalla, "Design guidelines in non-conventional composite laminate optimization," *J Aircraft*, vol. 54, no. 4, pp. 1454–1464, 2017.

[92] M. M. Abdalla, C. Kassapoglou, and Z. Gürdal, "Formulation of composite laminate robustness constraint in lamination parameters space," in *Proceedings of the 50th AIAA/ASME/ASCE/AHS/ASC structures, structural dynamics, and materials conference*, (Palm Springs, California), 2009.

[93] G. Caprino and I. C. Visconti, "A note on specially orthotropic laminates," *J Compos Mater*, vol. 16, no. 5, pp. 395–399, 1982.

[94] C. B. York, "Tapered hygro-thermally curvature-stable laminates with non-standard ply orientations," *Composites Part A*, vol. 44, pp. 140–148, 2013.

[95] C. B. York, "Characterization of non-symmetric forms of fully orthotropic laminates," *J Aircraft*, vol. 46, pp. 1114–1125, 2009.

[96] C. B. York, "On tapered warp-free laminates with single-ply terminations," *Composites Part A*, vol. 72, pp. 127–138, 2015.

[97] C. B. York and S. F. M. Almeida, "Tapered laminate designs for new non-crimp fabric architectures," *Composites Part A*, vol. 100, pp. 150–160, 2017.

[98] C. B. York and S. F. M. de Almeida, "On extension-shearing bending-twisting coupled laminates," *Compos Struct*, vol. 164, pp. 10–22, 2017.

[99] S. W. Tsai, "Weight and cost reduction by using unbalanced and unsymmetric laminates," in *Proceedings of the 18th International Conference on Composite Materials*, (Jeju, Korea), August 2011.

[100] T. A. Fletcher, R. Butler, and T. J. Dodwell, "Anti-symmetric laminates for improved consolidation and reduced warp of tapered C-sections," *Adv Manuf: Polymer and Composites Science*, vol. 1, no. 2, pp. 105–111, 2015.

[101] S. A. Hitchen and R. M. L. Kemp, "The effect of stacking sequence on impact damage in a carbon fibre/epoxy composite," *Composites*, vol. 26, no. 3, pp. 207–214, 1995.

[102] R. Butler, A. T. Rhead, W. Liu, and N. Kontis, "Compressive strength of delaminated aerospace composites," *Phil Trans Roy Soc A*, vol. 370, pp. 1759–1779, 2012.

[103] A. T. Nettles and M. J. Douglas, "A comparison of quasi-static indentation testing to low velocity impact testing, Composite Materials: Testing, Design and Acceptance Criteria," tech. rep., ASTM STP 141, 2000.

[104] M. H. Keegan, D. H. Nash, and M. M. Stack, "On erosion issues associated with the leading edge of wind turbine blades," *J Phys. D: Appl Phys*, vol. 46, no. 38, 2012.

[105] J. Rhymer, H. Kim, and D. Roach, "The damage resistance of quasi-isotropic carbon/epoxy composite tape laminates impacted by high velocity ice," *Composites Part A*, vol. 43, pp. 1134–1144, 2012.

[106] M. R. L. Gower, R. M. Shaw, and G. D. Sims, "Evaluation of the repeatability under static loading of a compression-after-impact test method proposed for ISO standardisation," tech. rep., National Physics Laboratory, Middlesex, UK, 2005. DEPC-MN 036.

[107] A. T. Rhead and R. Butler, "Compressive static strength model for impact damaged laminates," *Compos Sci Technol*, vol. 69, no. 14, pp. 2301–2307, 2009.

[108] K. N. Shivakumar, W. Elber, and W. Illg, "Prediction of low-velocity impact damage in thin circular laminates," *AIAA J*, vol. 23, no. 3, pp. 442–449, 1985.

[109] W. C. Jackson and C. C. Poe, "The use of impact force as a scale parameter for the impact response of composite laminates," tech. rep., NASA Technical Memorandum, 1992. 104189.

[110] A. L. Highsmith, "A study of the use of contact loading to simulate low velocity impact," tech. rep., NASA Contractor Report, 97–206121, 1997.

[111] S. Abrate, "Impact on laminated composite materials," *Appl Mech Rev*, vol. 44, no. 4, pp. 155–190, 1991.

[112] S. Abrate, *Impact on Composite Structures*. Cambridge University Press, 1998.

[113] H. Suemasu and O. Majima, "Multiple delaminations and their severity in nonlinear circular plates subjected to concentrated loading," *J Compos Mater*, vol. 32, no. 2, pp. 123–140, 1998.

[114] S. Hong and D. Liu, "On the relationship between impact energy and delamination area," *Exper Mech*, vol. 29, no. 2, pp. 115–120, 1989.

[115] P. O. Sjoblom, J. T. Hartness, and T. M. Cordell, "On low-velocity impact testing of composite materials," *J Compos Mater*, vol. 22, no. 1, pp. 30–52, 1988.

[116] A. L. Pilchak, T. Uchiyama, and D. Liu, "Low velocity impact response of small-angled laminated composites," *AIAA J*, vol. 44, no. 12, pp. 3080–3087, 2006.

[117] A. M. Amaro, P. N. B. Reis, A. G. Magalhes, and M. F. S. F. de Moura, "The effect of the impactor diameter and boundary conditions on low velocity impact composites behaviour," *Appl Mech Mater*, vol. 7, no. 8, p. 217, 2007.

[118] G. A. O. Davies and R. Olsson, "Impact on composite structures," *Aeronaut J*, vol. 108, pp. 541–563, 2004.

[119] C. Bouvet, B. Castani, M. Bizeul, and J. Barrau, "Low velocity impact modelling in laminate composite panels with discrete interface elements," *Int J Solids Struct*, vol. 46, no. 14, pp. 2809–2821, 2009.

[120] C. Garnier, M. Pastor, F. Eyma, and B. Lorrain, "The detection of aeronautical defects in situ on composite structures using non destructive testing," *Compos Struct*, vol. 93, no. 5, pp. 1328–1336, 2011.

[121] A. S. Chen, D. P. Almond, and B. Harris, "Acoustography as a means of monitoring damage in composite plates," *Meas Sci Technol*, vol. 12, pp. 151–156, 2001.

[122] L. Lammerant and I. Verpoest, "Modelling of the interaction between matrix cracks and delaminations during impact of composite plates," *Compos Sci Technol*, vol. 56, no. 10, pp. 1171–1178, 1996.

[123] G. Clark, "Modelling of impact damage in composite laminates," *Composites*, vol. 20, no. 3, pp. 209–214, 1989.

[124] A. M. Amaro, P. N. B. Reis, M. F. S. F. de Moura, and M. A. Neto, "Buckling analysis of laminated composite plates submitted to compression," *Fibers and Polymers*, vol. 15, no. 3, pp. 560–565, 2014.

[125] Y. Zhang and S. Wang, "Buckling, post-buckling and delamination propagation in debonded composite laminates, part I: Theoretical development," *Compos Struct*, vol. 88, pp. 121–130, 2009.

[126] S. Wang and Y. Zhang, "Buckling, post-buckling and delamination propagation in debonded composite laminates, Part 2: Numerical applications," *Compos Struct*, vol. 88, no. 1, pp. 131–146, 2009.

[127] Z. Aslan and M. Sahin, "Buckling behaviour and compressive failure of composite laminates containing multiple large delaminations," *Compos Struct*, vol. 89, pp. 382–390, 2009.

[128] H. Suemasu, T. Irie, and T. Ishikawa, "Buckling and post-buckling behaviour of composite plates containing multiple delaminations," *J Compos Mater*, vol. 43, pp. 191–202, 2009.

[129] R. Craven, L. Iannuci, and R. Olsson, "Delamination buckling: A finite element study with realistic delamination shapes, multiple delaminations and fibre fracture cracks," *Composites Part A*, vol. 441, pp. 684–692, 2010.

[130] A. Tafreshi and T. Oswald, "Global buckling behaviour and local damage propagation in composite plates with embedded delaminations," *Int J Pressure Vessels and Piping*, vol. 80, pp. 9–20, 2003.

[131] G. W. Hunt, B. Hu, R. Butler, D. P. Almond, and J. E. Wright, "Nonlinear modelling of delaminated struts," *AIAA J*, vol. 42, no. 11, pp. 2364–2372, 2004.

[132] H. Kim and K. T. Kedward, "A method for modeling the local and global buckling of delaminated composite plates," *Compos Struct*, vol. 44, pp. 43–53, 1998.

[133] G. L. Melin and J. Schön, "Buckling behaviour and delamination growth in impacted composite specimens under fatigue load: an experimental study," *Compos Sci Technol*, vol. 61, pp. 1841–1852, 2001.

[134] I. Sheinman, G. A. Kardomateas, and A. A. Pelegri, "Delamination growth during pre- and post-buckling phases of delaminated composite laminates," *Int J Solids Struct*, vol. 35, no. 1–2, pp. 19–31, 1998.

[135] E. S. Greenhalgh and S. Singh, "Investigation of the failure mechanisms for delamination growth from embedded defects," in *Proceedings of the 12th International Conference on Composite Materials*, (Paris, France), 1999.

[136] T. Gottesman, S. Girchovich, E. Drukker, N. Sela, and J. Loy, "Residual strength of impacted composites: analysis and tests," *J Compos Technol*, vol. 16, no. 3, pp. 244–255, 1994.

[137] Y. Xiong, C. Poon, P. V. Straznicky, and H. Vietinghoff, "A prediction method for the compressive strength of impact damaged composite laminates," *Compos Struct*, vol. 30, no. 4, pp. 357–367, 1995.

[138] J. Y. Huang, "Prediction of the residual strength of laminated composites subjected to impact loading," *J Mater Process Technol*, vol. 4, pp. 15–44, 1995.

[139] F. W. Williams, D. Kennedy, M. S. Anderson, and R. Butler, "Viconopt-program for exact vibration and buckling analysis for design of prismatic plate assemblies," *AIAA J*, vol. 29, pp. 1927–1928, 1991.

[140] M. W. D. Nielsen, "Damage tolerance of steered fibre composite laminates," tech. rep., University of Bath, 2013. Final Year MEng Project Report.

[141] A. A. Baker, R. Jones, and R. J. Callinan, "Damage tolerance of graphite/epoxy composites," *Compos Struct*, vol. 4, pp. 15–44, 1985.

[142] T. L. Anderson, *Fracture Mechanics: Fundementals and Applications, Third Edition.* CRC Press, 2005.

[143] H. Chai, C. D. Babcock, and W. G. Knauss, "One dimensional modelling of failure in laminated plates by delamination buckling," *Int J Struct*, vol. 17, no. 11, pp. 1069–1083, 1981.

[144] C. Soutis and P. T. Curtis, "Prediction of the post-impact compressive strength of CFRP laminated composites," *Compos Sci Tech*, vol. 56, no. 6, pp. 677–684, 1996.

[145] C. Soutis and N. A. Fleck, "Failure prediction technique for compression-loaded carbon fibre-epoxy laminate with open holes," *J Compos Mater*, vol. 25, pp. 1476–1498, 1991.

[146] A. T. Rhead, R. Butler, W. Liu, and N. Baker, "The influence of surface ply fibre angle on the compressive strength of composite laminates containing delamintion," *Aeronaut J*, vol. 116, no. 1186, pp. 1315–1330, 2012.

[147] M. Bloomfield, J. E. Herencia, and P. M. Weaver, "Optimisation of anisotropic composite plates incorporating non-conventional ply orientations," in *Proceedings of the 49th AIAA/ASME/ASCE/AHS/ASC structures, structural dynamics and materials conference*, (Schaumburg, Illinois), 2008.

[148] G. Guillamet, Y. Liv, A. Turon, L. Marin, E. V. Gonzalez, J. A. Mayugo, and J. Costa, "Design of non-conventional CFRP laminates for improved damage resistance and damage tolerance," in *Proceedings of the 16th European Conference on Composite Materials*, (Seville, Spain), 2014.

[149] P. Ladevèze, "Multiscale modelling and computational strategies for composites," *Int J Numer Meth Eng*, vol. 60, no. 1, pp. 233–253, 2004.

[150] A. Reinarz, T. Dodwell, T. Fletcher, L. Seelinger, R. Butler, and R. Scheichl, "dune-composites- A new framework for high-performance finite element modelling of laminates." Submitted for publication, 2017.

[151] M. U. Kismarton and T. B. Company, "Composite stiffeners for aerospace vehicles," May 13 2014. US Patent 8,720,825.

[152] M. W. D. Nielsen, A. T. Rhead, and R. Butler, "Structural efficiency via minimisation of elastic energy in damage tolerant laminates," in *Proceedings of the 16th European Conference on Composite Materials*, (Seville, Spain), June 2014.

[153] MATLAB, 2015. R2015b The MathWorks Inc.

[154] D. E. Goldberg, *Genetic algorithms in search, optimization and machine learning.* Boston: Addison-Wesley Longman, 1989.

[155] A. R. Conn, N. I. M. Gould, and P. L. Toint, "A globally convergent augmented lagrangian algorithm for optimization with general constraints and simple bounds," *SIAM J Numer Anal*, vol. 28, no. 2, pp. 545–572, 1991.

[156] A. R. Conn, N. I. M. Gould, and P. L. Toint, "A globally convergent augmented lagrangian barrier algorithm for optimization with general inequality constraints and simple bounds," *Math Comput*, vol. 66, no. 217, pp. 261–288, 1997.

[157] M. C. Y. Niu, *Airframe structural design- Practical design information and data on aircraft structures.* Hong Kong: Conmilit Press Limited, 1999.

[158] C. G. Diaconu and H. Sekine, "Layup optimization for buckling of laminated composite shells with restricted layer angles," *AIAA J*, vol. 42, no. 10, pp. 2153–2163, 2004.

[159] A. S. Kaddour and M. J. Hinton, "Maturity of 3D failure criteria for fibre-reinforced composites: Comparison between theories and experiments: Part B of WWFE-II," *J Compos Mater*, vol. 47, pp. 925–966, 2013.

[160] L. J. Hart-Smith, "Some observations about test specimens and structural analysis for fibrous composites," in *Composite Materials: Testing and Design (Ninth Volume) ASTM STP 1059* (S. P. Garbo, ed.), pp. 86–120, Philadephia, USA: American Society for Testing and Materials, 1990.

[161] M. W. D. Nielsen, K. J. Johnson, A. T. Rhead, and R. Butler, "Laminate design for optimised in-plane performance and ease of manufacture," *Compos Struct*, vol. 177, pp. 119–128, 2017.

[162] S. J. Winckler, "Hygrothermally curvature stable laminates with tension-torsion coupling," *J Am Helicopter Soc*, vol. 31, pp. 56–58, 1985.

[163] K. Potter, "Bias extension measurements on cross-plied unidirectional prepreg," *Composites Part A*, vol. 33, no. 1, pp. 63–73, 2002.

[164] P. Hallender, M. Akermo, C. Mattei, M. Petersson, and T. Nyman, "An experimental study of mechanisms behind wrinkle development during forming of composite laminates," *Composites Part A*, vol. 50, pp. 54–64, 2013.

[165] M. Elkington and C. Ward, "Time dependence of multi-ply forming over doubly curved shapes," in *Proceedings of the 17th European Conference on Composite Materials (ECCM17)*, (Munich, Germany), June 2016.

[166] Z. Gürdal, B. Tatting, and C. Wu, "Variable stiffness composite panels: Effects of stiffness variation on the in-plane and buckling response," *Composites Part A*, vol. 39, no. 5, pp. 911–922, 2008.

[167] MATLAB, 2013. R2013b The MathWorks Inc.

[168] S. Erland, T. J. Dodwell, and R. Butler, "Characterisation of inter-ply shear in uncured carbon fibre prepreg," *Composites Part A*, vol. 77, pp. 210–218, 2015.

[169] N. P. M. Werter and R. D. Breuker, "Aeroelastic tailoring and structural optimisation using an advanced dynamic aeroelastic framework," in *Proceedings of the IFASD 2015: 16th International Forum on Aeroelasticity and Structural Dynamics*, (Saint Petersburg, Russia), June–July 2015.

[170] G. Shijun, C. Weyuan, and C. Degang, "Aeroelastic tailoring of composite wing structures by laminate layup optimization," *AIAA J*, vol. 44, no. 12, pp. 3146–3150, 2006.

[171] M. Xia, H. Takayanagi, and K. Kemmochi, "Analysis of multi-layered filament-wound composite pipes under internal pressure," *Compos Struct*, vol. 53, no. 4, pp. 483–491, 2001.

[172] T. Y. Kam, Y. M. Liu, and F. T. Lee, "First-ply failure strength of laminated composite pressure vessels," *Compos Struct*, vol. 38, no. 1–4, pp. 65–70, 1997.

[173] J. Renze and E. W. Weisstein, "Extreme Value Theorem." [Online], Accessed: $8^{th} March 2018$.

[174] A. T. Rhead, *Analysis and optimisation of postbuckled damage tolerant composite laminates*. PhD thesis, University of Bath, 2009.

[175] D. Kennedy, F. W. Williams, and M. S. Anderson, "Buckling and vibration analysis of laminated panels using VICONOPT," *J Aerospace Eng*, vol. 7, pp. 245–262, 1994.

[176] A. T. Rhead, R. Butler, and G. Hunt, "Post-buckled propagation model for compressive fatigue of impact damaged laminates," *Int J Sols Struct*, vol. 45, pp. 4349–4361, 2008.

[177] L. E. Culliford, "Unexpected failure of aerospace composite laminates with high Poisson's ratio," tech. rep., University of Bath, 2016. Final Year MEng Project Report.

[178] J. Tomblin, T. Lacy, B. Smith, S. Hooper, A. Vizzini, and S. Lee, "Review of Damage Tolerance for Composite Sandwich Airframe Structures," tech. rep.,

U.S. Department of Transportation: Federal Aviation Adminstration, August 1999. DOT/FAA/AR-99/49.

[179] R. Butler, "Buckling and compressive strength of laminates with optimized fibre-steering and layer-stacking for aerospace applications," in *Polymer Composites in the Aerospace Industry*, Springer, 2015.

[180] J. D. Whitcomb and K. N. Shivakumar, "Strain-energy release rate analysis of plates with post-buckled delaminations," *Compos Mater*, vol. 23, no. 7, pp. 714–734, 1989.

[181] R. Hill, *The Mathematical Theory of Plasticity*. Oxford: Oxford U.P., 1950.

[182] S. W. Tsai, "Fundamental aspects of fibre reinforced plastic composites," in *Strength Theories of Filamentary Structures* (R. T. Schwartz and H. S. Schwartz, eds.), ch. 1, New York: Interscience, 1968.

[183] V. D. Azzi and S. W. Tsai, "Anisotropic strength of composites," *Exp Mech*, vol. 5, no. 9, pp. 283–288, 1965.

[184] S. W. Tsai and E. M. Wu, "A general theory of strength for anisotropic materials," *J Compos Mat*, vol. 5, no. 1, pp. 58–80, 1971.